AD_____

Award Number: W81XWH-06-1-0293

TITLE: Characterization of Neurofibromas of the Skin and Spinal Roots in a Mouse Model

PRINCIPAL INVESTIGATOR: Dr. Yuan Zhu

CONTRACTING ORGANIZATION: University of Michigan
Ann Arbor, MI 48109

REPORT DATE: February 2011

TYPE OF REPORT: Final

PREPARED FOR: U.S. Army Medical Research and Materiel Command
Fort Detrick, Maryland 21702-5012

REPORT DOCUMENTATION PAGE

Form Approved
OMB No. 0704-0188

1. REPORT DATE *(DD-MM-YYYY)*	**2. REPORT TYPE**	**3. DATES COVERED** *(From - To)*
01-02-2011	Final	25 JAN 2006 - 24 JAN 2011

4. TITLE AND SUBTITLE
Characterization of Neurofibromas of the Skin and Spinal Roots in a Mouse Model

5a. CONTRACT NUMBER

5b. GRANT NUMBER
W81XWH-06-1-0293

5c. PROGRAM ELEMENT NUMBER

6. AUTHOR(S)
Dr. Yuan Zhu

E-Mail: yuanzhu@umich.edu

5d. PROJECT NUMBER

5e. TASK NUMBER

5f. WORK UNIT NUMBER

7. PERFORMING ORGANIZATION NAME(S) AND ADDRESS(ES)
University of Michigan
Ann Arbor, MI 48109

8. PERFORMING ORGANIZATION REPORT NUMBER

9. SPONSORING / MONITORING AGENCY NAME(S) AND ADDRESS(ES)
U.S. Army Medical Research and Materiel Command
Fort Detrick, Maryland 21702-5012

10. SPONSOR/MONITOR'S ACRONYM(S)

11. SPONSOR/MONITOR'S REPORT NUMBER(S)

12. DISTRIBUTION / AVAILABILITY STATEMENT
Approved for Public Release; Distribution Unlimited

13. SUPPLEMENTARY NOTES

14. ABSTRACT
Benign neurofibromas and malignant peripheral nerve sheath tumors (MPNSTs) contribute to the majority of morbidity and mortality associated with NF1. The proposed studies are attempting to provide insights into one of the fundamental questions in neurofibroma biology: whether bi-allelic NF1 inactivation is necessary for neurofibroma formation. The objectives of this proposal are to use a series of newly established mouse models to (1) identify and characterize neurofibromas that are exclusively or predominantly comprised of NF1+/- cells (designated NF1+/- neurofibromas hereafter) in the skin and spinal roots; and (2) determine whether in this model, neurofibromas in the skin are similar to human dermal neurofibromas and thus are fundamentally different from the plexiform neurofibromas found in spinal roots. Previous studies of human tumors suggest that dermal and plexiform neurofibromas have fundamental differences in their dependence on the NF1 heterozygous environment and have different malignant transformation potentials. We have made substantial progress in the past four years of the award. For Task 1, we demonstrated that bi-allelic inactivation of Nf1 in neural crest stem cells is required for neurofibroma formation. These results resulted in publication of 3 manuscripts in 2008 (see appendices). For Task 2, we have determined that the Nf1 heterozygous environment promotes neurofibroma progression, but is not required for tumor initiation. For Task 3, we demonstrate that the Nf1 heterozygous environment is not required for malignant transformation of neurofibroma. We have established novel mouse models for MPNST, in which neurofibroma arises first followed by MPNST formation – a stepwise process that closely resembles the progressive nature of human MPNST. We are currently working on a manuscript to publish these results. We have written a manuscript based upon the results from Task 2 and Task 3, which will be submitted next month.

15. SUBJECT TERMS
neurofibroma, plexiform neurofibroma, mouse model, Schwann cell development, non-myelinating Schwann cells, myelinating Schwann cells, mast cell inflammation, axonal degeneration

16. SECURITY CLASSIFICATION OF:			**17. LIMITATION OF ABSTRACT**	**18. NUMBER OF PAGES**	**19a. NAME OF RESPONSIBLE PERSON**
a. REPORT	**b. ABSTRACT**	**c. THIS PAGE**			USAMRMC
U	U	U	UU	160	**19b. TELEPHONE NUMBER** *(include area code)*

Table of Contents

Page

Introduction

Benign neurofibromas and malignant peripheral nerve sheath tumors (MPNSTs) contribute to the majority of morbidity and mortality associated with NF1. The proposed studies attempt to provide insights into one of the fundamental questions in neurofibroma biology: whether biallelic *NF1* inactivation is necessary for neurofibroma formation. The objectives of this proposal are to use a series of newly established genetically engineered mouse (GEM) models to (1) identify and characterize neurofibromas that are exclusively or predominantly comprised of $Nf1^{+/-}$ cells (designated $Nf1^{+/-}$ neurofibromas hereafter) in the skin and spinal roots; and (2) determine whether in this model, neurofibromas in the skin are similar to human dermal neurofibromas and thus are fundamentally different from the plexiform neurofibromas found in spinal roots. Previous studies of human tumors suggest that dermal and plexiform neurofibromas have fundamental differences in their dependence on the *Nf1* hetereozygous environment and have different malignant transformation potentials. Thus, we will test three hypotheses: (1) bi-allelic *Nf1* inactivation is not necessary for neurofibroma formation; (2) An *Nf1* heterozygous environment is not essential for neurofibroma formation in the skin; (3) neurofibromas in the skin and spinal roots have distinct tumorigenic potential in response to subsequent p53-mediated malignant transformation. To test these hypotheses, we propose the following specific aims.

Body

We have completed all the proposed studies in the last 5 years of funding, which includes the first 4 years as requested and the 5th year as no-cost one-year extension. I received this grant shortly after I started my independent career as an assistant professor in the Department of Internal Medicine at the University of Michigan. This important funding provided a tremendous boost for my research program. During this funding period, I was able to publish several important papers including two Cancer Cell papers and was promoted to associate professor with tenure. More importantly, we made several fundamental discoveries regarding the pathogenesis of NF1-associated peripheral nerve sheath tumor, some of which provide novel insights on how to design novel therapies for preventing and treating these incurable tumors in humans. Based upon the results derived from this grant, I submitted two NIH R01 applications last year: one received the priority score of 13 and 1.0 percentile and the other received the priority score of 28 and 13.0 percentile. These NIH grants will ensure the continuation of these important studies. I am deeply appreciated by the funding resources provided by the Department of Defense NF Research Program.

Task 1. To determine whether *Nf1* heterozygous cells exclusively can give rise to neurofibromas in the skin and spinal roots.

The hypothesis for this task is that **bi-allelic *Nf1* inactivation is not absolutely necessary for neurofiborma formation**. The hypothesis predicts that at least some neurofibromas, particularly those formed in the skin, can be formed exclusively by *Nf1* heterozygous cells. To test this hypothesis, we employed two Cre transgenic strains, P0A-cre and Krox20-cre, which respectively target an *Nf1* mutation into neural crest stem cells (NCSCs) and more differentiated Schwann cells in mouse sciatic nerves. As shown in Figure 1, P0A-cre is expressed in NCSCs during embryonic nerve development (Figure 1). By analyzing these two *Nf1* tissue-specific knockout (KO) mouse models that are hereafter referred to as $Nf1^{P0A}$KO and $Nf1^{Krox20}$KO, respectively, we demonstrated that, to efficiently induce neurofibroma formation, *Nf1* must be deleted in NCSCs (Figure 2A-H), but not in more differentiated Schwann cells (Figure 2I-2P). However, surprisingly, *Nf1*-null NCSCs appear to differentiate according to a normal

developmental schedule. No abnormalities in cell density and the number of myelinating and nonmyelinating Schwann cells were observed in *Nf1*^{P0A}KO mutant sciatic nerves (Figure 3B, 3D, 3E, 3F) as compared to controls (Figure 3A, 3C). Through detailed analyses of peripheral nerves in these *Nf1*^{P0A}KO mutant mice, we found that loss of *Nf1* disrupted the ordered association of nonmyelinating Schwann cells with axons in an axon/Schwann cell structure known as Remark bundle (Figure 3G-3L). Over time these abnormally differentiated Remak bundles dissociated from their axons and the number of nonmyelinating Schwann cells increased (Figure 4A-4F). We further demonstrated that the expanded cell populations in *Nf1*^{P0A}KO mutant nerves exhibited morphological features of nonmyelinating Schwann cells including the presence of continuous basal lamina and ensheathed various numbers of unmyelinated axons (Figure 4G-4O), and had the lineage marker expression pattern similar to nonmyelinating Schwann cells (Sox10^{-} /GFAP^{+}/p75^{+}) (Figure 5A-5J). These expanded nonmyelinating Schwann cells also displayed several fundamental features of neurofibroma cells: hyperproliferation and clustering (Figure 5K-5Q). More importantly, these early-stage neurofibroma cells were invariably *Nf1* deficient (Figure 6). **In summary, we demonstrate that bi-allelic inactivation of *Nf1* is absolutely required for neurofibroma formation in mice. Furthermore, to efficiently induce plexiform neurofibroma formation, inactivation of both alleles of *Nf1* must occur in the early stages of Schwann cell development (e.g. neural crest stem cells or Schwann cell precursors).** In addition, these results suggest that nonmyelinating Schwann cells are a cell-of-origin of plexiform neurofibroma, and more importantly, that the *Nf1* deficient cells, but not *Nf1* heterozygous cells, initiate neurofibroma formation.

It is worth noting that the type of neurofibromas observed in the skin of the *Nf1*^{P0A}KO model may not fully resemble human dermal neurofibromas. Thus, we cannot completely rule out the possibility that some human dermal neurofibromas might arise from NF1 heterozygous cells. However, **these studies, for the first time, shed the insights into the cell-of-origin and critical cellular events during early phases of neurofibroma development.** These results may lay the foundation to design novel therapies for neurofibroma prevention and to target neurofibromas at early stages of development.

Task 2. To examine whether an *Nf1* heterozygous environment is essential for neurofibroma formation in the skin and spinal roots.

While Task 1 aims to understand the role of the *Nf1* homozygous cells in neurofibroma development, Task 2 is investigating the contribution of the *Nf1* heterozygous cells to neurofibroma formation. The hypothesis for this Task is whether an *Nf1* heterozygous environment is required for neurofibroma formation in the peripheral nerves, but not in the skin. This hypothesis predicts that the requirement of the *Nf1* heterozygous environment for neurofibroma formation is distinct, which depends on the sites of neurofibromas. Specifically, we hypothesize that plexiform neurofibromas arising from the peripheral nerves require the contribution of the *Nf1* heterozygous environment whereas the neurofibromas in the skin can form in the wild-type environment. The "hidden" hypothesis for this Task is that, in the $Nf1^{P0A}$KO model, the neurofibromas arising from the peripheral nerves resemble human plexiform neurofibromas that are almost exclusively identified in NF1 patients, whereas the neurofibromas in the skin are similar to dermal neurofibromas that can be found in the both NF1 patients and general populations. To examine the contribution of the *Nf1* heterozygous environment to neurofibroma development, we have constructed two *Nf1* mutant strains (Figure 7). The first strain is hereafter referred to as P0A-cre-driven *Nf1* conditional knockout 1 ($Nf1^{P0A}$CKO1) mice with the genotype of P0Acre+;$Nf1^{KO/flox}$, which genetically similar to NF1 patients, carry a germline *Nf1* mutation as well as harbor *Nf1* homozygous cells in the P0A-cre-expressing neural crest/Schwann cell lineages. The second strain with the genotype of P0Acre+;$Nf1^{flox/flox}$ harbor *Nf1* homozygous cells in the neural crest/Schwann cell lineages, but in a *Nf1* wild-type environment (referred to as $Nf1^{P0A}$CKO2).

Despite that $Nf1^{P0A}$CKO1 and $Nf1^{P0A}$CKO2 mice were morphologically indistinguishable, we found that there was significant difference in tumor penetrance throughout the peripheral nervous system (PNS) between the two age-matched mutant strains. Specifically, in sciatic nerves, approximately 65% of $Nf1^{P0A}$CKO1 mice developed full-blown neurofibromas whereas none of the $Nf1^{P0A}$CKO2 mice exhibited evidence of neurofibroma formation (Figure 8A, 8F). Similar results were also obtained in the trigeminal nerves (Figure 8B, 8F). The most severe lesions observed in the sciatic nerves and trigeminal nerves of $Nf1^{P0A}$CKO2 mice were hyperplastic

lesions with focal areas exhibiting characteristics of neurofibromas (Figure 8E, 8G). These results indicate that the *Nf1* heterozygous environment is absolutely required for neurofibroma formation in at least some of the peripheral nerves. However, *Nf1*^{P0A}CKO2 mice did develop neurofibromas in cutaneous/subcutaneous nerves, dorsal root ganglia (DRG) and spinal roots, and brachial plexus (Figure 8C to 8F). Of note, although neurofibromas were identified in the *Nf1*^{P0A}CKO2 mice, the size of these tumors was significantly smaller those observed in age-matched *Nf1*^{P0A}CKO1 nerves (Figure 8A-8F). Moreover, the neurofibroma penetrance in nerves of *Nf1*^{P0A}CKO2 mice was always lower than that in age-matched *Nf1*^{P0A}CKO1 mice. Together, these results indicate that the *Nf1* heterozygous environment is critical for neurofibroma development, albeit not absolutely required in some of peripheral nerves.

Given the high neurofibroma penetrance observed in some internal peripheral nerves of *Nf1*^{P0A}CKO2 mice (e.g. brachial plexus or DGR/spinal roots), we do not believe that neurofibromas observed in the cutaneous/subcutaneous nerves of the skin are significantly different from those arising from internal peripheral nerves in the *Nf1*^{P0A}KO mouse models. These results suggest that we need to employ a different targeting strategy to develop a mouse model for dermal neurofibromas. We are currently investigating the molecular and cellular mechanisms underlying the contribution of the *Nf1* heterozygous environment to neurofibroma development. We are preparing a manuscript on these results and expect to submit it some time this year.

Task 3. To determine the malignant transformation potential of neurofibromas in the skin and spinal roots.

The "hidden" hypothesis for Task 3 is the same as that for Task 2: **neurofibromas in the skin and peripheral nerves of *Nf1*^{P0A}KO mouse models are distinct and hence should exhibit different potentials for p53-mediated malignant transformation.** As observed in Task 2, we did not observe any difference in malignant transformation potential between neurofibromas in the different sites of peripheral nerves and skin. Thus, we disprove the "hidden" hypothesis of this proposal and we are focusing on the role of *Nf1* heterozygous environment in malignant transformation of neurofibroma in this Task. For the experiments proposed for this Task, **we**

have established the first mouse models that develop both benign and malignant peripheral nerve sheath tumors – a cardinal feature of human MPNST. We established the genetic cross between P0A-cre+;cisp53$^{KO/+}$;*Nf1*$^{flox/+}$ and *Nf1*$^{KO/flox}$ mice to generate two P0A-cre driven *Nf1*/p53 (NP) mutant mice: (1) P0A-cre+;p53$^{KO/+}$;*Nf1*$^{flox/KO}$ (NP mutants on the *Nf1* heterozygous background) and (2) P0A-cre+;p53$^{KO/+}$;*Nf1*$^{flox/flox}$ (NP mutants on the *Nf1* wild type background) along with control mice. We hereafter referred these two NP mutant mice to as NP^{P0A}CKO1 and NP^{P0A}CKO2, respectively. Furthermore, we monitored age-matched P0A-cre+;cisp53$^{KO/+}$;*Nf1*$^{flox/+}$ mice (referred to as NP^{P0A}cis) for tumor development. The genetic configurations of these three *Nf1*/p53 mutant strains are listed in Figure 9A.

Thus far, we have generated and analyzed 20 NP^{P0A}CKO1, 34 NP^{P0A}CKO2, and 34 NP^{P0A}cis mice. Similar to *Nf1*^{P0A}CKO1 and *Nf1*^{P0A}CKO2 mice, both NP^{P0A}CKO1 and NP^{P0A}CKO2 mice developed hyperplasia and neurofibromas throughout the peripheral nerves, though the severity of nerve lesions was greater in NP^{P0A}CKO1 mice (Figure 9B). These observations further confirmed that the *Nf1* heterozygous environment is critical for neurofibroma progression (see Task 2). Furthermore, NP^{P0A}cis mice exhibited no abnormalities in peripheral nerves (Figure 9B), which is consistent with our conclusion that *Nf1* heterozygous cells are not sufficient to initiate neurofibroma formation (see Task 1). Unexpectedly, however, all three *Nf1*/p53 mutant strains exhibited similar survival profiles (Figure 9C), rates of MPNST development (Figure 9D), and tumor spectrum (Figure 9E). These results suggest that none of the following factors: the *Nf1* heterozygous environment, the presence of degenerative nerves or the degree of neurofibroma burden, plays a significant role in MPNST development in mice. It appears that the only rate-limiting factor for developing MPNSTs in these three models is the loss of both *Nf1* and p53 (Figure 9A). To determine the status of *Nf1* and p53 in MPNSTs, we performed PCR analyses (Figure 9F). For comparison, we analyzed non-MPNST sarcomas identified in NP^{P0A}CKO1 and NP^{P0A}CKO2 mice. These tumors retained the wild-type *Nf1* allele (*Nf1*flox) and showed no evidence of Cre-mediated recombination on the *Nf1*flox alleles. In contrast, they exhibited loss of the wild-type p53 alleles via loss of heterozygosity (LOH, blue arrows in Figure 9F). Particularly, the sarcoma identified in a NP^{P0A}CKO1 mouse showed loss of both the wild-type p53 allele and *Nf1* KO allele, which are located on the same of chromosome indicating co-LOH of these two alleles (Figure 9A, F). This observation supports the previous finding that loss

of the entire or large segment of a chromosome is the most common mechanism leading to LOH in mice, as loss of the *Nf1* KO allele will not provide growth advantage for tumor cells. Consistently, MPNSTs identified in NP^{P0A}cis mice exhibited Cre-mediated deletion of the *Nf1*flox allele as well as loss of both *Nf1* and p53 wild-type alleles, which supports that co-LOH simultaneously inactivates both *Nf1* and p53 tumor suppressor genes in this model (Figure 9A, F). In contrast, all the MPNSTs from NP^{P0A}CKO1 and NP^{P0A}CKO2 mice exhibited Cre-mediated deletion in the *Nf1*flox alleles indicative of *Nf1* deficiency. Furthermore, most of these MPNSTs showed p53 LOH indicating loss of p53 function. However, all the MPNSTs identified in NP^{P0A}CKO1 mice retained the *Nf1* KO allele, suggesting that p53 LOH was not involved in the tightly linked *Nf1* KO allele (Figure 9A, F and G). It is worth noting that a subset of MPNSTs from 2 of 5 NP^{P0A}CKO1 and 1 of 8 NP^{P0A}CKO2 mice did not exhibit LOH at the p53 wild-type allele (Figure 9G). These MPNSTs may inactivate p53 via different mechanisms, as none of these tumors expressed p53 at mRNA or protein levels. Taken together, these results demonstrate that similar to human counterparts, NP^{P0A}CKO1 and NP^{P0A}CKO2 mice developed MPNSTs in a stepwise manner: P0A-cre-mediated recombination inactivates *Nf1* leading to benign neurofibroma formation, and subsequently p53 LOH or other mechanisms disrupts p53 functions inducing MPNST formation (Figure 9A).

The MPNSTs observed in all three *Nf1*/p53 models exhibited the morphological and immunohistchemical characteristics indistinguishable from those observed in human NF1 patients (Figure 10A-C). Drs. Eric Legius and Raf Sciot at the Catholic University of Leuven, Belgium, provided us the human MPNSTs for comparison. Furthermore, these P0A-cre driven MPNSTs expressed markers in the neural crest/Schwann cell lineages such as $p75^{NGFR}$, BLBP, S100, GFAP and Sox10 (Figure 10B). It is worth noting that the degree of the lineage marker expression varies among as well as within individual MPNSTs, indicating the heterogeneous nature of these malignant tumors. Although both mouse and human neurofibromas exhibited the traits of differentiated Schwann cells (e.g. presence of continuous basal lamina, insets, Figure 10C), MPNSTs from *Nf1*/p53 models and human NF1 patients lost the differentiated characteristics of a peripheral nerve cell and resembled more stem or progenitor cells during nerve development (Figure 10C). The stem/progenitor-like traits of MPNST cells may render these cells grow in an environment that does not depend on the presence of *Nf1* heterozygous

cells, abnormal nerves, or neurofibromas. **Finally, many NP^{P0A}CKO1 and NP^{P0A}CKO2 mice developed MPNSTs, which were often found adjacent to plexiform neurofibromas (Fig. 11) – another cardinal feature of human MPNSTs.** Together, these results suggest that *Nf1* heterozygous cells is specifically critical for neurofibroma formation, but not for neurofibroma initiation or malignant transformation. Furthermore, these observations imply that we need to design different therapeutic strategies to target different stages of MPNST. For example, the strategy aiming to target *Nf1* heterozygous environment will not be efficient of MPNSTs. These results are included in a manuscript, which is attached in the Appendix.

Key research accomplishments

1. We demonstrate that bi-allelic inactivation of *Nf1* is required for neurofibroma formation in mice. Specifically, neural crest stem cells and progenitor cells at early stages of nerve development are particularly susceptible to *Nf1*-mediated transformation.

2. We provide evidence that Remak bundles with "pocket defects" are a cell-of-origin for plexiform neurofibroma.

3. We have generated a robust mouse model for neurofibroma, which develops plexiform neurofibromas throughout the peripheral nervous system as well as discrete cutaneous neurofibromas in the skin.

4. We demonstrated that the *Nf1* heterozygous environment is critical, albeit not essential for, neurofibroma development throughout the peripheral nervous system.

5. Our data suggest that the *Nf1* heterozygous environment is not required for malignant formation of plexiform neurofibroma.

6. We develop the first mouse models that develop both benign and malignant peripheral nerve sheath tumors.

Reportable outcomes

1. Manuscripts (see appendix):

1. Zheng, H., Chang, L., Patel, N., Yang, J., Lowe, L., Burns, D.K. and **Zhu, Y.** (2008). Induction of abnormal proliferation by non-myelinating Schwann cells triggers neurofibroma formation. *Cancer Cell,* 13:117-128.

2. Joseph, N.M., Mosher, J.T., Buchstaller, J., Snider, P., McKeever, P.E., Lim, M., Conway, S.J., Parada, L.F., **Zhu, Y** and Morrison, S.J. (2008). The loss of *Nf1* transiently promotes selfrenewal but not tumorigenesis by neural crest stem cells. *Cancer Cell,* 13:129-140.

Notes: Both papers were highlighted in *Nature Reviews Cancer* and *Nature Medicine*. In addition, these two papers were also appeared in several public media including the home page of USAMRMC Neurofibromatosis Research Program, Children's Tumor Foundation, and the University of Michigan.

3. Roth, T.M., Ramamurthy, P., Muir, D., Wallace, M.R., **Zhu, Y.**, Chang, L. and Barald, K.F. (2008). Influence of hormones and hormone metabolites on the growth of Schwann Cells derived from embryonic stem cells and tumor cell lines expressing variable levels of neurofibromin. *Development Dynamics,* 237:513-524.

4. Chang, L., Zheng, H., Lee, J., Li, Y., Treisman, D.T., Akgül, S., Patel, N., Lowe L., Lucas, D.R., Sciot, R., Legius, E., Parada, L.F., Giovannini M. and **Zhu, Y**. (2011). Development of mouse models of NF1-associated progressive peripheral nerve sheath tumor with therapeutic implications. In preparation.

2. Platform presentations and abstracts:

2006

1. "Genetic analysis of peripheral nerve sheath tumor", 2006 Children's Tumor Foundation International Neurofibromatosis Consortium, Aspen, Colorado, June 4–6, 2006.
Presenter: **Yuan Zhu (PI).**

2007

1. "Identification of a susceptible cell type and three distinct stages for neurofibromatosis type 1 associated neurofibroma formation", 2007 Children's Tumor Foundation International Neurofibromatosis Consortium, Park City, Utah, June 10–12, 2007.
Presenter: **Yuan Zhu (PI).**

2. "The role of Neurofibromatosis type 1 (NF1) in Schwann cell development and tumorigenesis", 2007 Great Lakes Glia Meeting, Traverse City, MI, Sept. 29 – Oct. 1, 2007.
Presenter: **Yuan Zhu (PI).**

3. "NCI Education Day/Mouse Models Consortium", Annual Meeting of Society of Neurooncology, Grapevine, TX, November 15, 2007.
Presenter: **Yuan Zhu (PI).**

4. "Abnormal differentiation of stem/progenitor cells leads to tumor formation in peripheral nerves", Stem Cells & Aging: Balancing Regeneration and Cancer Workshop, University of Michigan Comprehensive Cancer Center, May 15, 2007.
Presenter: **Yuan Zhu (PI).**

2008

1. "A cell-of-origin for plexiform neurofibroma in mice", 2008 Children's Tumor Foundation International Neurofibromatosis Consortium, Bonita Springs, Florida, June 6 – 10, 2008.
Presenter: **Yuan Zhu (PI).**

2. "Cell migration in Development and Disease I", Session Chair, Annual Meeting, Society for

Neuroscience, Washington D.C., November 15-19, 2008.
Presenter: **Yuan Zhu (PI).**

3. "Induction of abnormal proliferation by non-myelinating Schwann cells triggers neurofibroma formation", American Association for Cancer Research Annual Meeting 2008, San Diego, California, April 12th-16th, 2008. Presenter: **Huarui Zheng (Post-doctoral fellow).**

4. "Cancer stem cells and the tumor environment in Neurofibromatosis Type I", Neuroscience 2008, the 38th annual meeting of the Society for Neuroscience, Washington, D.C., November 15th – 19th, 2008.
Presenter: **Lou Chang** (**Graduate student)**.

2009

1. Forum "Cancer Stem Cells: Advances and Challenges", Annual Meeting of the American Association for Cancer Research (AACR), Denver, CO, April 18-22, 2009.
Presenter: **Yuan Zhu (PI).**

2. "Role of Nf1 heterozygous environment in initiation, progression and transformation of plexiform neurofibroma", 2009 Children's Tumor Foundation International Neurofibromatosis Consortium, Portland, OR, June 14-16, 2009.
Presenter: **Yuan Zhu (PI).**

3. "Novel Murine Models of Malignant Peripheral Nerve Sheath Tumors ". Chang L, Zheng H, Zhu Y. 2009 Children's Tumor Foundation International Neurofibromatosis Consortium, Portland, OR, June 14-16, 2009.
Presenter: **Lou Chang** (**Graduate student)**.

4. "Novel Murine Models of Malignant Peripheral Nerve Sheath Tumors". Chang L, Zheng H, Zhu Y 2009. Poster presentation, Cell and Developmental Biology Retreat, Battle Creak, MI.
Presenter: **Lou Chang** (**Graduate student)**.

5. “Novel Murine Models of Malignant Peripheral Nerve Sheath Tumors ”. Chang L, Zheng H, Zhu Y 2009. Poster presentation, Cancer Center Fall Research Symposium, Ann Arbor, MI.
Presenter: **Lou Chang (Graduate student)**.

6. “Novel Murine Models of Malignant Peripheral Nerve Sheath Tumors ”. Chang L, Zheng H, Zhu Y 2009. Poster presentation, Cellular & Molecular Biology Annual Symposium and Poster Session, Ann Arbor, MI.
Presenter: **Lou Chang (Graduate student)**.

7. “Therapeutic intervention of preclinical symptoms in a NF1 mouse model”. Huarui Zheng, Lou Chang and Yuan Zhu. Poster presentation, 2009 Children’s Tumor Foundation International Neurofibromatosis Consortium, Portland, OR, June 14-16, 2009.
Presenter: **Huarui Zheng (Post-doctoral fellow).**

2010
1. “Tumor suppression mechanisms in neural stem cells”, House Ear Institute, Los Angeles, CA, March 22, 2010.
Presenter: **Yuan Zhu (PI).**

2 “Dissecting molecular and cellular mechanisms underlying Nf1 haploinsufficient tumor microenvironment”, 2010 Children’s Tumor Foundation International Neurofibromatosis Consortium, Baltimore, MD, June 5-8, 2010.
Presenter: **Yuan Zhu (PI).**

3. Mouse Models

We have developed a robust neurofibroma model, which should serve as a valuable tool for studying the pathogenesis of the NF1 disease and for testing novel therapies. These results were published in the February issue of Cancer Cell (See appendix). Furthermore, we have generated and characterized new models for human malignant peripheral nerve sheath tumor (MPNST).

4. Funding

1. ***National Institutes of Health (NIH)***

"The role of mTORC1 in the development and therapeutic targeting of NF1-associated benign and malignant peripheral nerve sheath tumor"

25% effort

Principal Investigator: Yuan Zhu

Role: PI

Type: R01

$1,093,750 (Direct cost)

4/1/2011 – 2/29/2016

The goals of this grant are to determine the role of mTORC1 signaling pathway in the development of benign and malignant peripheral nerve sheath tumor and to identify the therapeutic windows for rapamycin in treating NF1-related peripheral nerve sheath tumors.

Notes: The preliminary data for this NIH R01 grant were mostly obtained from the proposed work in this DOD.

2. ***National Institutes of Health (NIH)***

"Tumor suppression mechanisms in the peripheral nervous system"

25% effort

Principal Investigator: Yuan Zhu

Role: PI

Type: R01

$1,125,000 (Direct cost)

12/1/2011 – 11/30/2016

The major goal in this project is to understand cellular and molecular pathogenesis of MPNST initiation and progression. These studies may lay the foundation for designing novel strategies to improve early diagnosis and to effectively treat NF1-associated MPNSTs. Moreover, as mutations in NF1 (or deregulation of Ras), p53 and INK4a/ARF tumor suppressors are frequently found in common solid tumors in humans, our studies may have broad implications for the understanding of the pathogenesis of human cancers.

Status: A0 submission (Score: 27 and Percentile: 15.0)

A1 submission: (Score: 28 and Percentile: 13.0)

3. Dr. Huarui Zheng received a prestigious “Young Investigator Award” from Children’s Tumor Foundation (2007 to 2009).

Conclusion

We have made substantial progress in the past 5 years of the funding period. For Task 1, we demonstrated that bi-allelic inactivation of *Nf1* in neural crest stem cells is required for neurofibroma formation. These studies resulted in publication of 3 manuscripts (see appendices). For Task 2, we have determined that the *Nf1* heterozygous environment is critical, albeit not essential for, neurofibroma development throughout the peripheral nervous system. For Task 3, we demonstrate that the *Nf1* heterozygous environment is not required for malignant transformation and developed two robust models for human MPNST. We are currently preparing a manuscript for publishing these results (see Appendix).

Notes

Detailed methodologies for the experiments can be found in the "Supplemental Materials" of Zheng et al. Cancer Cell paper attached in the Appendix.

Figure 1

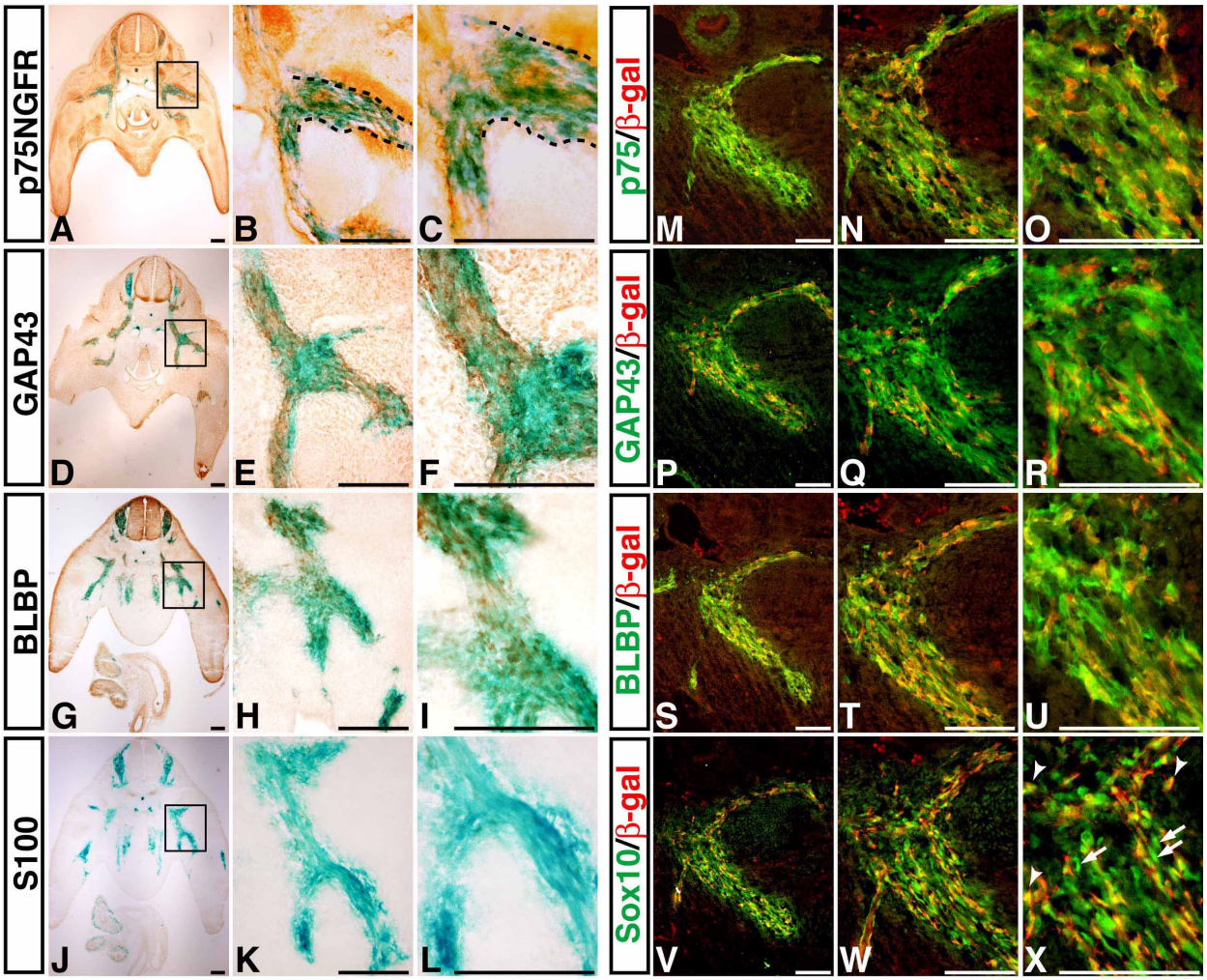

Figure 1. P0A-cre mediated recombination in NCSCs.
Transverse sections from the lumbar region of X-gal stained E12.5 P0A-cre/R26R-LacZ double transgenic embryos were stained with anti-$p75^{NGFR}$ (A-C), GAP43 (D-F), BLBP (G-I), and S100 (J-L) antibodies. The dashed lines (B, C) mark the $p75^{NGFR}$ and b-gal double positive developing peripheral nerves. The expression of the neural crest/Schwann cell lineage markers $p75^{NGFR}$ (M-O), GAP43 (P-R), BLBP (S-U), or Sox10 (V-X) in b-gal positive cells was further confirmed by double immuofluorescence. Nearly all the b-gal positive cells express these lineage markers whereas only a subset of the NCSCs are positive for b-gal. For example, arrowheads and arrows in X point to Sox10/b-gal double positive cells and Sox10-positive/b-gal-negative cells, respectively. Scale bar: (A-L), 50 mm ; (M-X), 25 mm.

Figure 2

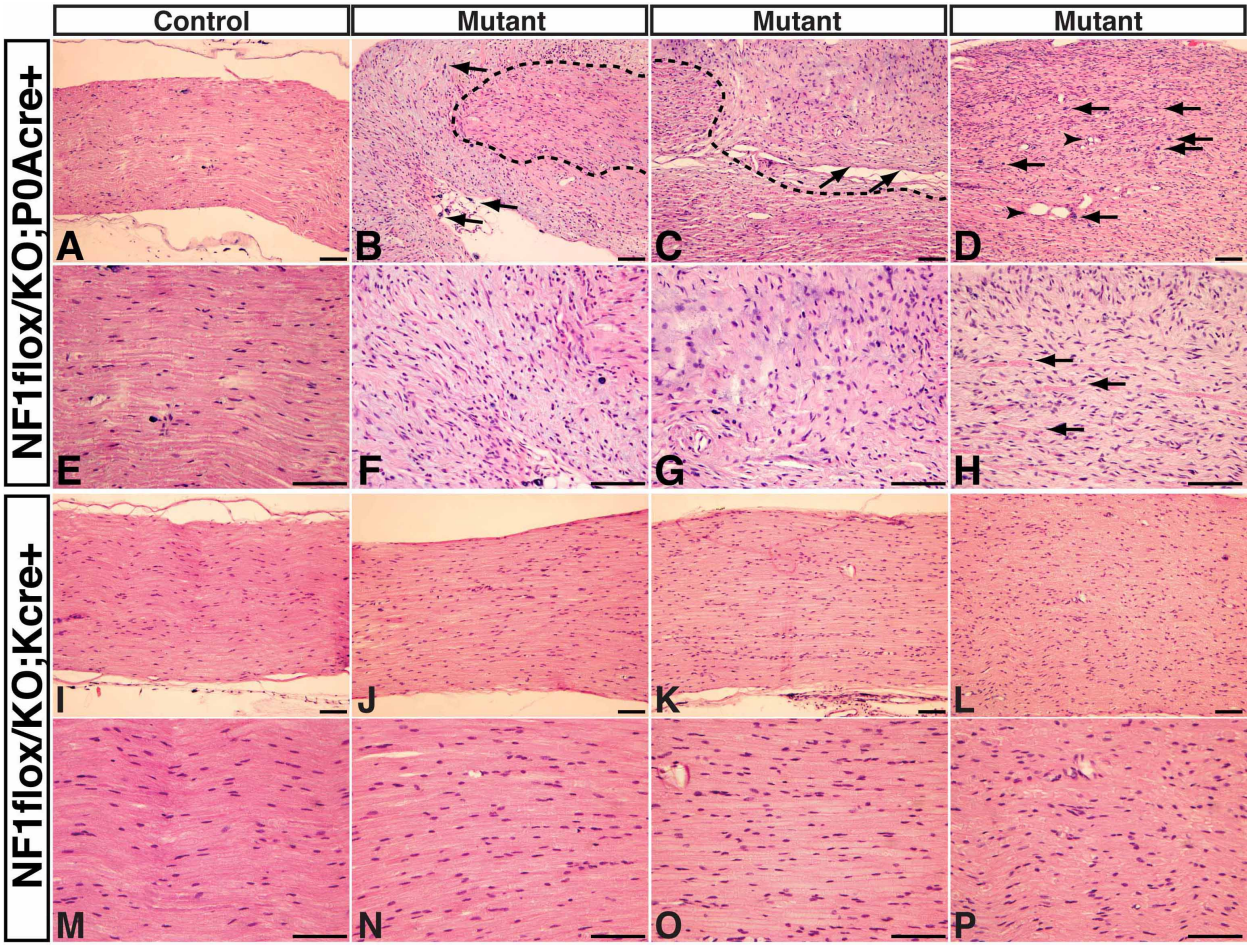

Figure 2. Histological analysis of control and mutant sciatic nerves.
Sciatic nerves from control (A, E) and three $Nf1^{P0A}KO$ mutant mice (B and F, C and G, D and H) were sectioned and stained with hematoxylin and eosin (H&E). The dashed lines (B, C) mark the border of neurofibromas (arrows, C) and hyperplasia in mutant nerves. Arrows in B, D point to infiltrating mast cells and arrowheads (D) point to blood vessels. Sections from sciatic nerves of control (I, M) and three $Nf1^{krox20}KO$ mutant (J and N, K and O, L and P) mice were stained with H&E. These mutant mice only developed varying degrees of hyperplasia in sciatic nerves. The histopathological distinctions between hyperplasia and neurofibroma used in this study was based upon the degree of derangement of the nerve architecture, namely the presence or absence of well-organized myelinated fibers within the proliferation in hyperplasia and neurofibroma. Scale bar: 100 μm.

Figure 3

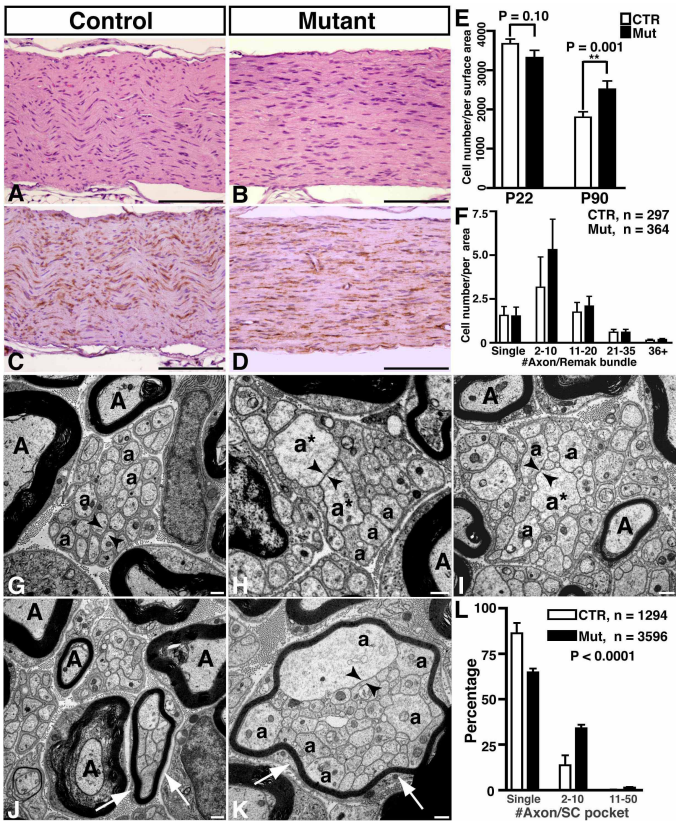

Figure 3. Abnormal Remak bundles in NF1 mutant sciatic nerves.
Sections of sciatic nerves from P22 control and $NF1^{P0A}KO$ mutant mice were stained with H&E (A, B) and anti-$p75^{NGFR}$ antibody (C, D). (E) Quantification of the number of cells per surface area (mm^2) in P22 and P90 control and mutant sciatic nerves. For P22 analysis, 8 control and 3 mutant mice were used; and for P90 analysis, 3 control and 7 mutant mice were used. Cell density for the P22 and P90 is plotted as mean ± SEM. (F) The numbers of Remak bundles per surface area (1,000 mm^2) in control and mutant P22 sciatic nerves were categorized into five groups based upon the number of axons that they ensheathed. N values represent Remak bundles quantified for each genotype. Sciatic nerves from 2 control and 4 mutant P22 mice were used for this analysis. No significant difference was found between control and mutant distributions. Transmission electron microscopy (TEM) analysis of Remak bundles in sciatic nerves of P22 control (G, J) and mutant (H, I, K) mice show abnormal axonal segregation in the mutant mice. Arrowheads in G indicate Schwann cell cytoplasm between different axons, which isolates each individual axon into a dedicated Schwann cell pocket in the Remak bundle. Mutant Remak bundles contain unsegregated axons, which remain directly apposed to each other (arrowheads, H, I, K). (J, K) The number of myelinated Schwann cells ensheathing multiple axons (arrows) is significantly increased in mutants compared to controls ($P = 0.0036$). (L) The percentage distribution of axons per Schwann cell pocket in control and mutant nerves. N values indicate the number of Schwann cell pockets counted for each genotype. The majority of axons in control nerves were segregated into individual pockets, while the number of axons properly segregated was dramatically reduced in mutant nerves (Chi-squared goodness-of-fit test, $P < 0.0001$). "A", myelinated axons; "a", unmyelinated axons; and "a*", dilated axons. Scale bar: (A-D), 100 mm; (G-K), 1 mm.

Figure 4

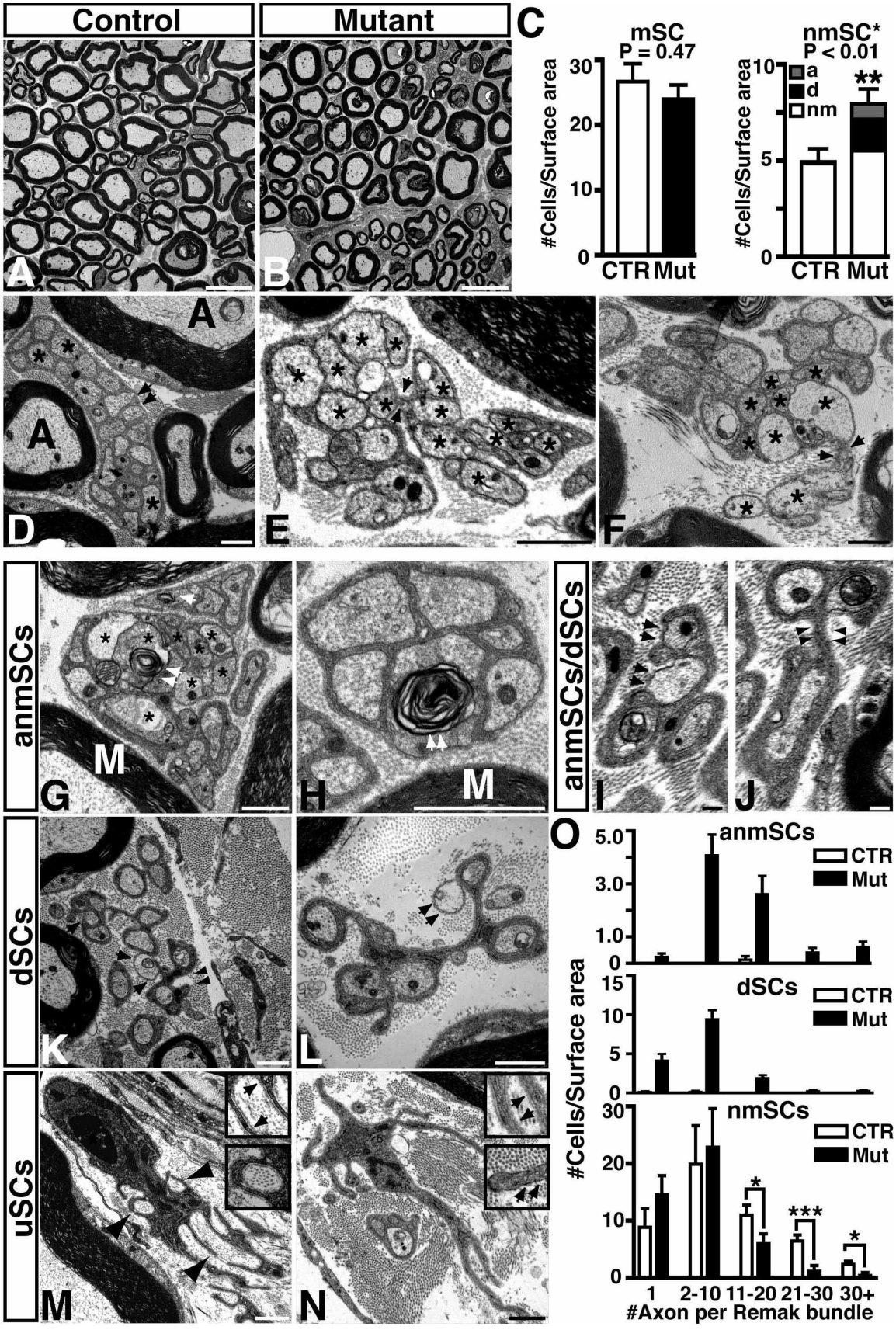
Control
Mutant
A
B
C
mSC
P = 0.47
#Cells/Surface area
30
20
10
0
CTR Mut
nmSC*
P < 0.01
a
d
nm
**
10
5
0
CTR Mut
D
E
F
anmSCs
G
M
H
M
anmSCs/dSCs
I
J
dSCs
K
L
uSCs
M
N
O
anmSCs
5.0
3.0
1.0
0
CTR
Mut
dSCs
15
10
5
0
nmSCs
30
20
10
0
*
***
*
#Cells/Surface area
1
2-10
11-20
21-30
30+
#Axon per Remak bundle

Figure 4. Degeneration of NF1 mutant Remak bundles at P90.
Electron micrographs show cross sections of P90 control (A, D) and mutant (B, E, F) sciatic nerves. (C) The number of myelinating (mSC) and non-myelinating (nmSC) Schwann cells in P90 control and mutant sciatic nerves was presented by the cell number per surface area (mean ± SEM). The identity of mSCs and nmSCs was determined by its distinct morphology on EM images. No difference was observed in the mSC lineage whereas a significant increase was identified in the nmSC lineage in P90 mutant nerves. "a" stands for abnormal nmSCs, "d" stands for dissociating SCs, and "nm" stands for normal nmSCs. Arrows in D point to a typical Remak bundle in control nerves containing multiple unmyelinated axons (a). E and F show two examples of abnormally differentiated Remak bundles with "broken pockets" that have dissociating axons. Arrows in E and F point to unsegregated axons (*) dissociating from each other. G and H show two representative anmSCs containing "naked" axons and myelin-like fragments, possibly representing membranous remnants of degenerating cells (arrows). M, normal myelin. I and J show the morphological similarity between a pair of anmSC and dSC. Arrows in I point to "naked" axons in an anmSC, whose degeneration likely generates free Schwann cell processes seen in a dSC (arrowheads, J). (K, L) Two examples of dSCs with free Schwann cell processes (arrowheads, K) and degenerating unmyelinated axons (arrows). (M, N) Two examples of unassociated Schwann cells (uSCs) with continuous basal lamina and no axon contact. Arrowheads in M point to collagen fibers ensheathed by uSCs, which were also shown in Insets (M) with higher magnification. Arrows in the Insets of M and N (top) point to continuous basal lamina in uSCs as compared to a fibroblast process (arrows, bottom Inset in N). (O) The numbers of Remak bundles per surface area (1,000 mm^2) in control and mutant sciatic nerves were categorized into five groups based upon the number of axons that they ensheathed. Top panel: abnormal non-myelinating Schwann cells (anmSCs); Middle panel: dissociating Schwann cells (dSCs); Bottom panel: normal non-myelinating Schwann cells (nmSCs). * and *** denote $P < 0.05$ and $P < 0.001$, respectively. Specific loss of the normal Remak bundles ensheathing >10 axons was found in mutant nerves. Scale bar: 1 mm.

Figure 5

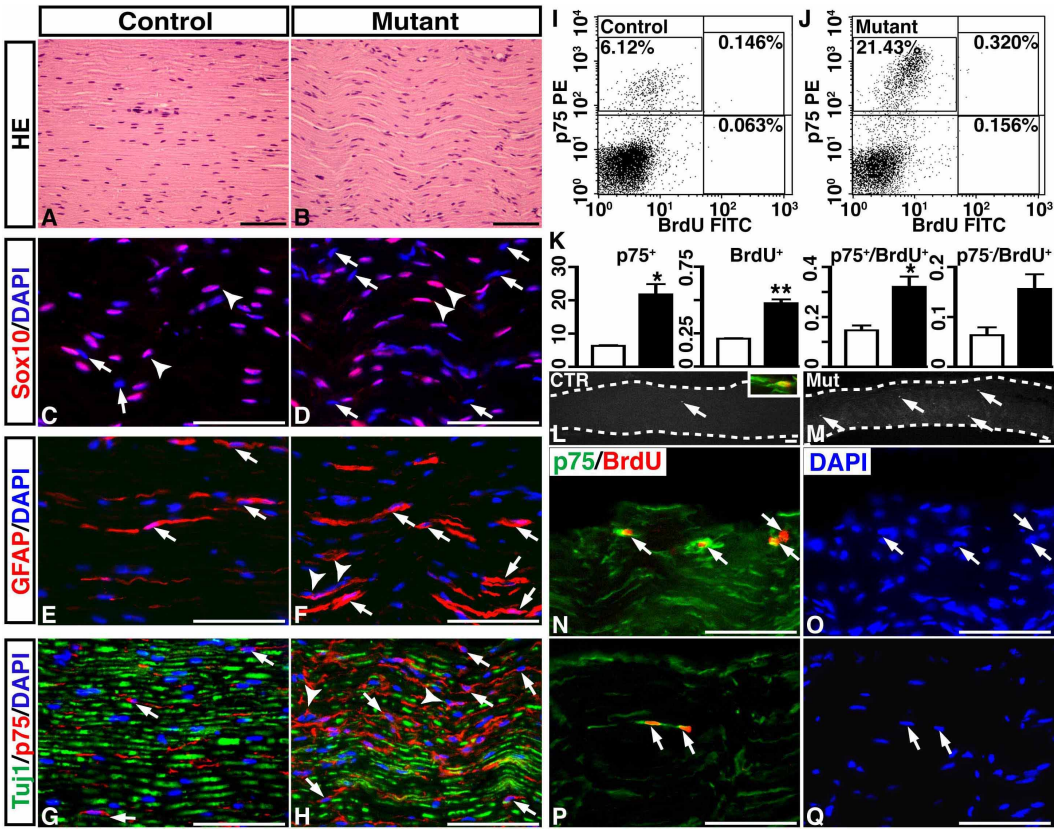

Figure 5. The expanded cellular populations in P90 mutant nerves express lineage markers similar to those by non-myelinating Schwann cells.

Sections from sciatic nerves of P90 control and mutant mice were stained with H&E (A, B), Sox10/DAPI (DAPI stains for cell nuclei) (C, D), GFAP/DAPI (E, F), and Tuj1/p75/DAPI (G, H). Arrows and arrowheads in C and D point to Sox10-negative and Sox10-positive cells, respectively. The number of GFAP-positive and $p75^{NGFR}$-positive cells was conspicuously increased in mutant nerves (arrows, F, H) compared to controls (arrows, E, G). Arrowheads in F and H point to a cluster of GFAP-positive and $p75^{NGFR}$-positive nuclei in mutant nerves, which were never seen in controls. Although some axons express $p75^{NGFR}$, on 5 m paraffin sections, most of $p75^{NGFR}$ expression was found in non-myelinating Schwann cells, as it has almost no overlapping expression with an axonal marker, Tuj1 (G, H and Suppl. Fig. 12). Representative flow-cytometry plots demonstrate approximately a 2.5 fold increase in frequency of $p75^{NGFR}$-positive cells in mutant nerves (21.75%, J) compared to that in control (6.27%, I), and a 1.3 fold increase in frequency of BrdU-positive cells in mutant (0.476%, J) nerves compared to controls (0.209%, I) nerves. Data in K represent mean ± SEM from two independent experiments using age-matched control (n = 2) and mutant (n = 4) mice. * $P < 0.05$, **$P < 0.01$. Statistical significance is indicated by * or **. Sections from sciatic nerves of BrdU-treated control (L) and mutant (M) mice were stained with anti-BrdU. The number of BrdU-positive cells is significantly more in mutant nerves (arrows, M) than that in controls (arrow, L). The inset in L shows a $p75^{NGFR}$/BrdU double positive cell in a control nerve. (N, O and P, Q) Two representative mutant nerves showing a cluster of $p75^{NGFR}$/BrdU double positive cells (arrows). Scale bar: 50 mm.

Figure 6

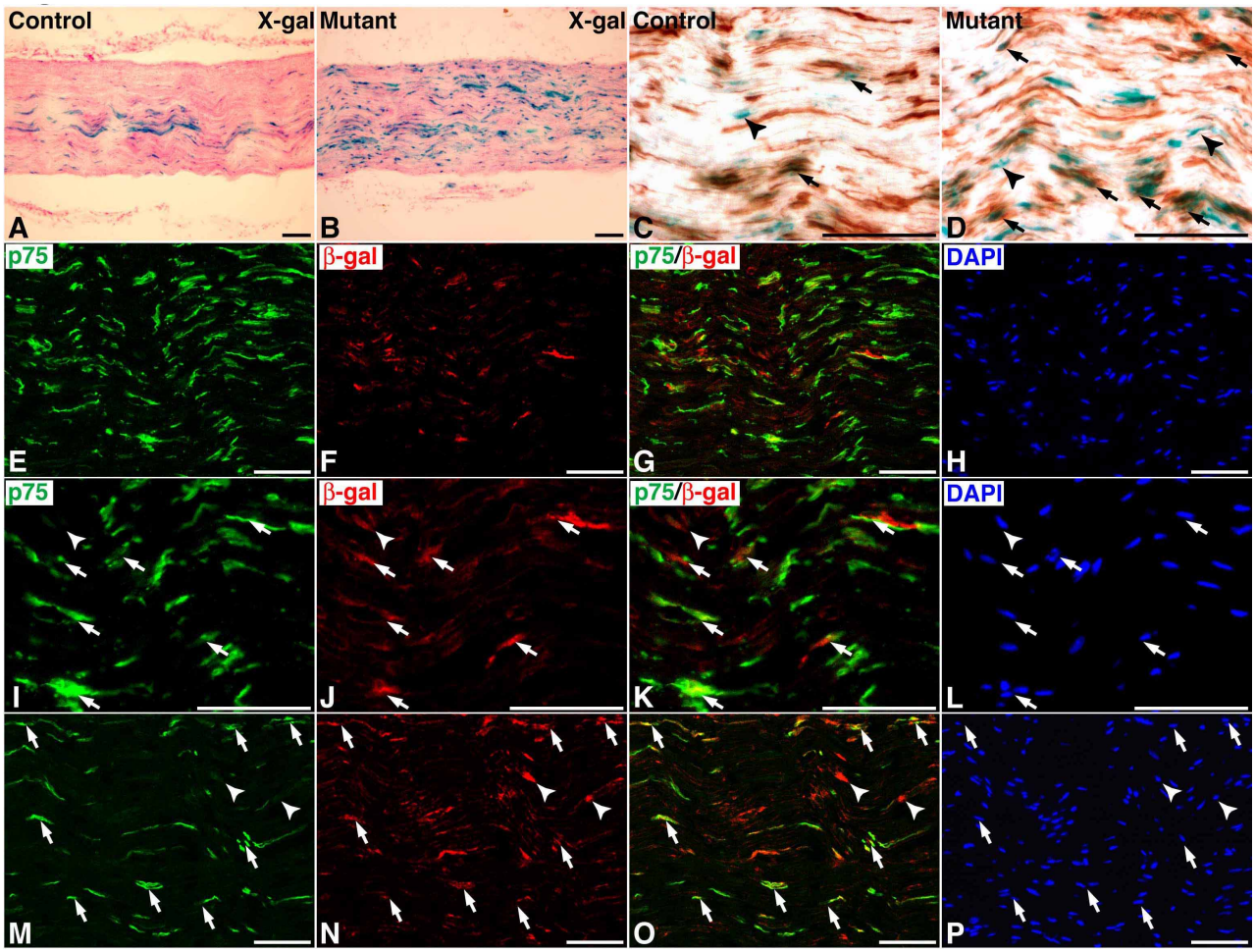

Figure 6. The expanded NF1 deficient cells in P90 mutant nerves express $p75^{NGFR}$ and GFAP. The R26R-LacZ allele was introduced to the control and $NF1^{P0A}$KO mutant mice. Sciatic nerves from P90 mice were sectioned and stained with X-gal (A, B) and X-gal/anti-$p75^{NGFR}$ antibody (C, D). Sections from mutant nerves were triple-labeled by anti-$p75^{NGFR}$ (E, I), anti-b-gal (F, J) and DAPI (H, L). Overlay images are shown in G and K. Arrows and an arrowhead in the panels I to L point to $p75^{NGFR}$/b-gal double positive cells and a $p75^{NGFR}$-/b-gal+ single positive cell, respectively . Sections from mutant nerves were triple-labeled by anti-GFAP (M), anti-b-gal (N) and DAPI (P). Overlay images are shown in panel O. Arrows in panels M to P point to GFAP/b-gal double positive cells and arrowheads in the same panels show a small number of b-gal positive cells that do not express GFAP. Scale bar: 50 mm.

Figure 7

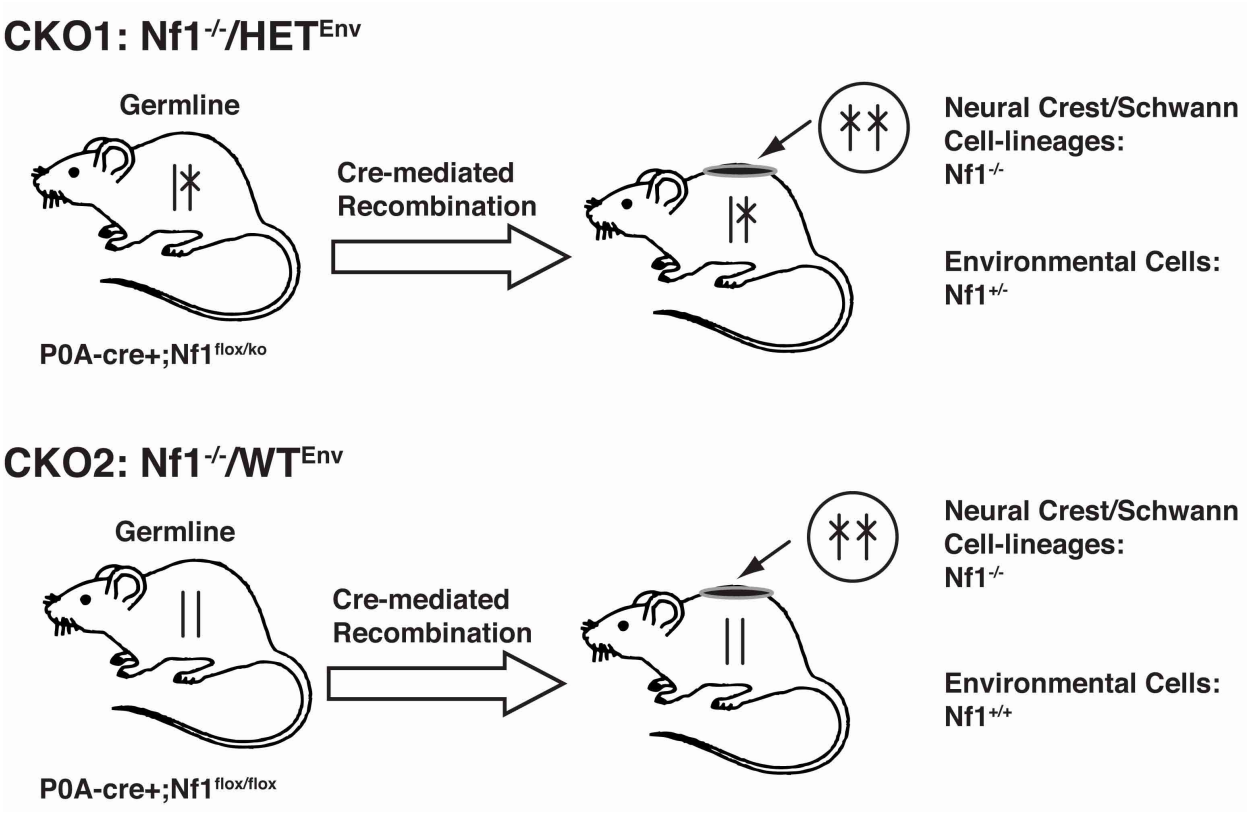

Figure 7. Experimental Strategy.
Two mouse models were generated in order to compare the effect of an *Nf1* heterozygous environment in neurofibroma formation. *Nf1*^{P0A}CKO1 mice, also designated *Nf1*$^{-/-}$/HET^{Env}, have the genotype of P0A-cre+;*Nf1*$^{flox/ko}$. The *Nf1*^{P0A}CKO1 mice undergo P0A-cre-mediated recombination, leading to *Nf1* inactivation in the neural crest/Schwann cell-lineages and *Nf1* heterozygous cells in the environment. *Nf1*^{P0A}CKO2 mice, also designated *Nf1*$^{-/-}$/WT^{Env}, have the genotype of P0A-cre+;*Nf1*$^{flox/flox}$, which undergo P0A-cre-mediated *Nf1* deletion in the neural crest/Schwann cell-lineages in the wild-type environment. These two mouse models directly allow the comparison of the role of the *Nf1* heterozygosity in neurofibroma formation.

Figure 8

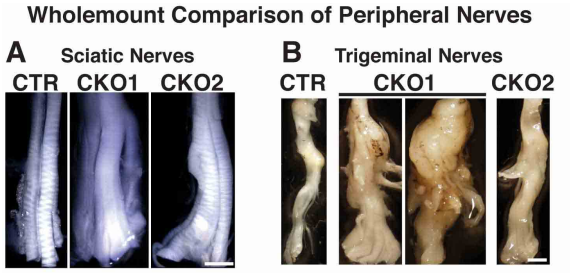

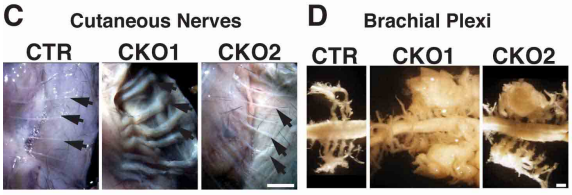

F Summary of Neurofibroma penetrance by site

Site	CKO1	CKO2	P-value
Sciatic	65% (n=20)	0% (n=13)	0.0002
Trigeminal	36% (n=14)	0% (n=12)	0.0425
Cutaneous	100% (n=20)	54% (n=13)	0.0015
CDRG*	73% (n=12)	35% (n=10)	0.027
TDRG*	58% (n=12)	31% (n=9)	0.086
LDRG*	36% (n=12)	23% (n=10)	0.472
Brachial Plexus	92% (n=13)	70% (n=10)	0.2806

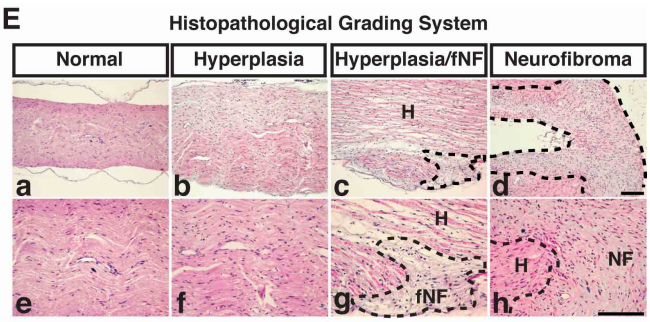

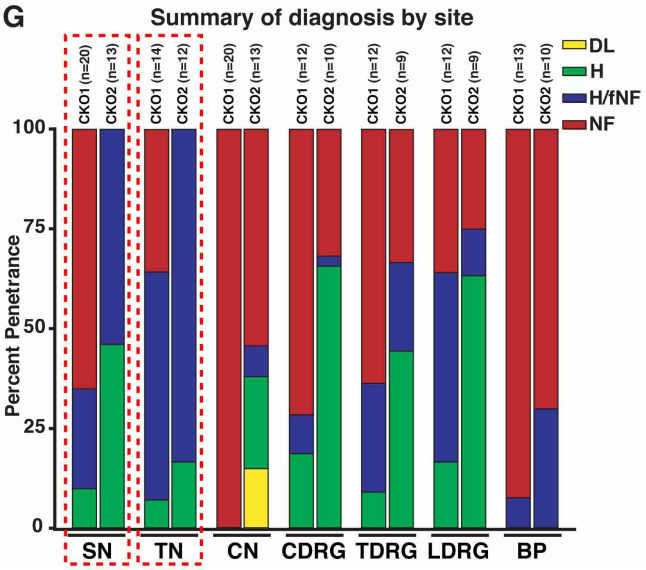

Figure 8. *Nf1* heterozygosity in the environment promotes neurofibroma development.
Representative whole-mount comparison of sciatic nerves (A), trigeminal nerves (B), cutaneous/subcutaneous nerves (C), and brachial plexus (D) from control, *Nf1*^{P0A}CKO1 and *Nf1*^{P0A}CKO2 mice demonstrate that the enlarged nerve size of mutant mice is sensitive to genotype of environmental cells. Despite both enlarged compared to controls, *Nf1*^{P0A}CKO1 nerves are markedly larger in size than those from age-matched *Nf1*^{P0A}CKO2 mice. The largest *Nf1*^{P0A}CKO1 trigeminal nerves (B, right panel) is also presented to demonstrate the range of trigeminal nerve sizes, while *Nf1*^{P0A}CKO2 trigeminal nerves have lower variation. (E) Based upon previously established histological grading criteria, each nerve was diagnosed into one of four categories based primarily on H&E staining. Normal nerves (a, e) have low cellularity and well organized. Hyperplastic nerves (b, f) exhibit higher cellularity, often accompanied by increased blood vessels and mast cells. Hyperplastic nerves with focal neurofibroma (c, g) resemble hyperplastic nerves (H), however, contain focal areas of tumor appearance (fNF). Finally, frank neurofibromas (d, h; NF region) resemble human neurofibromas with high levels of collagen deposition, disruption of the Schwann cell orientation and greatly increased cellularity (compare H with NF). (F) From these histological criteria, the penetrance of neurofibroma (I) was determined for seven sites: sciatic nerves, cutaneous/subcuteneous nerves, trigeminal nerves, brachial plexi, cervical dorsal root ganglia (C-DRG), thoracic DRG (T-DRG) and lumbar DRG (L-DRG). For sciatic nerve, cutaneous/subcutaneous nerves, trigeminal nerves and brachial plexi, one nerve examined for each mouse. For DRGs, from 1-6 DRGs were examined for each site in each mouse, and used to generate an average penetrance of all DRG per mouse. Specifically, 46 C-DRG from 12 *Nf1*^{P0A}CKO1, 45 C-DRG from 10 *Nf1*^{P0A}CKO2; 23 T-DRG from 12 *Nf1*^{P0A}CKO1, 16 T-DRG from 9 *Nf1*^{P0A}CKO2; 29 L-DRG from 12 *Nf1*^{P0A}CKO1 and 20 L-DRG from *Nf1*^{P0A}CKO2 mice were analyzed. A Z-test was used to determine whether a difference in neurofibroma penetrance exists based on the environmental genotype for sciatic nerves, cutaneous/subcutaneous nerves, trigeminal nerves and brachial plexus. Linear mixed modeling was used to determine whether the penetrance in DRGs was different based on *Nf1* heterozygosity in the environment. (G) The summary of the diagnostics for all nerves examined, based on genotype, is presented. Frank neurofibromas (NF) are labeled by red, hyperplasia (H) by green, focal neurofibroma (H/fNF) by blue, and non-neurofibroma, degenerative lesions (DF) by yellow. Bars representing *Nf1*^{P0A}CKO1 are on the left while *Nf1*^{P0A}CKO2 are on the right. A pattern emerges across the board, where the *Nf1* heterozygosity in the environment enhances the neurofibroma phenotypes of *Nf1* deficiency in the neural crest/Schwann cell lineages. Scale bars: (A-D) 1 mm. (E) 50 μm.

Figure 9

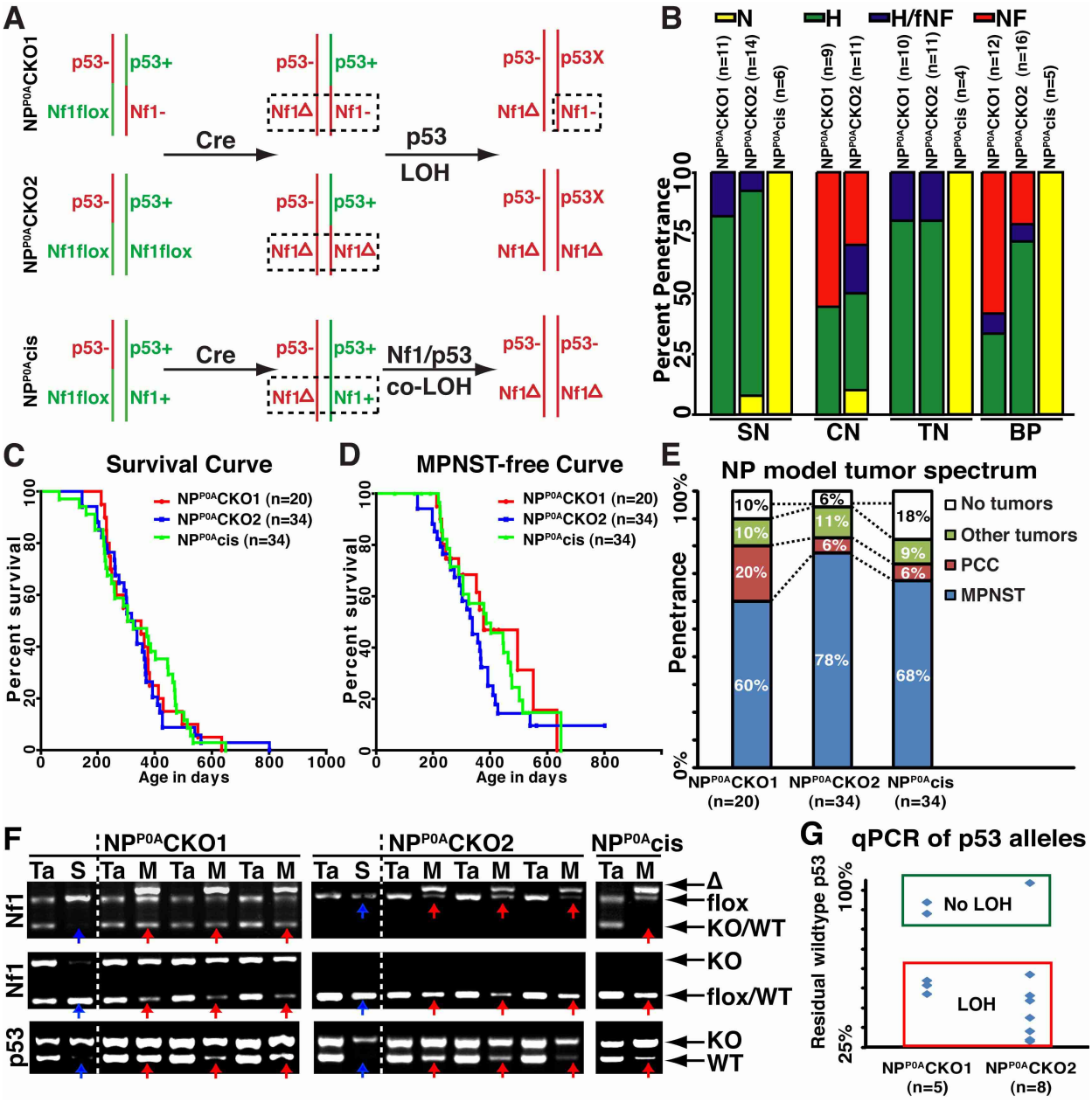
A
NP^P0ACKO1
p53-
p53+
Nf1flox
Nf1-
Cre
Nf1Δ
p53
LOH
p53X
NP^P0ACKO2
NP^P0Acis
Nf1/p53
co-LOH
Nf1+
B
N
H
H/fNF
NF
Percent Penetrance
SN
CN
TN
BP
C
Survival Curve
Percent survival
Age in days
D
MPNST-free Curve
E
NP model tumor spectrum
Penetrance
No tumors
Other tumors
PCC
MPNST
F
Ta
S
M
Nf1
p53
Δ
flox
KO/WT
KO
flox/WT
WT
G
qPCR of p53 alleles
Residual wildtype p53
No LOH
LOH

Figure 9. Progressive mouse models of neurofibroma and MPNSTs.
(A) Schematic of the genetic configurations of NP^{P0A}CKO1 , NP^{P0A}CKO2 and NP^{P0A}cis mice. The green color is used to label functional alleles, including the wild-type allele (+) and the floxed allele (x1); the red color is used to label non-functional alleles, including the recombined floxed allele (Δ) and the knockout allele (−). Both NP^{P0A}CKO configurations generate *Nf1* homozygous cells in the same cell lineages upon Cre-mediated recombination. However, the unrecombined cells in NP^{P0A}CKO1 are Nf1 heterozygous while the unrecombined cells in NP^{P0A}CKO2 are *Nf1* wild-type. NP^{P0A}CKO mice require an LOH event at the p53 locus after Cre-mediated Nf1 deletion, while the NP^{P0A}cis mice require a co-LOH event after recombination, to generate a cell deficient for both *Nf1* and p53 activity. (B) Nerves from NP^{P0A}CKO1 and NP^{P0A}CKO2 mice develop benign peripheral nerve sheath tumors, but with greater severity when the environment is heterozygous. No abnormalities were detected in NP^{P0A}cis nerves. (C) The survival curve and (D) MPNST-free curve for NP^{P0A}CKO1, NP^{P0A}CKO2 and NP^{P0A}cis mice were nearly identical, with the majority of the mice euthanized due to presence of body tumor or abdominal mass. The rates at which our three mouse models developed MPNSTs were indistinguishable ($p > 0.5$). (E) The tumor spectrum of NP^{P0A}CKO1 (n=18 tumors), NP^{P0A}CKO2 (n=34 tumors) and NP^{P0A}cis (n=34) mice are relatively similar, with MPNSTs the predominant tumors generated (60%, 78% and 68%, respectively). Malignant pheochromocytoma accounted for 20% of tumors in NP^{P0A}CKO1 mice, and only 6% in both NP^{P0A}CKO2 and NP^{P0A}cis mice. In some instances (10%, 11% or 18% for NP^{P0A}CKO1, NP^{P0A}CKO2 and NP^{P0A}cis respectively), tumors that arose from tissue that had not undergone Cre-mediated recombination. (F) PCR analysis of MPNST tissues confirms our schematic model of MPNST generation in these mice. All MPNSTs from these mice demonstrate recombination of the *Nf1* allele, and commonly demonstrate LOH of the p53 allele. However, there is significant contamination with unrecombined tissue, resulting in a fainter band, as opposed to complete absence of band. (G) Scatter plot of residual wild-type p53 allele, as measured by qPCR of genomic DNAs with primers against exons 6 and 7 of p53.

Figure 10

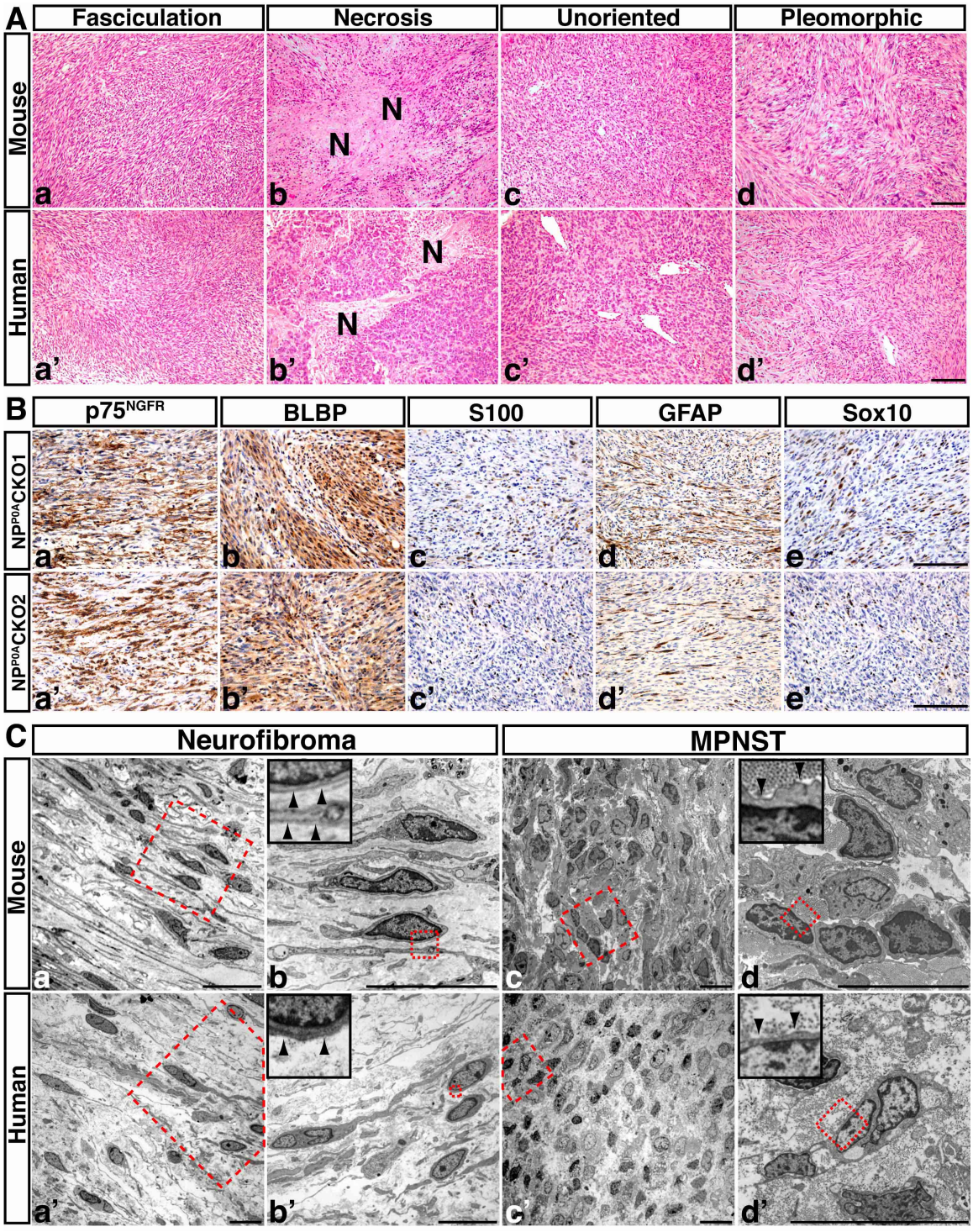
A
Fasciculation
Necrosis
Unoriented
Pleomorphic
Mouse
Human
N
N
N
N
a
b
c
d
a'
b'
c'
d'
B
p75NGFR
BLBP
S100
GFAP
Sox10
NP P0ACKO1
NP P0ACKO2
a
b
c
d
e
a'
b'
c'
d'
e'
C
Neurofibroma
MPNST
Mouse
Human
a
b
c
d
a'
b'
c'
d'

Figure 10. Mouse model recapitulates human peripheral nerve sheath features and MPNSTs display immature neural crest features.
(A) Tumors collected from $NP^{P0A}CKO1$ and $NP^{P0A}CKO2$ mice recapitulate common histopathological features of human MPNSTs. Commonly found features in mice are malignant spindle cells arranged in intertwining fascicles, with ill-defined cytoplasms and a high mitotic rate (a, a'). Occasionally, geographic necrosis can be found, sometimes accompanied by peripheral palisading malignant spindle cells (b, b'). Another manifestation of MPNSTs seen is unoriented malignant cells dispersed in sheets (c, c'). In some tumors, nuclear pleomorphism can be found, with marked variation in size and shape of cells (d, d'). (B) MPNSTs collected from these mouse models often express $p75^{NGFR}$ (a, a') and BLBP (b, b') throughout the tumor tissues. Less frequently, MPNSTs express S100 (c, c'), GFAP (d, d'), and/or Sox10 (e, e') in approximately 50% of tumors analyzed, without correlations in expression patterns. While immunohistological markers varied highly between MPNSTs, staining patterns were indistinguishable between the $NP^{P0A}CKO$ mice. (C) Ultrastructural analysis of murine benign (a, b) and malignant (c, d) peripheral nerve sheath tumors reveal a high degree of similarity with their human counterparts (a'-d'). Benign tumor cells retain differentiated phenotype: continuous basal lamina (inset, arrows), extended Schwann cell processes, sheet-like organization, low rates of proliferation. MPNST have immature and tumor phenotypes: loss of basal lamina (inset, arrows), prominent nuclei, ovoid shape, crowded and highly proliferative. Scale bars: (A, B) 50 μm, (C) 10 μm.

Figure 11

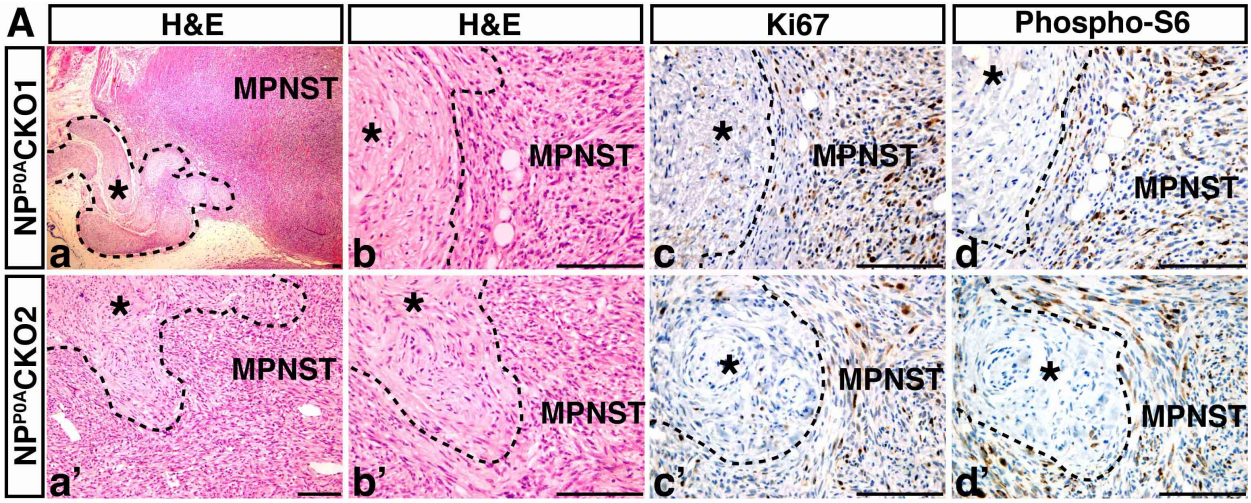

Figure 11. NP^{P0A}CKO mice developed MPNSTs adjacent to plexiform neurofibromas.
(A) In some tumor samples, regions containing neurofibromas (* inside dashed lines) juxtaposed to MPNSTs can be identified **(a and b; a' and b')**. The regions containing neurofibromas and MPNSTs show marked difference in proliferation marked by Ki67 **(c, c')**, and mTOR activity marked by phosphorylated S6 **(d, d')**. Scale bar: 50 μm.

Appendices and supporting data

Manuscripts:

1. Zheng, H., Chang, L., Patel, N., Yang, J., Lowe, L., Burns, D.K. and **Zhu, Y.** (2008). Induction of abnormal proliferation by non-myelinating Schwann cells triggers neurofibroma formation. *Cancer Cell,* 13:117-128 (including supplemental materials).

2. Joseph, N.M., Mosher, J.T., Buchstaller, J., Snider, P., McKeever, P.E., Lim, M., Conway, S.J., Parada, L.F., **Zhu, Y** and Morrison, S.J. (2008). The loss of *Nf1* transiently promotes selfrenewal but not tumorigenesis by neural crest stem cells. *Cancer Cell,* 13:129-140.

3. Roth, T.M., Ramamurthy, P., Muir, D., Wallace, M.R., **Zhu, Y.**, Chang, L. and Barald, K.F. (2008). Influence of hormones and hormone metabolites on the growth of Schwann Cells derived from embryonic stem cells and tumor cell lines expressing variable levels of neurofibromin. *Development Dynamics,* 237:513-524.

4. Chang, L., Zheng, H., Lee, J., Li, Y., Treisman, D.T., Akgül, S., Patel, N., Lowe L., Lucas, D.R., Sciot, R., Legius, E., Parada, L.F., Giovannini M. and **Zhu, Y**. (2011). Development of mouse models of NF1-associated progressive peripheral nerve sheath tumor with therapeutic implications. In preparation.

Cancer Cell
Article

Induction of Abnormal Proliferation by Nonmyelinating Schwann Cells Triggers Neurofibroma Formation

Huarui Zheng,[1,5] Lou Chang,[1,5] Neha Patel,[1,2] Jiong Yang,[1] Lori Lowe,[3] Dennis K. Burns,[4] and Yuan Zhu[1,*]
[1]Division of Molecular Medicine and Genetics, Departments of Internal Medicine and Cell and Developmental Biology
[2]Department of Pediatrics and Communicable Diseases
[3]Departments of Dermatology and Pathology
University of Michigan Medical School, Ann Arbor, MI 48109, USA
[4]Department of Pathology, University of Texas Southwestern Medical Center, Dallas, TX 75390, USA
[5]These authors contributed equally to this work.
*Correspondence: yuanzhu@umich.edu
DOI 10.1016/j.ccr.2008.01.002

SUMMARY

Recent evidence suggests that alterations in the self-renewal program of stem/progenitor cells can cause tumorigenesis. By utilizing genetically engineered mouse models of neurofibromatosis type 1 (NF1), we demonstrated that plexiform neurofibroma, the only benign peripheral nerve sheath tumor with potential for malignant transformation, results from *Nf1* deficiency in fetal stem/progenitor cells of peripheral nerves. Surprisingly, this did not cause hyperproliferation or tumorigenesis in early postnatal period. Instead, peripheral nerve development appeared largely normal in the absence of *Nf1* except for abnormal Remak bundles, the nonmyelinated axon-Schwann cell unit, identified in postnatal mutant nerves. Subsequent degeneration of abnormal Remak bundles was accompanied by initial expansion of nonmyelinating Schwann cells. We suggest abnormally differentiated Remak bundles as a cell of origin for plexiform neurofibroma.

INTRODUCTION

The hallmark feature of neurofibromatosis type 1 (NF1) is the development of benign peripheral nerve sheath tumor, termed neurofibroma (Cichowski and Jacks, 2001; Riccardi, 1992; Zhu and Parada, 2002). NF1 is a common inherited neurological disease, affecting 1 in 3500 newborns worldwide. Individuals afflicted with NF1 are predisposed to a wide spectrum of derangements, including tumors in the peripheral and central nervous system (PNS and CNS), myeloid leukemia, hyperpigmentation defects of the skin, bone abnormalities, and learning disabilities. The *NF1* gene encodes a protein product (neurofibromin) composed of 2818 amino acids, which is highly conserved during evolution. Neurofibromin is a functional Ras *G*TPase-*a*ctivating *p*rotein (RasGAP) that negatively regulates Ras signaling by accelerating conversion of activated Ras-GTP to inactive Ras-GDP (Ballester et al., 1990; Xu et al., 1990).

Plexiform neurofibroma is the only neurofibroma subtype that has the potential to undergo malignant transformation and progress to malignant peripheral nerve sheath tumors (MPNSTs). MPNST is the most common malignancy associated with NF1 and is responsible for the majority of mortality observed in human NF1 patients (Korf, 1999; Woodruff, 1999). Microscopically, neurofibromas are heterogeneous proliferations composed of a mixture of cells found in normal peripheral nerves, including Schwann cells, fibroblasts, perineurial-like fibroblasts, axons, and mast cells. Recent studies from human tumors (Rutkowski et al., 2000; Serra et al., 2000; Sheela et al., 1990) and mouse models (Zhu et al., 2002) have established the Schwann cell lineage as the true neoplastic element in

SIGNIFICANCE

Identification of cancer stem cells raises the possibility that human cancers likely arise from the stem or progenitor cells possessing self-renewal capabilities. However, the nature of the cell(s) of origin of central and peripheral nervous system tumors remains largely unknown. The development of plexiform neurofibroma during early childhood raises the possibility that this tumor arises from the transformation of fetal stem/progenitor cells during nerve development. Our study demonstrated that early tumor formation is characterized by an expansion of fully differentiated nonmyelinating Schwann cells in a microenvironment with degeneration of normal nonmyelinated axon/Schwann cell relationships and mast cell infiltration. These observations suggest potential future therapies for preventing neurofibroma formation by stabilizing axon-Schwann cell interactions and reducing mast cell infiltration.

neurofibromas. In a mature peripheral nerve, there are two types of Schwann cells: myelinating and nonmyelinating Schwann cells (Jessen and Mirsky, 2005). Myelinating Schwann cells encircle large-diameter (>1 μm) axons with concentric layers of cell membrane in a 1:1 relationship to form lipid-rich, multilamellar myelin sheaths. Small-diameter axons are embedded within and separated by cytoplasmic processes of nonmyelinating Schwann cells. These Schwann cell/axonal complexes, termed Remak bundles, may contain up to 30 or 40 axons in mature nerves (Taveggia et al., 2005). If a fully differentiated Schwann cell is assumed to be the cell of origin of neurofibromas, it remains to be explained how loss of NF1 function leads to the transformation of axon-bearing differentiated Schwann cells into the axon-free Schwann cells that populate neurofibromas.

Clinical studies indicate that plexiform neurofibromas are often identified during early childhood (Waggoner et al., 2000). It has been suggested that these tumors are congenital lesions that arise from fetal stem or progenitor cells during nerve development (Riccardi, 1992). The development of the Schwann cell lineage is a complex process that includes multiple transition phases from migrating neural crest cells to glial restricted progenitor cells (Schwann cell precursors) to two mature cell types—myelinating and nonmyelinating Schwann cells (see Figure S1 available with this article online) (Jessen and Mirsky, 2005). Although Schwann cell precursors (SCPs) were originally identified and widely viewed as glial restricted progenitors that only give rise to Schwann cells in developing peripheral nerves (Dong et al., 1999; Jessen et al., 1994), more recent evidence suggests that at least some of these cells are multipotent and give rise to both Schwann cells and myofibroblasts during development (Joseph et al., 2004; Morrison et al., 1999). Consequently, these cells were also referred to as neural crest stem cells (NCSCs) (Morrison et al., 1999). In this study, we refer to these stem/progenitor cells as SCP/NCSCs, which function as an intermediate cell type between classic migrating neural crest cells and lineage-committed Schwann cells during nerve development (Jessen and Mirsky, 2005). Since loss of heterozygosity (LOH) or biallelic inactivation of the *NF1* gene is a rate-limiting step for neurofibroma formation (Cichowski et al., 1999; Serra et al., 1997, 2000), the question arises whether the key LOH event must occur in fetal stem/progenitor cells during nerve development to initiate plexiform neurofibroma formation. In spite of the importance of NF1 as a model for understanding tumor suppressor gene function, it remains uncertain which cell type(s) in the neural crest/Schwann cell lineage during development and/or in adulthood is the cellular target for *NF1* mutation and how loss of *NF1* in these cells leads to neurofibroma formation.

RESULTS

Targeting an *Nf1* Mutation into Fetal Stem/Progenitor Cells during Nerve Development

We previously showed that *n*eural *c*rest-specific *Nf1* mutant mice ($Nf1^{NC}$) developed hyperplastic lesions in NC-derived sympathetic ganglia and adrenal medulla and died at birth (Gitler et al., 2003). To circumvent early lethality of the $Nf1^{NC}$ mice, we utilized a previously published Cre transgenic strain under the control of the P0 promoter (*P0A*-cre) (Giovannini et al., 2000), which expresses Cre in significantly fewer cells within the PNS during development. We crossed the P0A-cre transgenic mice to a Rosa26-LacZ Reporter strain (R26R-LacZ) that allows us to examine Cre recombinase activity by expression of the β-galactosidase (β-gal) gene (Soriano, 1999). *P0A*-cre-mediated recombination, revealed by X-gal staining, was first detected in neural crest and its derived tissues in cranial-facial regions at embryonic day 9.5 (E9.5) (Figure S2). However, significant β-gal activity was not detected until E11.5 in the trunk region (Figures S3Aa–S3Ad). At E12.5, when peripheral nerves start to innervate both forelimbs and hindlimbs, intense X-gal staining was detected in these peripheral nerves (arrows, Figures S3Ba–S3Bd). To assess the specificity of *P0A*-cre-mediated recombination, we performed X-gal staining on serial transverse sections prepared from the trunk region of E12.5 *P0A*-cre+/R26R-LacZ double transgenic embryos. As shown in Figure 1, β-gal positive cells are specifically distributed throughout the PNS including developing peripheral nerves (Figures 1A–1L). In peripheral nerves, β-gal positive cells are colocalized with three neural crest/Schwann cell lineage markers: $p75^{NGFR}$ (a marker that is expressed in both migrating neural crest cells and SCP/NCSCs) (Figures 1A–1C), GAP43 (Figures 1D–1F), and BLBP (brain lipid binding protein, also known as BFABP or Fabp7) (Figures 1G–1I). Both GAP43 and BLBP are expressed in SCP/NCSCs, but not in migrating neural crest cells (Jessen and Mirsky, 2005). It is worth noting that unlike GAP43 and BLBP, $p75^{NGFR}$ is not neural-specific, as it is expressed in both developing nerves and adjacent muscle cells (Figures 1B and 1C) (Wheeler et al., 1998). The nonneural expression of $p75^{NGFR}$ was further confirmed by double-labeling of $p75^{NGFR}$ with an axonal marker, Tuj1 (arrows, Figure S4). Furthermore, most of these β-gal-positive cells in sciatic nerves did not express S100, a marker for differentiated Schwann cells (Figures 1J–1L) (Jessen and Mirsky, 2005; Murphy et al., 1996). Of note, peripheral nerve development in the thoracic region occurs earlier than in lumbar region. Consistently, a significant number of S100-positive cells were observed in peripheral nerves in the thoracic region (arrows, Figure S3C). At the lumbar region, the transition from migrating neural crest cells to SCP/NCSCs occurs between E10 and E11 (Britsch et al., 2001). Because E11.5 is the earliest time point that we could detect significant β-gal activity in the trunk, we conclude that the major cell type in the peripheral nerves in the lumbar region including sciatic nerves undergoing P0A-cre-mediated recombination is the SCP/NCSC. To further confirm these results, we performed double immunofluorescence and attempted to colocalize the β-gal protein with $p75^{NGFR}$ (Figures 1M–1O), GAP43 (Figures 1P–1R), BLBP (Figures 1S–1U), and Sox10 (Figures 1V–1X) (a marker that is expressed in both migrating neural crest cells and SCP/NCSCs) (Britsch et al., 2001). Collectively, these double-labeling experiments demonstrated that most, if not all of, the β-gal positive cells expressed all four markers. However, only a subset of $p75^{NGFR}$, GAP43, BLBP, or Sox10 positive cells expressed β-gal protein. To inactivate *Nf1* in SCP/NCSCs during nerve development, we bred *P0A*-cre transgenic mice to the $Nf1^{flox/-}$ mice (Zhu et al., 2001) and subsequently generated *Nf1* mutant mice with genotypes of $Nf1^{flox/-}$;*P0A*-cre+ (hereafter, $Nf1^{P0A}KO$).

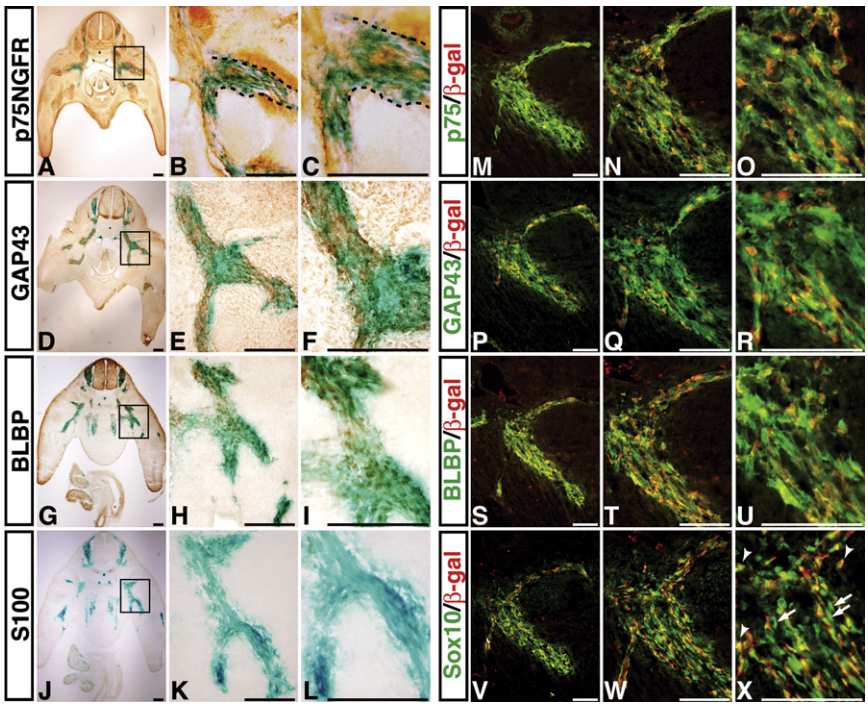

Figure 1. *P0A*-cre-Mediated Recombination in SCP/NCSCs

Transverse sections from the lumbar region of X-gal-stained E12.5 P0A-cre/R26R-LacZ double transgenic embryos were stained with anti-$p75^{NGFR}$ (A–C), GAP43 (D–F), BLBP (G–I), and S100 (J–L) antibodies. The dashed lines (B and C) mark the $p75^{NGFR}$ and β-gal double-positive developing peripheral nerves. The expression of $p75^{NGFR}$ (M–O), GAP43 (P–R), BLBP (S–U), or Sox10 (V–X) in β-gal positive cells was further confirmed by double immuofluorescence. Arrowheads and arrows in X point to Sox10/β-gal double-positive cells and Sox10-positive/β-gal-negative cells, respectively. Scale bars: (A)–(L), 50 μm; (M)–(X), 25 μm.

Loss of *Nf1* in SCP/NCSCs Induces Neurofibroma Formation with High Frequency

The $Nf1^{P0A}$KO mutant mice were viable, fertile, and indistinguishable from their control littermates. However, in the second year of life, all the mutant mice developed signs of sickness including lethargy, ruffled hair, skin lesions, or hindlimb paralysis. Histological analysis revealed that all of the sick mutant mice (n = 14) exhibited neurofibroma formation throughout the PNS. We focused our analysis on sciatic nerves, because these nerves are the only parts of the PNS in which the timing and stages of Schwann cell development are well established (Jessen and Mirsky, 2005). As compared to control nerves (Figures 2A and 2E), all mutant sciatic nerves were significantly enlarged (Figures 2B–2D). Histological examinations of sciatic nerves revealed that 10 of 14 (71%) mutant mice developed full-blown plexiform neurofibromas (NF), which, like human counterparts (Kleihues and Cavenee, 2000), were composed of increased numbers of elongated spindle-shape cells and infiltrating mast cells in a matrix rich in collagen fibers (Figures 2B and 2F and Figures 2C and 2G). All the neurofibromas analyzed in this model expressed S100 and $p75^{NGFR}$ (Figure S5), which often serve as diagnostic markers for human neurofibromas. The neurofibroma tissues were always identified adjacent to preneoplastic lesions (referred to as hyperplasia, Figures 2B and 2C). The major histopathological distinction between hyperplasia and a fully developed neurofibroma is that hyperplasia does not disrupt normal nerve structure in spite of increased cellularity. Figure 2D illustrates an example of advanced hyperplasia, characterized by dramatically increased cellularity with numerous blood vessels (arrowheads) and infiltrating mast cells (arrows), but with persistence of normally arrayed axons. In contrast, a neurofibroma identified in adjacent areas was characterized histologically by complete disruption of nerve structure with only small numbers of residual myelinated nerve fibers (arrows, Figure 2H). In contrast to normal (Figure 2E) and hyperplastic (Figure 2D) nerves in which Schwann cells distribute parallel to nerve fibers, neurofibroma cells are completely disorganized and randomly oriented in a collagen-rich matrix (Figures 2F–2H). The remaining mutant mice without evidence of neurofibroma formation in sciatic nerves (n = 4, 29%) developed an intermediate lesion that we referred to as "hyperplasia with focal neurofibroma" (hyperplasia/NF). Histopathologically, hyperplasia/NF is characterized as an overall hyperplastic lesion with focal areas displaying the disruption of peripheral nerve architecture characteristics of neurofibroma (Figures 7C, 7G, and 7K). Notably, all of these 4 mutant mice also developed large cutaneous or subcutaneous neurofibromas (data not shown), raising the question of whether the presence of these lesions in some way precludes hyperplasia/NF in sciatic nerves from progressing to full-blown neurofibromas. Together, these observations indicate that *Nf1* inactivation in SCP/NCSCs in sciatic nerves induces neurofibroma formation with high frequency.

To test whether differentiated Schwann cells are susceptible to neurofibroma formation, we analyzed sciatic nerves of a previously characterized *Nf1* mutant strain ($Nf1^{flox/-}$;*Krox20*-cre+, referred to as $Nf1^{Krox20}$*KO*) (Zhu et al., 2002). In sciatic nerves, the *Krox20*-cre transgene (also known as Egr2-cre) is first expressed at E15.5 $S100^{+}$ immature Schwann cells at moderate levels. *Krox20*-cre becomes highly expressed during myelination and is maintained in myelinating Schwann cells in adulthood (Figure S1) (Garratt et al., 2000; Ghislain et al., 2002; Voiculescu et al., 2000). None of the sciatic nerves analyzed from 16 aged $Nf1^{Krox20}$*KO* mutant mice along with 3 control littermates (12–16 months old) exhibited any evidence of neurofibroma formation (Figures 2I–2P). In contrast, all of these mutant mice developed multiple neurofibromas in cranial nerves and spinal roots (Zhu et al., 2002) where *Krox20*-cre is expressed in E10.5 neural stem/progenitor cells during early nerve development (Figures S6A–S6C) (Hjerling-Leffler et al., 2005; Maro et al., 2004). The level of *Krox20*-cre-mediated *Nf1* deletion between sciatic nerves and spinal roots was not significantly different (Figure S6D). Furthermore, the level of Cre-mediated recombination in adult sciatic nerves between *P0A*- and *Krox20*-cre transgenic

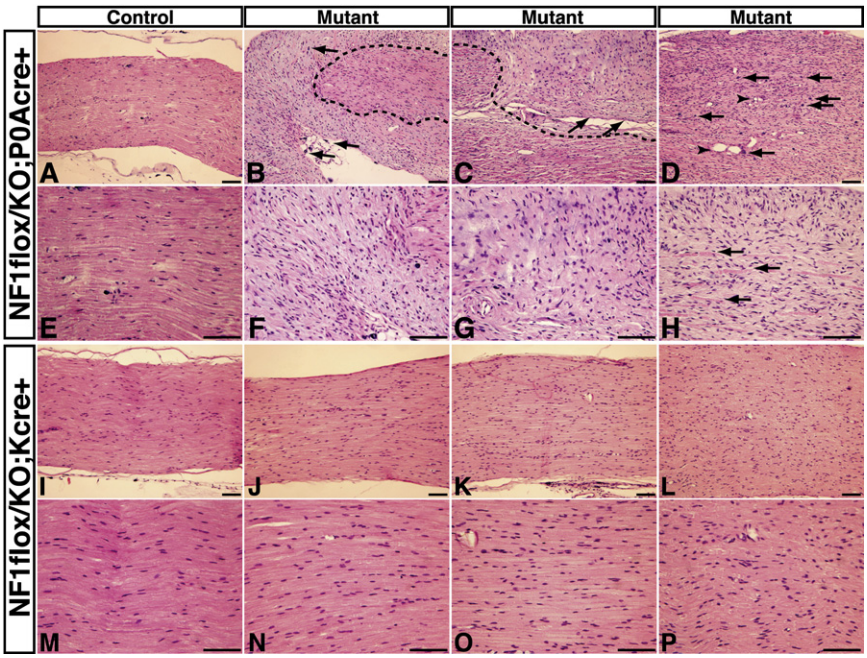

Figure 2. Histological Analysis of Control and Mutant Sciatic Nerves

Sciatic nerves from control (A and E) and three *Nf1*^{P0A}*KO* mice ([B] and [F], [C] and [G], and [D] and [H]) were sectioned and stained with hematoxylin and eosin (H&E). The dashed lines (B and C) mark the border of neurofibromas (arrows, [C]) and hyperplasia in mutant nerves. Arrows in (B) and (D) point to infiltrating mast cells and arrowheads (D) point to blood vessels. Sections from sciatic nerves of control (I and M) and three *Nf1*^{krox20}*KO* ([J] and [N], [K] and [O], and [L] and [P]) mice were stained with H&E. These mutant mice only developed varying degrees of hyperplasia in sciatic nerves. Scale bar, 100 μm.

mice was also not significantly different (Figures S6E and S6F). Therefore, these results suggest that the timing of *Nf1* inactivation, but not the number of *Nf1*-deficient cells generated by *Krox20*- and *P0A*-cre transgenes in peripheral nerves, is critical for the discrepancy in tumor penetrance observed in these two neurofibroma models. Together, these results suggest that in order to efficiently form neurofibromas, *Nf1* must be deleted from fetal stem/progenitor cells (SCP/NCSCs) in developing peripheral nerves.

The Role of *Nf1* in Schwann Cell Development

The genetic studies described above raise the question of whether *Nf1* deficiency leads to the hyperproliferation of fetal stem/progenitor cells (SCP/NCSCs) throughout the late gestation and the early postnatal period, despite the fact that tumors did not become grossly evident until late adulthood. To test this, we examined sciatic nerves of the *Nf1*^{P0A}*KO* mutant mice at postnatal day 22 (P22), a time point when Schwann cell development is nearly complete. Surprisingly, no significant difference in cell density and p75^{NGFR} expression was detected between sciatic nerves of control and mutant mice (Figures 3A–3E). Moreover, ultrastructural analysis obtained with transmission electron microscopy (TEM) revealed no difference in the number of myelinating and nonmyelinating Schwann cells between control and mutant sciatic nerves (Figure S7A). The number of axons within the Remak bundles of mutant sciatic nerves was not significantly altered when compared to the control nerves (Figure 3F, Figure S7B). These observations indicate that *Nf1* does not regulate the generation or overall differentiation of myelinating or nonmyelinating Schwann cells from fetal stem/progenitor cells in developing peripheral nerves. However, unlike control Remak bundles (Figure 3G) in which most of individual axons were segregated into single Schwann cell pockets (Taveggia et al., 2005), some mutant Remak bundles exhibited a Schwann cell "pocket defect" that contained aberrantly large numbers of unseparated axons (Figures 3H, 3I, and 3L), a significant number of which had an abnormal "dilated" morphology in cross sections. The maximum number of axons per pocket in the control nerves was 17 as compared to 41 in the mutant nerves. In addition, some of the abnormal Remak bundles with poorly segregated and dilated axons underwent aberrant myelination (Figure 3K), a phenomenon that was never observed in wild-type nerves (CTR versus Mut, $p = 0.004$). Myelinated Remak bundles with smaller numbers of axons were found in one *Nf1* heterozygous mouse (Figure 3J). Thus, these data suggest that *Nf1* is required for appropriate axonal segregation and suppression of myelination in at least some nonmyelinating Schwann cells.

Degeneration of Abnormal Remak Bundles

To investigate the possible mechanisms by which abnormal Remak bundles lead to neurofibroma formation, we analyzed sciatic nerves of control and *Nf1*^{P0A}*KO* mutant mice at older ages. At 3 months of age (P90), although there was no significant difference in size between control and mutant sciatic nerves, the cellular density of mutant sciatic nerves was significantly increased as compared to that of control nerves (Figures S9A and S9B; Figure 3E). EM analysis indicated that the number of myelinating Schwann cells in mutant P90 sciatic nerves was not significantly different from that of controls (Figures 4A–4C; Figure S7C). Thus, these observations indicate that myelinating Schwann cells do not contribute to initial cellular expansion in P90 mutant nerves. In the nonmyelinating Schwann cell lineage, most of the abnormally differentiated Remak bundles with unseparated or poorly segregated axons observed in P22 mutant sciatic nerves were no longer detected. The small number of such abnormal Remak bundles identified at P90 had "broken" Schwann cell pockets in which axons were dissociating from each other and from their supporting Schwann cells (arrows, Figures 4E and 4F), which was never observed in control Remak bundles (Figure 4D). Since these abnormal Remak bundles typically contained more than 10 axons (10+), we compared the number of axons ensheathed by nonmyelinating Schwann cells within each Remak bundle between control and mutant nerves. Consistent with the degenerating morphology of abnormal Remak

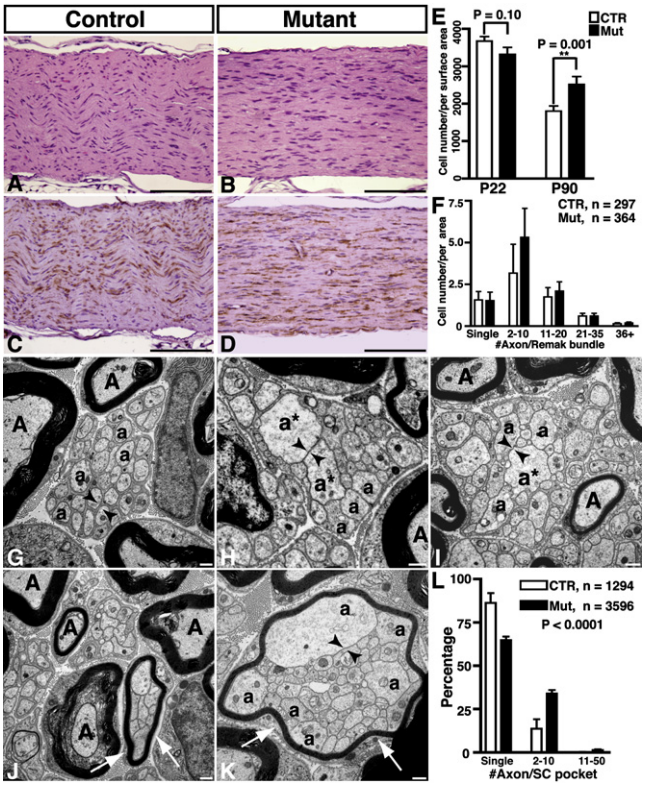

Figure 3. Abnormal Remak Bundles in *Nf1* Mutant Sciatic Nerves

Sections of sciatic nerves from P22 control and $Nf1^{P0A}KO$ mutant mice were stained with H&E (A and B) and anti-$p75^{NGFR}$ antibody (C and D). (E) Quantification of the number of cells per surface area (mm^2) in P22 and P90 control and mutant sciatic nerves. For P22 analysis, 8 control and 3 mutant mice were used, and for P90 analysis, 3 control and 7 mutant mice were used. Cell density for the P22 and P90 is plotted as mean ± SEM. (F) The numbers of Remak bundles per surface area (1,000 μm^2) in control and mutant P22 sciatic nerves were categorized into five groups based upon the number of axons that they ensheathed. N values represent Remak bundles quantified for each genotype. Data in (F) represent mean ± SEM from 2 control and 4 mutant nerves. Transmission electron microscopy (TEM) analysis of Remak bundles in sciatic nerves of P22 control (G and J) and mutant (H, I, and K) mice show abnormal axonal segregation in the mutant mice. Arrowheads in [G] indicate Schwann cell cytoplasm between different axons, which isolates each individual axon into a dedicated Schwann cell pocket in the Remak bundle. Mutant Remak bundles contain unsegregated axons, which remain directly apposed to each other (arrowheads, [H], [I], and [K]). (J and K) The number of myelinated Schwann cells ensheathing multiple axons (arrows) is significantly increased in mutants compared to controls ($p = 0.0036$). (L) The percentage distribution of axons per Schwann cell pocket in control and mutant nerves. N values indicate the number of Schwann cell pockets counted for each genotype (mean ± SEM). The majority of axons in control nerves were segregated into individual pockets, while the number of axons properly segregated was dramatically reduced in mutant nerves (Chi-square goodness-of-fit test, $p < 0.0001$). A, myelinated axons; a, unmyelinated axons; a*, dilated axons. Scale bars: (A)–(D), 100 μm; (G)–(K), 1 μm.

bundles, we found that the normal Remak bundles containing 10+ axons in mutant nerves were dramatically reduced as compared to controls (bottom panel, Figure 4O). Loss of the specific populations of the normal Remak bundles (10+) in P90 mutant nerves suggests that these cells either died or converted to other abnormal cells. To test these two possibilities, we first employed three independent assays to examine whether excess apoptotic cells were present in mutant nerves. No excess apoptotic cells were identified by expression of activated Caspase 3 or by a TUNEL assay in control or mutant sciatic nerves of P22 and P90 mice (Figures S8A–S8H). Furthermore, by using EM, we examined the morphology of over 1,500 nonmyelinating Schwann cells in control and mutant sciatic nerves of P22 and P90 mice. No cell exhibited classic morphology of apoptotic Schwann cells such as coarse chromatin, aggregation in the nucleus, vacuolation in the cytoplasm (Figure S8I) (Feldman et al., 1999). These results indicate that excess apoptosis is not likely to account for the loss of abnormally differentiated Remak bundles observed in mutant nerves.

Next, to test the possibility whether these abnormal Remak bundles converted into other cells, we quantified the number of the different cell types in control and mutant sciatic nerves of P90 mice by EM (Figure S7C). The cells with Schwann cell morphology, defined by presence of a continuous basal lamina and association with axon(s), constitute approximately 98% of the total cells in the endoneurial space in these EM cross sections of both control and mutant nerves. We identified three abnormal Schwann cell populations in mutant nerves that were rarely seen in control nerves (Figures 4D–4O). Abnormal nonmyelinating Schwann cells (anmSCs) were characterized by an association of morphologically abnormal axons (e.g., dilated or naked axons), many of which had myelin-like fragments (Figures 4G–4I). Dissociating Schwann cells (dSCs) were characterized by presence of free Schwann cell processes (arrowheads, Figures 4J and 4K), which progressively dissociated from axons leading to degeneration of unmyelinated axons (arrows, Figures 4K and 4L). Unassociated Schwann cells (uSCs) completely lost axonal contact in spite of presence of a continuous basal lamina that sometimes encircled collagen fibers (Figures 4M and 4N). The uSCs are morphologically identical to the tumor cells observed in both human and mouse neurofibromas (Figure S14) (Cichowski et al., 1999; Lassmann et al., 1977; Zhu et al., 2002). Both anmSCs and dSCs share fundamental features with nonmyelinating Schwann cells: ensheathing small-diameter axon(s) and possessing a continuous basal lamina (Figures 4G–4L). However, most of these abnormal Schwann cells, particularly dSCs, contained fewer numbers of axons (<10) compared to normal nonmyelinating Schwann cells (Figure 4O). Together, these observations suggest that the Remak bundles with large numbers of axons (10+), which were specifically lost in mutant nerves, had broken down into bundles with smaller numbers of axons that were identified within both normal and abnormal (anmSCs and dSCs) Remak bundles. Consistent with this, when we counted and pooled the total axons from all three populations of nonmyelinating Schwann cells in mutant nerves (nmSCs, anmSCs, and dSCs), we found that, as compared to controls, mutant nerves contained significantly fewer Remak bundles ensheathing more than 20 axons, but had increased numbers of Remak bundles containing 10 or fewer axons (Figure S7D). Thus, these results collectively suggest that abnormally differentiated Remak bundles in mutant nerves are unstable and degenerate into anmSCs and dSCs. The presence of anmSCs and dSCs leads to approximately 61% increase ($p < 0.01$) in the number of nonmyelinating Schwann cells in the EM cross sections of P90 mutant nerves as compared to controls

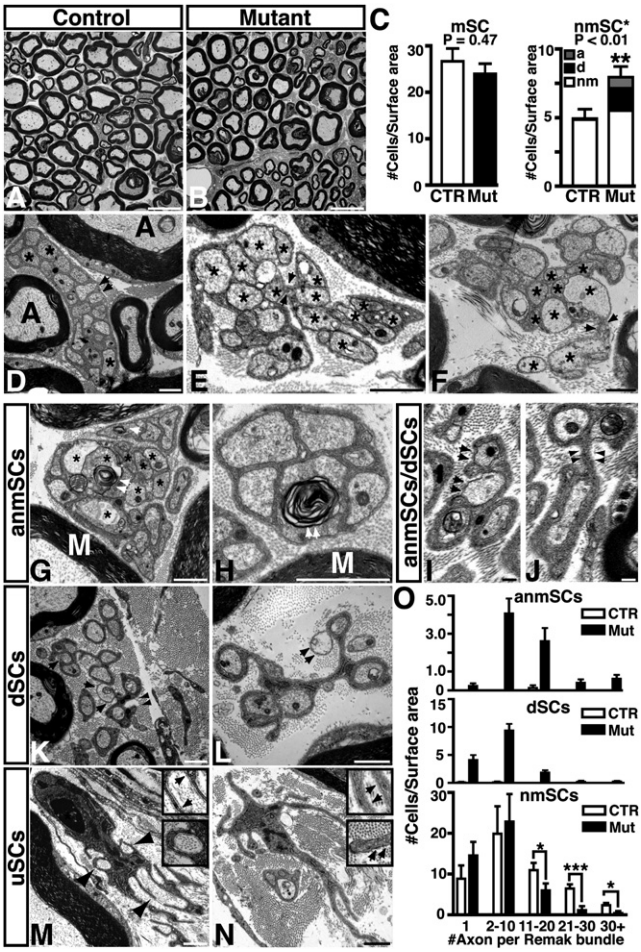

Figure 4. Degeneration of *Nf1* Mutant Remak Bundles at P90

Electron micrographs show cross-sections of P90 control (A and D) and mutant (B, E, and F) sciatic nerves. (C) The number of myelinating (mSC) and nonmyelinating (nmSC) Schwann cells in P90 control and mutant sciatic nerves was presented by the cell number per surface area (mean ± SEM). a, abnormal nmSCs; d, dissociating SCs; nm, normal nmSCs. Arrows in (D) point to a typical Remak bundle in control nerves containing multiple unmyelinated axons (*). (E) and (F) show two examples of abnormally differentiated Remak bundles with "broken pockets" that have dissociating axons. Arrows in (E) and (F) point to unsegregated axons (*) dissociating from each other. (G) and (H) show two representative anmSCs containing "naked" axons and myelin-like fragments (arrows). M, normal myelin. (I) and (J) show the morphological similarity between a pair of anmSC and dSC. Arrows in (I) point to "naked" axons in an anmSC whose degeneration likely generates free Schwann cell processes seen in a dSC (arrowheads, [J]). (K and L) Two examples of dSCs with free Schwann cell processes (arrowheads, [K]) and degenerating unmyelinated axons (arrows). (M and N) Two examples of unassociated Schwann cells (uSCs) with continuous basal lamina and no axon contact. Arrowheads in (M) point to collagen fibers ensheathed by uSCs, which were also shown in Insets (M) with higher magnification. Arrows in the Insets of (M) and (N) (top) point to continuous basal lamina in uSCs as compared to a fibroblast process (arrows, bottom inset in [N]). (O) The numbers of Remak bundles per surface area (1,000 μm^2) in control and mutant sciatic nerves were categorized into five groups based upon the number of axons that they ensheathed. Data in [O] represent mean ± SEM from 2 control and 3 mutant nerves. Top panel, abnormal nonmyelinating Schwann cells (anmSCs); middle panel, dissociating Schwann cells (dSCs); bottom panel, normal nonmyelinating Schwann cells (nmSCs). *$p < 0.05$, ***$p < 0.001$. Scale bar, 1 μm.

(Figure 4C and Figure S7C). uSCs represented a minor population of cells in P90 mutant nerves. Because some of them exhibited only parts of Schwann cell-like processes in the EM images and, hence, are difficult to quantify accurately, we did not include uSCs in this analysis. Therefore, the 61% increase of nonmyelinating Schwann cells observed in P90 mutant nerves most likely is a slight underestimation.

Expansion of Nonmyelinating Schwann Cells

To investigate whether the initial expanded nonmyelinating Schwann cells observed in mutant nerves are neurofibroma cells in the early stages of tumorigenesis, we first attempted to identify specific markers for these cells. Under the light microscope, except for presence of mild hyperplasia, mutant sciatic nerves were relatively normal compared to controls at P90 (Figures 5A and 5B; Figures S9A and S9B). Furthermore, the presence of excess cells in mutant nerves did not alter overall nerve structure and differentiation of myelinating Schwann cells, revealed by S100 staining (Figures S9C and S9D). These observations are consistent with the EM analysis that the myelinating Schwann cells were not affected in these hyperplastic mutant nerves. Since Sox10 is primarily expressed in myelinating Schwann cells of adult nerves (Berger et al., 2006; Peirano et al., 2000), we used Sox10 immunofluorescence to quantify the number of myelinating Schwann cells in control and mutant nerves. Sox10-positive cells (arrowheads) were comparable in control and mutant nerves, whereas mutant nerves had significantly more Sox10-negative cells (arrows, Figures 5C and 5D; Figure S10). These results are consistent with the EM analysis described above (Figure 4C) that the cells in the nonmyelinating, but not in the myelinating, Schwann cell lineage, are expanded in P90 mutant nerves. In addition, these observations also suggest that the initial expanded cellular population in mutant nerves does not resemble fetal stem or progenitor cells with regard to Sox10 expression. To further confirm these results, we employed three additional neural crest/Schwann cell lineage markers, BLBP, GFAP (glial fibrillary acidic protein), and $p75^{NGFR}$. The expression of BLBP is downregulated in mature Schwann cells (Kurtz et al., 1994; Miller et al., 2003). Consistently, no BLBP expression was found in control or mutant sciatic nerves of P90 mice (data not shown). GFAP is probably one of the most reliable markers for nonmyelinating Schwann cells (Jessen and Mirsky, 2005). Accordingly, we observed a conspicuous increase in GFAP-positive cells in mutant nerves as compared to controls (Figures 5E and 5F; Figure S11). Similar to Sox10, $p75^{NGFR}$ is expressed in both migrating neural crest cells and SCP/NCSCs during early nerve development. However, in contrast to Sox10, $p75^{NGFR}$ is only expressed in the nonmyelinating Schwann cell populations in adult nerves. In conjunction with the ultrastructural changes noted above, the expression pattern of Sox10 and BLBP provide compelling evidence that no stem or progenitor cells persisted into adult *Nf1* mutant nerves. Hence, the expression of $p75^{NGFR}$ can be used as a surrogate marker for nonmyelinating Schwann cells in adult mutant nerves. The increased number of $p75^{NGFR}$-expressing cells was identified in mutant nerves compared to controls. These results were demonstrated by two independent assays: immuohistochemistry (Figures 5G and 5H; Figures S9E, S9F, and S12) and flow cytometry (Figures 5I and 5J). Because both GFAP and $p75^{NGFR}$ have diffuse

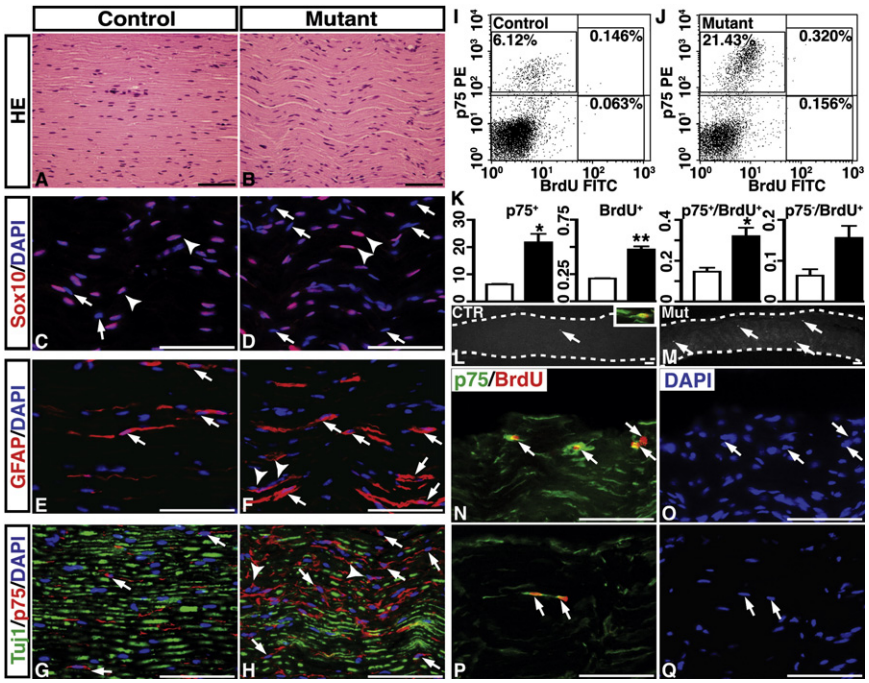

Figure 5. The Expanded Cellular Populations in P90 Mutant Nerves Express Lineage Markers by Nonmyelinating Schwann Cells

Sections from sciatic nerves of P90 control and mutant mice were stained with H&E (A and B), Sox10/DAPI (DAPI stains for cell nuclei) (C and D), GFAP/DAPI (E and F), and Tuj1/p75/DAPI (G and H). Arrows and arrowheads in (C) and (D) point to Sox10-negative and Sox10-positive cells, respectively. The number of GFAP-positive and $p75^{NGFR}$-positive cells was conspicuously increased in mutant nerves (arrows, [F] and [H]) compared to controls (arrows, [E] and [G]). Arrowheads in (F) and (H) point to a cluster of GFAP-positive and $p75^{NGFR}$-positive nuclei in mutant nerves, which were never seen in controls. Representative flow-cytometry plots demonstrate approximately a 2.5-fold increase in frequency of $p75^{NGFR}$-positive cells in mutant nerves (21.75%, [J]) compared to that in control (6.27%, [I]) and a 1.3-fold increase in frequency of BrdU-positive cells in mutant (0.476%, [J]) nerves compared to controls (0.209%, [I]) nerves. Data in (K) represent mean ± SEM from two independent experiments using age-matched control (n = 2) and mutant (n = 4) mice. *$p < 0.05$, **$p < 0.01$. Statistical significance is indicated by * or **. Sections from sciatic nerves of BrdU-treated control (L) and mutant (M) mice were stained with anti-BrdU. The inset in (L) shows a $p75^{NGFR}$/BrdU double-positive cell in a control nerve. ([N] and [O] and [P] and [Q]) Two representative mutant nerves showing a cluster of $p75^{NGFR}$/BrdU double-positive cells (arrows). Scale bar, 50 μm.

expression pattern in the cytoplasm that could not always readily be colocalized with the cell nuclei, we employed flow cytometry to quantify the number of $p75^{NGFR}$-expressing cells in sciatic nerves. In two independent experiments, the frequency of $p75^{NGFR}$-expressing cells isolated by fluorescence-activated cell sorting (FACS) was approximately 2.5-fold higher in mutant nerves than that in controls (Figures 5I–5K), which agreed very well with the increase in Sox10-negative cells (2.1-fold increase; Figure S10K). It is worth noting that the increase observed in the Sox10-negative or $p75^{NGFR}$-positive cell populations of mutant nerves is markedly higher than the increased numbers of non-myelinating Schwann cells obtained from EM analysis (61%). This discrepancy could reflect the fact that we were using longitudinal sections for quantifying Sox10-positive or -negative cells whereas EM images were taken from cross-sections of the nerves. Together, these results demonstrate that the expanded cellular populations in P90 mutant nerves not only morphologically resemble differentiated nonmyelinating Schwann cells at ultrastructural level (e.g., ensheathing small-diameter axons), but also exhibited molecular characteristics that are similar to nonmyelinating Schwann cells ($BLBP^-/Sox10^-/GFAP^+/p75^+$), but not to the fetal stem/progenitor cells ($BLBP^+/Sox10^+/GFAP^-/p75^+$).

The Expanded Nonmyelinating Schwann Cells Exhibit the Characteristics of Early-Stage Neurofibroma Cells

To investigate whether the expanded nonmyelinating Schwann cells in *Nf1* mutant nerves exhibit the characteristics of tumor cells, we examined proliferation of these cells. In normal P90 nerves, only about 0.2% of the total cells were proliferating, revealed by BrdU staining in the FACS plot (Figure 5I). There was nearly 1.3-fold increase in the number of BrdU-positive cells in mutant nerves (Figure 5J) as compared to controls (Figure 5I). Although the number of BrdU-positive cells was increased in both $p75^{NGFR}$-positive and $p75^{NGFR}$-negative cellular compartments, only the $p75^+/BrdU^+$ cells were statistically significant more in mutant nerves than those in control nerves (Figure 5K). To confirm these FACS analyses, we performed BrdU-labeling experiments on the tissue sections from P90 control and mutant sciatic nerves. Consistent with the FACS results, very few BrdU-positive cells could be identified in control nerves, which were evenly distributed throughout the nerve (Figure 5L). In contrast, significantly more BrdU-positive cells were identified in mutant nerves (arrows, Figure 5M; $p = 0.02$). Many of the mutant BrdU-positive cells also expressed $p75^{NGFR}$ and distributed in clusters (Figures 5N–5Q), a characteristic of tumor cells that was never observed in control nerves. Furthermore, a cluster of GFAP or $p75^{NGFR}$-positive nuclei could readily be identified in mutant nerves (arrowheads, Figures 5F and 5H), but not in controls (Figures 5E and 5G).

Both human genetic studies and mouse models have demonstrated that NF1 deficiency and expansion of $NF1^{-/-}$ cells drive neurofibroma formation. If the expanded $p75^{NGFR}$-expressing cells in mutant nerves are early-stage neurofibroma cells, they should be genetically *Nf1* deficient. To mark *Nf1*-deficient cells in intact nerve tissues, we introduced the R26R-LacZ allele to control and mutant mice. Consequently, we could mark $Nf1^{+/-}$ and $Nf1^{-/-}$ cells as β-gal-positive cells in control ($Nf1^{flox/+}$;*P0A*-cre+;R26RLacZ) and mutant ($Nf1^{flox/-}$;*P0A*-cre+;R26RLacZ) nerves, respectively. As compared to controls (Figure 6A), the number of β-gal-positive cells in mutant (Figure 6B) sciatic nerves were significantly increased, indicating expansion of $Nf1^{-/-}$ cellular compartment. In control nerves (Figure 6C),

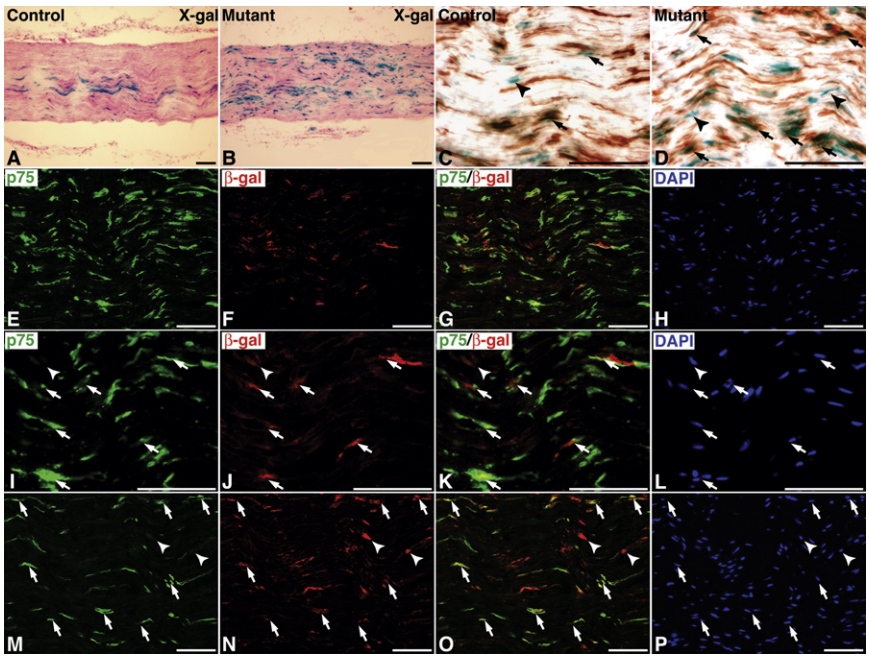

Figure 6. The Expanded *Nf1*-Deficient Cells in P90 Mutant Nerves Express $p75^{NGFR}$ and GFAP

The R26R-LacZ allele was introduced to the control and $Nf1^{P0A}KO$ mutant mice. Sciatic nerves from P90 mice were sectioned and stained with X-gal (A and B) and X-gal/anti-$p75^{NGFR}$ antibody (C and D). Sections from mutant nerves were triple-labeled by anti-$p75^{NGFR}$ (E and I), anti-β-gal (F and J), and DAPI (H and L). Overlay images are shown in (G) and (K). Arrows and an arrowhead in (I) to (L) point to $p75^{NGFR}$/β-gal double-positive cells and a $p75^{NGFR-}$/β-gal+ single positive cell, respectively. Sections from mutant nerves were triple-labeled by anti-GFAP (M), anti-β-gal (N) and DAPI (P). An overlay image is shown in panel (O). Arrows in (M)–(P) point to GFAP/β-gal double positive cells and arrowheads in the same panels show a small number of β-gal positive cells that do not express GFAP. Scale bars, 50 μm.

β-gal-positive cells were found in both $p75^{NGFR}$-positive (arrows) and negative (arrowhead) cell compartments, indicating that P0A-cre was targeted to both nonmyelinating and myelinating Schwann cell lineages. Most of the β-gal positive cells in mutant nerves expressed $p75^{NGFR}$ (Figures 6D and 6E–6L), indicating expansion of the β-gal^{+}/$p75^{NGFR+}$ cellular population. Furthermore, these β-gal positive cells also expressed GFAP (arrows, Figures 6M–6P), further confirming that they are in the nonmyelinating Schwann cell lineage. Together, these results indicate that the expanded nonmyelinating Schwann cells exhibited the key features of neurofibroma cells: increased proliferation, clustering, and most importantly, *Nf1* deficiency. Expansion of the nonmyelinating Schwann cells was accompanied by degeneration of unmyelinated axons, which was revealed by EM analysis (Figures 4K and 4L) and focal loss of Tuj1 expression in mutant nerves (compare Figures S12E and S12M to Figures S12A and S12I). Axonal degeneration also correlated with an inflammatory response. At P22, no mast cells were identified in either control or mutant sciatic nerves. In contrast, mutant nerves recruited over 2.5-fold more mast cells than did controls at P90, a time point when initial cellular expansion was observed in mutant nerves (Figure S13). The degenerative microenvironment and accompanying mast cell infiltration may provide a favorable niche for proliferation of early-stage tumor cells.

Progression Stages of Neurofibroma Development

The morphological, molecular and genetic analyses described above suggest that the expanded $p75^{+}$/$GFAP^{+}$/β-gal^{+} (*Nf1* deficient) nonmyelinating Schwann cells observed in P90 $Nf1^{P0A}KO$ mutant sciatic nerves are tumor cells engaged in the early stages of neurofibroma development. To determine the role of these early-stage tumor cells during tumor progression, we analyzed 6 healthy *Nf1* mutant mice at 6 to 12 months of age, in which we identified the preneoplastic lesions in sciatic nerves similar to those seen in end-stage mutant nerves as described above (Figure 2). These observations suggest that hyperplasia and hyperplasia/NF are the precursors for neurofibroma. However, unlike the hyperplastic lesions observed in sciatic nerves of younger P90 mutant mice (Figure 5B; Figures S9B and S9D), similar lesions in aged mutant nerves exhibited focal loss of myelinated axons, revealed by loss of S100 staining (arrows, Figure 7B) as compared to age-matched controls (Figure 7A). Significantly increased $p75^{NGFR}$ expression also occurred in these mutant nerves (arrows, Figure 7F) compared to controls (Figure 7E), indicating further expansion of these $p75^{NGFR}$-expressing cell populations (compare Figures 7F and 7J to Figures 7E and 7I). In semithin sections, control nerves were tightly packed with myelinated axons with only a small intervening interstitial space (Figures 7M and 7Q). Aged hyperplastic mutant nerves, in contrast, were significantly enlarged by an expanded interstitial compartment (Figures 7N and 7R). The expression pattern of S100 and $p75^{NGFR}$ revealed that hyperplasia/NF (Figures 7C, 7G, and 7K) and neurofibromas (Figures 7D, 7H, and 7L) had continuous expansion of the $p75^{NGFR}$-expressing cells similar to that observed in hyperplasia, leading to further increased interstitial cellularity and depletion of myelinated axons (Figures 7O and 7S, 7P and 7T, and Figure S14). The expanded cell population also expressed GFAP and was *Nf1* deficient, revealed by increased numbers of GFAP-positive (Figures 8A–8I) and R26R-LacZ positive cells (Figure S15) in mutant nerves during tumor progression. Consistent with loss of myelinated axons at later stages of neurofibroma development, gradual loss of Sox10-positive cells was observed in these mutant nerves during tumor progression (Figures 8J–8O). Furthermore, no BLBP expression was observed in these aged mutant nerves (data not shown). Together, these results suggest that neurofibroma progression is driven by continuous expansion of the *Nf1*-deficient cells with molecular characteristics of nonmyelinating Schwann cells ($BLBP^{-}$/$Sox10^{-}$/$GFAP^{+}$/$p75^{+}$) similar to the early-stage tumor cells that were identified in sciatic nerves of younger P90 mutant mice.

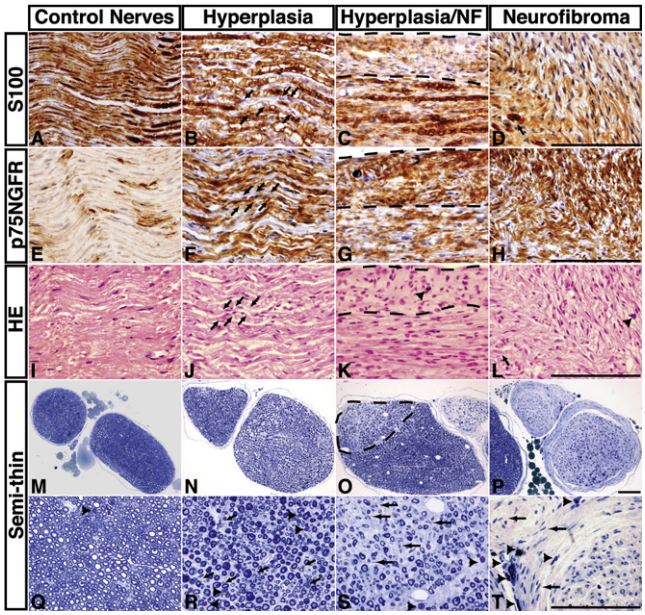

Figure 7. Progression Stages of Neurofibroma Formation

Sciatic nerves from control (A, E, and I) and *Nf1*^{P0A}*KO* mutant mice harboring hyperplasia (B, F, and J), hyperplasia with focal neurofibroma (C, G, and K), and neurofibroma (D, H, and L) were sectioned and stained with anti-S100, anti-p75^{NGFR}, and H&E. Arrows in (B), (F) and (J) point to focal loss of S100-positive myelin sheath that was accompanied by increased numbers of p75^{NGFR}-expressing cells. The dashed lines in (C, G, and K) mark the border of hyperplasia and neurofibroma tissues. Arrows in (D) and (L) point to residual S100-positive myelin sheath in a neurofibroma. Arrowheads in (K) and (L) point to infiltrating mast cells in neurofibroma tissues. Semithin sections of sciatic nerves from control (M and Q) and mutant mice harboring hyperplasia (N and R), hyperplasia with focal NF (O and S), and neurofibroma (P and T) were stained with toluidine blue. The dashed lines in (O) mark the areas undergoing transition from hyperplasia to neurofibroma, which is characterized by significant loss of myelinated axons at ultrastructural levels. Arrows in (R), (S), and (T) point to increased numbers of cells between myelinated axons in mutant nerves compared to controls. Arrowheads (Q–T) point to infiltrating mast cells, staining metachromatically in this preparation. Scale bars, 100 μm.

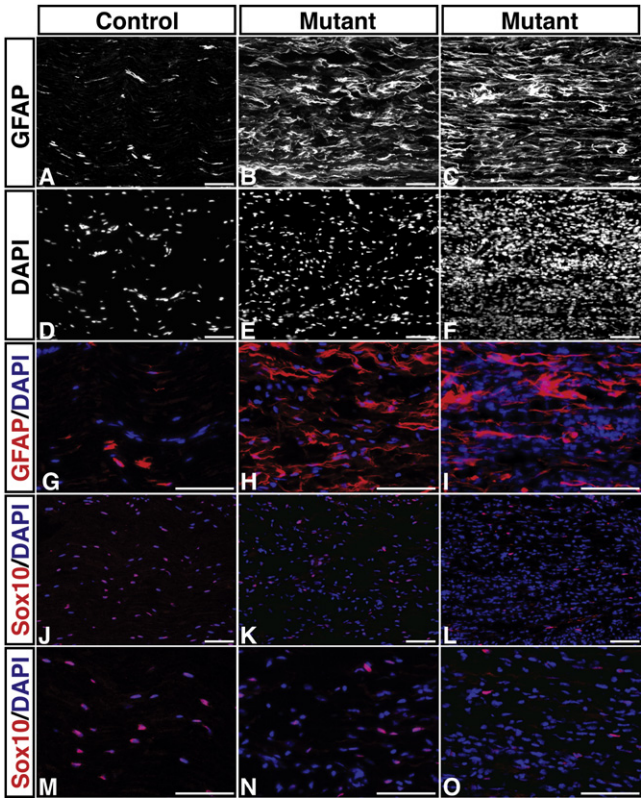

Figure 8. The Number of GFAP-Positive Cells Is Gradually Increased during Neurofibroma Progression with a Concomitant Decrease in Sox10-Expressing Cells

Adjacent sections from sciatic nerves of aged control and two *Nf1*^{P0A}*KO* mutant mice were stained with GFAP (A, B, and C), DAPI (D, E, and F), GFAP/DAPI (overlay images, [G], [H], and [I]), and Sox10/DAPI (J, K, and L). (M), (N), and (O) represent high magnification views of (J), (K), and (L). Scale bars, 50 μm.

DISCUSSION

Cell of Origin for Plexiform Neurofibroma

In this study, we employed two Cre transgenic strains, *P0A*-cre and *Krox20*-cre, which, respectively, target an *Nf1* mutation into stem/progenitor cells and more differentiated Schwann cells in sciatic nerves. The *Nf1*^{P0A}*KO* mice, but not the age-matched *Nf1*^{Krox20}*KO* mice, developed plexiform neurofibromas in sciatic nerves. These genetic studies provide compelling evidence that plexiform neurofibromas arise most efficiently as a result of *Nf1* deletion from fetal stem/progenitor cells in developing peripheral nerves.

No stem/progenitor cells (NCSCs) have been identified in normal adult peripheral nerves (Kruger et al., 2002). Thus, the possible mechanisms underlying transformation of fetal stem/progenitor cells are that NF1 deficiency (1) promotes self-renewal of fetal stem/progenitor cells to form hyperplasia or tumors during or after nerve development is complete and/or (2) inhibits differentiation of the fetal stem/progenitor cells that leads to at least some of these undifferentiated cells persisting into adult nerves and forming tumors at later stages. Our data show that *Nf1*-deficient fetal stem/progenitor cells differentiate according to a normal time course into Schwann cells. In addition, EM analysis and expression of neural crest/Schwann cell lineage markers revealed no evidence of stem/progenitor cells persisting into adult mutant nerves. By employing a well-established neural stem cell assay (Morrison et al., 1999), Joseph et al. found no evidence for the persistence of NCSCs in *Nf1*-deficient nerves based upon functional clonal assays for the presence of self-renewing, multipotent stem cells (Joseph et al., 2008). Together, these data suggest that it is unlikely that persisting *Nf1*-deficient fetal stem/progenitor cells serve as a direct cell of origin for plexiform neurofibroma. Rather, the only subtle phenotypic abnormality identified in postnatal *Nf1*^{P0A}*KO* mutant nerves is the presence of a subset of the Remak bundles with a Schwann cell "pocket defect," which failed to appropriately segregate ensheathed axons. Abnormal axonal segregation phenotypes observed in *Nf1* mutant Remak bundles are reminiscent of those seen in mice with targeted mutations in the type III neuregulin-1 (NRG1) (Taveggia et al., 2005) or β-secretase BACE1 that is normally required for cleaving the type III NRG1 precursor into the functional form (Hu et al., 2006; Willem et al., 2006), suggesting that *NF1* may be an intracellular component of NRG1/ErbB signaling pathway.

Our data indicate that the abnormally differentiated Remak bundles with the "pocket defect" were degenerating in sciatic nerves of P90 *Nf1*^{P0A}*KO* mutant mice. Most strikingly, degeneration of the abnormal Remak bundles was accompanied by initial cellular expansion in *Nf1*^{P0A}*KO* mutant nerves. At the ultrastructural level, the expanded cell populations exhibited an intermediate morphology between fully differentiated nonmyelinating Schwann cells and neurofibroma cells. Thus, the majority of the expanded cells were morphologically characterized as anmSCs or dSCs, both of which displayed the defining features of nonmyelinating Schwann cells (e.g., ensheathing various numbers of small-diameter axons). When we compared the axon number within each Remak bundle between control and mutant nerves, there is a conspicuous shift in axonal distribution from the more Remak bundles ensheathing >20 axons in control nerves to the more Remak bundles with <10 axons in mutant nerves. Thus, the morphological similarities of and the differences in axon number ensheathed by control and mutant nonmyelinating Schwann cells suggest a lineage relationship between the degenerating abnormally differentiated Remak bundles with the "pocket defect" and anmSCs/dSCs/uSCs. Specifically, we propose a model for neurofibroma initiation (Figure S16): degeneration of abnormally differentiated Remak bundles in mutant nerves, which progressively dissociate from axons and breaks into bundles with smaller numbers of axons, a sequence which eventually generates a continuum of abnormal Remak bundles, ranging from anmSC, dSCs to uSCs. The clinical observation that plexiform neurofibroma is almost exclusively found in individuals with *NF1* germline mutations (Halliday et al., 1991; Woodruff, 1999) also supports the notion that *NF1* plays a critical function(s) during early nerve development. Together, our results implicate the abnormally differentiated Remak bundles as a cell of origin for early-stage neurofibroma cells.

Early-Stage Tumor Cells versus Tumor-Initiating Cells

Our morphological and molecular analyses demonstrate that initial hyperplasia observed in P90 *Nf1* mutant nerves is not due to expansion by stem or progenitor cells, but rather by fully differentiated nonmyelinating Schwann cells. To establish a cell or cells as a cell of origin for a tumor, it is necessary to determine whether these cells are responsible for initiation and progression of tumors. The term "tumor-initiating cells" was recently used to describe a subset of human tumor cells that possess stem cell-like properties and are capable of regenerating tumors when transplanted into immunodeficient mice (Al-Hajj et al., 2003; Singh et al., 2004). The "tumor-initiating cells" were often referred to as cancer stem cells. However, these tumor-initiating cells were isolated from end-stage established tumors, which typically have accumulated numerous mutations that support its growth upon xenotransplantation. Therefore, the tumor-initiating cells or cancer stem cells probably have little or no resemblance to the early-stage tumor cells, which harbor fewer mutations and are responsible for initiating tumor formation in primary tumor sites.

Because the early-stage tumor cells typically are present in smaller numbers and have limited tumorigenic capacities, we designed several in vivo assays to determine their tumor cell characteristics. Given that no stem or progenitor cells were observed in adult *Nf1* mutant nerves, we were able to use p75^{NGFR} as a surrogate for the expanded nonmyelinating Schwann cells. First, both our immunofluorescence and FACS data demonstrate that most of the proliferating cells were identified in the p75^{NGFR}-positive cellular compartment, which were significantly increased in *Nf1* mutant nerves. Second, the proliferating p75^{NGFR}-positive cells histopathologically exhibited an important characteristic of tumor cells, namely a tendency to form clusters, a phenomenon that was never observed in control nerves. Third, most importantly, many of the p75^{NGFR}-positive cells are genetically *Nf1* deficient. Finally, during neurofibroma progression, the continuously expanded cellular populations share the molecular and genetic characteristics (BLBP^{-}/Sox10^{-}/GFAP^{+}/p75^{+}/*Nf1*$^{-/-}$) with those early-stage tumor cells. Taken together, our data suggest that the initially expanded nonmyelinating Schwann cells are early-stage tumor cells, which are responsible for both the initiation and progression of plexiform neurofibromas.

Clinical Implication

Previous studies showed that overexpression of epidermal growth factor receptor (EGFR) or dominant negative ErbB4 induced similar hyperplastic lesions to that seen in P90 *Nf1*^{P0A}*KO* mutant nerves (Chen et al., 2003; Ling et al., 2005). However, these transgenic mice did not develop neurofibromas. Therefore, there must be some intrinsic increase of tumorigenic potential in *Nf1*$^{-/-}$ dSCs and uSCs and/or extrinsic field effects of *Nf1*$^{+/-}$ microenvironment. Intriguingly, we detected unmyelinated axonal degeneration and mast cell infiltration at the initiation phase of neurofibroma formation. Joseph et al. transplanted *Nf1*$^{-/-}$ NCSCs into sciatic nerves of adult *Nf1*$^{+/-}$ mice and observed no tumor formation 20 months after injection (Joseph et al., 2008 [this issue of Cancer Cell]). Therefore, it is tempting to speculate that such a degenerative and inflammatory microenvironment could provide a favorable niche for initial proliferation of *Nf1*$^{-/-}$ cells. Thus, the present study suggests potential future therapies for prevention and treatment of neurofibroma by stabilizing axon-Schwann cell interactions and reducing mast cell infiltration.

EXPERIMENTAL PROCEDURES

Control and Conditional Mutant Mice

The control mice used in this study are a pool of phenotypically indistinguishable mice with four genotypes: *Nf1*$^{flox/+}$;*P0A*-cre+, *Nf1*$^{flox/flox}$;*P0A*-cre−, *Nf1*$^{flox/-}$;*P0A*-Cre−, and *Nf1*$^{+/-}$. The mutant mice used were of the genotype, *Nf1*$^{flox/-}$;P0A-cre (mutants). The P0A-cre transgenic strain was initially generated on the FVB background (Giovannini et al., 2000). After five generations of being backcrossed to the 129 Svj background, the P0A-cre transgenic mice were crossed to the *Nf1*$^{flox/-}$ mice that were maintained on the 129 Svj background. Subsequent crosses generated control and mutant mice for analysis. The Rosa26-LacZ allele was maintained on the mixed 129 Svj and C57Bl6 backgrounds. The mutant mice with or without the Rosa26-LacZ allele exhibited similar phenotypes. All mice in this study were cared for according to the guidelines that were approved by the Animal Care and Use Committees of the University of Michigan at Ann Arbor.

Histological, Molecular, FACS, and Statistical Analyses

Detailed descriptions for these experimental procedures are provided in the Supplemental Data.

Supplemental Data

The Supplemental Data include Supplemental Experimental Procedures and 16 supplemental figures and can be found with this article online at http://www.cancercell.org/cgi/content/full/13/2/117/DC1/.

ACKNOWLEDGMENTS

We thank M. Hancock, J. Tomasek, L. Liu, and A. Wang for technical assistance; members of the Zhu lab for support; Dr. N. Joseph for assistance on FACS analysis; Drs. L. Parada and M. Giovannini for providing critical mouse strains and generous support in the early phases of the project; Dr. P. Charnay for *Krox20*-cre mice; S. Meshinchi at the MIL core facility for EM analysis; J. Kazemi at CSCAR for statistical analysis; Dr. N. Heintz for BLBP antibody and Drs. Y. Shen and K. Meiri for GAP-43 antibody; and Drs. E. Fearon, S. Morrison, and S. Weiss for critically reading the manuscript. This work is supported by grants from the American Cancer Society (ACS, no. RSG DDC-110857), the Department of Defense (DOD, NF050041), the Comprehensive Cancer Center and Biological Sciences Scholars Program of the University of Michigan (Y.Z.). Y.Z. is an ACS, GMCR, and BSSP Scholar.

Received: June 4, 2007
Revised: November 12, 2007
Accepted: January 3, 2008
Published: February 4, 2008

REFERENCES

Al-Hajj, M., Wicha, M.S., Benito-Hernandez, A., Morrison, S.J., and Clarke, M.F. (2003). Prospective identification of tumorigenic breast cancer cells. Proc. Natl. Acad. Sci. USA *100*, 3983–3988.

Ballester, R., Marchuk, D., Boguski, M., Saulino, A., Letcher, R., Wigler, M., and Collins, F. (1990). The NF1 locus encodes a protein functionally related to mammalian GAP and yeast IRA proteins. Cell *63*, 851–859.

Berger, P., Niemann, A., and Suter, U. (2006). Schwann cells and the pathogenesis of inherited motor and sensory neuropathies (Charcot-Marie-Tooth disease). Glia *54*, 243–257.

Britsch, S., Goerich, D.E., Riethmacher, D., Peirano, R.I., Rossner, M., Nave, K.A., Birchmeier, C., and Wegner, M. (2001). The transcription factor Sox10 is a key regulator of peripheral glial development. Genes Dev. *15*, 66–78.

Chen, S., Rio, C., Ji, R.R., Dikkes, P., Coggeshall, R.E., Woolf, C.J., and Corfas, G. (2003). Disruption of ErbB receptor signaling in adult non-myelinating Schwann cells causes progressive sensory loss. Nat. Neurosci. *6*, 1186–1193.

Cichowski, K., and Jacks, T. (2001). NF1 tumor suppressor gene function: narrowing the GAP. Cell *104*, 593–604.

Cichowski, K., Shih, T.S., Schmitt, E., Santiago, S., Reilly, K., McLaughlin, M.E., Bronson, R.T., and Jacks, T. (1999). Mouse models of tumor development in neurofibromatosis type 1. Science *286*, 2172–2176.

Dong, Z., Sinanan, A., Parkinson, D., Parmantier, E., Mirsky, R., and Jessen, K.R. (1999). Schwann cell development in embryonic mouse nerves. J. Neurosci. Res. *56*, 334–348.

Feldman, E.L., Russell, J.W., Sullivan, K.A., and Golovoy, D. (1999). New insights into the pathogenesis of diabetic neuropathy. Curr. Opin. Neurol. *12*, 553–563.

Garratt, A.N., Voiculescu, O., Topilko, P., Charnay, P., and Birchmeier, C. (2000). A dual role of erbB2 in myelination and in expansion of the schwann cell precursor pool. J. Cell Biol. *148*, 1035–1046.

Ghislain, J., Desmarquet-Trin-Dinh, C., Jaegle, M., Meijer, D., Charnay, P., and Frain, M. (2002). Characterisation of cis-acting sequences reveals a biphasic, axon-dependent regulation of Krox20 during Schwann cell development. Development *129*, 155–166.

Giovannini, M., Robanus-Maandag, E., van der Valk, M., Niwa-Kawakita, M., Abramowski, V., Goutebroze, L., Woodruff, J.M., Berns, A., and Thomas, G. (2000). Conditional biallelic Nf2 mutation in the mouse promotes manifestations of human neurofibromatosis type 2. Genes Dev. *14*, 1617–1630.

Gitler, A.D., Zhu, Y., Ismat, F.A., Lu, M.M., Yamauchi, Y., Parada, L.F., and Epstein, J.A. (2003). Nf1 has an essential role in endothelial cells. Nat. Genet. *33*, 75–79.

Halliday, A.L., Sobel, R.A., and Martuza, R.L. (1991). Benign spinal nerve sheath tumors: their occurrence sporadically and in neurofibromatosis types 1 and 2. J. Neurosurg. *74*, 248–253.

Hjerling-Leffler, J., Marmigere, F., Heglind, M., Cederberg, A., Koltzenburg, M., Enerback, S., and Ernfors, P. (2005). The boundary cap: a source of neural crest stem cells that generate multiple sensory neuron subtypes. Development *132*, 2623–2632.

Hu, X., Hicks, C.W., He, W., Wong, P., Macklin, W.B., Trapp, B.D., and Yan, R. (2006). Bace1 modulates myelination in the central and peripheral nervous system. Nat. Neurosci. *9*, 1520–1525.

Jessen, K.R., and Mirsky, R. (2005). The origin and development of glial cells in peripheral nerves. Nat. Rev. Neurosci. *6*, 671–682.

Jessen, K.R., Brennan, A., Morgan, L., Mirsky, R., Kent, A., Hashimoto, Y., and Gavrilovic, J. (1994). The Schwann cell precursor and its fate: a study of cell death and differentiation during gliogenesis in rat embryonic nerves. Neuron *12*, 509–527.

Joseph, N.M., Mukouyama, Y.S., Mosher, J.T., Jaegle, M., Crone, S.A., Dormand, E.L., Lee, K.F., Meijer, D., Anderson, D.J., and Morrison, S.J. (2004). Neural crest stem cells undergo multilineage differentiation in developing peripheral nerves to generate endoneurial fibroblasts in addition to Schwann cells. Development *131*, 5599–5612.

Joseph, N.M., Mosher, J.T., Buchstaller, J., Snider, P., McKeever, P.E., Lim, M., Conway, S.J., Parada, L.F., Zhu, Y., and Morrison, S.J. (2008). The loss of Nf1 transiently promotes self-renewal but not tumorigenesis by neural crest stem cells. Cancer Cell *13*, this issue, 129–140.

Kleihues, P., and Cavenee, W.K. (2000). Pathology and Genetics of Tumors of the Nervous System (Lyon, France: iARC Press).

Korf, B.R. (1999). Plexiform neurofibromas. Am. J. Med. Genet. *89*, 31–37.

Kruger, G.M., Mosher, J.T., Bixby, S., Joseph, N., Iwashita, T., and Morrison, S.J. (2002). Neural crest stem cells persist in the adult gut but undergo changes in self-renewal, neuronal subtype potential, and factor responsiveness. Neuron *35*, 657–669.

Kurtz, A., Zimmer, A., Schnutgen, F., Bruning, G., Spener, F., and Muller, T. (1994). The expression pattern of a novel gene encoding brain-fatty acid binding protein correlates with neuronal and glial cell development. Development *120*, 2637–2649.

Lassmann, H., Jurecka, W., Lassmann, G., Gebhart, W., Matras, H., and Watzek, G. (1977). Different types of benign nerve sheath tumors. Light microscopy, electron microscopy and autoradiography. Virchows Arch. *375*, 197–210.

Ling, B.C., Wu, J., Miller, S.J., Monk, K.R., Shamekh, R., Rizvi, T.A., Decourten-Myers, G., Vogel, K.S., DeClue, J.E., and Ratner, N. (2005). Role for the epidermal growth factor receptor in neurofibromatosis-related peripheral nerve tumorigenesis. Cancer Cell *7*, 65–75.

Maro, G.S., Vermeren, M., Voiculescu, O., Melton, L., Cohen, J., Charnay, P., and Topilko, P. (2004). Neural crest boundary cap cells constitute a source of neuronal and glial cells of the PNS. Nat. Neurosci. *7*, 930–938.

Miller, S.J., Li, H., Rizvi, T.A., Huang, Y., Johansson, G., Bowersock, J., Sidani, A., Vitullo, J., Vogel, K., Parysek, L.M., et al. (2003). Brain lipid binding protein in axon-Schwann cell interactions and peripheral nerve tumorigenesis. Mol. Cell. Biol. *23*, 2213–2224.

Morrison, S.J., White, P.M., Zock, C., and Anderson, D.J. (1999). Prospective identification, isolation by flow cytometry, and in vivo self-renewal of multipotent mammalian neural crest stem cells. Cell *96*, 737–749.

Murphy, P., Topilko, P., Schneider-Maunoury, S., Seitanidou, T., Baron-Van Evercooren, A., and Charnay, P. (1996). The regulation of Krox-20 expression reveals important steps in the control of peripheral glial cell development. Development *122*, 2847–2857.

Peirano, R.I., Goerich, D.E., Riethmacher, D., and Wegner, M. (2000). Protein zero gene expression is regulated by the glial transcription factor Sox10. Mol. Cell. Biol. *20*, 3198–3209.

Riccardi, V.M. (1992). Neurofibromatosis: Phenotype, Natural History, and Pathogenesis, Second Edition (Baltimore and London: Johns Hopkins University Press).

Rutkowski, J.L., Wu, K., Gutmann, D.H., Boyer, P.J., and Legius, E. (2000). Genetic and cellular defects contributing to benign tumor formation in neurofibromatosis type 1. Hum. Mol. Genet. *9*, 1059–1066.

Serra, E., Puig, S., Otero, D., Gaona, A., Kruyer, H., Ars, E., Estivill, X., and Lazaro, C. (1997). Confirmation of a double-hit model for the NF1 gene in benign neurofibromas. Am. J. Hum. Genet. *61*, 512–519.

Serra, E., Rosenbaum, T., Winner, U., Aledo, R., Ars, E., Estivill, X., Lenard, H.G., and Lazaro, C. (2000). Schwann cells harbor the somatic NF1 mutation in neurofibromas: evidence of two different Schwann cell subpopulations. Hum. Mol. Genet. *9*, 3055–3064.

Sheela, S., Riccardi, V.M., and Ratner, N. (1990). Angiogenic and invasive properties of neurofibroma Schwann cells. J. Cell Biol. *111*, 645–653.

Singh, S.K., Hawkins, C., Clarke, I.D., Squire, J.A., Bayani, J., Hide, T., Henkelman, R.M., Cusimano, M.D., and Dirks, P.B. (2004). Identification of human brain tumour initiating cells. Nature *432*, 396–401.

Soriano, P. (1999). Generalized lacZ expression with the ROSA26 Cre reporter strain. Nat. Genet. *21*, 70–71.

Taveggia, C., Zanazzi, G., Petrylak, A., Yano, H., Rosenbluth, J., Einheber, S., Xu, X., Esper, R.M., Loeb, J.A., Shrager, P., et al. (2005). Neuregulin-1 type III determines the ensheathment fate of axons. Neuron *47*, 681–694.

Voiculescu, O., Charnay, P., and Schneider-Maunoury, S. (2000). Expression pattern of a Krox-20/Cre knock-in allele in the developing hindbrain, bones, and peripheral nervous system. Genesis *26*, 123–126.

Waggoner, D.J., Towbin, J., Gottesman, G., and Gutmann, D.H. (2000). Clinic-based study of plexiform neurofibromas in neurofibromatosis 1. Am. J. Med. Genet. *92*, 132–135.

Wheeler, E.F., Gong, H., Grimes, R., Benoit, D., and Vazquez, L. (1998). p75NTR and Trk receptors are expressed in reciprocal patterns in a wide variety of non-neural tissues during rat embryonic development, indicating independent receptor functions. J. Comp. Neurol. *391*, 407–428.

Willem, M., Garratt, A.N., Novak, B., Citron, M., Kaufmann, S., Rittger, A., DeStrooper, B., Saftig, P., Birchmeier, C., and Haass, C. (2006). Control of peripheral nerve myelination by the beta-secretase BACE1. Science *314*, 664–666.

Woodruff, J.M. (1999). Pathology of tumors of the peripheral nerve sheath in type 1 neurofibromatosis. Am. J. Med. Genet. *89*, 23–30.

Xu, G.F., Lin, B., Tanaka, K., Dunn, D., Wood, D., Gesteland, R., White, R., Weiss, R., and Tamanoi, F. (1990). The catalytic domain of the neurofibromatosis type 1 gene product stimulates ras GTPase and complements ira mutants of S. cerevisiae. Cell *63*, 835–841.

Zhu, Y., and Parada, L.F. (2002). The molecular and genetic basis of neurological tumours. Nat. Rev. Cancer *2*, 616–626.

Zhu, Y., Romero, M.I., Ghosh, P., Ye, Z., Charnay, P., Rushing, E.J., Marth, J.D., and Parada, L.F. (2001). Ablation of NF1 function in neurons induces abnormal development of cerebral cortex and reactive gliosis in the brain. Genes Dev. *15*, 859–876.

Zhu, Y., Ghosh, P., Charnay, P., Burns, D.K., and Parada, L.F. (2002). Neurofibromas in NF1: Schwann cell origin and role of tumor environment. Science *296*, 920–922.

Supplemental experimental procedures

Tissue Processing

For histological analysis, we utilized both paraffin sections and frozen sections. For both section techniques, control and mutant littermates at P22, P90, 6-12 months and 12-20 months of age were perfused with 4% paraformaldehyde (PFA). For paraffin sections, sciatic nerves were dissected, post-fixed in PFA overnight at 4°C, and processed for paraffin embedding. Sciatic nerves were sectioned longitudinally at 5 μm thickness. For frozen sections, sciatic nerves were dissected, post-fixed in PFA for 2 hours at 4°C and transferred to 30% sucrose overnight at 4°C. Tissue was embedded in using O.C.T. compound (Tissue-Tek) and frozen in crushed dry ice. Sciatic nerves were sectioned longitudinally at 6 or 14 μm thickness.

Histology and tumor grading

Two to three paraffin sectioned slides were stained with hematoxylin/eosin (H&E). Diagnosis for each sciatic nerve lesion was generated based upon histology from H&E stained sections under the light microscopy. The penetrance and frequency of neurofibromas or pre-neoplastic lesions in control and mutant mice was quantified based upon sciatic nerve diagnoses. Quantification of the number of cells per surface area (mm^2) in P22 and P90 control and mutant sciatic nerves was performed using ImageJ on digital images of H&E stained sections. For PCR analysis, tissues were dissected in ice-cold PBS and digested with proteinase K as described (Zhu et al., 2005).

Immunohistochemistry and Immunofluorescence

Immunohistochemistry was performed on both paraffin and frozen sections. The visualization of primary antibodies was performed with the avidin-biotin horseradish peroxidase system (Vectastain ABC kit, Vector). The dilutions of primary antibodies used on paraffin sections in this study were: anti-S100 (rabbit, 1:100, Signet), anti-$p75^{NGFR}$ (rabbit, 1:4,000, Chemicon). The dilutions of primary antibodies used on frozen sections in this study were: anti-S100 (rabbit, 1:300, Signet), anti-BLBP (rabbit, 1:5,000, a gift from N. Heintz), anti-GAP43 (mouse, 1:500, a gift from Drs. Y. Shen and K. Meiri)

and anti-$p75^{NGFR}$ (rabbit, 1:8,000, Chemicon).

Immunofluorescence was performed on both paraffin and frozen sections. Visualization of primary antibodies was performed by using Cy3-conjugated anti-rabbit/goat/rat and Cy2-conjugated anti-mouse/rabbit secondary antibodies (1:200, Jackson ImmunoResearch). The dilutions of primary antibodies used in this study are as follows: anti-BLBP (rabbit, 1:2,000, a gift from N. Heintz), anti-GAP43 (mouse, 1:2,000, a gift from Drs. Y. Shen and K. Meiri), anti-$p75^{NFGR}$ (rabbit, 1:10,000, Chemicon), anti-Sox10 (rabbit, 1:500, Chemicon), anti-β-gal (goat, 1:10,000, AbD Serotec), anti-GFAP (rabbit, 1:2,000, DAKO), anti-BrdU (rat, 1:500, Abcam) and anti-Tuj1 (mouse, 1:1,000, Covance). DAPI (1μg/ml, Molecular Probes) was used to visualize nuclei. Sections were examined under a fluorescence microscope (Olympus).

Semithin and ultrathin preparation

Control and mutant littermates were perfused with 4% PFA and 2.5% gluteraldehyde. Sciatic nerves were dissected and post-fixed in 4% PFA and 2.5% gluteraldehyde overnight at 4°C. Nerves were then post-fixed in OsO_4 for 1 hour and embedded in epoxy resin. Semithin sections were cut with a glass knife at 0.5 μm and stained with toluidine blue for visualization. Ultrathin sections were cut with a diamond knife at 75 nm and visualized using transmission electron microscope (TEM). For P22 pups, 2 control and 4 mutant sciatic nerves were analyzed using four or five low magnification fields from each nerve. For P90 mice, 2 controls nerves and 3 mutant nerves were analyzed using seven or nine low magnification fields from each nerve. Each field was taken at the same low magnification, and total endoneurial area in each image calculated by the ImageJ software package. Higher magnification images for most areas in each field were taken. The number of mSCs, nmSCs, anmSCs, and dSCs were quantified for each field based on morphology in high magnification images. The axon number per Remak bundle for which nmSCs, anmSCs or dSCs ensheathed was counted and categorized into single, 2-10, 11-20, 21-30 or greater than 30. Axons in each Schwann cell pocket was counted and categorized into single, 2-10 or 11-50. The cell density for each population was normalized by the surface area sampled.

Statistical analysis for EM data

Cell densities from the same low magnifications image cannot be considered independent since cells from the same nerve tend to be correlated as evident by an interclass correlation coefficient (ICC) of 0.2. Thus, we utilized linear mixed models from the SPSS 15 statistical package in order to determine if there was a difference in population for nmSC, anmSC, dSC, mSC and axons per Remak bundle in control and mutant nerves. Genotype was set as the fixed factor while nerve was set as a random factor in order to generate accurate P-values and error bars. Chi-squared goodness-of-fit tests were used to compare control and mutant distributions for axon pocketing at P22. $P < 0.05$ was considered to be statistically significant. One mutant P90 sciatic nerve had an intermediate phenotype between that of control and mutants. For the purposes of nmSC distribution and axon density distribution into axons per Remak bundle analysis, this mutant was excluded in order to better document the changes in cellular distribution of the more severely affected mutant mice.

LacZ staining

The R26R-LacZ allele was introduced to the control and mutant mice. Mice with genotypes of $NF1^{flox/+}$;P0A-cre+;R26R-LacZ+ (control) and $NF1^{flox/-}$;P0A-cre+;R26R-LacZ+ (mutant) were generated. Embryos from double transgenic P0A-cre/R26R-LacZ mice were collected at E9.5, E10.5, E11.5, and E12.5, and subjected to whole-mount X-gal staining as described previously (Zhu et al., 2001). Fifty μm vibratome sections and 14 μm frozen sections were generated from the whole-mount stained embryos. Serial sections from multiple levels of the sciatic nerve were subjected to nuclear fast red counterstaining, immunohistochemistry or immunofluorescence. Similarly, sciatic nerves from control and mutant mice carrying the R26R-LacZ allele at P90 were dissected and frozen sections were analyzed with X-gal and X-gal/anti-$p75^{NGFR}$ antibody staining.

BrdU assay

Control and mutant mice were pulsed with 50 μg/g (gram, body mass) of BrdU five times a day at 2-hour intervals. Mice were perfused with 4% PFA 2 hours after the last pulse.

Sciatic nerves were prepared for frozen sections. BrdU immunofluorescence was performed as described previously (Zhu et al., 1998). The number of BrdU-positive cells was quantified and statistical analysis was carried out using two tail Student's *t*-test. $P < 0.05$ was considered to be statistically significant.

FACS Analysis

Age matched 3 month to 5 month old $NF1^{flox/-}$;P0A-cre+, $NF1^{flox/flox}$;P0A-cre+ and $NF1^{flox/flox}$; P0A-cre- mice were injected with BrdU at 50 μg/g for 5 consecutive days. At these stages, $NF1^{flox/-}$;P0A-cre+ and $NF1^{flox/flox}$;P0A-cre+ mutant mice exhibited indistinguishable phenotypes in sciatic nerves. BrdU was also added to the drinking water of the mice at 1 mg/ml for the duration of the injections. Sciatic nerves were dissected from BrdU treated mice following the final day of treatment and collected in ice-cold Ca, Mg-free HBSS. Nerves were dissociated for 30 min at 37°C in 1 mg/ml type IV collagenase (Worthington) followed by 20 min at 37°C in 0.5% trypsin/EDTA (Invitrogen). The reaction was quenched with staining medium: L15 medium containing 1 mg/ml BSA (Sigma A-3912), 10 mM HEPES (pH 7.4), 1% penicillin/streptomycin (BioWhittaker), and 25 mg/ml deoxyribonuclease type 1 (DNase1, Sigma D-4527). Cells were centrifuged, resuspended in staining medium without DNase, triturated, and filtered through nylon screen (45 mm, Sefar America) to remove aggregates. Cell suspensions were stained with antibodies against $p75^{NGFR}$ (rabbit, 1:2,000, Chemicon) and BrdU (FITC BrdU Flow Kit, BD Pharmagen) for analysis of the frequency of $p75^{NGFR}$+ and BrdU+ cells by flow-cytometry (Bixby et al., 2002). Flow-cytometry was performed with a FACSVantage SE-dual laser, three-line flow-cytometer (Becton-Dickinson). For statistical analysis, two tailed Student's *t*-tests were performed to compare differences in population distribution of $p75^{NGFR}$-/BrdU-, $p75^{NGFR}$-/BrdU+, $p75^{NGFR}$+/BrdU-, $p75^{NGFR}$+/BrdU+, $p75^{NGFR}$+ and BrdU+ FACS sorted cells from $NF1^{flox/-}$;P0A-cre+ and $NF1^{flox/flox}$;P0A-cre+ nerves. For each category compared, a P-value of > 0.5 was obtained. Thus, we grouped mice with genotypes of $NF1^{flox/-}$;P0A-cre+ and $NF1^{flox/flox}$;P0A-cre+ together as the Mutants category. Two tailed Student's *t*-tests was conducted between Mutants and $NF1^{flox/flox}$; P0A-cre- (Control) for each of the above categories. $P < 0.05$ was considered to be statistically significant.

Apoptosis analysis

TUNEL staining (ApopTag Peroxidase In Situ Apoptosis Detection Kit, Chemicon) was performed on paraffin sections. Immunofluorescence with antibody against Cleaved caspase-3 (rabbit, 1:800, Cell Signaling) was performed on frozen sections. Electron micrographs from P22 and P90 nerves were analyzed for apoptotic Schwann cells, as defined by coarse chromatin, aggregation in the nucleus, vacuolation in the cytoplasm and condensed rough endoplasmic reticulum associated with loss of perikaryal volume (Feldman et al., 1999).

Mast cell quantification

One to three H&E stained slides of sciatic nerves were taken from 22 days old and 90 days old mice for mast cells quantification. All of these H&E stained slides were scanned and the sections that had best histology were selected for analysis. Mast cells were counted for each section individually using 40X magnification under a light microscope. The area of the nerve was calculated using the ImageJ software package and mast cell density was calculated as the number of cells per surface area (mm^2). Statistical analysis was carried out using two tail Student's *t*-test. $P < 0.05$ was considered to be statistically significant.

Supplemental figure legends

Supplemental Figure 1. The scheme of Schwann cell development in mouse sciatic nerves and the expression pattern of Krox20-cre and P0A-cre transgenes.

The terms used for describing Schwann cells at different developmental stages were based upon a recent review by Jessen and Mirsky (Jessen and Mirsky, 2005). NCC, neural crest cell; SCP/NCSC, Schwann cell precursor/Neural crest stem cell; SC, Schwann cell; nmSC, non-myelinating Schwann cell; mSC, myelinating Schwann cell.

Supplemental figure 2. P0A-cre mediated recombination at E9.5 and E10.5.

Embryos with both P0A-cre and R26R-LacZ transgenes at E9.5 (A) and E10.5 (B-D)

were subjected to whole-mount X-gal staining. Arrows in A, B point to cranial-facial staining of the embryos. Of note, at these stages, except for the notochord, no Cre-mediated β-gal expression was detected in the trunk region. Scale bar: 1 mm.

Supplemental Figure 3. P0A-cre mediated recombination at E11.5 and E12.5.

Embryos with both P0A-cre and R26R-LacZ transgenes at E11.5 (A) and E12.5 (B) were subjected to X-gal staining. (Aa-Ad and Ba-Bd) High magnification views of the E11.5 (A) and E12.5 (B) embryos show that P0A-cre-mediated recombination in peripheral nerves is more robust in the lumbar region (arrows, Ac and Bc) than in the thoracic region (Aa and Ba). The dashed lines in Aa, Ba mark the border of the thoracic and lumbar regions. Arrows in Ab,d and Bb,d point to peripheral nerves innervating both forelimbs (Ab, Bb) and hindlimbs (Ad, Bd). The LacZ staining pattern suggests that Cre-mediated recombination occurs broadly throughout the developing peripheral nerves when SCP/NCSCs are first generated. (C) Thoracic sections from X-gal stained E12.5 embryos were subsequently stained with BLBP (Ca-Cc), and S100 (Cd-Cf) antibodies. Arrows in Cf point to a group of S100-positive cells in the peripheral nerves in the thoracic region of E12.5 embryos. Presence of S100-positive cells is consistent with the observation that nervous system development occurs earlier in thoracic regions than lumbar regions. Scale bar: (A, B), 1 mm; (C), 50 μm.

Supplemental Figure 4. $p75^{NGFR}$ expression is not restricted to developing peripheral nervous system.

Double immunofluorescence was performed with antibodies against Tuj1 and $P75^{NGFR}$ (A, C, E) or Tuj1 and BLBP (B, D, F) on lumbar sections from E12.5 embryos. Tuj1 and BLBP staining are both restricted to developing peripheral nerves, but $p75^{NGFR}$ staining also can be seen in non-neural tissue (arrows). Scale bar: 50 μm.

Supplemental figure 5. Immunohistochemical analysis of neurofibromas in sciatic nerves.

Sciatic nerves from mutant mice harboring neurofibromas were sectioned and stained with anti-S100 and anti-$p75^{NGFR}$ antibodies. The expression levels of S100 and $p75^{NGFR}$

are variable in neurofibromas. Some tumors have high levels of S100 and p75NGFR expression (A and E, B and F) while other tumors have relatively lower expression levels (C and G, D and H). Furthermore, there is variation in expression level of these markers between cells within the same neurofibroma (A and E, C and G, D and H), indicating heterogeneous nature of these tumors. The dashed lines (D and H) mark the border of hyperplasia and neurofibroma. Scale bar: 50 μm.

Supplemental figure 6. Analysis of Krox20-cre-mediated recombination.
(A-C) E12.5 double transgenic Krox20-cre/R26R-LacZ embryos were subjected to a X-gal staining assay. Cre-mediated β-gal expression is restricted to cranial nerves and proximal parts of spinal nerves (spinal roots, arrows, B) in E12.5 embryos. Arrows in A point to forelimb and hindlimb, confirming no β-gal expression in distal parts of spinal nerves including sciatic nerves. (D) Verification that Krox20-cre induces recombination of the NF1 flox allele only in Schwann cell containing tissues. Genomic DNAs were extracted from adult $NF1^{flox/+}$;Krox20-cre+ mice and were subjected to PCR analysis. Lane 1, forebrain; lane 2, brainstem; lane 3, cerebellum; lane 4, spinal cord; lane 5, lung; lane 6, kidney; lane 7 liver; lane 8, muscle; lane 9, skin; lane 10, spinal roots; lane 11, sciatic nerve; lane 12, trigeminal nerve. Only tissues having significant numbers of Schwann cells such as spinal roots, sciatic nerves and trigeminal nerves (*lane 10-12) have the recombined (Rcre) flox allele. Sciatic nerves from Krox20-cre/R26R-LacZ (E) and P0A-cre/R26R-LacZ (F) double transgenic mice at ages of 12 months were sectioned and stained with a X-gal staining assay. No significant difference in β-gal staining was observed in sciatic nerves between these two Cre transgenic strains. Scale bar: (A-C), 1 mm; (E, F), 50 μm.

Supplemental figure 7. Summary statistics of electron microscopic quantification of P22 and P90 sciatic nerves.
(A) Quantification of the numbers of mSCs and nmSCs per surface area (1,000 μm^2) in P22 control and mutant sciatic nerves. (B) The numbers of Remak bundles per surface area (1,000 μm^2) in control and mutant P22 sciatic nerves were categorized into five groups based upon the number of axons that they ensheathed. Mean and 95% confidence

intervals are generated from summary statistics. P-values are generated using linear mixed models. (C) Distribution of endoneurial cell types in P90 control and mutant sciatic nerves. Pooled nmSC represent combined putative nmSC-lineage cells, including anmSC and dSC. Mean and 95% confidence intervals are generated from summary statistics. P-values are generated using linear mixed models. Note that the majority of cell types in both mutant and control are in the Schwann cell lineage. Three cell types or tissues including mast cells, macrophages, and blood vessels were labeled with asterisks (*) because the number of these cells in cross EM sections was too few to get any significance between control and mutant nerves. (D) Axonal distribution into Remak bundles. Remak bundles analyzed are from the pooled nmSC population including nmSCs, anmSCs and dSCs. The numbers of axons per surface area (1,000 μm^2) in P90 control (green) and mutant (red) sciatic nerves were categorized into five groups based upon the number of axons within each Remak bundle. For mutant nerves, the axon number was pooled from all three non-myelinating Schwann cell populations (nmSCs, anmSCs and dSCs). As compared to controls, axonal distribution in mutant nerves is shifted from Remak bundles with >20 axons to Remak bundles that ensheath <11 axons. This shift in distribution suggests that the Remak bundles ensheathing a large number of axons are replaced by multiple Remak bundles ensheathing fewer axons in mutant nerves. The total number of axons is slightly reduced in mutant sciatic nerves.

Supplemental figure 8. Little evidence of apoptosis in P22 and P90 sciatic nerves.
TUNEL was performed on sections of DNase I treated (A), control (B) and mutant sciatic nerves (C, D) from P90 mice. DNase I treated sections served as a positive control. A cluster of positive cells was detected in only one of ten mutant nerves analyzed (D, arrow). Immunofluorescence was performed with antibodies against cleaved caspase 3 on sectioned MPNST (E) and P90 control (F) and mutant sciatic nerves (G, H). Sections from MPNSTs served as a positive control. (I) Summary of three independent methods to detect apoptotic cells. Apoptosis via TUNEL staining was below detection limit for P22 and P90 control nerves, while only a single cluster of positive cells was detected in one P90 mutant nerve. Cleaved caspase-3 immunofluorescence was not detected in either control or mutant nerves. No Schwann cells that displayed apoptotic morphology were

detected via electron microscopy in either control or mutant nerves. Together, this data suggests that no excess apoptosis was observed in P22 or P90 NF1 mutant nerves. Scale bar: 50 μm.

Supplemental figure 9. NF1 deficiency leads to increased numbers of $p75^{NGFR}$-expressing cells during young adulthood.

Sciatic nerves from P90 mice were sectioned and stained with H&E (A, B), anti-S100 (C, D) and anti- $p75^{NGFR}$ (E, F) antibodies. There is an appreciable increase in cellularity in the mutant nerves (B) compared to control nerves (A). While there is no change in the S100 expression pattern (C, D), mutant nerves (F) have increased numbers of p75NGFR staining cells compared to control nerves (E). Together, this data suggests an expansion of the nmSC lineage in mutant nerves. Scale bar: 50 μm.

Supplemental figure 10. NF1 deficiency leads to increased numbers of Sox10 negative cells during young adulthood.

Immunofluorescence was performed with antibodies against Sox10 (A, D, G, I), a marker specific for mSCs in adult nerves, and counterstained with DAPI (B, E, H, J) on P90 control and mutant sciatic nerves. Although similar number of Sox10-positive nuclei was observed between control (C) and mutant nerves (F), more Sox10-negative nuclei were identified in mutant nerves. (K) Quantification of Sox10 positive (arrowheads in G-J) and negative (arrows in G-J) nuclei. Together, these data suggest that there is no expansion in the mSC lineage. As SCs constitute the majority of nuclei in adult nerves, this data also suggests that the expansion in the nmSC lineage accounts for cellular hyperplasia. Scale bar: 50 μm.

Supplemental figure 11. NF1 deficiency leads to increased numbers of GFAP-expressing cells during young adulthood.

Immunofluorescence was performed with antibodies against GFAP (A, D, G, J) and counterstained with DAPI (B, E, H, K) on P90 control and mutant sciatic nerves. Mutant sciatic nerves (F, L) have conspicuously more GFAP-positive cells than those in controls (C, I), suggesting an expansion in the nmSC lineage. Arrows in G to L point to GFAP-

positive cells in control and mutant nerves. Arrowheads in L point to a cluster of GFAP-positive nuclei. Scale bar: 50 μm.

Supplemental figure 12. NF1 deficiency leads to increased numbers of $p75^{NGFR}$-expressing cells with focal loss of Tuj1-positive axons during young adulthood.
Immunofluorescence was performed with antibodies against Tuj1 (A, E, I, M), $p75^{NGFR}$ (B, F, J, N), Tuj1/$p75^{NGFR}$ (Overlay images, C, G, K, O) and counterstained with DAPI (D, H, L, P) on P90 control and mutant sciatic nerves. In these 5 μm thin paraffin sections, most of $p75^{NGFR}$-expression do not overlap with axonal Tuj1 staining, suggesting that the increased $p75^{NGFR}$ expression in mutant nerves (F, N) compared to controls (B, J) was due to cellular expansion in non-myelinating Schwann cells. Arrows point to $p75^{NGFR}$-expressing cells in control (K, L) and mutant (O, P) nerves. Arrowheads in O and P point to clusters of $p75^{NGFR}$-positive nuclei. The dashed lines in M to P mark the area in mutant nerves with focal increase in $p75^{NGFR}$-positive cells that was accompanied by focal loss of Tuj1 staining. Scale bar: 50 μm.

Supplemental figure 13. NF1 deficiency leads to increase in mast cell infiltration into the sciatic nerve during young adulthood.
Sciatic nerves from P22 and P90 control and mutant mice were sectioned and H&E stained. Mast cells were identified by their distinct morphology with hematoxylin stained granulation. The number of mast cells was quantified and normalized by surface area. While mast cells have not yet infiltrated into nerves at P22, there is over a 2.5 fold increase in mast cells in the P90 mutant nerves as compared to control nerves. ***$P < 0.001$.

Supplemental figure 14. Ultrastructural analysis of neurofibroma.
Electron micrographs show control nerves (A, D), hyperplastic lesions (B, E), and neurofibromas (C, F) of mutant sciatic nerves. Arrows in E, F point to abnormal cells completely unassociated with axons (Ax). *, denoting degenerating axons. Very few normal non-myelinating Schwann cells were observed in neurofibromas, which is consistent with the observation that degeneration of this cell lineage was detected at the

initiation stage of neurofibroma formation. (G, H) Two examples of unassociated Schwann cells (uSCs) with continuous basal lamina (arrows). (I) A perineurial-like cell lacking a continuous basal lamina and surrounds axons in a concentric fashion. Scale bar: 1 μm.

Supplemental figure 15. Expansion of NF1 deficient cells in aged mutant sciatic nerves. The R26R-LacZ allele was introduced to the control and mutant mice. Sciatic nerves from aged mice were sectioned and stained with X-gal. The population of X-gal positive cells has greatly expanded while X-gal negative tissue has remained constant or has reduced. This suggests that NF1 deficient cells have a growth advantage and continuously expand during neurofibroma progression. Scale bar: 50 μm.

Supplemental figure 16. We propose a two-step model for neurofibroma formation. At the initiation phase, NF1 inactivation in fetal stem/progenitor cells (SCP/NCSCs) during development leads to abnormally differentiated Remak bundles with the "pocket defect", which are characterized by presence of poorly segregated axons and/or ectopic myelination. Schwann cells and axons in these abnormal Remak bundles are unstable and progressively lose contact, leading to axonal degeneration and generation of dissociated Schwann cells (dSCs) and unassociated Schwann cells (uSCs). The presence of these abnormal cells and axonal degeneration elicit an inflammatory response characterized by infiltration of mast cells, creating a permissive condition for expansion of dSCs and uSCs. Neurofibroma progression involves further expansion of dSCs and uSCs as well as the subsequent degeneration of myelinated axon-Schwann cell units. Black dot, collagen fiber; blue star and dot, mast cells; black circle, myelinating Schwann cells; red dot, dissociating/unassociated Schwann cells; green dot, fibroblasts; *, demyelination.

REFERENCES

Bixby, S., Kruger, G. M., Mosher, J. T., Joseph, N. M., and Morrison, S. J. (2002). Cell-intrinsic differences between stem cells from different regions of the peripheral nervous system regulate the generation of neural diversity. Neuron *35*, 643-656.

Britsch, S., Goerich, D. E., Riethmacher, D., Peirano, R. I., Rossner, M., Nave, K. A., Birchmeier, C., and Wegner, M. (2001). The transcription factor Sox10 is a key regulator of peripheral glial development. Genes Dev *15*, 66-78.

Feldman, E. L., Russell, J. W., Sullivan, K. A., and Golovoy, D. (1999). New insights into the pathogenesis of diabetic neuropathy. Current opinion in neurology *12*, 553-563.

Jessen, K. R., and Mirsky, R. (2005). The origin and development of glial cells in peripheral nerves. Nat Rev Neurosci *6*, 671-682.

Zhu, Y., Harada, T., Liu, L., Lush, M. E., Guignard, F., Harada, C., Burns, D. K., Bajenaru, M. L., Gutmann, D. H., and Parada, L. F. (2005). Inactivation of NF1 in CNS causes increased glial progenitor proliferation and optic glioma formation. Development *132*, 5577-5588.

Zhu, Y., Richardson, J. A., Parada, L. F., and Graff, J. M. (1998). Smad3 mutant mice develop metastatic colorectal cancer. Cell *94*, 703-714.

Zhu, Y., Romero, M. I., Ghosh, P., Ye, Z., Charnay, P., Rushing, E. J., Marth, J. D., and Parada, L. F. (2001). Ablation of NF1 function in neurons induces abnormal development of cerebral cortex and reactive gliosis in the brain. Genes Dev *15*, 859-876.

Supplemental Figure 1

Schwann cell development and the expression pattern of P0A and Krox20 promoters

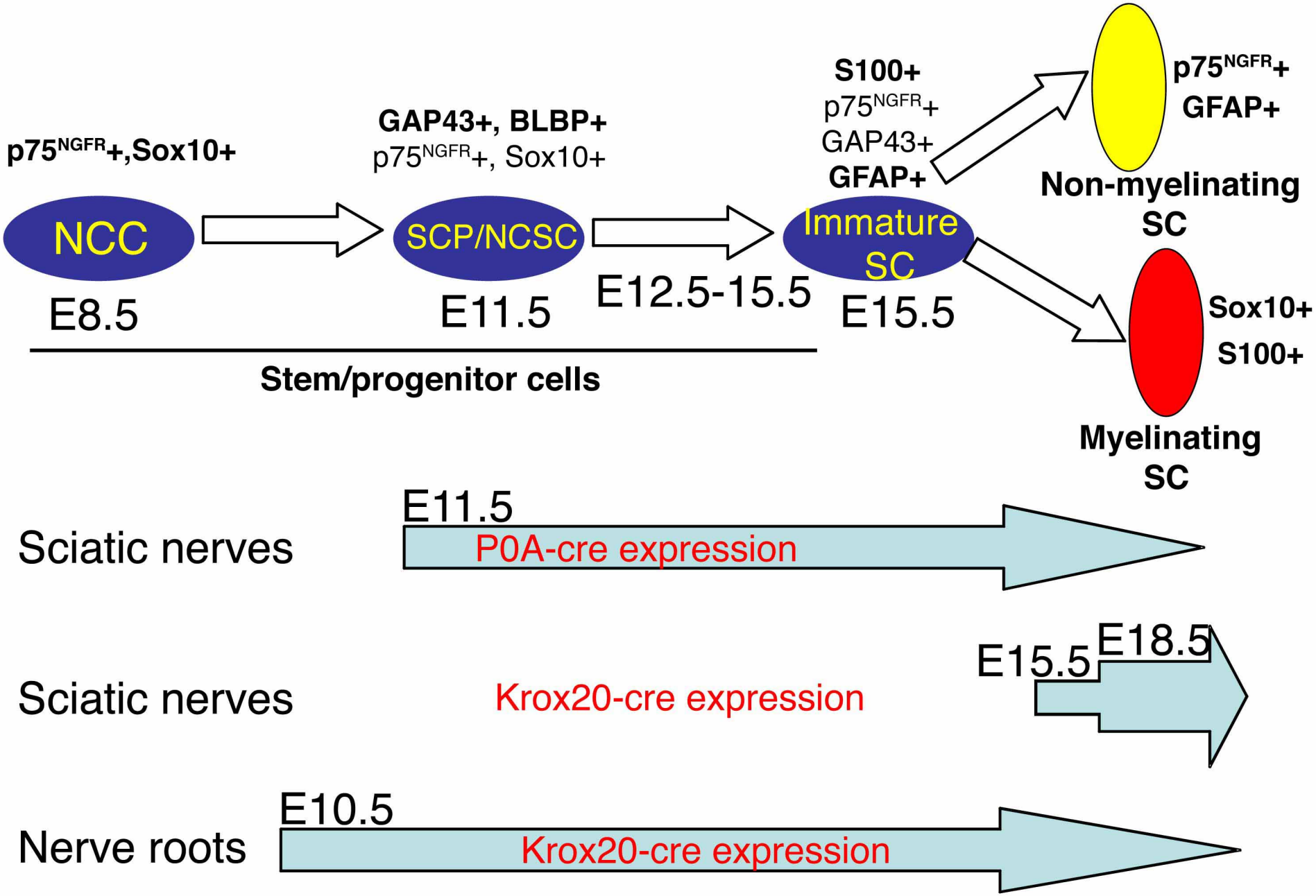

Supplemental Figure 2

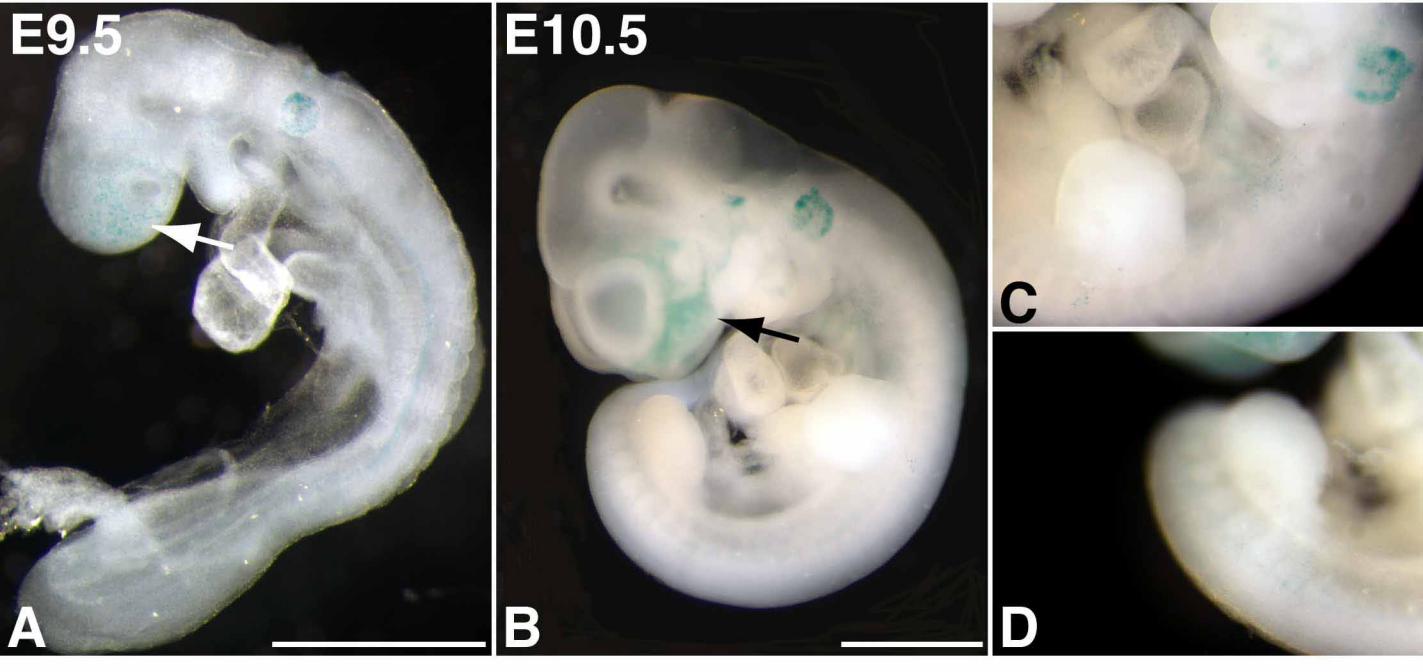

Supplemental Figure 3

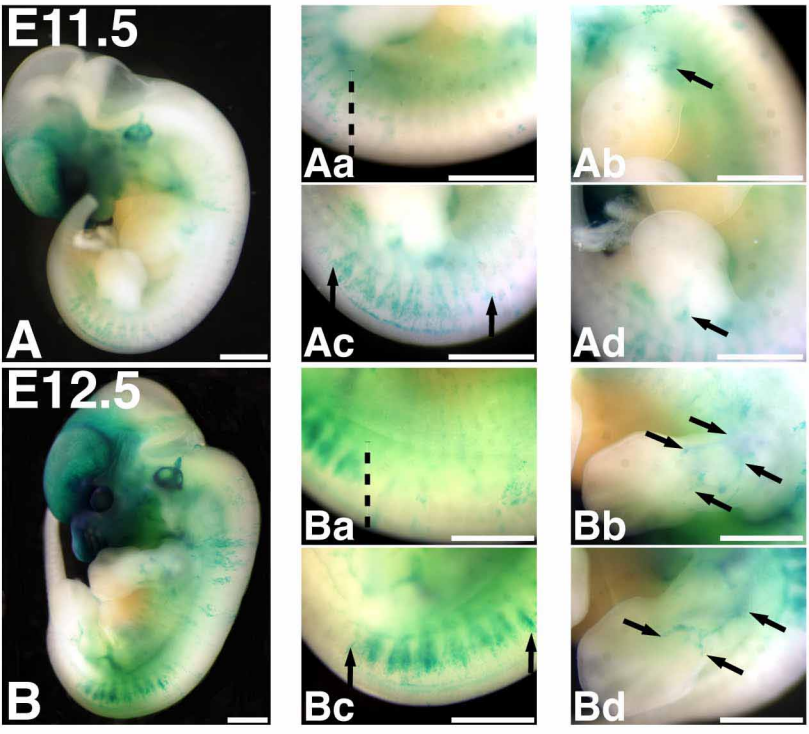

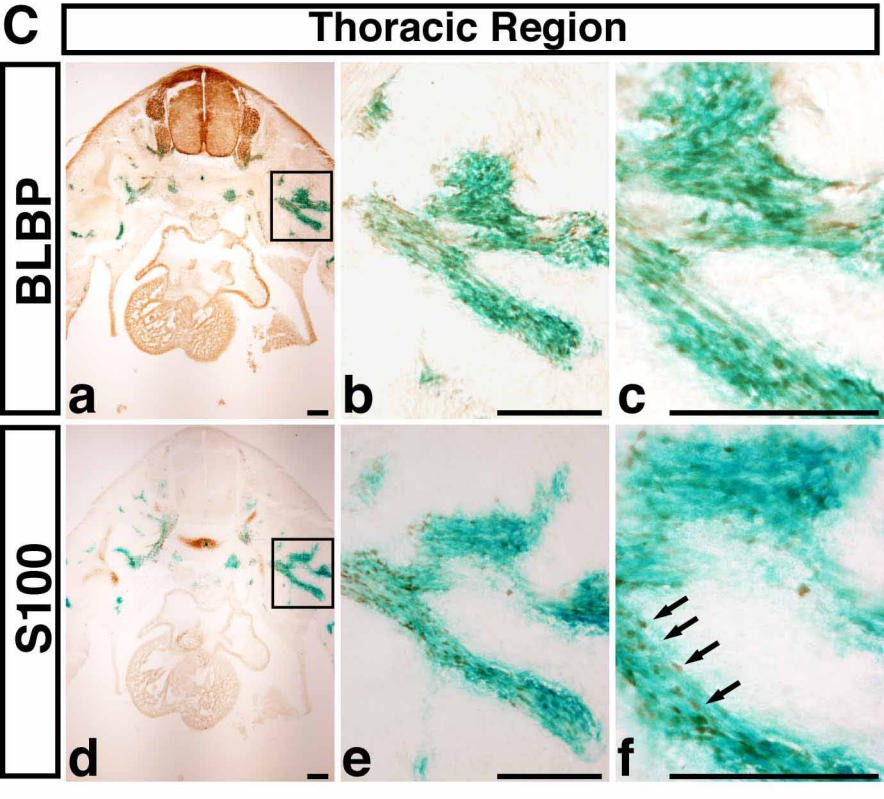

Supplemental Figure 4

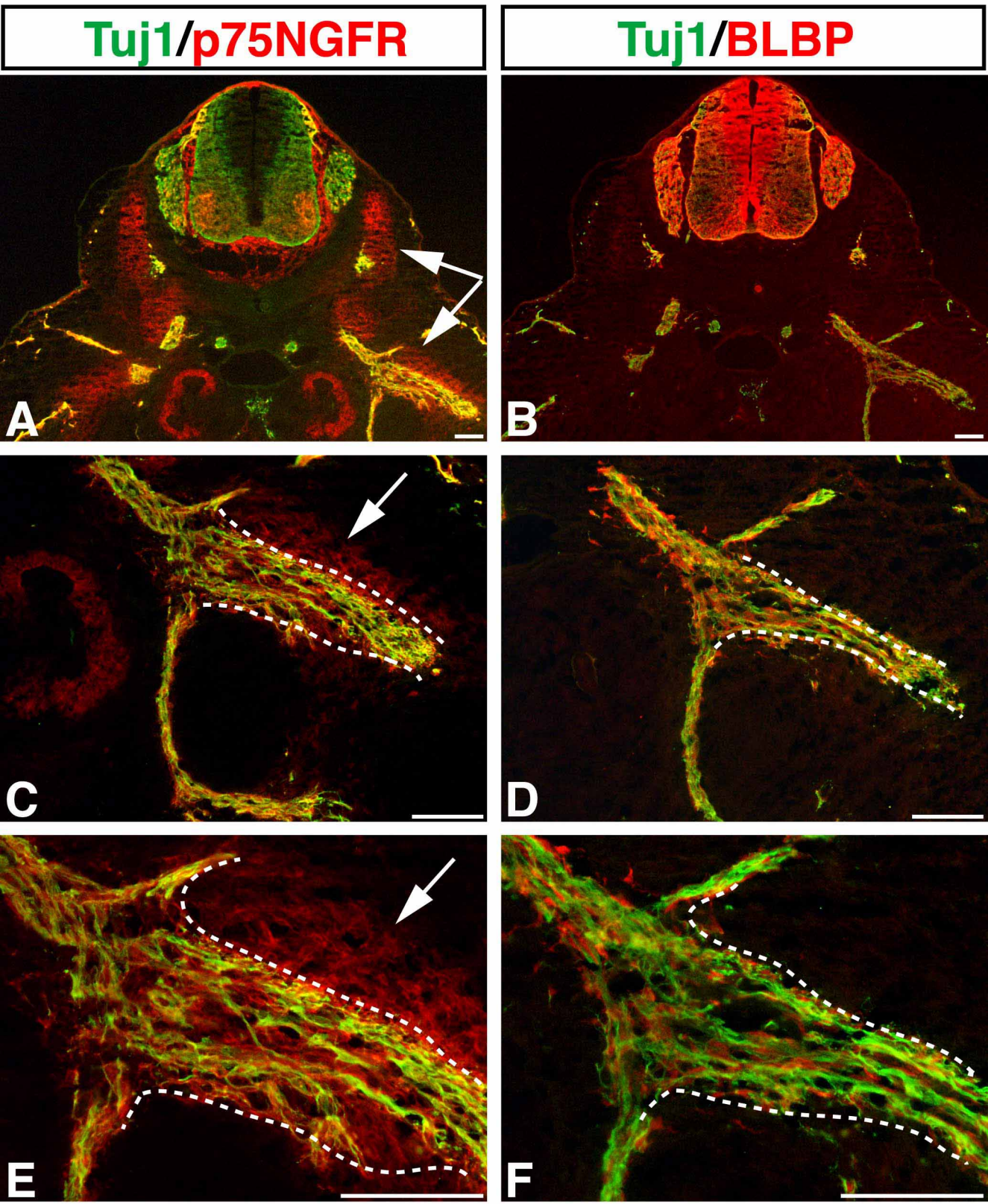

Supplemental Figure 5

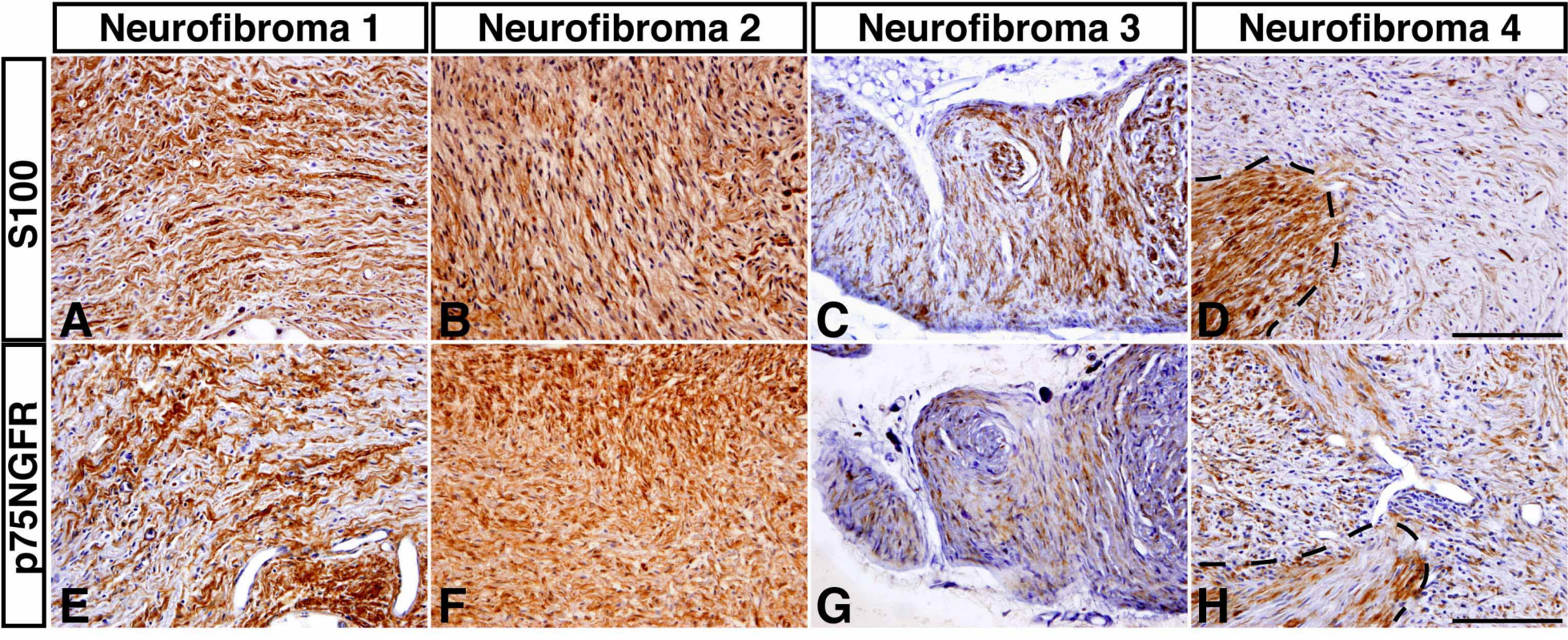

Supplemental Figure 6

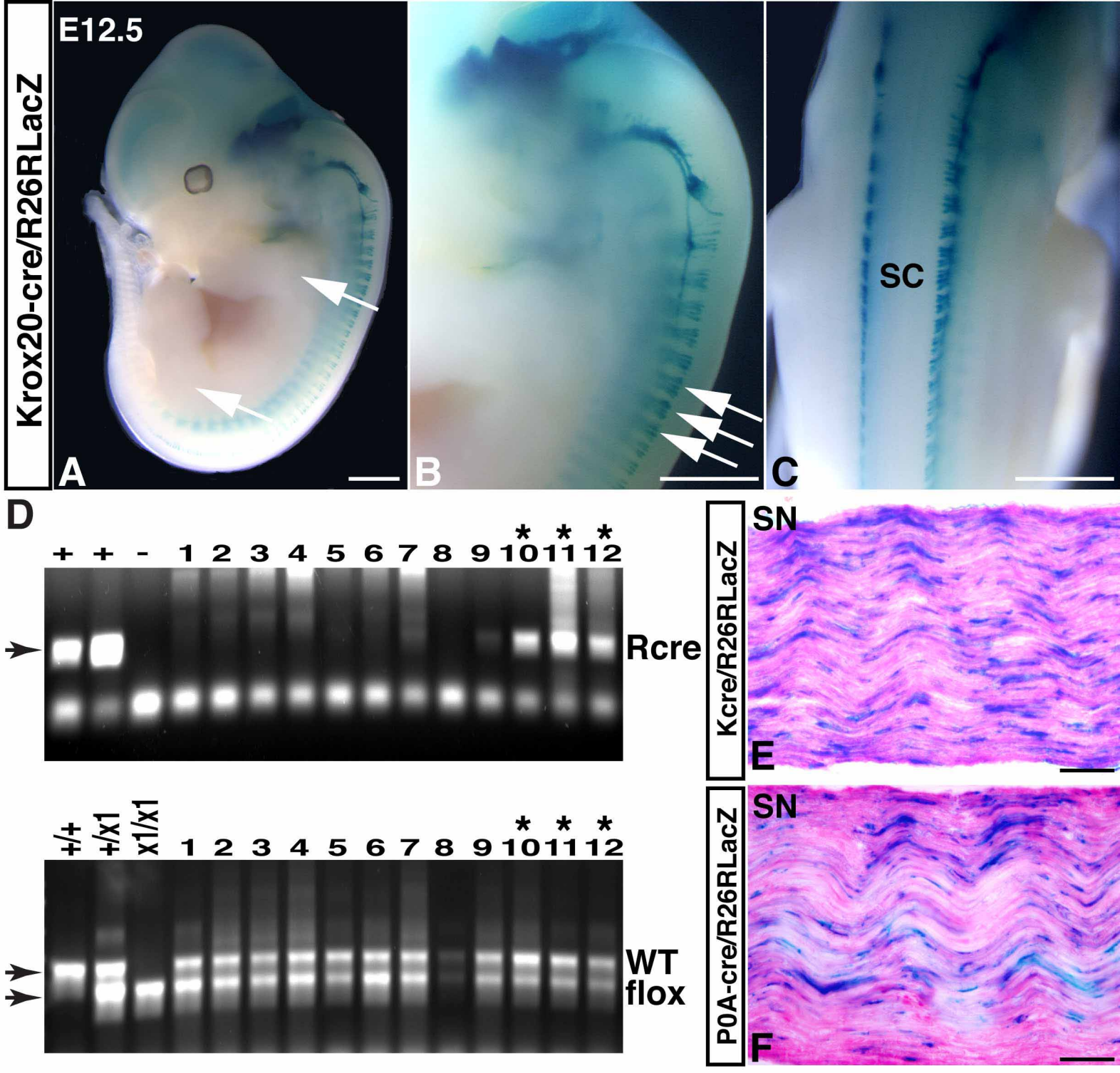

Supplemental Figure 7

A

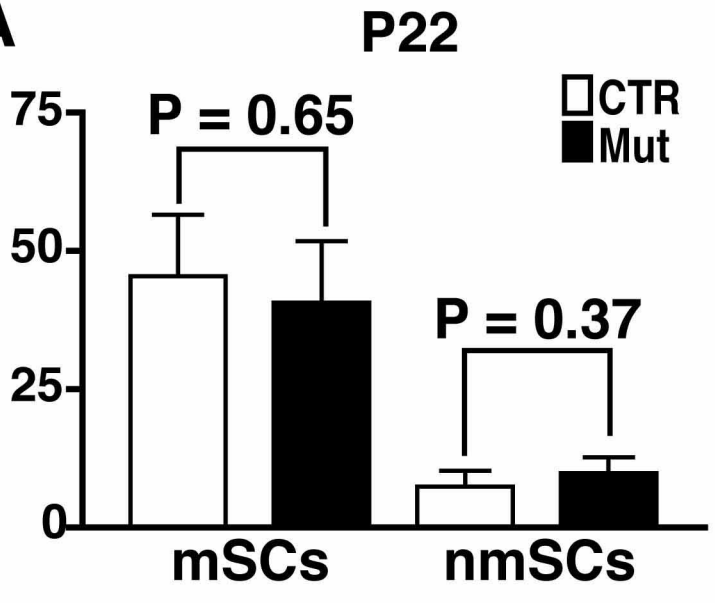

B

P22 Remak Bundle Distribution

Axons per Remak Bundle	Control	Mutant	P-value
Single Axon	1.58±0.39	1.53±0.56	0.93
2-10 Axons	3.15±0.87	5.30±2.11	0.08
11-20 Axons	1.73±0.25	2.06±0.72	0.41
21-35 Axons	0.61±0.24	0.60±0.43	0.99
36+ Axons	0.14±0.07	0.19±0.16	0.62

C

P90 Endoneurial Cells

Cell Type	Control	Mutant	P-value
Schwann cell lineages	98.6%	97.7%	
mSC	27.02±3.24	24.16±2.00	0.475
nmSC	4.89±1.34	5.56±1.31	0.655
dSC	0.03±0.03	1.58±0.34	0.000
anmSC	0.01±0.03	0.79±0.42	0.000
Pooled nmSC	4.93±1.21	7.94±1.52	0.009
Non-Schwann cell lineages	1.4%	2.3%	
Fibroblasts	0.40±0.11	0.75±0.14	0.001
Mast Cells*	0.00±0.00	0.02±0.02	0.479
Macrophages*	0.01±0.02	0.05±0.03	0.163
Blood Vessels*	0.13±0.07	0.14±0.06	0.882

D

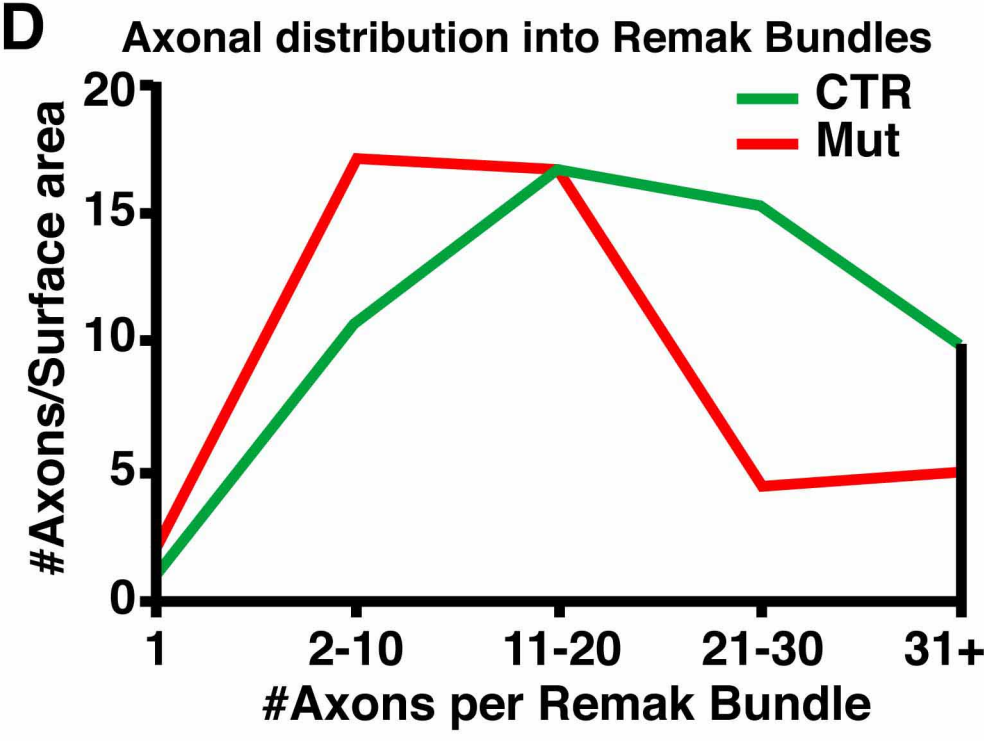

Supplemental Figure 8

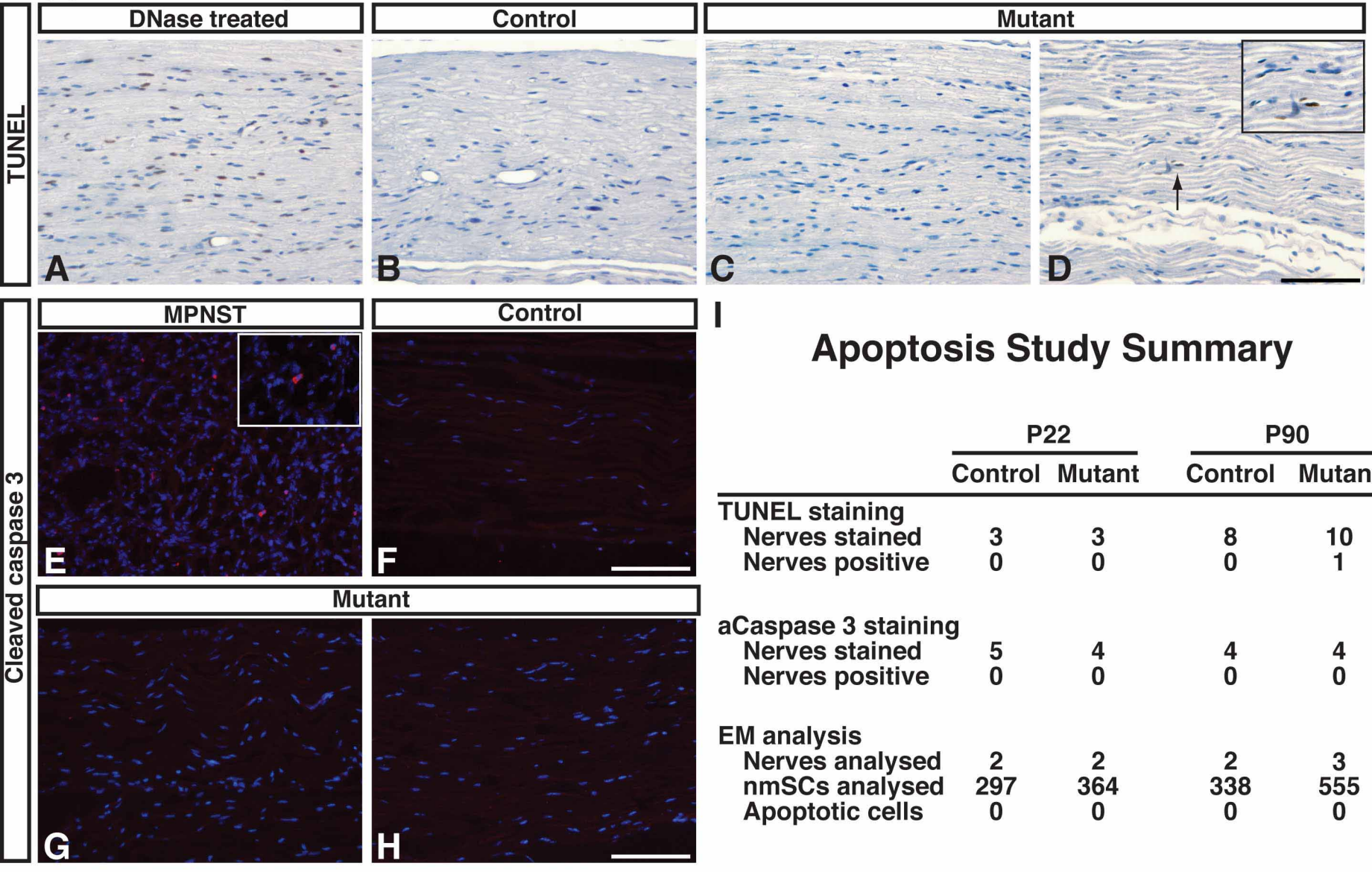

I

Apoptosis Study Summary

	P22		P90	
	Control	Mutant	Control	Mutant
TUNEL staining				
Nerves stained	3	3	8	10
Nerves positive	0	0	0	1
aCaspase 3 staining				
Nerves stained	5	4	4	4
Nerves positive	0	0	0	0
EM analysis				
Nerves analysed	2	2	2	3
nmSCs analysed	297	364	338	555
Apoptotic cells	0	0	0	0

Supplemental Figure 9

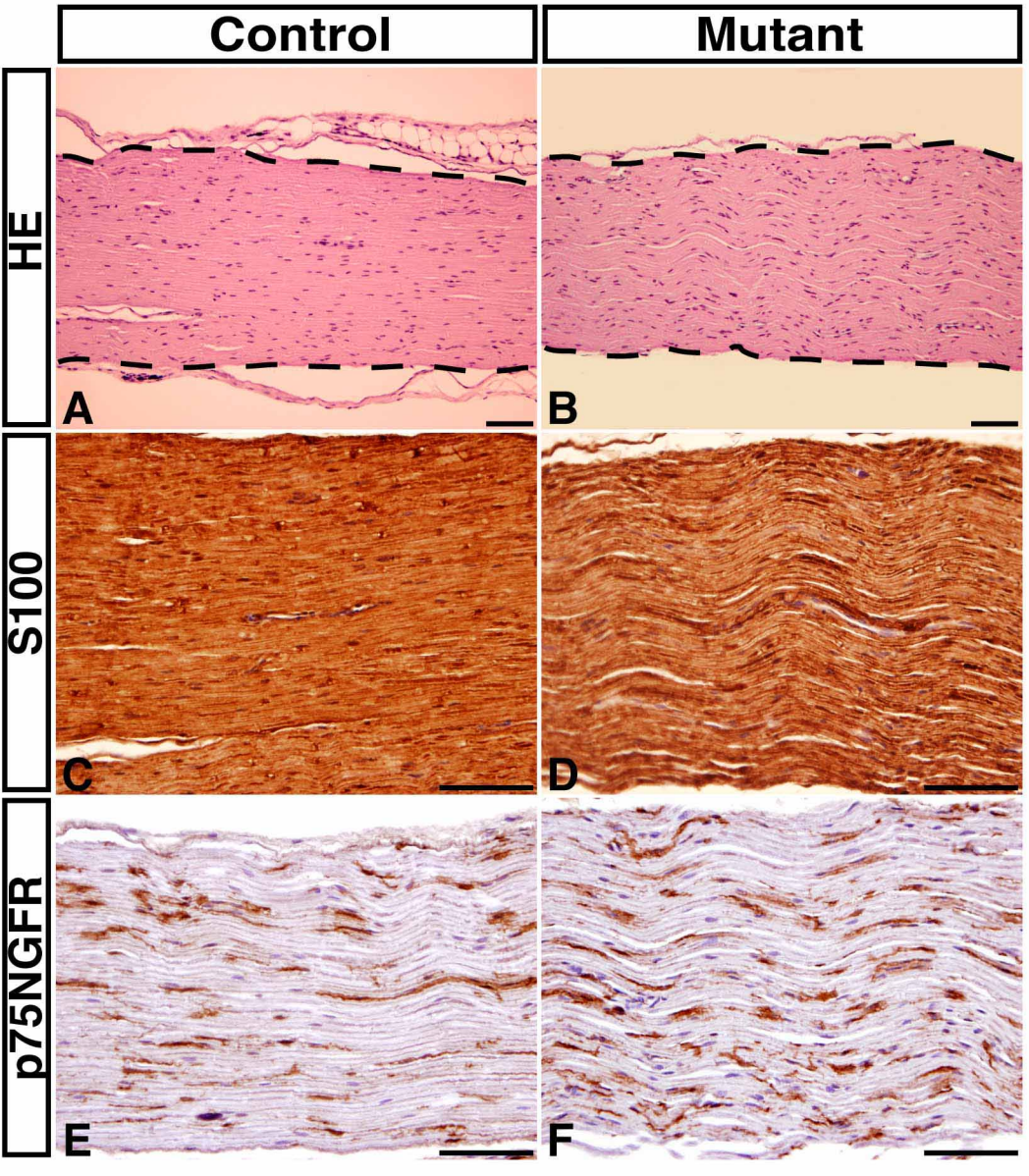

Supplemental Figure 10

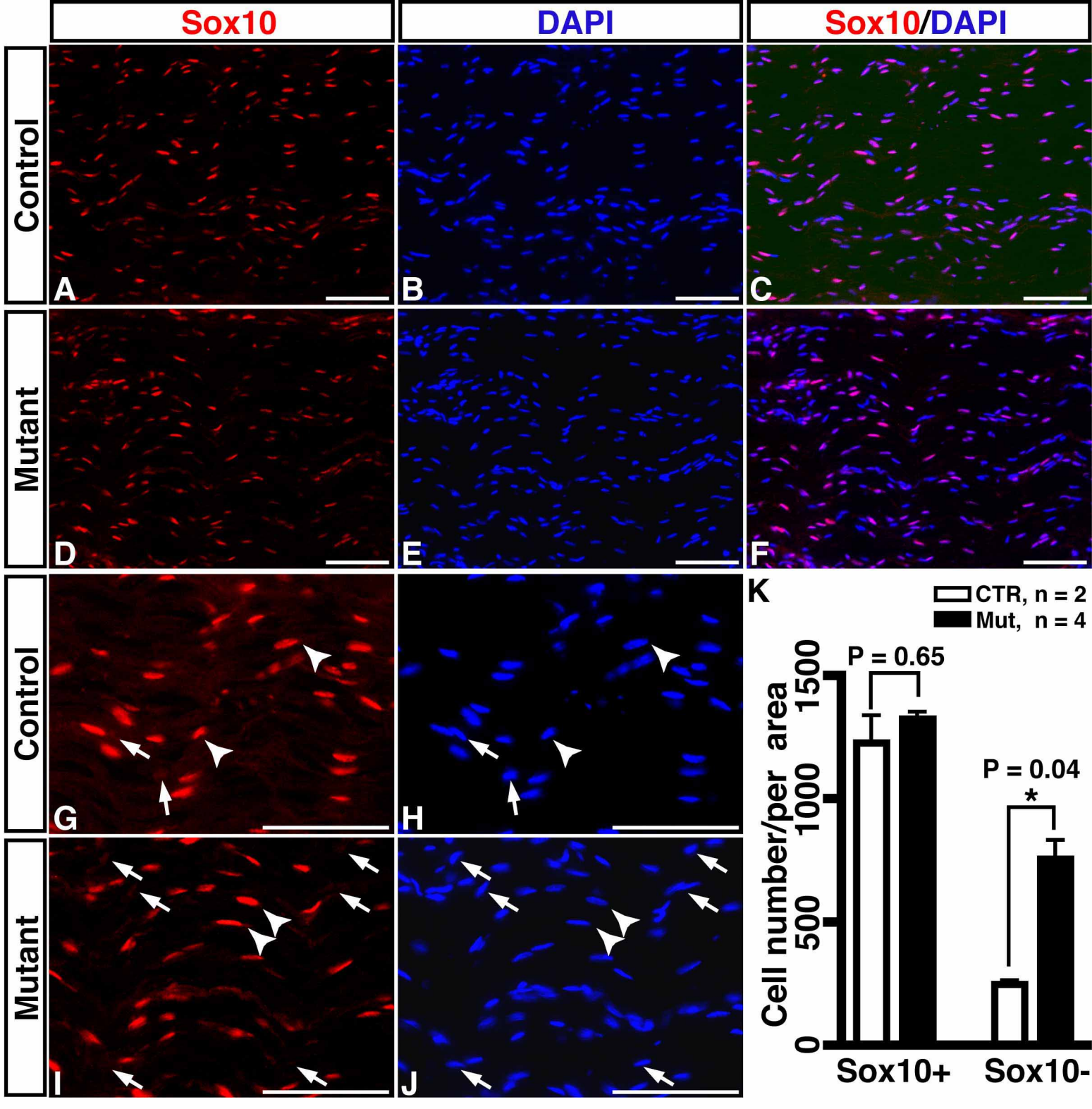

Supplemental Figure 11

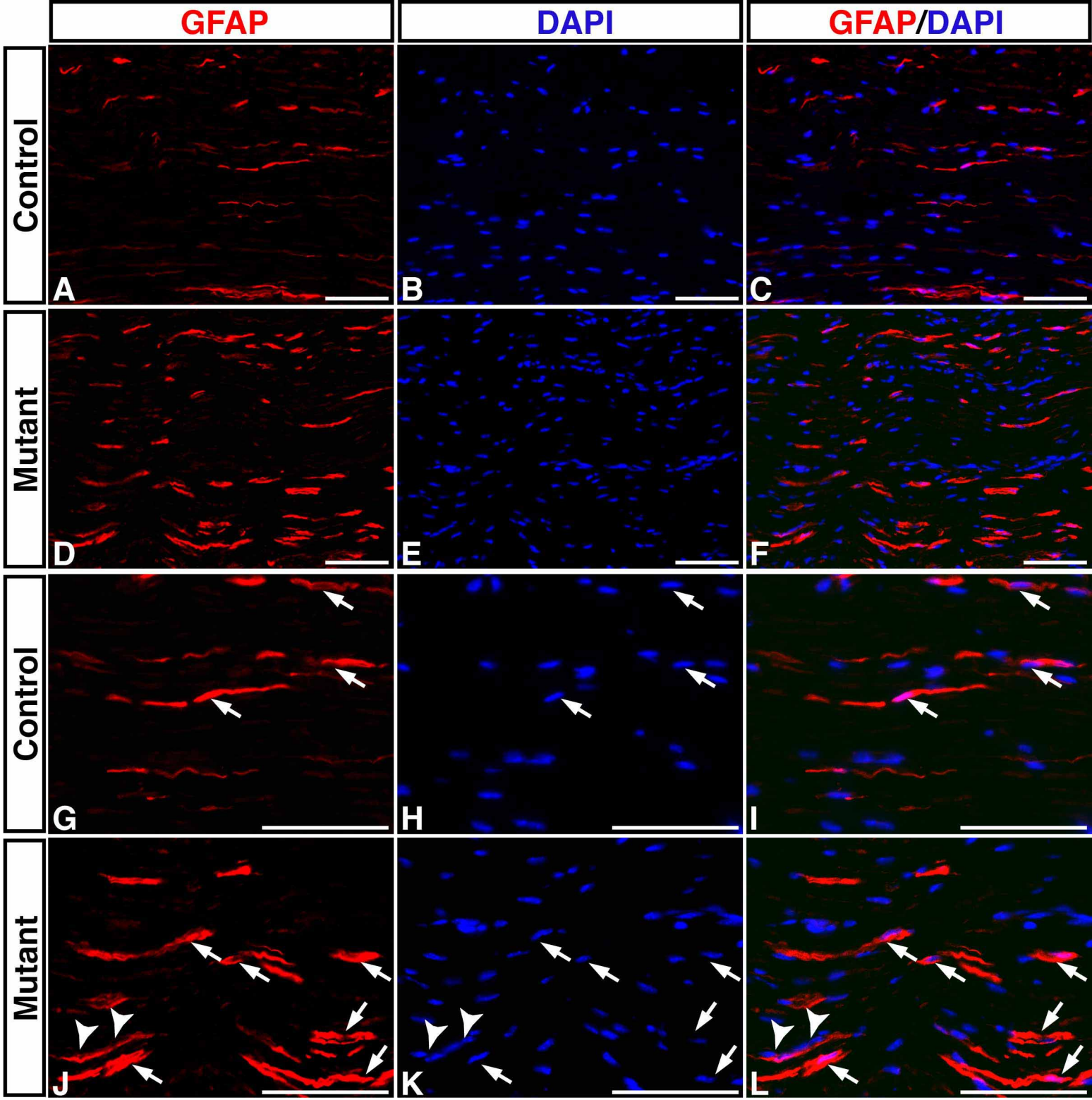

Supplemental Figure 12

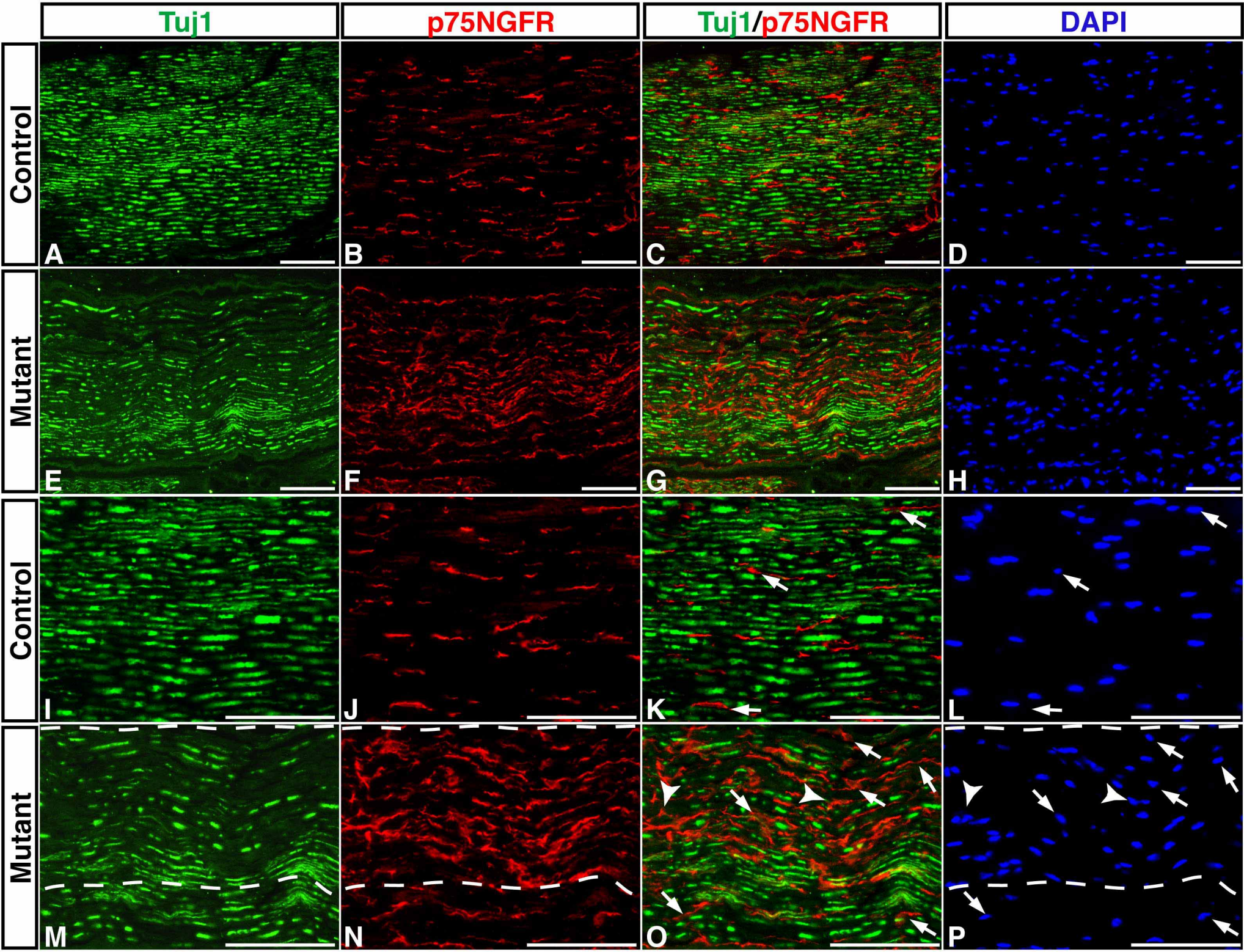

Supplemental Figure 13

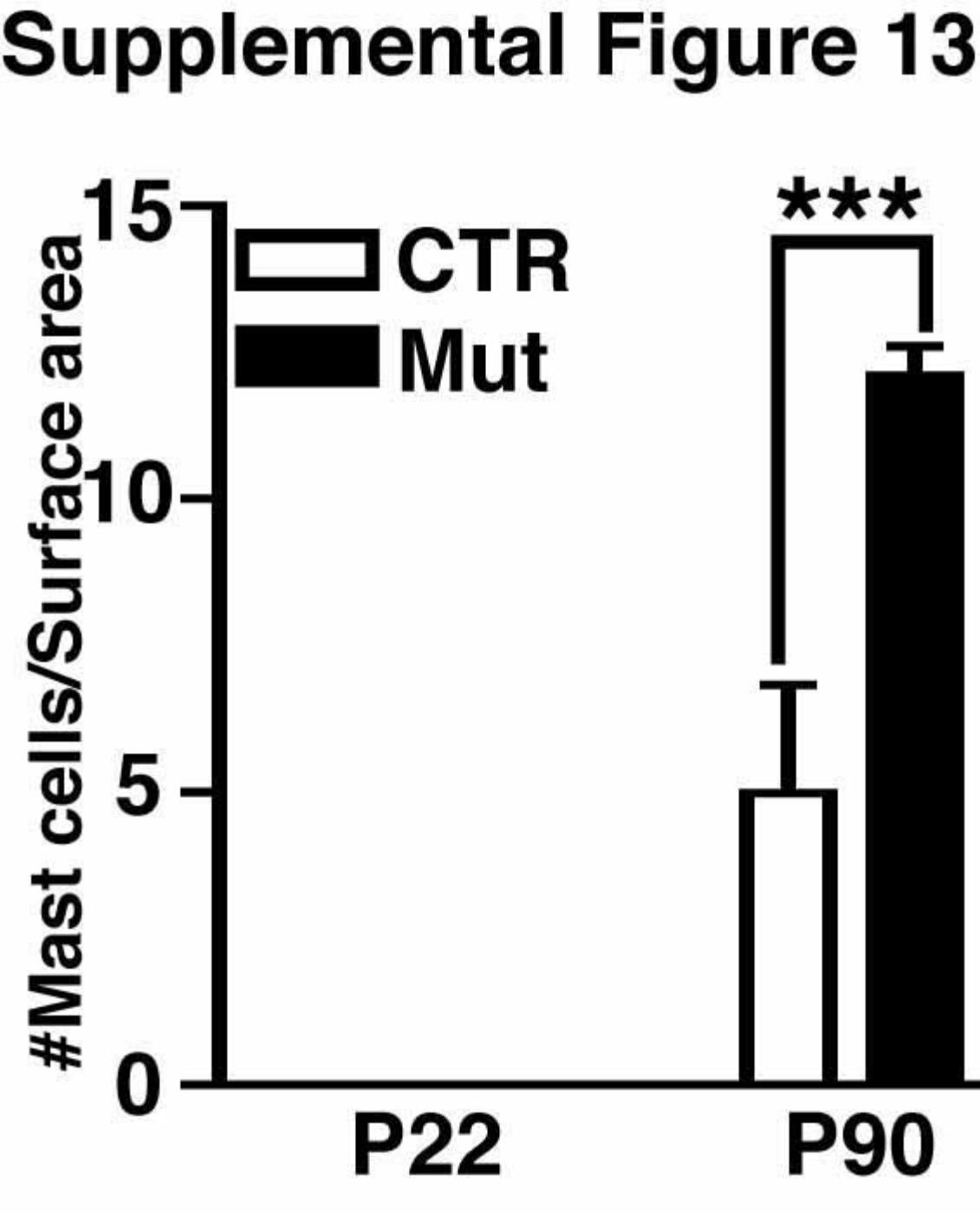

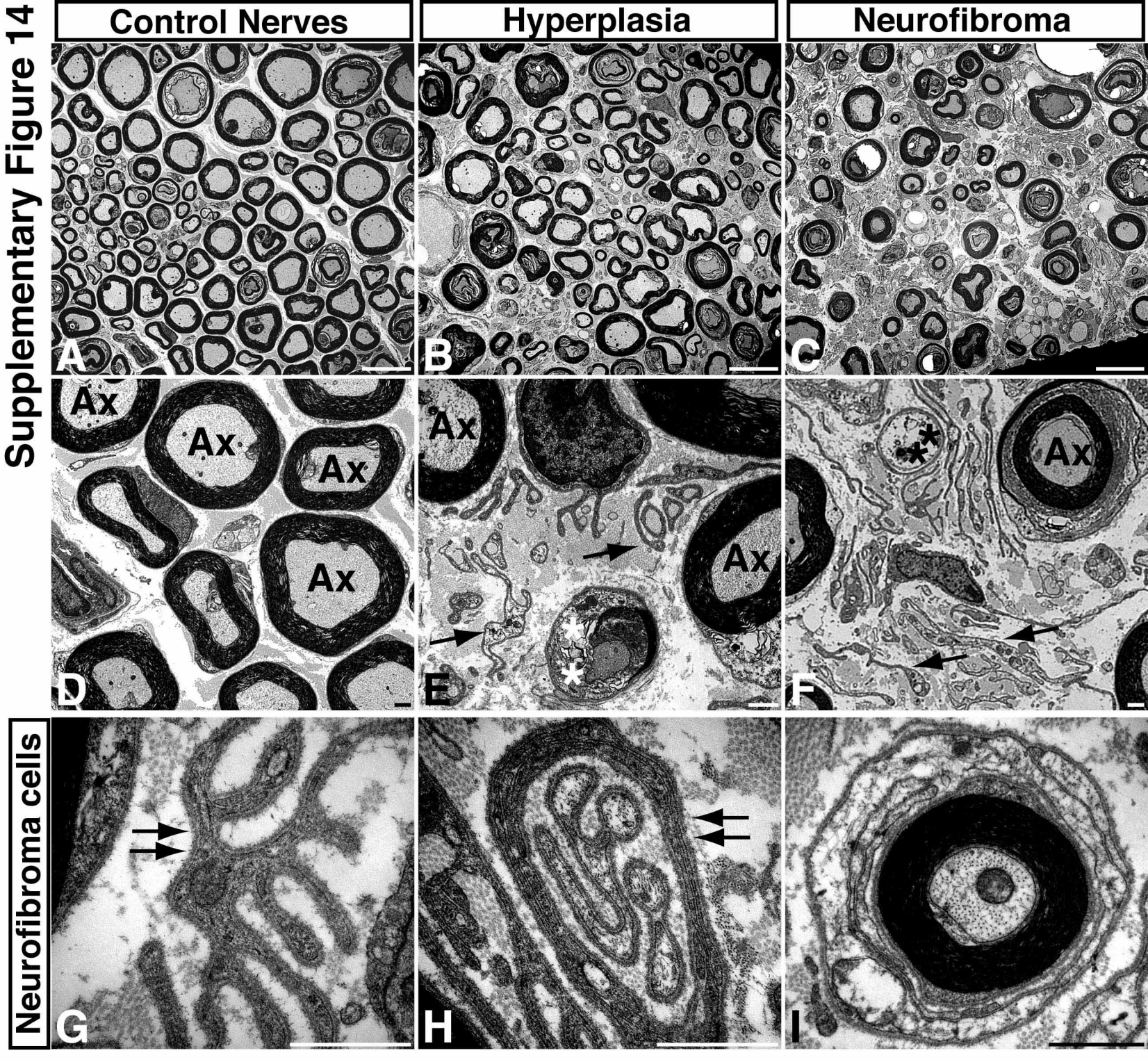
Supplementary Figure 14
Control Nerves
Hyperplasia
Neurofibroma
A
B
C
Ax
Ax
Ax
Ax
D
Ax
Ax
E
Ax
F
Neurofibroma cells
G
H
I

Supplemental Figure 15

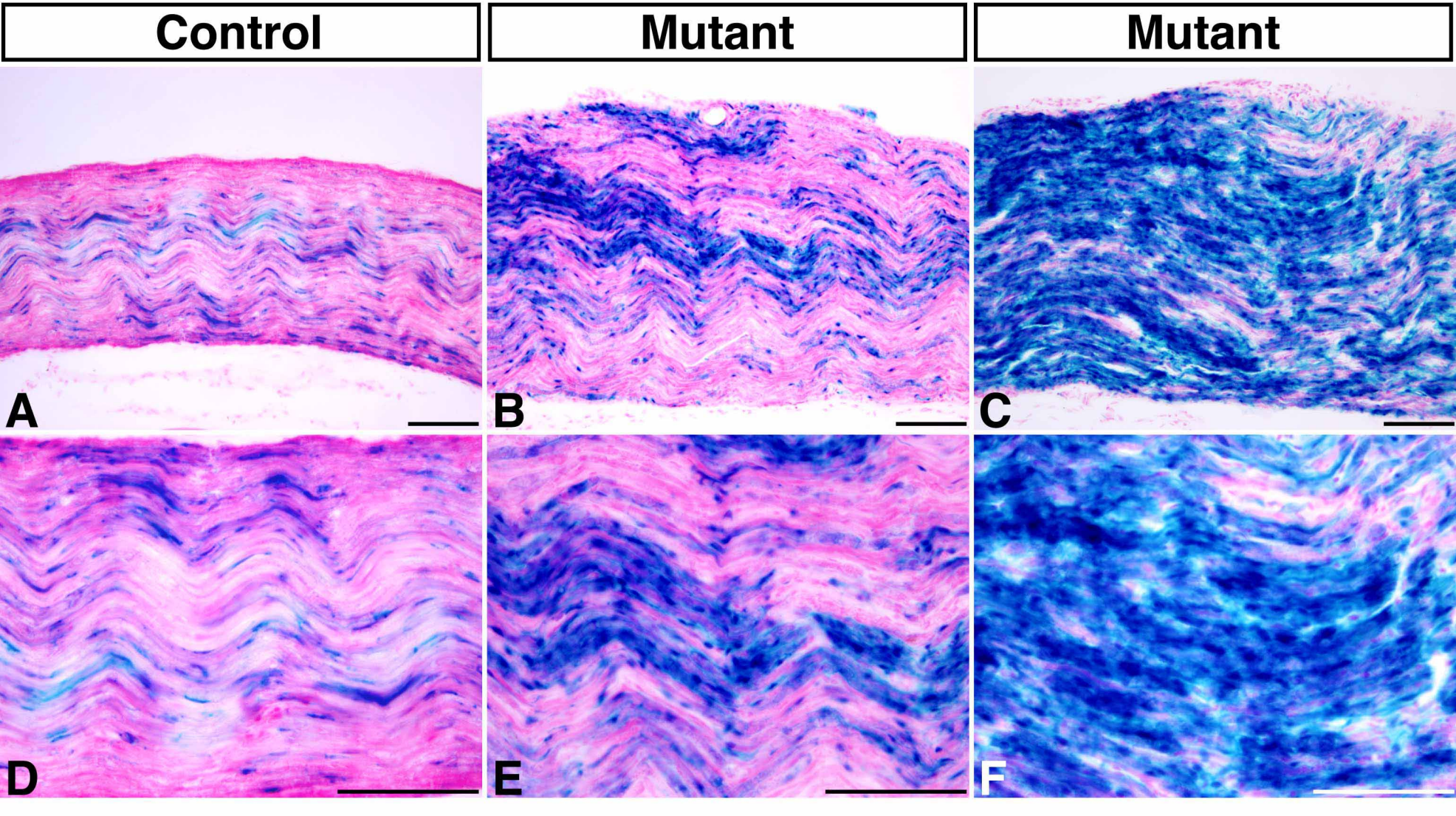

Supplemental Figure 16

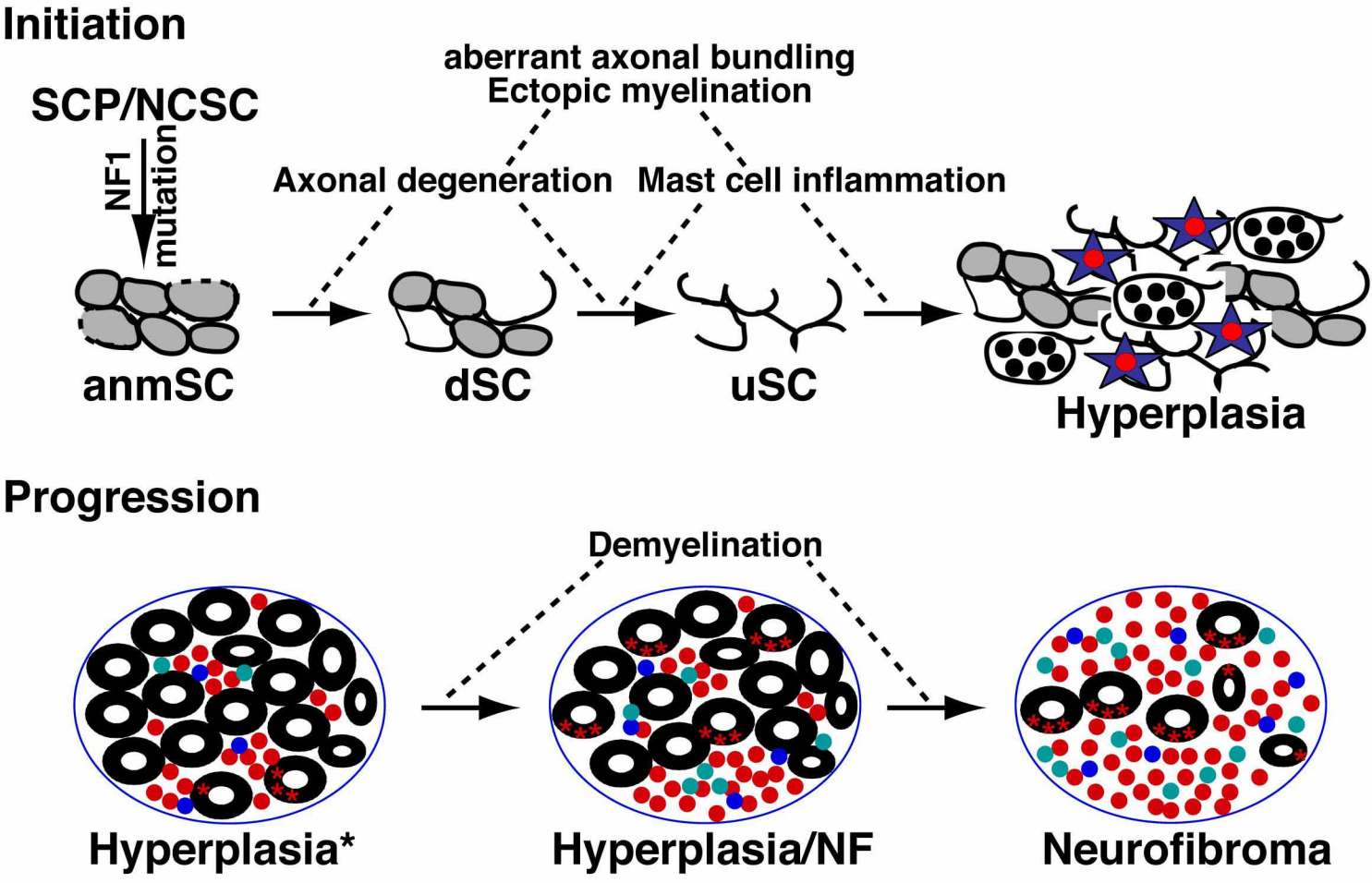

Cancer Cell
Article

The Loss of *Nf1* Transiently Promotes Self-Renewal but Not Tumorigenesis by Neural Crest Stem Cells

Nancy M. Joseph,[1,3,6] Jack T. Mosher,[1,3,6] Johanna Buchstaller,[1] Paige Snider,[4] Paul E. McKeever,[2] Megan Lim,[2] Simon J. Conway,[4] Luis F. Parada,[5] Yuan Zhu,[3] and Sean J. Morrison[1,3,*]
[1]Center for Stem Cell Biology, Howard Hughes Medical Institute, Life Sciences Institute
[2]Department of Pathology
[3]Division of Molecular Medicine and Genetics, Departments of Internal Medicine and Cell and Developmental Biology
University of Michigan, Ann Arbor, MI 48109-2216, USA
[4]Herman B. Wells Center for Pediatric Research, Indiana University School of Medicine, Indianapolis, IN 46202, USA
[5]Center for Developmental Biology, University of Texas Southwestern Medical Center, Dallas, TX 75235-9133, USA
[6]These authors contributed equally to this work.
*Correspondence: seanjm@umich.edu
DOI 10.1016/j.ccr.2008.01.003

SUMMARY

Neurofibromatosis is caused by the loss of *neurofibromin* (*Nf1*), leading to peripheral nervous system (PNS) tumors, including neurofibromas and malignant peripheral nerve sheath tumors (MPNSTs). A long-standing question has been whether these tumors arise from neural crest stem cells (NCSCs) or differentiated glia. Germline or conditional *Nf1* deficiency caused a transient increase in NCSC frequency and self-renewal in most regions of the fetal PNS. However, *Nf1*-deficient NCSCs did not persist postnatally in regions of the PNS that developed tumors and could not form tumors upon transplantation into adult nerves. Adult *P0a-Cre*$^{+}$*Nf1*$^{fl/-}$ mice developed neurofibromas, and *Nf1*$^{+/-}$*Ink4a/Arf*$^{-/-}$ and *Nf1/p53*$^{+/-}$ mice developed MPNSTs, but NCSCs did not persist postnatally in affected locations in these mice. Tumors appeared to arise from differentiated glia, not NCSCs.

INTRODUCTION

Neurofibromatosis type 1 is among the most prevalent disorders of the nervous system and is characterized by the formation of tumors throughout the PNS. It is an autosomal dominant disorder caused by mutations in the *neurofibromin* (*Nf1*) tumor suppressor, which encodes a GTPase activating protein that negatively regulates Ras signaling (Rubin and Gutmann, 2005). Patients typically inherit one *Nf1* mutant allele in the germline, and somatic mutations inactivate the other allele in cells that go on to form tumors. Tumors include discrete dermal neurofibromas that are associated with individual nerves as well as larger plexiform neurofibromas that arise from dorsal root ganglia (DRGs), spinal nerve roots, or nerve plexuses (Riccardi, 1999). In addition to these benign tumors, neurofibromatosis patients can also develop MPNSTs, which often bear additional mutations in *p53* and/or *Ink4a/Arf* (Agesen et al., 2005; Menon et al., 1990; Perrone et al., 2003). Neurofibromas and MPNSTs contain a mixture of normal and neoplastic cells including hyperproliferative Schwann cells as well as fibroblasts and other nerve components in addition to inflammatory cells.

A long-standing question relates to the cell of origin for neurofibromas and MPNSTs. Schwann cells are the most prevalent cell type in these tumors and have bialleleic *Nf1* mutations (Rubin and Gutmann, 2005). This suggests that these tumors arise from Schwann cells or their progenitors. Nonetheless, important questions remain regarding the stage of Schwann cell development that is rendered tumorigenic by *Nf1* deficiency. Mature Schwann cells fail to become hyperproliferative upon *Nf1* deletion or Ras activation (Kim et al., 1995). In contrast, conditional deletion of *Nf1* from fetal nerve progenitors using *Krox20-Cre* leads to plexiform neurofibromas in spinal nerve roots (Zhu et al., 2002).

SIGNIFICANCE

Cancers are often proposed to arise from stem cells that have been transformed by mutations that inappropriately activate self-renewal mechanisms. Neurofibromas and MPNSTs arise from neural crest-derived cells and sometimes arise congenitally, raising the question of whether they arise from NCSCs. We found that *Nf1* transiently inhibits the expansion of NCSCs during midgestation but that *Nf1*-deficient NCSCs appear to acquire normal differentiated fates, do not become tumorigenic, and do not persist postnatally. Instead, MPNSTs and plexiform neurofibromas appeared to arise from differentiated glia that began proliferating inappropriately postnatally or during adulthood. Cancer and benign tumors in the PNS can, therefore, arise from differentiated glia.

Krox20 is expressed by nerve NCSCs (T. Iwashita and S.J.M., unpublished data) in addition to Schwann cells and their committed progenitors (Topilko et al., 1994; Zhu et al., 2002). Fate mapping of *Krox20-Cre* expressing cells demonstrates that these cells undergo multilineage differentiation in DRGs (Maro et al., 2004; Zhu et al., 2002). These observations raise the question of whether neurofibromas and MPNSTs arise from NCSCs or from differentiated Schwann cells.

The neural crest is a heterogeneous population of progenitors that migrates from the dorsal neural tube in early to midgestation and gives rise to the neurons and glia of the PNS. NCSCs are a subset of neural crest cells and are defined by the ability of individual cells to self-renew and to undergo multilineage differentiation into neurons, glia, and myofibroblasts (Morrison et al., 1999; Stemple and Anderson, 1992). Postmigratory NCSCs have been found in all regions of the fetal PNS including peripheral nerves, sympathetic chain, DRGs, and gut (enteric nervous system) (Bixby et al., 2002; Morrison et al., 1999). In peripheral nerves, NCSCs give rise to myelinating and nonmyelinating Schwann cells as well as endoneurial fibroblasts (Joseph et al., 2004), cell types that are present in neurofibromas.

NCSCs persist throughout adult life in the gut (Kruger et al., 2002). However, in other regions of the PNS, including those that develop neurofibromas, NCSCs terminally differentiate by late gestation and cannot be detected postnatally (Kruger et al., 2002). Nonetheless, NCSCs could still be rendered tumorigenic by *Nf1* mutations as plexiform neurofibromas and MPNSTs can arise from mutations that occur during fetal development. Some tumors are even evident in patients at birth (Rubin and Gutmann, 2005). Other tumors develop around puberty or during adulthood. Thus, if NCSCs are rendered tumorigenic by *Nf1* deficiency, then deletion of *Nf1* from fetal NCSCs should lead to a sustained expansion of these cells, and their postnatal persistence, such that they can give rise to neonatal or adult tumors.

Many cancers appear to arise from mutations that transform normal stem cells by inappropriately activating self-renewal pathways (Pardal et al., 2003; Reya et al., 2001). *Nf1* inhibits the proliferation, survival, and glial differentiation of CNS stem cells (Dasgupta and Gutmann, 2005) and the proliferation of CNS glial progenitors (Zhu et al., 2005b). These effects of *Nf1* on CNS stem cells and glial progenitors appear to explain the astrocytomas that arise in neurofibromatosis patients (Zhu et al., 2005a). Although PNS tumors are more common than CNS tumors in neurofibromatosis, the origin of PNS tumors remains unknown.

We found that *Nf1*-deficient NCSCs from fetal DRGs, sciatic nerves, and sympathetic ganglia exhibited increased frequency, proliferation, self-renewal, and gliogenesis. To test whether these effects were sustained, we examined mice in which *Nf1* was conditionally deleted from the PNS using *Wnt1-Cre*, *P0a-Cre*, or *3.9Periostin-Cre*. We did not detect the persistence of *Nf1*-deficient NCSCs in the postnatal DRG, sciatic nerve, or sympathetic ganglia and NCSCs in the postnatal gut were not affected by *Nf1* deficiency. Yet *P0a-Cre*$^{+}$*Nf1*$^{fl/-}$ mice developed plexiform neurofibromas from adult nerves (Zheng et al., 2008 [this issue of *Cancer Cell*]). NCSCs also did not persist postnatally in the DRGs, sciatic nerves, trigeminal nerve, brachial plexus, or sympathetic ganglia of *Nf1/p53*$^{+/-}$ mice or *Nf1*$^{+/-}$*Ink4a/Arf*$^{-/-}$ mice. Yet, these mice developed MPNSTs as adults. NCSCs are, therefore, not rendered tumorigenic by *Nf1* deficiency. Instead, plexiform neurofibromas and MPNSTs appear to arise from differentiated glia.

RESULTS

Nf1 Regulates NCSC Frequency throughout Much of the Developing PNS

Germline *Nf1*$^{-/-}$ embryos die from a cardiac defect by embryonic day (E)14.5 (Brannan et al., 1994; Jacks et al., 1994). Therefore, to test whether *Nf1* regulates NCSC function, we cultured NCSCs from various regions of the PNS from E13 *Nf1*$^{-/-}$ embryos and littermate controls. NCSC frequency was assessed as the percentage of cells from each region of the PNS that could form self-renewing neurospheres that underwent multilineage differentiation (Iwashita et al., 2003; Molofsky et al., 2005) (see Figure S1 available with this article online). The sympathetic chain, DRG, and sciatic nerve from *Nf1*$^{-/-}$ embryos contained a significantly higher percentage of cells (3- to 6-fold higher; $p < 0.05$) that formed multipotent neurospheres in culture compared to littermate controls (Figures 1A–1C). In contrast, *Nf1*-deficiency did not increase the frequency of gut cells that formed multipotent neurospheres. This suggests that *Nf1* negatively regulates the frequency of NCSCs from many, but not all, PNS regions.

To test whether the increased frequency of *Nf1*$^{-/-}$ NCSC colonies was attributable to an increased frequency of NCSCs in vivo or increased survival by NCSCs in culture, we assayed the frequency of p75$^{+}\alpha_4^{+}$ cells among uncultured DRG, sciatic nerve, sympathetic chain, and gut cells by flow-cytometry. p75$^{+}\alpha_4^{+}$ cells from the fetal PNS are enriched for NCSCs (Iwashita et al., 2003; Molofsky et al., 2005). Freshly dissociated *Nf1*$^{-/-}$ DRG, sciatic nerve, and sympathetic chain all had significantly ($p < 0.05$) higher frequencies of p75$^{+}\alpha_4^{+}$ cells (Figures 1A–1C). In contrast, we did not observe a significantly higher frequency of p75$^{+}\alpha_4^{+}$ cells in the gut of *Nf1*$^{-/-}$ mice (Figure 1D). These data suggest that NCSC frequency is increased in vivo at E13 by *Nf1* deficiency.

Nf1 Regionally Regulates NCSC Proliferation and Self-Renewal in the Developing PNS

In PNS regions where *Nf1* negatively regulated NCSC frequency, *Nf1* also negatively regulated proliferation from NCSCs in culture. Multipotent neurospheres formed by NCSCs from DRG, sciatic nerve, and sympathetic chain were significantly larger in the absence of *Nf1* (Figures 1A–1C). All cultures were initiated with very low densities of cells (1000 to 5000 cells per 35 mm dish forming up to 30 neurospheres per dish) so as to minimize fusion between neurospheres. To ensure that the increased size of colonies reflected increased proliferation by *Nf1*$^{-/-}$ NCSCs, we also cultured these cells adherently. Adherent multilineage colonies cultured at clonal density from DRG and sympathetic chain were also significantly larger in the absence of *Nf1* (Figure S2). Increased proliferation contributed to the increased size of NCSC colonies in the absence of *Nf1* as we detected a significantly increased rate of BrdU incorporation into *Nf1*$^{-/-}$ colonies but no decrease in the frequency of cells undergoing cell death (Figure S2I). In contrast, adherent NCSC colonies cultured from the gut were not significantly larger nor did they exhibit an increased rate of BrdU incorporation (Figure S2I).

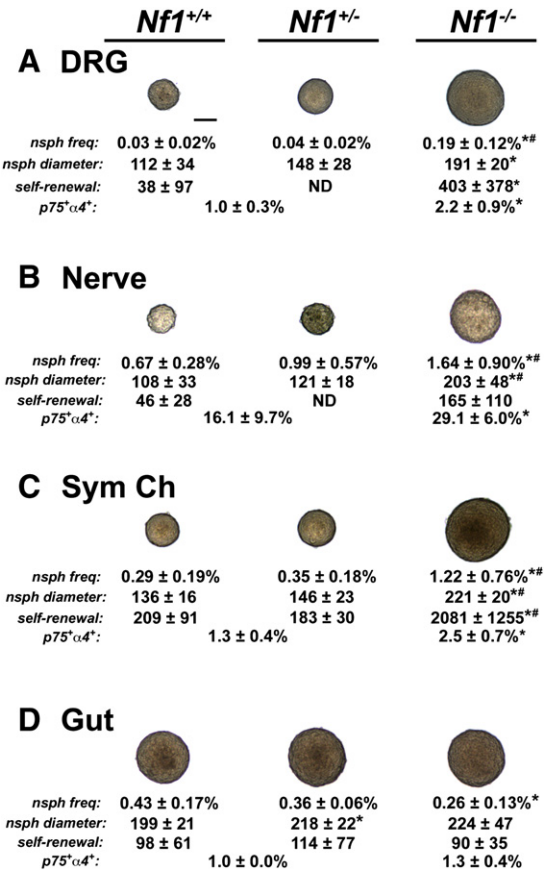

Figure 1. *Nf1* Negatively Regulates the Frequency, Proliferation, and Self Renewal of NCSCs in Most Regions of the Fetal PNS

DRG (A), sciatic nerve (B), sympathetic chain (C), and gut (D) were dissected from E13 $Nf1^{+/+}$, $Nf1^{+/-}$, and $Nf1^{-/-}$ mouse embryos. Dissociated cells were plated into nonadherent cultures at low density (1000 to 2500 cells/35 m well for most tissues; 5000 for DRG). Neurospheres were cultured non-adherently for 10 days, followed by 4 days in adherent cultures before being stained for neurons, glia, and myofibroblasts. Typical neurospheres are shown along with the percentage of freshly dissociated cells that formed neurospheres that underwent multilineage differentiation (nsph freq), the diameter of these neurospheres, and the number of multipotent secondary neurospheres generated per primary neurosphere upon subcloning (self-renewal) (*$p < 0.05$ versus wild-type; #$p < 0.05$ versus heterozygous). The scale bar (100 μm) in (A) applies to all panels. The frequency of $p75^{+}\alpha_4{}^{+}$ cells among freshly dissociated cells was significantly increased in DRG (A), sciatic nerve (B), and sympathetic chain (C), but not gut (D). Culture data represent 8 to 12 experiments and flow-cytometry data represent 4 to 7 experiments per tissue. All statistics are mean ± SD.

To test whether the increased proliferation of NCSCs also reflected increased self-renewal, we dissociated primary neurospheres and subcloned them into secondary cultures to determine the number of multipotent daughter neurospheres that arose per primary neurosphere. Secondary neurospheres were always differentiated to assess multipotency (Figure S1). When cultured from the DRG, nerve, or sympathetic chain, $Nf1^{-/-}$ neurospheres gave rise to 4 to 10 times as many multipotent daughter neurospheres as compared to control neurospheres (Figures 1A–1C). In contrast, we detected no increase in self-renewal by $Nf1^{-/-}$ gut neurospheres (Figure 1D). *Nf1* negatively regulates NCSC self-renewal in most regions of the developing PNS.

Increased Ras Signaling, Gliogenesis, and Growth Factor Sensitivity by *Nf1*-Deficient NCSCs

$Nf1^{-/-}$ cells exhibit increased sensitivity to growth factors that signal through the Ras pathway (Vogel et al., 1995). To test whether this was the case in NCSCs, we cultured NCSCs from the gut, sciatic nerve, DRG, and sympathetic chain of E13 $Nf1^{-/-}$ and littermate control embryos. Western blot demonstrated increased phosphorylated Erk (pErk) in the $Nf1^{-/-}$ colonies, consistent with increased Ras signaling in these cells (Figure 2A). Gut neural crest cells also exhibited increased pErk in the absence of *Nf1* (Figure 2A) despite the fact that these cells did not exhibit increased proliferation. The increased Ras signaling by $Nf1^{-/-}$ NCSCs suggests that these cells may exhibit increased responses to growth factors that signal through Ras, including factors that regulate survival, like FGF2, and gliogenesis, like Neuregulin (Nrg1). Indeed, addition of a short pulse of Nrg1 to NCSC cultures increased pErk levels in wild-type cells and further increased the elevated levels observed in $Nf1^{-/-}$ cells (Figure 2B).

To test whether *Nf1*-deficiency affected the differentiation of NCSCs, we cultured neurospheres from E13 $Nf1^{-/-}$ and control littermate embryos, then replated them in adherent cultures and stained the colonies for neurons, glia, and myofibroblasts. Multipotent $Nf1^{-/-}$ colonies exhibited much more exuberant gliogenesis (Figures 2E and 2H) as compared to control colonies (Figures 2C, 2D, 2F, and 2G). These colonies exhibited a dramatic increase in the absolute numbers of glia per colony without exhibiting decreases in the numbers of neurons or myofibroblasts per colony (data not shown). Similar results were obtained with nerve NCSCs, but we did not generally observe increased gliogenesis by cultured gut NCSCs (data not shown). This indicates that *Nf1* negatively regulates gliogenesis from NCSCs, though we do not know whether this reflects effects on glial lineage determination, proliferation, or survival.

$Nf1^{-/-}$ NCSCs also survived under adverse culture conditions in which FGF2 and chick embryo extract concentrations were reduced to levels that were non-permissive for the survival of wild-type NCSCs. $Nf1^{+/+}$ and $Nf1^{+/-}$ sympathetic chain or DRG progenitors formed only rare colonies that contained small numbers of myofibroblasts in this medium, while $Nf1^{-/-}$ cells formed multilineage colonies (Figure 2), albeit at a reduced frequency as compared to standard medium (Figures 2L and 2M; *$p < 0.05$).

Nf1-Deficient NCSCs Do Not Persist Postnatally outside of the Gut

To test whether *Nf1* deficiency leads to an ongoing postnatal expansion of NCSCs, we conditionally deleted *Nf1* from neural crest cells by crossing *Wnt1-Cre* mice (Danielian et al., 1998) with $Nf1^{fl}$ mice (Zhu et al., 2001). *Wnt1-Cre*$^{+}Nf1^{fl/-}$ mice die at birth (Gitler et al., 2003), so cells were cultured from E17 to E19 embryos. We were never able to culture multilineage NCSC colonies from the sciatic nerve or DRG of *Wnt1-Cre*$^{+}Nf1^{fl/-}$ embryos or controls (Table 1). We were able to culture rare NCSC colonies from the sympathetic chain and gut of *Wnt1-Cre*$^{+}Nf1^{fl/-}$ embryos and littermate controls, though their

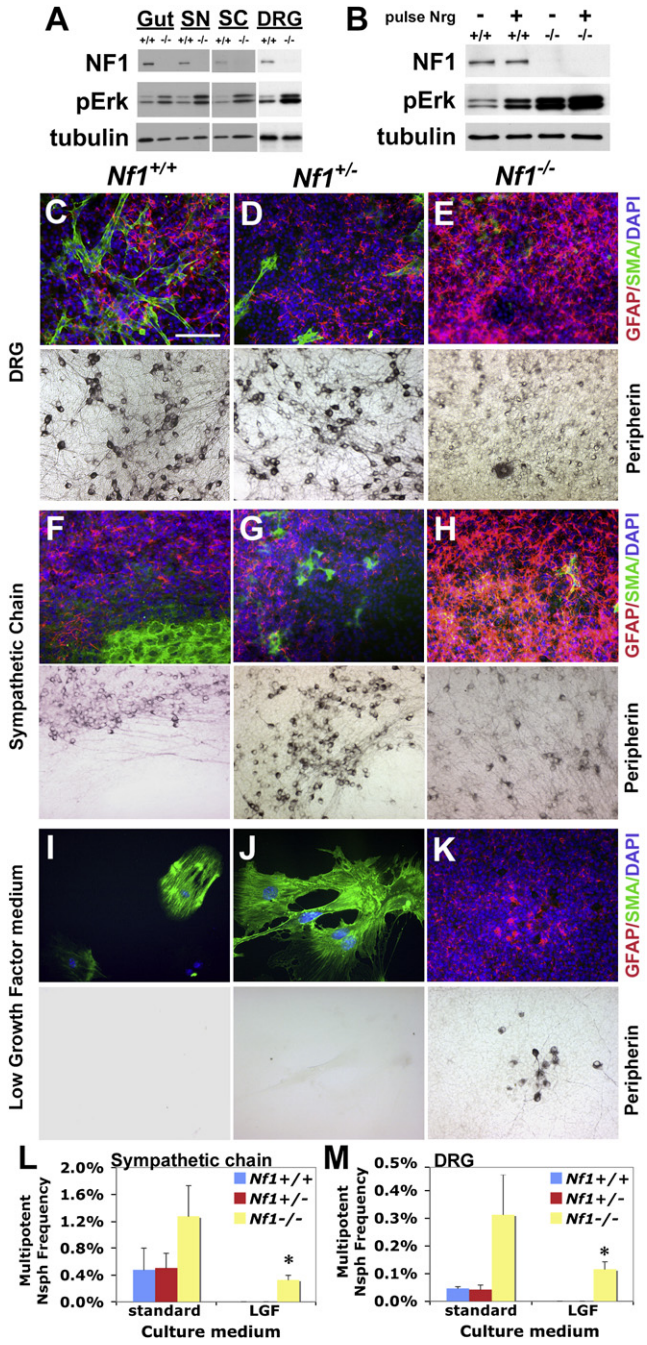

Figure 2. *Nf1*-Deficient NCSCs Exhibit Increased Ras Signaling, Increased Gliogenesis, and Increased Survival in Low Growth Factor Cultures

(A) Cell lysates from $Nf1^{+/+}$ and $Nf1^{-/-}$ neurospheres were analyzed for NF1 and phosphorylated Erk 42/44 (pErk) protein levels. (B) When $Nf1^{+/+}$ and $Nf1^{-/-}$ NCSC cultures from sympathetic chain were pulsed with Nrg-1, pErk levels increased in both $Nf1^{+/+}$ and $Nf1^{-/-}$ cells, but were highest in $Nf1^{-/-}$ cells. NCSCs cultured from E13 $Nf1^{+/+}$, $Nf1^{+/-}$, and $Nf1^{-/-}$ DRGs (C–E) and sympathetic chain (F–H) underwent multilineage differentiation, forming peripherin$^+$ neurons, GFAP$^+$ glia, and SMA$^+$ myofibroblasts. More gliogenesis (red) was observed from $Nf1^{-/-}$ NCSCs from DRG (E) and sympathetic chain (H). $Nf1^{+/+}$ and $Nf1^{+/-}$ cells from sympathetic chain (I–J and L) and DRG (M) failed to form multilineage colonies in low growth factor cultures (LGF), while $Nf1^{-/-}$ cells continued to do so ([K]; SMA+ myofibroblasts were present in this colony outside of the field of view) ([L and M]; *$p < 0.05$ versus control cultures). Brightfield (peripherin) and fluorescence (GFAP, SMA) images always represent the same field of view within a single colony. The scale bar (100 μm) in (C) applies to all panels. Data represent 3–5 independent experiments and error bars represent SD.

Table 1. *Nf1* Deficiency Does Not Lead to the Persistence of Expanded Numbers of NCSCs into Late Gestation or Postnatally

E17 to E19	Cells that Formed Multipotent Neurospheres	
	Littermate Controls	*Wnt1-Cre*$^+$*Nf1*$^{fl/-}$
DRG	0 ± 0%	0 ± 0%
Sciatic nerve	0 ± 0%	0 ± 0%
Sympathetic chain	0.03 ± 0.03%	0.05 ± 0.04%
Gut	0.08 ± 0.10%	0.08 ± 0.10%
P30 to P60	**Cells that Formed Multipotent Neurospheres**	
	Littermate Controls	*3.9Periostin-Cre*$^+$*Nfl*$^{fl/-}$
DRG	0 ± 0%	0 ± 0%
Sciatic nerve	0 ± 0%	0 ± 0%
Sympathetic chain	0 ± 0%	0 ± 0%
Gut	0.8 ± 0.6%	1.1 ± 0.8%

Tissues were dissected, dissociated, and added to nonadherent cultures. Neurospheres were replated to test multilineage differentiation into neurons, glia, and myofibroblasts. We were unable to detect NCSCs from the DRGs, sciatic nerves, or sympathetic chain of young adult (P30 to P60) *3.9Periostin-Cre*$^+$*Nfl*$^{fl/-}$ mice or littermate controls. All data represent mean ± SD for 3 to 5 independent experiments per PNS region.

frequency was similar in $Nf1^{+/+}$ and $Nf1^{-/-}$ embryos (Table 1). The expansion of $Nf1^{-/-}$ NCSCs at E13 does not lead to the inappropriate expansion or persistence of $Nf1^{-/-}$ NCSCs at later stages of development.

To test when $Nf1^{-/-}$ NCSCs are lost from the developing PNS, we analyzed *Wnt1-Cre*$^+$*Nf1*$^{fl/-}$ embryos and littermate controls at E13, E15, and E17–19. Like germline *Nf1*-deficient mice (Figure 1), we observed increased NCSC frequencies in E13 *Wnt1-Cre*$^+$*Nf1*$^{fl/-}$ embryos as compared to littermate controls in the sympathetic chain, sciatic nerve, and DRG, but not in the gut (Figures S3A–S3D). Nonetheless, the frequency of *Nf1*-deficient NCSCs declined in all regions of the PNS by E15 and declined further by E17. By E17–19, *Nf1*-deficient multipotent neurospheres could only be detected in the sympathetic chain and gut and did not differ in frequency as compared to littermate controls. We confirmed that *Nf1* was efficiently deleted from NCSCs in these experiments by genotyping individual neurospheres cultured from the sympathetic chain, sciatic nerve, DRG, and gut of E13 *Wnt1-Cre*$^+$*Nf1*$^{fl/-}$ embryos: all of the 25 neurospheres exhibited deletion of the *Nf1*^{fl} allele (Figure S3H). These data suggest that *Nf1*-deficient NCSCs differentiate during late gestation according to a similar time course as wild-type NCSCs.

To independently test whether *Nf1* deficiency leads to the postnatal persistence of NCSCs, we generated *3.9Periostin-Cre*$^+$*Nf1*$^{fl/-}$ mice. *3.9Periostin-Cre* conditionally deletes throughout the Schwann cell lineage after E11, at a later stage of development than *Wnt1-Cre* (Lindsley et al., 2007). We also observed an increase in the frequency of NCSCs within the sympathetic chain and sciatic nerve, but not the gut, of E15 *3.9Periostin-Cre*$^+$*Nf1*$^{fl/-}$ mice as compared to littermate controls (Figures

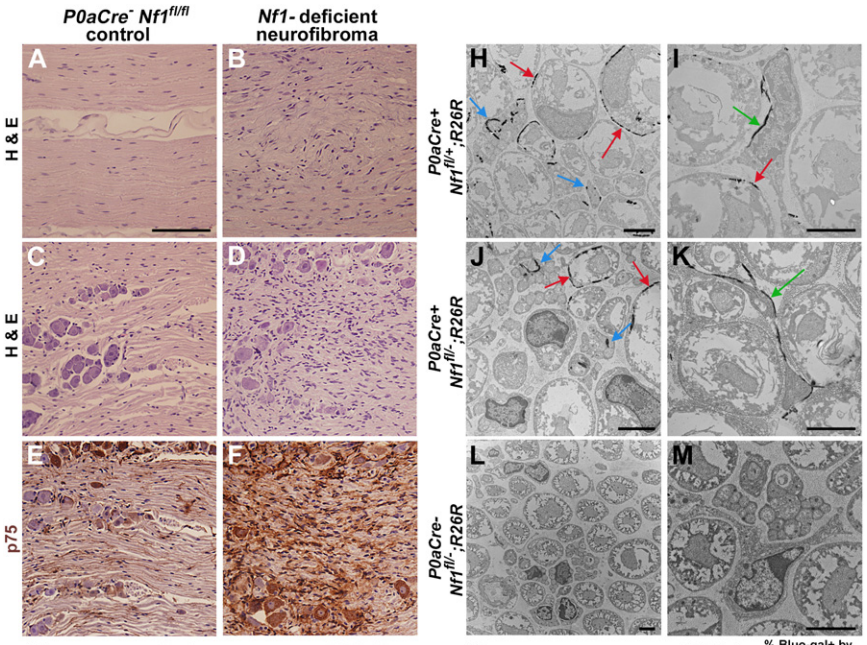

G

	Fraction sorted	*P0aCre-Nf1fl/fl* control	*Nf1*-deficient neurofibroma
DRG	unfractionated	0 ± 0%	0 ± 0%
	p75+	0 ± 0%	0 ± 0%
Sciatic Nerve	unfractionated	0 ± 0%	0 ± 0%
	p75+	0 ± 0%	0 ± 0%
Trigeminal Nerve	unfractionated	0 ± 0%	0 ± 0%
	p75+	0 ± 0%	0 ± 0%
Brachial Plexus	unfractionated	0 ± 0%	0 ± 0%
	p75+	0 ± 0%	0 ± 0%
Sympathetic Ch	unfractionated	0 ± 0%	0 ± 0%
	p75+	0 ± 0%	0 ± 0%
Gut	p75+	10 ± 6%	4 ± 3%

N

	Genotype	Total # of cells counted	% Bluo-gal+ by Electron Microscopy
myelinating Schwann cells	*P0aCre+Nf1fl/+;R26R*	928	35.8%
	P0aCre+Nf1fl/-;R26R	525	35.0%
	P0aCre-Nf1fl/-;R26R	487	0.0%
non-myelinating Schwann cells	*P0aCre+Nf1fl/+;R26R*	161	40.4%
	P0aCre+Nf1fl/-;R26R	78	39.7%
	P0aCre-Nf1fl/-;R26R	109	0.0%
endoneurial fibroblasts	*P0aCre+Nf1fl/+;R26R*	63	55.6%
	P0aCre+Nf1fl/-;R26R	52	59.6%
	P0aCre-Nf1fl/-;R26R	48	0.0%

Figure 3. Adult *P0aCre*$^{+}$*Nf1*$^{fl/-}$ Mice Developed Plexiform Neurofibromas but NCSCs Appeared to Differentiate Normally and Did Not Persist Postnatally

P0aCre^{+} *Nf1*-deficient mice developed plexiform neurofibromas in adult peripheral nerves (B) and DRGs (D), marked by increased cellularity and disorganization relative to control nerves (A) and DRGs (C). Neurofibromas also exhibited increased p75 (F) staining relative to control nerves (E). Multipotent neurospheres arose from control and *P0aCre*$^{+}$ *Nf1*-deficient gut, but not from other regions of the adult PNS (G). Neural crest progenitors in developing nerves were fate-mapped by staining sciatic nerves from postnatal day 20 *P0aCre*$^{+}$*Nf1*$^{fl/+}$*R26R* (H and I), *P0aCre*$^{+}$*Nf1*$^{fl/-}$*R26R* (J and K), and *P0aCre*$^{-}$*Nf1*$^{fl/-}$*R26R* (L and M) pups with bluo-gal (Joseph et al., 2004). We detected no defects in nerve development in *Nf1* mutant mice. A similar percentage of endoneurial fibroblasts (green arrows) as well as myelinating (red arrows) and nonmyelinating (blue arrows) Schwann cells were bluo-gal+ in *P0aCre*$^{+}$*Nf1*$^{fl/-}$*R26R* nerves as compared to littermate controls (N). No bluo-gal staining was observed in *P0aCre*$^{-}$*Nf1*$^{fl/-}$*R26R* negative control nerves (L and M). The scale bar (100 μm) in (A) applies to panels (A)–(F). Scale bars in (H)–(M) equal 2.5 μm. (n = 3–6 mice/genotype for [A]–[G] and 2 mice/genotype for [H]–[N]). All statistics are mean ± SD.

S3E–S3G). Genotyping of individual neurospheres showed that *Nf1* was efficiently deleted from these cells: 30 out of 30 neurospheres exhibited deletion of the *Nf1*^{fl} allele (data not shown).

Most *3.9Periostin-Cre*$^{+}$*Nf1*$^{fl/-}$ mice died by 4 weeks after birth. Of 32 expected *3.9Periostin-Cre*$^{+}$*Nf1*$^{fl/-}$ mice, only 6 survived more than 4 weeks after birth. In these surviving mice, NCSCs did not persist into adulthood in sciatic nerve, DRG, or sympathetic chain in either *3.9Periostin-Cre*$^{+}$*Nf1*$^{fl/-}$ mice or littermate controls (Table 1). As expected, NCSCs did persist postnatally in the guts of *3.9Periostin-Cre*$^{+}$*Nf1*$^{fl/-}$ mice and littermate controls, but there was no difference in the frequency of gut NCSCs in these mice (Table 1). Genotyping of individual neurospheres cultured from the guts of adult *3.9Periostin-Cre*$^{+}$*Nf1*$^{fl/-}$ mice showed that *Nf1* was efficiently deleted from these cells: 35 out of 35 neurospheres exhibited deletion of the *Nf1*^{fl} allele (data not shown). The expansion of NCSCs that was observed at E13 in germline and conditional *Nf1*$^{-/-}$ embryos was therefore only transient: *Nf1*$^{-/-}$ NCSCs did not persist postnatally in regions of the PNS where plexiform neurofibromas form.

NCSCs Do Not Persist Postnatally in Mice that Develop Plexiform Neurofibromas

We never detected PNS tumors in the limited number of *3.9Periostin-Cre*$^{+}$*Nf1*$^{fl/-}$ mice that survived into adulthood (two mice were analyzed at 3 weeks of age and six from 4 to 8 weeks of age). To study mice that consistently survived into adulthood after *Nf1* deletion, we conditionally deleted *Nf1* using *P0a-Cre*, which deletes in trunk neural crest by E11.5 and in peripheral nerves by E12.5 (Giovannini et al., 2000). P0 is expressed by early migrating and multipotent neural crest cells (Hagedorn et al., 1999; Lee et al., 1997). We sacrificed six *P0a-Cre*$^{+}$ *Nf1*-deficient mice and six littermate controls between 15 and 20 months of age and analyzed sciatic nerves, DRGs, trigeminal nerves, and brachial plexi for plexiform neurofibromas. All six of the *P0a-Cre*$^{+}$ *Nf1*-deficient mice, but none of the littermate controls, exhibited neurofibromas (Figures 3A–3F). Classic features of plexiform neurofibromas were evident in each case, including grossly enlarged peripheral nerves and DRGs, with increased cell density, nerve disorganization, and expression of p75 and S100 within the tumors (Figures 3B, 3D, and 3F).

To assess whether NCSCs persist into adulthood in these mice, we dissociated and plated DRG, sciatic nerve, trigeminal nerve, brachial plexus, sympathetic chain, and gut cells from the *P0a-Cre*$^{+}$ *Nf1*-deficient mice and littermate controls into culture as described above. In each case, we sorted both unfractionated cells as well as p75^{+} cells into culture. p75^{+} cells from the gut of *P0a-Cre*$^{+}$ *Nf1*-deficient mice and littermate controls formed multipotent neurospheres in culture (Figure 3G). However, no neurospheres formed in culture from any other region

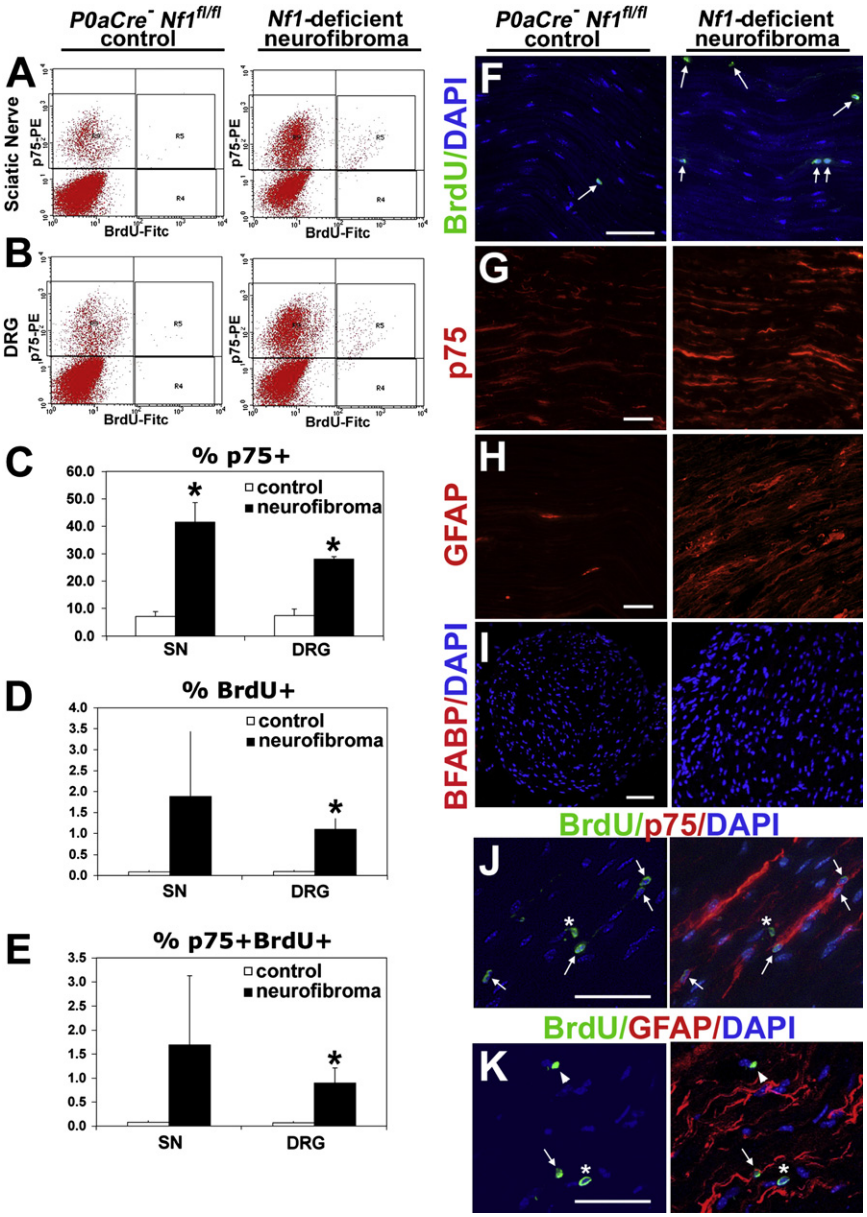

Figure 4. Proliferating Cells within Plexiform Neurofibromas Were p75+ and Expressed Markers of Nonmyelinating Schwann Cells

Sciatic nerves (A, C–E, and F–K) and DRGs (B–E) were dissected from adult *P0aCre*$^{+}$ *Nf1*-deficient mice with plexiform neurofibromas and littermate controls. Mice were administered BrdU for 4 days prior to being sacrificed. By flow-cytometry, neurofibromas contained significantly higher frequencies of p75+ cells (A–C), BrdU+ cells (A, B, and D), and p75+BrdU+ cells (A, B, and E). The vast majority of dividing cells within neurofibromas were p75+ (upper right quadrant of plots in [A] and [B]). Immunofluorescence in sections confirmed the increased frequency of BrdU+ cells ([F]; arrows), p75+ cells (G), and GFAP+ cells (H) in neurofibromas (right column) as compared to control nerves (left column). Normal nerves and neurofibromas lacked BFABP staining (I). Most BrdU+ cells costained with p75 (J), and many costained with GFAP (K), markers of nonmyelinating Schwann cells. In (J) and (K), double-positive cells are indicated with arrows, while possible double-positive cells are indicated with asterisks, and cells that are only BrdU positive are indicated with arrowheads. Scale bars in (F)–(K) equal 50 μm. Error bars represent SD.

of the PNS. These results demonstrate that we were able to culture adult NCSCs from the guts of these mice, but that NCSCs did not persist postnatally in regions of the PNS affected by neurofibromas.

NCSCs Appear to Differentiate Normally in the Nerves of Mice that Develop Neurofibromas

We fate-mapped neural crest progenitors in developing nerves by generating *P0a-Cre*$^{+}$*Nf1*$^{fl/-}$*R26R*$^{+}$ mice and littermate controls. In these mice, the fate of *P0a-Cre* expressing progenitors can be followed based on LacZ expression (R26R). Sciatic nerves were dissected from postnatal day 20 mice of each genotype, stained with bluo-gal, and analyzed by electron microscopy (Joseph et al., 2004). We detected no gross abnormalities in the size, composition, or histology of these postnatal nerves from *P0a-Cre*$^{+}$*Nf1*$^{fl/-}$*R26R*$^{+}$ mice as compared to littermate controls. Bluo-gal+ endoneurial fibroblasts as well as myelinating and nonmyelinating Schwann cells arose with similar frequencies from *P0a-Cre*$^{+}$*Nf1*$^{fl/-}$*R26R* mice as compared to *P0a-Cre*$^{+}$*Nf1*$^{fl/+}$*R26R* controls (Figures 3H–3N). These data suggest that *Nf1*-deficient neural crest progenitors acquired appropriate fates in developing peripheral nerves. Consistent with this, the only abnormality in *P0a-Cre*$^{+}$*Nf1*$^{fl/-}$ nerve development detected in a companion paper was the presence of rare nonmyelinating Schwann cells that were associated with abnormal numbers of axons (Zheng et al., 2008). These data suggest that *Nf1*-deficiency did not grossly alter nerve development or the differentiated fates of neural crest progenitors.

Nonmyelinating Schwann Cells Proliferate within Plexiform Neurofibromas

To address what cells were proliferating within the neurofibromas that arose after *Nf1* deletion with *P0a-Cre*, we analyzed the neurofibromas by flow-cytometry and immunohistochemistry. We observed a significant increase (4.0- to 6.4-fold; $p < 0.01$) in the frequency of p75+ cells within the plexiform neurofibromas in sciatic nerves and DRGs as compared to normal nerves and DRGs from littermate controls (Figures 4A–4C). By administering BrdU to mice for 4 days before analysis, we also found that these p75+ cells were much more likely to be dividing in neurofibromas as compared to normal tissue from littermate

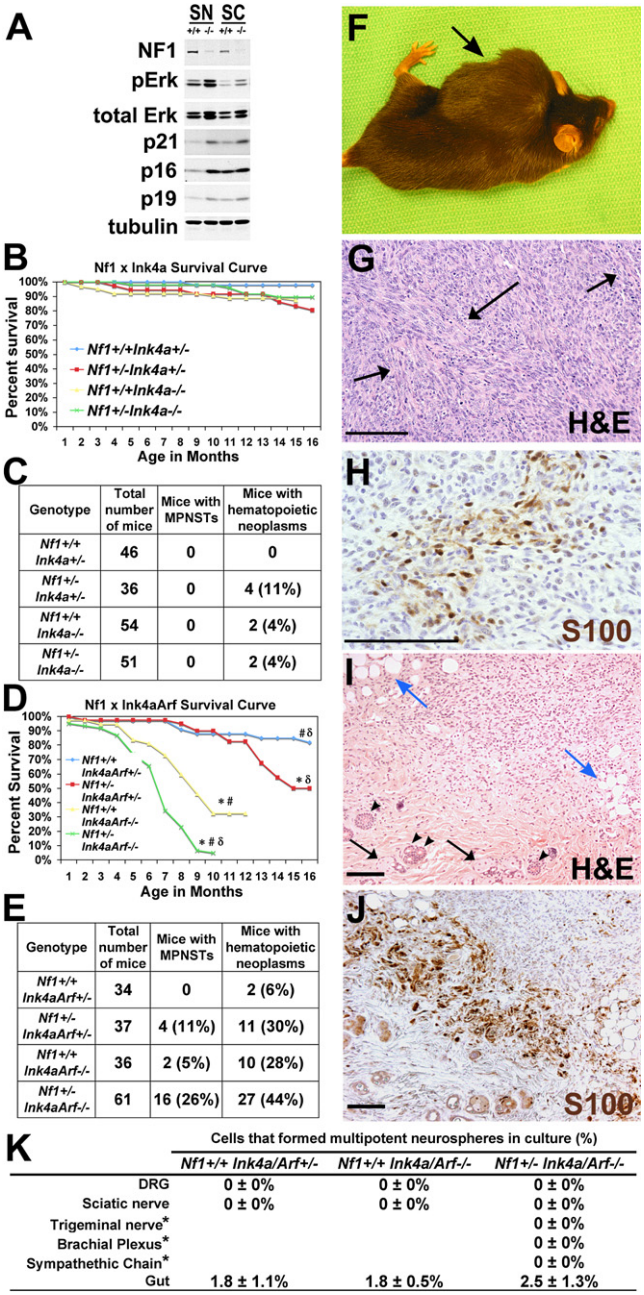

Figure 5. *Ink4a/Arf* Deficiency, but Not *Ink4a* Deficiency, Collaborates with *Nf1* Mutations to Generate MPNSTs without the Postnatal Persistence of NCSCs

(A) $Nf1^{+/+}$ and $Nf1^{-/-}$ neural crest cells cultured from sciatic nerve (SN) and sympathetic chain (SC) were analyzed by western blot. (B) *Ink4a* deficiency did not significantly affect the survival of $Nf1^{+/-}$ mice. (C) We detected no MPNSTs among $Nf1^{+/-}Ink4a^{-/-}$ mice or littermate controls. (D) The lifespan of $Nf1^{+/-}$ mice was significantly ($p < 0.05$) decreased by *Ink4a/Arf* deficiency as compared to littermate controls (* versus $Nf1^{+/+}Ink4aArf^{+/-}$; # versus $Nf1^{+/-}Ink4aArf^{+/-}$; δ versus $Nf1^{+/+}Ink4aArf^{-/-}$). Each line in (B) and (D) represents a cohort of 34–61 mice per genotype (see numbers in [C] and [E]). $Nf1^{+/-}Ink4a/Arf^{-/-}$ mice developed MPNSTs (E–J) as early as P30 but more commonly after 4–6 months of age. Tumors were typically large ([F], arrow). Paraffin sections exhibited classic features of MPNSTs including fascicular patterns of tightly packed spindle cells ([G], arrows) with hyperchromatic nuclei and frequent mitoses (G). These tumors contained $S100^{+}$ cells (H), a marker used in the diagnosis of MPNSTs. Some tumors were found embedded in the dermis (I and J) surrounding fat cells ([I], blue arrows), sebaceous glands ([I], arrows), and hair follicles ([I], arrowheads). Dermal tumors stained more intensely for S100 (J) than MPNSTs outside of the dermis (H). Scale bars in (G)–(J) equal 100 μm. (K) Multipotent neurospheres consistently arose from $Nf1^{+/-}$ *Ink4a/Arf* $^{-/-}$ and control guts, but not from other regions of the adult PNS (*these tissues were analyzed relative to age-matched wild-type controls). Statistics represent mean ± SD for 3–6 independent experiments.

controls (Figures 4A, 4B, 4D, and 4E). Indeed, virtually all of the dividing cells (BrdU+ cells) within neurofibromas were p75+ (Figures 4A and 4B). Since we could not culture NCSCs from the nerves or DRGs of these adult mice, these data suggest that nonmyelinating Schwann cells were proliferating within neurofibromas, as nonmyelinating Schwann cells also express p75 (Jessen et al., 1990).

To test whether the proliferating p75+ cells within plexiform neurofibromas expressed other markers of nonmyelinating Schwann cells, we stained tumor sections with antibodies against BrdU, p75, GFAP, and BFABP. We observed increased numbers of BrdU+ cells (Figure 4F), p75+ cells (Figure 4G), and p75+BrdU+ cells (Figure 4J) in neurofibromas as compared to normal nerves, just as we had observed by flow cytometry (Figures 4A–4E). We also observed greatly increased numbers of GFAP+ cells in neurofibromas (Figure 4H) and at least some of these GFAP+ cells also appeared to be BrdU+ (Figure 4K), though this was difficult to assess because GFAP is expressed mainly in cell processes while BrdU is nuclear. Since GFAP is expressed by nonmyelinating Schwann cells, but not by primitive glial progenitors in E13 fetal nerves (which include NCSCs and restricted Schwann cell precursors) (Jessen and Mirsky, 2005; Jessen et al., 1990; Morrison et al., 1999), these data suggest that GFAP+ nonmyelinating Schwann cells contribute to the growth of neurofibromas. Neither normal nerves nor neurofibromas exhibited detectable BFABP (also known as BLBP or Fabp7) staining (Figure 4I). Primitive glial progenitors in embryonic nerves express BFABP, but adult nonmyelinating Schwann cells do not (Britsch et al., 2001; Jessen and Mirsky, 2005). The presence of large numbers of p75+, GFAP+, and BFABP− cells in neurofibromas, at least some of which are dividing, suggests that nonmyelinating Schwann cells contribute to the growth of neurofibromas.

Nf1 and *p53* Mutations Lead to MPNSTs but Not to the Postnatal Persistence of NCSCs

$Nf1/p53^{+/-}$ mice formed MPNSTs by 6 months of age (Figures S4A–S4C) as previously reported (Cichowski et al., 1999; Vogel et al., 1999). To test whether these mice maintained postnatal NCSCs, we cultured dissociated cells from DRG, sciatic nerve, trigeminal nerve, sympathetic chain, and gut of adult $Nf1/p53^{+/-}$ mice. Gut cells from $Nf1/p53^{+/-}$ mice and littermate controls formed NCSC colonies in culture, but *Nf1/p53* heterozygosity did not affect the frequency or growth of these cells (Figure S4D). We did not detect cells from the DRG, sciatic nerve, trigeminal nerve, or sympathetic chain of $Nf1/p53^{+/-}$ mice or littermate controls that could form NCSC colonies (Figure S4D). *Nf1* and *p53* mutations did not affect the ability of fetal or adult NCSCs to form colonies in culture or to undergo multilineage differentiation (Figure S5A and S5E), so these mutations did not prevent us from

detecting NCSCs in culture. *Cis* deletion of *Nf1* and *p53* leads to the formation of MPNSTs during adulthood without promoting the postnatal persistence of NCSCs, suggesting that MPNSTs do not arise from NCSCs.

We also examined DRGs, sciatic nerves, trigeminal nerves, brachial plexi, and sympathetic ganglia from 3- to 6-month-old *Nf1/p53*$^{+/-}$ mice prior to the formation of MPNSTs to assess whether there were any abnormalities in PNS development. Except for a single *Nf1/p53*$^{+/-}$ brachial plexus that exhibited hyperproliferation, we were unable to distinguish *Nf1/p53*$^{+/-}$ tissues from wild-type tissues by histology or marker expression (Figure S6). We also did not detect any increase in the frequency of p75+ cells in adult *Nf1/p53*$^{+/-}$ tissues prior to the development of MPNSTs (Figure S6S). The failure to detect significantly increased numbers of p75+ cells in adult *Nf1/p53*$^{+/-}$ tissues prior to the development of tumors supports the conclusion that these tumors do not arise from the postnatal persistence of expanded populations of NCSCs.

Ink4a and *Arf* Deficiency Cooperate with *Nf1* Heterozygosity to Yield MPNSTs

To test whether the postnatal persistence of NCSCs might be inhibited by induction of p16^{Ink4a} or p19^{Arf} expression in *Nf1* mutant NCSCs we performed western blots on cultured NCSCs from the sciatic nerve and sympathetic chain. In both cases, we observed increased p19^{Arf} expression by *Nf1*$^{-/-}$ cells (Figure 5A). We also observed an increase in p16^{Ink4a} expression by *Nf1*$^{-/-}$ sciatic nerve cells, though the effect on p16^{Ink4a} expression in sympathetic chain cells was not as clear. Consistent with the known role for *p53* mutations in the formation of MPNSTs, we also observed a consistent increase in p21^{Cip1} expression by *Nf1*$^{-/-}$ NCSCs (Figure 5A). These observations raised the possibility that increased p16^{Ink4a} and p19^{Arf} expression by *Nf1*$^{-/-}$ NCSCs might retard the formation of MPNSTs.

To test this, we first generated mice bearing mutations in *Nf1* and *Ink4a* (leaving *Arf* intact). We aged cohorts of *Nf1*$^{+/-}$*Ink4a*$^{-/-}$ mice as well as various genotypes of littermate controls for up to 16 months. Overall mortality was low (Figure 5B). We never detected any MPNSTs or neurofibromas in these mice, though we did observe some hematopoietic neoplasms, particularly lymphoma (Figure 5C). The lack of grossly evident PNS tumors in these mice suggested that *Ink4a* deletion is not sufficient for tumorigenesis in an *Nf1* heterozygous background. *Nf1*$^{+/-}$ mice were previously generated on an *Arf*-deficient background and also did not develop neurofibromas or MPNSTs (King et al., 2002). These observations are consistent with genetic analyses of MPNSTs in patients, which usually exhibit loss-of-function mutations in both the Rb and p53 pathways (Agesen et al., 2005; Perrone et al., 2003).

To develop a mouse model that more faithfully recapitulated the mutations observed in human MPNSTs, we generated mice bearing mutations in *Nf1* and *Ink4a/Arf* (lacking both *Ink4a* and *Arf*). We aged cohorts of *Nf1*$^{+/-}$*Ink4a/Arf*$^{-/-}$ mice as well as various genotypes of littermate controls for up to 16 months. Virtually all *Nf1*$^{+/-}$*Ink4a/Arf*$^{-/-}$ mice died by 10 months of age, more quickly than littermates with other genotypes (Figure 5D). *Nf1*$^{+/+}$*Ink4a/Arf*$^{+/-}$ control mice failed to develop MPNSTs or neurofibromas, but 26% of *Nf1*$^{+/-}$*Ink4a/Arf*$^{-/-}$ mice had to be euthanized due to the formation of MPNSTs (Figures 5E and 5F). Most of the MPNSTs developed by *Nf1*$^{+/-}$*Ink4a/Arf*$^{-/-}$ mice became grossly evident at 4 to 6 months of age. These MPNSTs tended to develop on the shoulders, ribs, or legs of mice, close to DRGs and peripheral nerves. Much lower rates of MPNSTs were observed among *Nf1*$^{+/-}$*Ink4a/Arf*$^{+/-}$ mice (Figure 5E), and only after 1 year of age. These statistics may underestimate the true frequency of MPNSTs, as smaller tumors may have gone undetected in mice that died due to other causes.

Histology of the MPNSTs revealed typical features including fascicular patterns of tightly packed spindle cells with hyperchromatic nuclei and frequent mitoses (Figure 5G) as well as S100 staining (Figure 5H). Five of the MPNSTs observed in *Nf1*$^{+/-}$*Ink4a/Arf*$^{-/-}$ mice were confined to the dermis and epidermis (Figure 5I), were much smaller than the more typical tumors imaged in Figure 5F, and stained more intensely for S100 (Figure 5J). These tumors may actually be dermal neurofibromas, though they were characterized as MPNSTs because the frequent mitotic figures and invasiveness were more consistent with a malignancy. These data demonstrate that *Ink4a/Arf* deficiency leads to the formation of MPNSTs in an *Nf1*$^{+/-}$ background.

In addition to forming MPNSTs, we observed a significant frequency of hematopoietic neoplasms among *Nf1*$^{+/-}$*Ink4a/Arf*$^{-/-}$, *Nf1*$^{+/-}$*Ink4a/Arf*$^{+/-}$, and *Nf1*$^{+/+}$*Ink4a/Arf*$^{-/-}$ mice (Figure 5E). These included mainly lymphomas and histiocytic neoplasms, but we observed some acute myeloid leukemias as well as some mice with myeloproliferative disease.

NCSCs Did Not Persist Postnatally in *Nf1*$^{+/-}$*Ink4a/Arf*$^{-/-}$ Mice

To test whether *Nf1*$^{+/-}$*Ink4a/Arf*$^{-/-}$ mice maintained postnatal NCSCs, we cultured dissociated cells from DRG, sciatic nerve, trigeminal nerve, brachial plexus, sympathetic chain, and gut of adult *Nf1*$^{+/-}$*Ink4a/Arf*$^{-/-}$ mice and littermate controls. Gut cells from *Nf1*$^{+/-}$*Ink4a/Arf*$^{-/-}$ mice and controls formed multilineage NCSC colonies in culture, but we did not detect a significantly increased frequency of NCSCs in *Nf1*$^{+/-}$*Ink4a/Arf*$^{-/-}$ mice (Figure 5K). *Nf1* deficiency also did not affect the size of gut NCSC colonies (data not shown). We did not detect cells from any other region of the PNS of *Nf1*$^{+/-}$*Ink4a/Arf*$^{-/-}$ mice or littermate controls that could form multipotent neurospheres (Figure 5K). *Nf1* and *Ink4a/Arf* mutations did not affect the ability of fetal or adult NCSCs to form colonies in culture or to undergo multilineage differentiation (Figures S5B and S5F), so these mutations did not prevent us from detecting NCSCs in culture.

We also examined DRGs, sciatic nerves, trigeminal nerves, and sympathetic ganglia from 3- to 6-month-old *Nf1*$^{+/-}$*Ink4a/Arf*$^{-/-}$ mice prior to the formation of MPNSTs to assess PNS development. We were unable to distinguish *Nf1*$^{+/-}$*Ink4a/Arf*$^{-/-}$ tissues from wild-type tissues by either histology or marker expression and did not detect a significant increase in the frequency of p75+ cells in adult *Nf1*$^{+/-}$*Ink4a/Arf*$^{-/-}$ tissues prior to the development of MPNSTs (Figure S6). The failure to detect significantly increased numbers of p75+ cells in adult *Nf1*$^{+/-}$*Ink4a/Arf*$^{-/-}$ tissues prior to the development of tumors supports the conclusion that these tumors do not arise from the postnatal persistence of expanded populations of NCSCs.

Clonogenic MPNST Cells Did Not Resemble NCSCs

To test whether clonogenic MPNST cells resembled NCSCs, tumors from *Nf1*$^{+/-}$*Ink4aArf*$^{-/-}$ mice or *Nf1/p53*$^{+/-}$ mice were

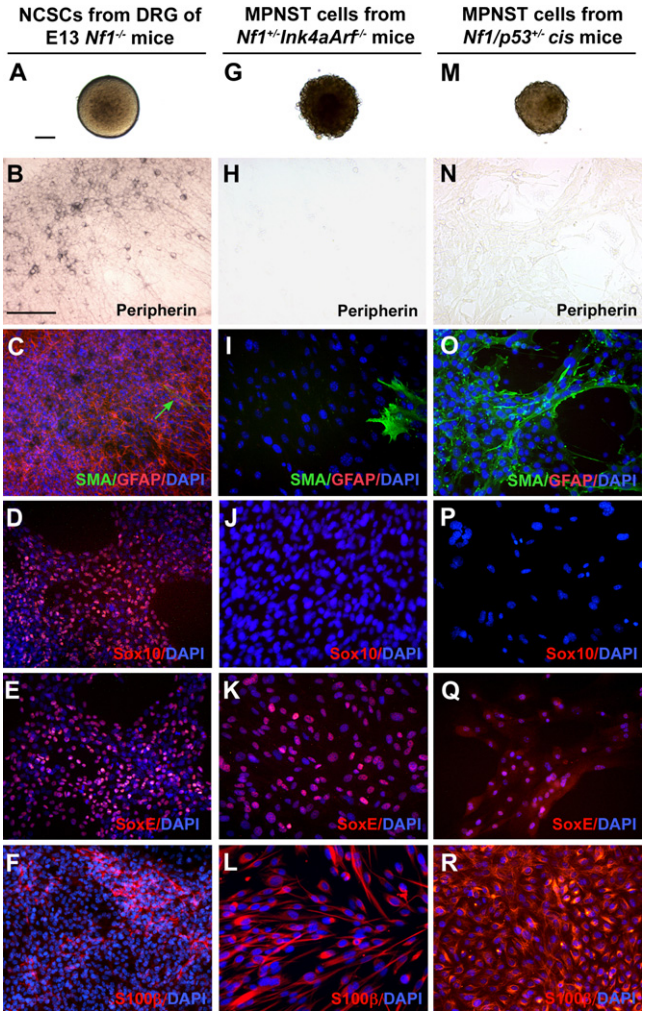

Figure 6. Self-Renewing Spheres Grew from *Nf1*$^{+/-}$*Ink4a/Arf* $^{-/-}$ and *Nf1/p53*$^{+/-}$ MPNSTs but Did Not Form Colonies that Resembled NCSCs Colonies

Some MPNST cells from *Nf1*$^{+/-}$*Ink4aArf*$^{-/-}$ mice and *Nf1/p53*$^{+/-}$ mice formed self-renewing spheres in culture. While all NCSCs generated peripherin^{+} neurons (B), GFAP^{+} glia (C), and SMA^{+} myofibroblasts ([C]; arrow), MPNST colonies from *Nf1*$^{+/-}$*Ink4aArf*$^{-/-}$ and *Nf1/p53*$^{+/-}$ mice failed to generate peripherin^{+} neurons (H and N) or GFAP^{+} glia (I and O). In contrast to *Nf1*$^{-/-}$ NCSC colonies (D), MPNST colonies exhibited little or no Sox10 staining (J and P). MPNST colonies typically contained cells with a glial morphology (data not shown) as well as SMA^{+} myofibroblasts (I and O). Like *Nf1*$^{-/-}$ NCSC colonies (E and F), most cells within MPNST colonies were SoxE^{+} (K and Q) and S100β^{+} (L and R). These represent typical colonies from six independent *Nf1*$^{+/-}$*Ink4a/Arf*$^{-/-}$ MPNSTs and four independent *Nf1/p53*$^{+/-}$ MPNSTs. The scale bar (100 μm) in (A) applies to (A), (G), and (M) while the scale bar (100 μm) in (B) applies to all other panels.

dissociated and cultured in the conditions we use for NCSCs. Some *Nf1*$^{+/-}$*Ink4a/Arf*$^{-/-}$ MPNST cells and *Nf1/p53*$^{+/-}$ MPNST cells formed spheres in culture (Figures 6G and 6M). These sphere-forming cells had self-renewal potential, giving rise to an average of 164 ± 133 and 104 ± 21 daughter spheres, respectively, when subcloned after 10 to 12 days of primary culture. These sphere-forming cells were unlikely to arise from normal cells in the tumors because we were unable to culture sphere-forming cells from normal adult nerves in control mice (Figure 5K). All *Nf1*$^{-/-}$ (Figures 6A–6F) and wild-type (Figures 2C and 2F) NCSC colonies formed peripherin^{+} neurons (Figure 6B), smooth muscle actin^{+} (SMA^{+}) myofibroblasts (Figure 6C), and GFAP^{+} glia (Figure 6C). Moreover, E13 *Nf1*$^{-/-}$*Ink4a/Arf*$^{-/-}$ and *Nf1/p53*$^{-/-}$ NCSCs also underwent multilineage differentiation, as did adult gut *Nf1*$^{+/-}$*Ink4a/Arf*$^{-/-}$ and *Nf1/p53*$^{+/-}$ NCSCs (Figure S5). These data demonstrate that *Nf1* deficiency, with or without additional mutations in *p53* or *Ink4a/Arf*, does not alter the ability of NCSCs to undergo multilineage differentiation. In contrast, the *Nf1*$^{+/-}$*Ink4a/Arf*$^{-/-}$ MPNST and *Nf1/p53*$^{+/-}$ MPNST colonies in the same culture conditions rarely generated peripherin^{+} neurons and never GFAP^{+} glia (Figure 6). Clonogenic MPNST cells fail to undergo multilineage differentiation characteristic of NCSCs.

While cells within NCSC colonies were Sox10^{+} as expected (Kim et al., 2003), MPNST cells stained weakly or not at all for Sox10, as previously reported (Levy et al., 2004; Miller et al., 2006) (Figure 6). Apart from the lack of GFAP staining, most cells in MPNST colonies otherwise resembled glia, as they were small, spindle-shaped cells that stained positively for SoxE (Sox8/9/10) and S100β (Figure 6). Increased Sox9 expression is typical of MPNSTs, and a subset of MPNSTs express S100β (Miller et al., 2006; Takeuchi and Uchigome, 2001). MPNST cells thus formed colonies that consistently differed from wild-type (Figures 2C and 2F), *Nf1*$^{-/-}$ (Figures 6A–6F), *Nf1*$^{-/-}$*Ink4aArf*$^{-/-}$ (Figure S5B), and *Nf1/p53*$^{-/-}$ (Figure S5A) NCSCs, though these cells did resemble Schwann cells based on morphology and expression of S100β and SoxE.

Nf1-Deficient NCSCs Are Not Tumorigenic

To test whether *Nf1*-deficient NCSCs could form tumors, we cultured NCSCs from E13 *Nf1*$^{+/+}$ or *Nf1*$^{-/-}$ mice or MPNST cells from *Nf1*$^{+/-}$*Ink4a/Arf*$^{-/-}$ mice, then transplanted these cells into the sciatic nerves of adult *Nf1*$^{+/-}$ mice. In some experiments, the *Nf1* mutant allele was bred onto a Rosa background so that we could monitor the engraftment of the transplanted cells. All mice (8/8) injected with 50,000 MPNST cells developed large tumors within 2 to 6 weeks of injection (Figures 7I and 7J). None of 12 mice injected with 50,000 to 100,000 *Nf1*$^{+/+}$ cells or 16 mice injected with 50,000 to 100,000 *Nf1*$^{-/-}$ cells developed tumors despite being monitored for up to 20 months after injection (Figure 7J). The *Nf1*$^{+/+}$ and *Nf1*$^{-/-}$ cells did engraft within nerves as indicated by the presence of LacZ expressing cells (Figures 7E–7H). However, these LacZ+ donor cells never formed tumors (Figures 7G and 7H). Together, our data indicate that NCSCs are not rendered tumorigenic by *Nf1* deficiency, but rather infrequent differentiated glia (such as nonmyelinating Schwann cells) begin proliferating inappropriately and form tumors in adults.

DISCUSSION

If NCSCs give rise to plexiform neurofibromas and MPNSTs, then *Nf1*-deficient NCSCs would be expected to persist in expanded numbers throughout late gestation and into the postnatal period. However, we did not detect the postnatal persistence of NCSCs in DRG, sympathetic chain, trigeminal ganglion, brachial plexus, or peripheral nerve of conditional *Nf1*-deficient mice (Table 1), even in mice that went on to develop plexiform neurofibromas (Figure 3G). The expansion of *Nf1*-deficient

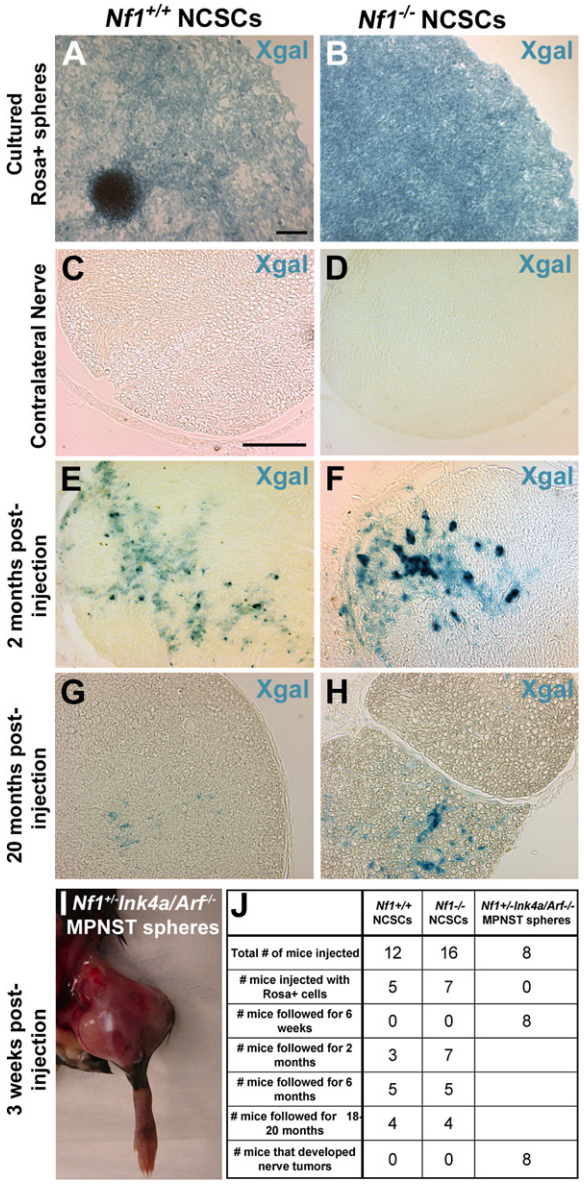

J	Nf1+/+ NCSCs	Nf1-/- NCSCs	Nf1+/-Ink4a/Arf-/- MPNST spheres
Total # of mice injected	12	16	8
# mice injected with Rosa+ cells	5	7	0
# mice followed for 6 weeks	0	0	8
# mice followed for 2 months	3	7	
# mice followed for 6 months	5	5	
# mice followed for 18-20 months	4	4	
# mice that developed nerve tumors	0	0	8

Figure 7. *Nf1*-Deficient NCSCs Are Not Tumorigenic In Vivo

We transplanted 50,000 MPNST cells or 50,000–100,000 $Nf1^{+/+}$ or $Nf1^{-/-}$ NCSCs into the nerves of adult $Nf1^{+/-}$ mice. NCSCs were grown as spheres from various regions of the E13 PNS of $Nf1^{+/+}$ and $Nf1^{-/-}$ mice that had been bred to Rosa mice in some experiments to allow the tracking of cells with Xgal staining (A and B). NCSC spheres were replated to adherent cultures, dissociated to single cell suspensions, and injected into the sciatic nerves of adult $Nf1^{+/-}$ mice. Contralateral nerves never showed X-gal+ cells (C and D) but nerves injected with Rosa+ cells consistently showed engraftment (E–H). MPNST spheres from $Nf1^{+/-}Ink4aArf^{-/-}$ mice were also dissociated and injected into the sciatic nerves of adult $Nf1^{+/-}$ mice (I). Tumors were never observed in mice injected with $Nf1^{+/+}$ or $Nf1^{-/-}$ neural crest cells, even after 20 months follow-up (E–J). MPNST cells gave rise to large tumors (I) in all recipients within 2–6 weeks after injection (J). The scale bar (100 μm) in (A) applies to (A) and (B) and the scale bar (100 μm) in (C) applies to (C)–(H).

NCSCs occurred only transiently during midgestation. Like wild-type NCSCs, *Nf1*-deficient NCSCs became increasingly rare in late gestation and failed to persist postnatally, precluding them from participating in tumorigenesis (Figure S3). NCSCs also did not persist postnatally in $Nf1^{+/-}Ink4aArf^{-/-}$ or $Nf1/p53^{+/-}$ mice (Figure 5K; Figure S4), despite the fact that they went on to develop MPNSTs as adults (Figure 5; Figure S4). Since NCSCs did not persist postnatally in regions of the PNS that formed plexiform neurofibromas or MPNSTs during adulthood, NCSCs could not have given rise to these tumors.

Our inability to detect *Nf1*-deficient NCSCs postnatally in regions of the PNS that developed tumors did not simply reflect altered differentiation or survival of these cells in culture. In all experiments, we were able to detect the postnatal persistence of both wild-type and *Nf1*-deficient NCSCs from the adult gut. This positive control demonstrated that we were able to culture adult NCSCs from each of the genetic backgrounds we studied. Moreover, *Nf1* deficiency increased the survival and proliferation of NCSCs in culture, making them easier, not more difficult, to grow (Figure 2). Furthermore, *Nf1* deficiency, with or without *p53* or *Ink4a/Arf* deficiency, did not alter the ability of NCSCs to undergo multilineage differentiation (Figure 2; Figure 6; Figure S1; Figure S5).

Nf1-deficient NCSCs appeared to differentiate normally in peripheral nerves during late gestation (Figure 3). We did not detect any gross alterations in nerve development in P20 *Nf1* mutant mice by electron microscopy (Figure 3). Rather, hyperplasia and increased frequencies of p75+ cells were not observed in $P0a\text{-}Cre^{+}Nf1^{fl/-}$ mice until around 3 months of age (Zheng et al., 2008). We also did not detect any gross alterations in PNS development or a significant increase in the frequency of p75+ cells in PNS tissues from $Nf1^{+/-}Ink4aArf^{-/-}$ or $Nf1/p53^{+/-}$ mice during early adulthood prior to the formation of tumors (Figure S6). When combined with the observation that *Nf1*-deficient NCSCs were lost from the late gestation PNS according to a similar time course as wild-type NCSCs (Figure S3), and the observation that *Nf1*-deficient NCSCs failed to form tumors after transplantation into adult $Nf1^{+/-}$ peripheral nerves (Figure 7), our data suggest that *Nf1*-deficient NCSCs terminally differentiate during late gestation and are long gone by the time tumors arise in the adult PNS.

Our data instead suggest that infrequent differentiated glia, such as nonmyelinating Schwann cells within peripheral nerves, begin proliferating inappropriately in the postnatal period and give rise to plexiform neurofibromas. The dividing cells within plexiform neurofibromas were almost exclusively p75+ (Figures 4A, 4B, and 4J). Many of these cells had a phenotype similar to nonmyelinating Schwann cells (and dissimilar to fetal NCSCs) as they were also GFAP+ and BFABP− (Figure 4). Proliferating cells within MPNSTs also expressed some differentiated glial markers as well as having a glial morphology (Figure 6).

Why would deletion of *Nf1* in fetal nerve progenitors lead to the formation of tumors that do not become evident until adulthood in mice (Zhu et al., 2002)? A cosubmitted manuscript by Zheng and colleagues concludes that abnormal differentiation of some nonmyelinating Schwann cells in the absence of *Nf1* leads to their association with unusually large numbers of axons (Zheng et al., 2008). These bundles degenerate postnatally, leading to inflammation that precedes Schwann cell hyperproliferation and the formation of plexiform neurofibromas. These observations suggest that *Nf1*-deficient Schwann cells differentiate perinatally and do not become hyperproliferative until early adulthood when their behavior is modified by epigenetic (i.e., inflammation,

hormones, and nerve damage) or genetic (i.e., secondary mutations) triggers.

Our results do not address the origin of dermal neurofibromas. Typical benign dermal neurofibromas did not arise in any of the mice we studied. Neural progenitors have been cultured from adult dermis and at least some of these are neural crest derived (Fernandes et al., 2004; Wong et al., 2006). While these cells express markers similar to NCSCs, the progenitors cultured from trunk skin have little capacity to make neurons (Wong et al., 2006), in contrast to the NCSC populations we have characterized (Bixby et al., 2002; Kruger et al., 2002; Morrison et al., 1999). More work will be required to identify the in vivo cells that give rise to the dermally derived neural progenitors. Nonetheless, this is a different neural progenitor population, in a different location, than the NCSC populations that we characterized in this study.

It is interesting that NF1 negatively regulates the frequency, self-renewal, growth factor sensitivity, and gliogenesis of NCSCs in most regions of the PNS but not in the gut. The basis for this regional difference in NF1 function is not clear. Nonetheless, these results are consistent with the observation that neurofibromatosis patients seem more likely to develop tumors from peripheral nerves, DRGs, and sympathetic ganglia than from the gut (Fuller and Williams, 1991). The failure of gut neural crest progenitors to exhibit increased proliferation or gliogenesis after *Nf1* deletion may partly explain this clinical observation.

While many cancers may arise from the transformation of stem cells, our results indicate that NCSCs are not rendered tumorigenic by mutations in *Nf1*. Benign tumors and cancers of the PNS can arise from differentiated glia.

EXPERIMENTAL PROCEDURES

All experiments using mice were performed in accordance with approved protocols by the University Committee on the Use and Care of Research Animals (UCUCA). Several *Nf1* alleles were used in these studies including $Nf1^{-}$ (germline mutant) mice (Jacks et al., 1994), $Nf1^{fl}$ mice for conditional deletion (Zhu et al., 2001), and $Nf1/p53^{-}$ *cis* mutant mice (Cichowski et al., 1999). For conditional deletion of *Nf1* we used *Wnt-1-Cre*$^{+}$ (Danielian et al., 1998), *3.9Periostin-Cre*$^{+}$ (Lindsley et al., 2007), and *P0a-Cre*$^{+}$ (Giovannini et al., 2000) mice. Compound mutant mice were generated by mating $Nf1^{+/-}$ mice with $Ink4a^{-/-}$ mice (Sharpless et al., 2001) or $Ink4aArf^{-/-}$ mice (Serrano et al., 1996).

Isolation of NCSCs

Timed pregnant matings of $Nf1^{+/-}$ mice were set up to obtain E13 $Nf1^{-/-}$ embryos. DRGs (cervical, thoracic, and lumbar), sciatic nerve, sympathetic chain, and gut (including stomach, small intestine, and hindgut) were dissected from E12.5 to E13.5 $Nf1^{+/+}$, $Nf1^{+/-}$, and $Nf1^{-/-}$ littermates and collected in ice-cold Ca, Mg-free HBSS. Tissues were dissociated for 4 min at 37°C in 0.05% trypsin/EDTA (Invitrogen, Carlsbad, California; diluted 1:10 in Ca, Mg-free HBSS) with 0.25 mg/ml type IV collagenase (Worthington, Lakewood NJ) then quenched with staining medium: L15 medium containing 1 mg/ml BSA (Sigma A-3912, St. Louis, MO), 10 mM HEPES (pH 7.4), 1% penicillin/streptomycin (BioWhittaker, Walkersville, MD), and 25 mg/ml deoxyribonuclease type 1 (DNase1, Sigma D-4527). Cells were centrifuged, resuspended in staining medium without DNase, triturated, filtered through nylon screen (45 μm, Sefar America, Kansas City, MO) to remove aggregates, counted by hemocytometer, and added to culture. In some experiments, cell suspensions were stained with antibodies against p75 (Ab 1554; Chemicon) and α_4 integrin (Becton Dickinson, San Jose, CA) for analysis by flow-cytometry (Bixby et al., 2002). In some experiments, cells were stained for BrdU using a flow-cytometry kit (BD PharMingen; cat. no. 559619). Flow cytometry was performed with a FACSVantage SE-dual laser, three-line flow-cytometer (Becton Dickinson).

See Supplementary Data for details regarding dissociation of adult cells, genotyping, cell culture, immunohistochemistry, western blots, nerve injections, and other methods.

Supplemental Data

The Supplemental Data include six supplemental figures and Supplemental Experimental Procedures and can be found with this article online at http://www.cancercell.org/cgi/content/full/13/2/129/DC1/.

ACKNOWLEDGMENTS

This work was supported by the NIH NINDS (R01 NS40750 to SJM) and the Howard Hughes Medical Institute. Generation of 3.9Periostin-Cre mice was supported by R01 HL077342 to S.J.C. and T32 HL079995 to P.S. Y.Z. was supported by grants from the American Cancer Society and Department of Defense. N.M.J was supported by an NRSA from the NINDS (F30 NS049761). J.T.M. was supported by the Aron Family NF Scholars Fellowship from the Children's Tumor Foundation. J.B. was supported by the Swiss National Science Foundation. Thanks to M. White and D. Adams for assistance with flow cytometry. Thanks to D. Sorensen for assistance with electron microscopy and to H. Zheng and L. Chang for assistance with *P0aCre* experiments. Thanks to Tyler Jacks for providing *Nf1*-deficient mice, to Karlyne Reilly for providing $Nf1/p53^{+/-}$ cis mice, and to Ron DePinho for providing *Ink4a* and *Ink4a/Arf* mice. Thanks to Alan Saltiel's and Kun-Liang Guan's laboratories for advice related to western blots. Thanks to Michael Wegner, David Anderson, and Thomas Muller for providing antibodies against SoxE, Sox10, and BFABP. Thanks to Paul Cederna and Deborah Yu for advice with nerve injections.

Received: June 5, 2007
Revised: November 15, 2007
Accepted: January 3, 2008
Published: February 4, 2008

REFERENCES

Agesen, T.H., Florenes, V.A., Molenaar, W.M., Lind, G.E., Berner, J.M., Plaat, B.E., Komdeur, R., Myklebost, O., van den Berg, E., and Lothe, R.A. (2005). Expression patterns of cell cycle components in sporadic and neurofibromatosis type 1-related malignant peripheral nerve sheath tumors. J. Neuropathol. Exp. Neurol. *64*, 74–81.

Bixby, S., Kruger, G.M., Mosher, J.T., Joseph, N.M., and Morrison, S.J. (2002). Cell-intrinsic differences between stem cells from different regions of the peripheral nervous system regulate the generation of neural diversity. Neuron *35*, 643–656.

Brannan, C.I., Perkins, A.S., Vogel, K.S., Ratner, N., Nordlund, M.L., Reid, S.W., Buchberg, A.M., Jenkins, N.A., Parada, L.F., and Copeland, N.G. (1994). Targeted disruption of the neurofibromatosis type-1 gene leads to developmental abnormalities in heart and various neural crest-derived tissues. Genes Dev. *8*, 1019–1029.

Britsch, S., Goerich, D.E., Riethmacher, D., Peirano, R.I., Rossner, M., Nave, K.-A., Birchmeier, C., and Wegner, M. (2001). The transcription factor Sox10 is a key regulator of peripheral glial development. Genes Dev. *15*, 66–78.

Cichowski, K., Shih, T.S., Schmitt, E., Santiago, S., Reilly, K., McLaughlin, M.E., Bronson, R.T., and Jacks, T. (1999). Mouse models of tumor development in neurofibromatosis type 1. Science *286*, 2172–2176.

Danielian, P.S., Muccino, D., Rowitch, D.H., Michael, S.K., and McMahon, A.P. (1998). Modification of gene activity in mouse embryos in utero by a tamoxifen-inducible form of Cre recombinase. Curr. Biol. *8*, 1323–1326.

Dasgupta, B., and Gutmann, D.H. (2005). Neurofibromin regulates neural stem cell proliferation, survival, and astroglial differentiation in vitro and in vivo. J. Neurosci. *25*, 5584–5594.

Fernandes, K.J., McKenzie, I.A., Mill, P., Smith, K.M., Akhavan, M., Barnabe-Heider, F., Biernaskie, J., Junek, A., Kobayashi, N.R., Toma, J.G., et al. (2004). A dermal niche for multipotent adult skin-derived precursor cells. Nat. Cell Biol. *6*, 1082–1093.

Fuller, C.E., and Williams, G.T. (1991). Gastrointestinal manifestations of type 1 neurofibromatosis (von Recklinghausen's disease). Histopathology *19*, 1–11.

Giovannini, M., Robanus-Maandag, E., van der Valk, M., Niwa-Kawakita, M., Abramowski, V., Goutebroze, L., Woodruff, J.M., Berns, A., and Thomas, G. (2000). Conditional biallelic Nf2 mutation in the mouse promotes manifestations of human neurofibromatosis type 2. Genes Dev. *14*, 1617–1630.

Gitler, A.D., Zhu, Y., Ismat, F.A., Lu, M.M., Yamauchi, Y., Parada, L.F., and Epstein, J.A. (2003). Nf1 has an essential role in endothelial cells. Nat. Genet. *33*, 75–79.

Hagedorn, L., Suter, U., and Sommer, L. (1999). P0 and PMP22 mark a multipotent neural crest-derived cell type that displays community effects in response to TGF-beta family factors. Development *126*, 3781–3794.

Iwashita, T., Kruger, G.M., Pardal, R., Kiel, M.J., and Morrison, S.J. (2003). Hirschsprung disease is linked to defects in neural crest stem cell function. Science *301*, 972–976.

Jacks, T., Shih, T.S., Schmitt, E.M., Bronson, R.T., Bernards, A., and Weinberg, R.A. (1994). Tumor predisposition in mice heterozygous for a targeted mutation in Nf1. Nat. Genet. *7*, 353–361.

Jessen, K.R., and Mirsky, R. (2005). The origin and development of glial cells in peripheral nerves. Nat. Rev. Neurosci. *6*, 671–682.

Jessen, K.R., Morgan, L., Steward, H.J.S., and Mirsky, R. (1990). Three markers of adult non-myelin-forming schwann cells, 217c(Ran-1), A5E3 and GFAP: Development and regulation by neuron-Schwann cell interactions. Development *109*, 91–103.

Joseph, N.M., Mukouyama, Y.S., Mosher, J.T., Jaegle, M., Crone, S.A., Dormand, E.L., Lee, K.F., Meijer, D., Anderson, D.J., and Morrison, S.J. (2004). Neural crest stem cells undergo multilineage differentiation in developing peripheral nerves to generate endoneurial fibroblasts in addition to Schwann cells. Development *131*, 5599–5612.

Kim, H.A., Rosenbaum, T., Marchionni, M.A., Ratner, N., and DeClue, J.E. (1995). Schwann cells from neurofibromin deficient mice exhibit activation of p21ras, inhibition of cell proliferation and morphological changes. Oncogene *11*, 325–335.

Kim, J., Lo, L., Dormand, E., and Anderson, D.J. (2003). SOX10 maintains multipotency and inhibits neuronal differentiation of neural crest stem cells. Neuron *38*, 17–31.

King, D., Yang, G., Thompson, M.A., and Hiebert, S.W. (2002). Loss of neurofibromatosis-1 and p19(ARF) cooperate to induce a multiple tumor phenotype. Oncogene *21*, 4978–4982.

Kruger, G.M., Mosher, J.T., Bixby, S., Joseph, N., Iwashita, T., and Morrison, S.J. (2002). Neural crest stem cells persist in the adult gut but undergo changes in self-renewal, neuronal subtype potential, and factor responsiveness. Neuron *35*, 657–669.

Lee, M., Brennan, A., Blanchard, A., Zoidl, G., Dong, Z., Tabernero, A., Zoidl, C., Dent, M.A., Jessen, K.R., and Mirsky, R. (1997). P0 is constitutively expressed in the rat neural crest and embryonic nerves and is negatively and positively regulated by axons to generate non-myelin-forming and myelin-forming Schwann cells, respectively. Mol. Cell. Neurosci. *8*, 336–350.

Levy, P., Vidaud, D., Leroy, K., Laurendeau, I., Wechsler, J., Bolasco, G., Parfait, B., Wolkenstein, P., Vidaud, M., and Bièche, I. (2004). Molecular profiling of malignant peripheral nerve sheath tumors associated with neurofibromatosis type 1, based on large-scale real-time RT-PCR. Mol. Cancer *3*, 20.

Lindsley, A., Snider, P., Zhou, H., Rogers, R., Wang, J., Olaopa, M., Kruzynska-Frejtag, A., Koushik, S.V., Lilly, B., Burch, J.B.E., et al. (2007). Identification and characterization of a novel Schwann and outflow tract endocardial cushion lineage-restricted periostin promoter. Dev. Biol., in press.

Maro, G.S., Vermeren, M., Voiculescu, O., Melton, L., Cohen, J., Charnay, P., and Topilko, P. (2004). Neural crest boundary cap cells constitute a source of neuronal and glial cells of the PNS. Nat. Neurosci. *9*, 930–938.

Menon, A.G., Anderson, K.M., Riccardi, V.M., Chung, R.Y., Whaley, J.M., Yandell, D.W., Farmer, G.E., Freiman, R.N., Lee, J.K., Li, F.P., et al. (1990). Chromosome 17p deletions and p53 gene mutations associated with the formation of malignant neurofibrosarcomas in von Recklinghausen neurofibromatosis. Proc. Natl. Acad. Sci. USA *87*, 5435–5439.

Miller, S.J., Rangwala, F., Williams, J., Ackerman, P., Kong, S., Jegga, A.G., Kaiser, S., Aronow, B.J., Frahm, S., Kluwe, L., et al. (2006). Large-scale molecular comparison of human schwann cells to malignant peripheral nerve sheath tumor cell lines and tissues. Cancer Res. *66*, 2584–2591.

Molofsky, A.V., He, S., Kruger, G.M., Bydon, M., Morrison, S.J., and Pardal, R. (2005). Bmi-1 promotes neural stem cell self-renewal and neural development but not mouse growth and survival by repressing the p16Ink4a and p19Arf senescence pathways. Genes Dev. *19*, 1432–1437.

Morrison, S.J., White, P.M., Zock, C., and Anderson, D.J. (1999). Prospective identification, isolation by flow cytometry, and in vivo self-renewal of multipotent mammalian neural crest stem cells. Cell *96*, 737–749.

Pardal, R., Clarke, M.F., and Morrison, S.J. (2003). Applying the principles of stem-cell biology to cancer. Nat. Rev. Cancer. *3*, 895–902.

Perrone, F., Tabano, S., Colombo, F., Dagrada, G., Birindelli, S., Gronchi, A., Colecchia, M., Pierotti, M.A., and Pilotti, S. (2003). p15INK4b, p14ARF, and p16INK4a inactivation in sporadic and neurofibromatosis type 1-related malignant peripheral nerve sheath tumors. Clin. Cancer Res. *9*, 4132–4138.

Reya, T., Morrison, S.J., Clarke, M.F., and Weissman, I.L. (2001). Stem cells, cancer, and cancer stem cells. Nature *414*, 105–111.

Riccardi, V.M. (1999). Neurofibromatosis: Phenotype, Natural History, and Pathogenesis, Third Edition (Baltimore: Johns Hopkins Univeristy Press).

Rubin, J.B., and Gutmann, D.H. (2005). Neurofibromatosis type 1 - a model for nervous system tumour formation? Nat. Rev. Cancer *5*, 557–564.

Serrano, M., Lee, H., Chin, L., Cordon-Cardo, C., Beach, D., and DePinho, R.A. (1996). Role of the INK4a locus in tumor suppression and cell mortality. Cell *85*, 27–37.

Sharpless, N.E., Bardeesy, N., Lee, K.-H., Carrasco, D., Castrillon, D.H., Aguirre, A.J., Wu, E.A., Horner, J.W., and DePinho, R.A. (2001). Loss of p16Ink4a with retention of p19Arf predisposes mice to tumorigenesis. Nature *413*, 86–91.

Stemple, D.L., and Anderson, D.J. (1992). Isolation of a stem cell for neurons and glia from the mammalian neural crest. Cell *71*, 973–985.

Takeuchi, A., and Uchigome, S. (2001). Diverse differentiation in malignant peripheral nerve sheath tumours associated with neurofibromatosis-1: An immunohistochemical and ultrastructural study. Histopathology *39*, 298–309.

Topilko, P., Schneider-Maunoury, S., Levi, G., Baron-Van Evercooren, A., Chennoufi, A.B., Seitanidou, T., Babinet, C., and Charnay, P. (1994). Krox-20 controls myelination in the peripheral nervous system. Nature *371*, 796–799.

Vogel, K.S., Brannan, C.I., Jenkins, N.A., Copeland, N.G., and Parada, L.F. (1995). Loss of neurofibromin results in neurotrophin-independent survival of embryonic sensory and sympathetic neurons. Cell *82*, 733–742.

Vogel, K.S., Klesse, L.J., Velasco-Miguel, S., Meyers, K., Rushing, E.J., and Parada, L.F. (1999). Mouse tumor model for neurofibromatosis type 1. Science *286*, 2176–2179.

Wong, C.E., Paratore, C., Dours-Zimmermann, M.T., Rochat, A., Pietri, T., Suter, U., Zimmermann, D.R., Dufour, S., Thiery, J.P., Meijer, D., et al. (2006). Neural crest-derived cells with stem cell features can be traced back to multiple lineages in the adult skin. J. Cell Biol. *175*, 1005–1015.

Zheng, H., Chang, L., Patel, N., Yang, J., Lowe, L., Burns, D.K., and Zhu, Y. (2008). Induction of abnormal proliferation by non-myelinating Schwann cells triggers neurofibroma formation. Cancer Cell, in press.

Zhu, Y., Romero, M.I., Ghosh, P., Ye, Z., Charnay, P., Rushing, E.J., Marth, J.D., and Parada, L.F. (2001). Ablation of NF1 function in neurons induces abnormal development of cerebral cortex and reactive gliosis in the brain. Genes Dev. *15*, 859–876.

Zhu, Y., Ghosh, P., Charnay, P., Burns, D.K., and Parada, L.F. (2002). Neurofibromas in NF1: Schwann cell origin and role of tumor environment. Science *296*, 920–922.

Zhu, Y., Guignard, F., Zhao, D., Liu, L., Burns, D.K., Mason, R.P., Messing, A., and Parada, L.F. (2005a). Early inactivation of p53 tumor suppressor gene cooperating with NF1 loss induces malignant astrocytoma. Cancer Cell *8*, 119–130.

Zhu, Y., Harada, T., Liu, L., Lush, M.E., Guignard, F., Harada, C., Burns, D.K., Bajenaru, M.L., Gutmann, D.H., and Parada, L.F. (2005b). Inactivation of NF1 in CNS causes increased glial progenitor proliferation and optic glioma formation. Development *132*, 5577–5588.

Influence of Hormones and Hormone Metabolites on the Growth of Schwann Cells Derived From Embryonic Stem Cells and on Tumor Cell Lines Expressing Variable Levels of Neurofibromin†

Therese M. Roth,[1] Poornapriya Ramamurthy,[1,2] David Muir,[3] Margaret R. Wallace,[4] Yuan Zhu,[1,5] Lou Chang,[1] and Kate F. Barald[1,2]*

Loss of neurofibromin, the protein product of the tumor suppressor gene neurofibromatosis type 1 (NF1), is associated with neurofibromas, composed largely of Schwann cells. The number and size of neurofibromas in NF1 patients have been shown to increase during pregnancy. A mouse embryonic stem cell (mESC) model was used, in which mESCs with varying levels of neurofibromin were differentiated into Schwann-like cells. NF1 cell lines derived from a malignant and a benign human tumor were used to study proliferation in response to hormones. Estrogen and androgen receptors were not expressed or expressed at very low levels in the NF1+/+ cells, at low levels in NF1+/− cells, and robust levels in NF1−/− cells. A 17β-estradiol (E2) metabolite, 2-methoxy estradiol (2ME2) is cytotoxic to the NF1−/− malignant tumor cell line, and inhibits proliferation in the other cell lines. 2ME2 or its derivatives could provide new treatment avenues for NF1 hormone-sensitive tumors at times of greatet hormonal influence. *Developmental Dynamics 237:513–524, 2008.* © 2008 Wiley-Liss, Inc.

Key words: Schwann cells; mouse ES cells; pregnancy hormones; steroid receptors

Accepted 3 December 2007

INTRODUCTION

Neurofibromatosis Type 1 Origin and Loss of Heterozygosity

Neurofibromatosis type 1 (NF1) is the most common human tumor predisposition syndrome of the nervous system, affecting 1/3,000 to 1/3,500 live births worldwide. Neurofibromas, the cardinal feature of NF1, are heterogeneous and composed of all the cellular components of peripheral nerves, including Schwann cells (SCs), fibroblasts, perineurial cells, axons, and mast cells. SCs or SC precursors have been shown to be the initiating cell type for tumorigenesis (Serra et al., 2001; Zhu et al., 2002). Loss of heterozygosity has been found in some, but not all neurofibromas, and in some but not all cell types within the neurofibroma (Menon et al., 1990; Daschner et al., 1997; Rasmussen et al., 2000). Although neurofibromin is generally a microtubule-associated cytoplasmic protein (Gregory et al., 1993),

†This article was accepted for inclusion in the Special Focus on Stem Cells—*Developmental Dynamics* 236 #2.
[1]Department of Cell and Developmental Biology, University of Michigan Medical School, Ann Arbor, Michigan
[2]Department of Biomedical Engineering, College of Engineering, University of Michigan, Ann Arbor, Michigan
[3]Department of Pediatrics, Neurology Division, University of Florida College of Medicine, Gainesville, Florida
[4]Department of Molecular Genetics and Microbiology, University of Florida College of Medicine, Gainesville, Florida
[5]Department of Internal Medicine-Molecular Medicine and Genetics, University of Michigan Medical School, Ann Arbor, Michigan
Grant sponsor: National Science Foundation; Grant number: 2004016780; Grant sponsor: NIH; Grant number: RO1 NS17262; Grant sponsor: AMRMC; Grant number: NF990027; Grant sponsor: DAMD; Grant number: 17-01-10707; Grant sponsor: DAMD; Grant number: 17-03-1-0224.
***Correspondence to: Kate F. Barald, Department of Cell and Developmental Biology, University of Michigan Medical School, 3053 BSRB, 109 Zina Pitcher Place, Ann Arbor, MI 48109-2200. E-mail: kfbarald@umich.edu**

DOI 10.1002/dvdy.21430
Published online 16 January 2008 in Wiley InterScience (www.interscience.wiley.com).

it has also been found to be actively transported to the nucleus (Vandenbroucke et al., 2004).

The manifestations of NF1 are highly variable, even among members of the same family, who presumably have the same mutation. Discrete cutaneous neurofibromas are usually benign and often first appear at puberty (McLaughlin and Jacks, 2003; Fishbein et al., 2007). Although these tumors are rarely present at birth, they are found in 48% of 10 year olds (notably, precocious puberty is a common feature of NF1; Virdis, 2000), 84% of 20 year olds, and virtually all NF1 patients over the age of 40 (McGaughran et al., 1999; DeBella et al., 2000). Neurofibromas can also arise from multiple nerves within nerve plexuses, which are termed plexiform neurofibromas (Woodruff, 1999; Gutmann and Giovannini, 2002). Plexiform neurofibromas are first seen in early childhood and are capable of aggressive growth, particularly as puberty approaches or during pregnancy (Dugoff and Sujansky, 1996). Approximately 5% of plexiform neurofibromas undergo malignant transformation and eventually become malignant peripheral nerve sheath tumors (MPNSTs; Korf, 1999; Woodruff, 1999). Contributions from other mutations, at *NF1* or other loci, environmental conditions including trauma and the elevated levels of specific hormones seen at puberty and during pregnancy, may also be "triggers" for tumorigenesis, enlargement, or tumor progression. Such stimuli could be responsible for initial growth of the tumors, for increases in tumor size and number during pregnancy, puberty, or exogenous hormonal stimulation and for malignant transformation (Posma et al., 2003). Reports indicate that up to 80% of pregnant women with NF1 experience an increase in tumor size and/or number during pregnancy, with one third of these lesions regressing in the postpartum period, suggesting a hormonal influence (Dugoff and Sujansky, 1996).

Hormonal Milieu During Pregnancy

Concentrations of the steroid hormones 17β-estradiol (E2), progesterone (P4), and testosterone (T) increase during pregnancy (Witorsch, 2002; Fernandez-Valdivia et al., 2005; Okada et al., 2005; Rodriguez-Cuenca et al., 2006). E2 has been shown to be involved in cell proliferation, and is a ligand for the estrogen receptor (ER; Revankar et al., 2005). P4 is modified to E2 and is involved in both proliferation and differentiation (Fernandez-Valdivia et al., 2005); P4 is the ligand for the progesterone receptor (PR) (Fernandez-Valdivia et al., 2005). The PR is regulated by E2 by transactivation through the ER (Fernandez-Valdivia et al., 2005; Okada et al., 2005). Testosterone is the primary circulating androgen, even in women, and is the ligand for the androgen receptor (AR), although it can rarely cross-react with both the ER and the PR with very low affinity (Gao et al., 2005). Steroids can rarely cross-react and bind to receptors other than their native receptor, because of the similarity of their receptor conformation, even though the actual sequence identity may be low (Gao et al., 2005). Hormone receptor-positive breast cancer cells were shown to be more likely to respond to hormone antagonist treatment (Jacobsen et al., 2003, 2005) than hormone receptor-negative breast cancer cells.

Antimetabolites/Antagonists for Hormones and Angiogenesis

2-Methoxy-estradiol (2ME2) is a naturally occurring E2 metabolite that rises in serum during pregnancy (Wang et al., 2000) and is a potent antiangiogenic factor, although it is not ER-dependent (Wang et al., 2000; Dingli et al., 2002). 2ME2 has been found to inhibit tumor cells (e.g., breast cancer, prostate cancer, and ovarian carcinoma) by destabilizing and depolymerizing microtubules (MT) and impairing hypoxia-inducible factor 1 (HIF-1) accumulation in the nucleus (Wang et al., 2000; Mabjeesh et al., 2003; Ireson et al., 2004). HIF-1 also induces vascular endothelial growth factor (VEGF) expression; therefore, inhibition of HIF-1 results in inhibition of VEGF expression that is required for angiogenesis (Mabjeesh et al., 2003). Tumors require angiogenesis to grow larger than 1 mm in size due to the limits of nutrient diffusion to cells, so that 2ME2 may be acting indirectly to inhibit tumor growth through inhibition of angiogenesis, although that cannot be the reason 2ME2 has apoptotic effects on cultured tumor cells (Mabjeesh et al., 2003; Wang et al., 2000). In such cells, 2ME2 acts by disrupting microtubules, with prolonged (24–72 hr) treatment of malignant tumor cells resulting in apoptosis (Wang et al., 2000; Mabjeesh et al., 2003).

Embryonic Stem Cell-Based Model of SC Differentiation for Studies of NF1 Tumorigenesis

We recently reported a new stem cell-based model for studies of tumorigenesis in NF1 (Roth et al., 2007). An in vitro system was used to differentiate mouse embryonic stem cells (mESCs), which are NF1 wild-type (+/+), heterozygous (+/−), or null (−/−) into SC-like cells for studies of NF1. In this hormone study, we have focused on the SC-like cells derived from these mouse embryonic stem cells.

RESULTS

The cell lines used for these studies include the NF1+/+ (D3) mES cell line (Doetschman, 1985), NF1+/− (SKO) mES cells (Jacks et al., 1994), NF1−/− (DKO) mES cell line (Jacks et al., 1994), SW10 (NF1+/+) mouse SC line that harbors a temperature sensitive SV40 large T antigen. When these cells are grown at 37°C (the nonpermissive temperature for transgene expression), they differentiate (ATCC; Hai et al., 2002). We also examined two human NF1 cell lines, pNF00.11 (referred to as PNF cells in this report; NF1−/−) a human plexiform neurofibroma SC-enriched culture (Muir et al., 2001), and ST88-14 (referred to as ST cells in this report; NF1−/−) derived from a human MPNST (a gift of Dr. Larry Sherman, Oregon Health Sciences University; Su et al., 2004). SC-like differentiated mES cells will be referred to as D3SC (NF1+/+), SKOSC (NF1+/−), and DKOSC (NF1−/−), depending on the number of NF1 alleles expressed.

Expression of Steroid Hormone Receptors Is Correlated With NF1 Expression in SC-Like mES-Derived Cells

To determine whether the mES-derived SC-like cells or human SC tumor

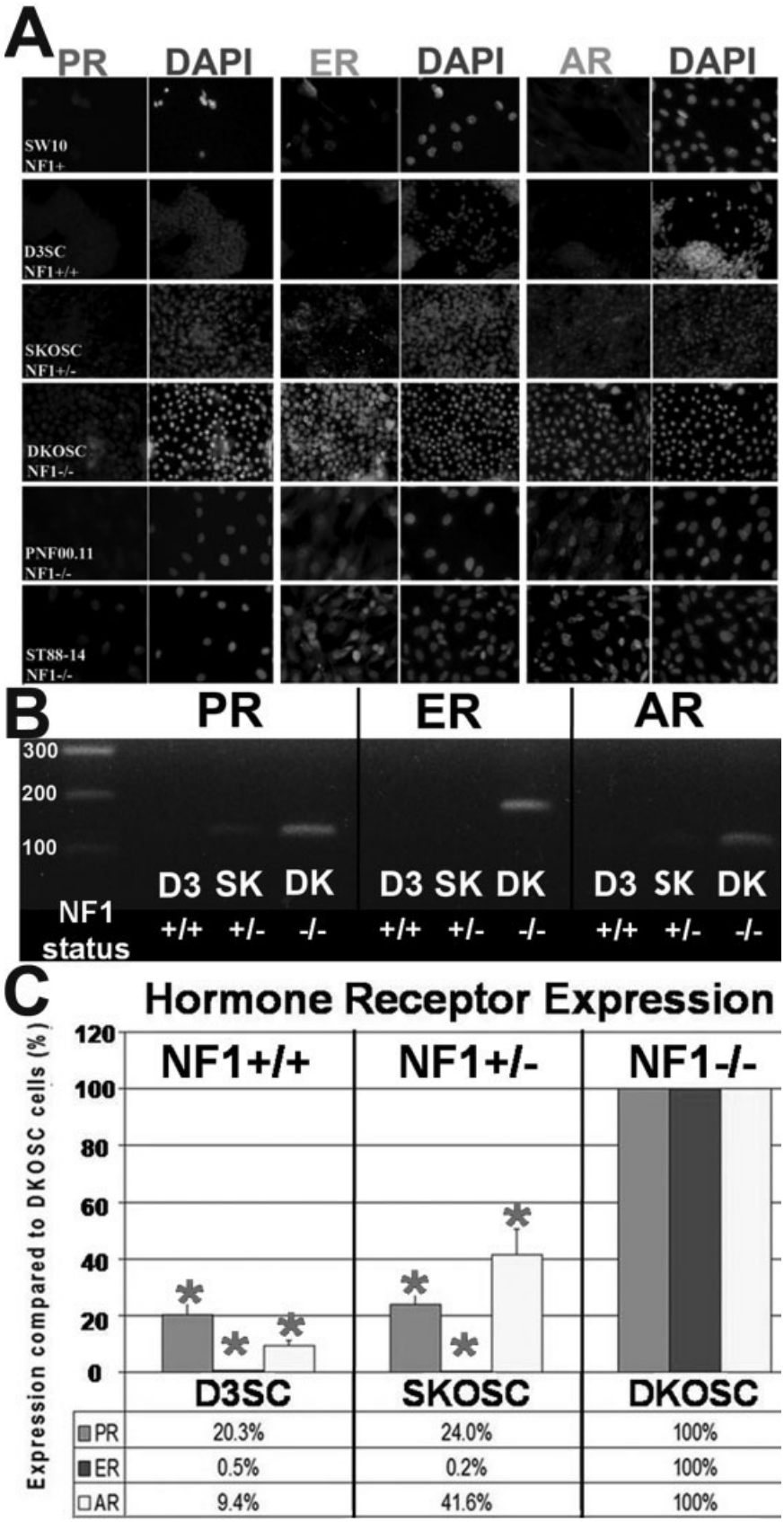

cell lines responded differently to the steroid hormones that are up-regulated during pregnancy (P4, E2, and T), we first determined whether these cells expressed the appropriate receptors (PR, ER, AR) for the relevant classic steroid receptor pathways at the protein level. We found that the level of classic receptor expression varied depending on the level of neurofibromin expressed by the cell type/line. Whereas PR (Fig.1A, first column) was not highly expressed in any of the cell lines, the NF1−/− (DKOSC, PNF, ST) cells had the most intense staining in the immunocytochemical experiments, although the SC line SW10 also showed some PR expression (Fig. 1A, bottom row, left). ER expression (Fig. 1A, third column) and AR expression (Fig. 1A, fifth column) followed similar patterns to each other, with little/no expression in the NF1+/+ (D3SC, SW10) cells, low levels of expression in NF1+/− (SKOSC) cells, and higher levels of expression in NF1−/− (DKOSC, PNF, ST) cells. Immunocytochemical analysis demonstrated that, although PR and AR expression was exclusively nuclear, ER

Fig. 1. A: Schwann cell (SC) -like cells and neurofibromatosis type 1 (NF1) tumor cells express varying levels of steroid hormone receptors. 4′,6-Diamidine-2-phenylidole-dihydrochloride (DAPI) staining of cell nuclei is shown to the right of the hormone receptor assayed. Left column, progesterone receptor (PR): Low levels of PR expression were seen in all cell types, with some up-regulation in NF1−/− (DKOSC, PNF, ST) cells. Third column, estrogen receptor (ER) and fifth column androgen receptor (AR): Very low levels of both ER and AR seen in NF1+/+ (D3SC, SW10) cells, a slightly higher level in NF1+/− (SKOSC) cells, and most intense levels in NF1−/− (DKOSC, PNF, ST) cells suggests a stronger ability of NF1−/− cells to respond to hormones up-regulated during pregnancy. Some cell types displayed both nuclear and cytoplasmic expression of ER. Photographs were taken at ×40 original magnification. **B:** Using gel visualization, expression of hormone receptors was verified by reverse transcriptase-polymerase chain reaction (RT-PCR; D3=D3SC, SK=SKOSC, DK=DKOSC). **C:** Real-time quantitative PCR (RTqPCR) shows percentage of hormone receptor expression of D3SC and SKOSC cells in comparison to DKOSC cells (DKOSC expression set at 100%). D3SC cells expressed 20% the amount of PR, 0.5% ER and 9.4% PR of DKOSC cells, while SKOSC cells expressed 24% the amount of PR, 0.25 ER, and 41.6% AR of DKOSC cells.

localization was seen in both the nucleus and the cytoplasm, as has been previously noted (Ho and Liao, 2002; Zhang et al., 2004; Revankar et al., 2005). The differences in expression levels were confirmed in mouse SC-like cells by real-time quantitative polymerase chain reaction (RTqPCR; Fig. 1B). In RTqPCR assessments, with the level of expression in DKOSC cells set at 100%, D3SC cells expressed 20% of the amount of PR, 0.5% of the ER, and 9.4% of the PR seen in DKOSC cells, whereas SKOSC cells expressed 24% of the amount of PR, 0.25% of the ER, and 41.6% of the AR expressed by DKOSC cells (Fig. 1C). We then costained for both steroid hormone receptors and SC markers in the same cells, which verified coexpression levels (Fig. 2A–C).

To assay whether in vivo mouse tissue with or without NF1 expression showed similar patterns of classic hormone receptor expression as mouse cells in vitro did, we obtained tissue from mice in which a P0-driven cre transgene targeted the loss of NF1 in cells only from the SC lineage (Zheng et al., in revision) and stained for classic hormone receptor expression. In this model, NF1 mutant mice (cre+) develop neurofibroma tumors in dorsal root ganglia (DRG; Fig. 3). High levels of ER (green, middle columns) and AR (green, right columns) were seen in NF1-deficient mouse tissue (cre+), but not in mouse tissue with normal NF1 expression levels (cre−), similar to the expression patterns seen in the cultured NF1-deficient mouse cells (Fig. 3). In contrast to the in vitro assays, however, high levels of PR (red, left columns) expression were

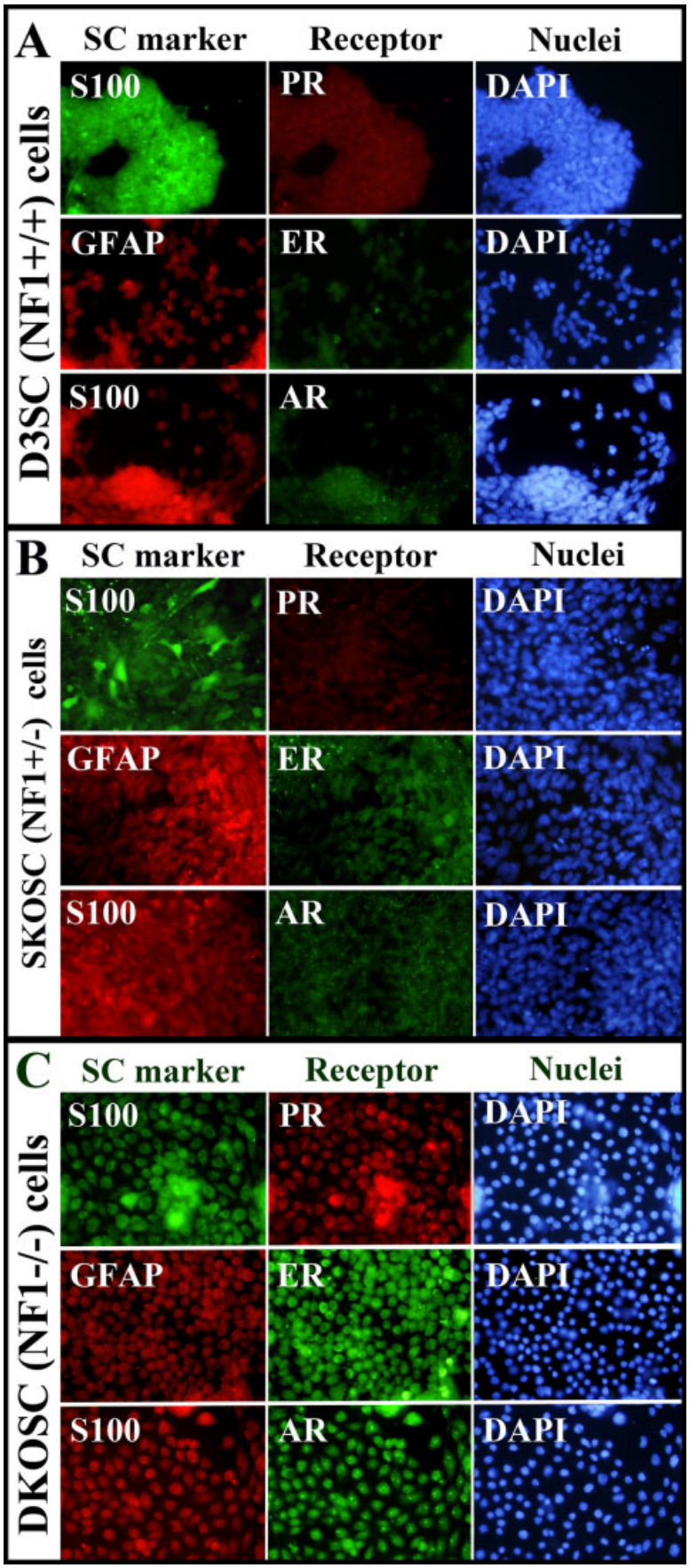

Fig. 2. Coexpression levels of classic hormone receptors and Schwann cell (SC) markers in SC-like differentiated mouse embryonic stem cells (mESCs). **A–C:** This finding confirms the coexpression levels of S100 and progesterone receptor (PR), glial fibrillary acidic protein (GFAP) and estrogen receptor (ER) or S100 and androgen receptor (AR) in NF1+/+ D3SC cells (A), NF1+/− SKOSC cells (B), and NF1−/− DKOSC cells (C). The staining for all three hormone receptors (PR, ER, AR) was most intense in the DKOSC (NF1−/−) cells (C), whereas all three cell types (D3SC NF1+/+, SKOSC NF1+/−, and DKOSC NF1−/−) expressed the SC markers S100 or GFAP. Photographs were taken at ×40 original magnification.

also seen in NF1-deficient mouse tissues (cre+; Fig. 3).

Hormonal Effects on Cell Proliferation

Because expression of hormone receptors was found to be associated with the level of NF1 expression in the cells tested, with DKOSC cells expressing much higher levels of the receptors than either the D3SC or SKOSC cells (Figs. 1B, 2A–C), we assayed the cells for hormonal effects on cell proliferation. Concentrations of the hormones were chosen based on dose–response curves that determined the optimal doses that induced proliferation rather than differentiation (not shown). After growing the cells overnight in hormone-free phenol-red free medium, we added one of the ligands for the steroid hormone receptors (P4, E2, and T) and/or its respective nuclear receptor inhibitor (RU486, ICI 182, 780, or flutamide; Wang et al., 2000; Witorsch, 2002; Fig. 4). Addition of P4 (Fig. 4 P4) increased proliferation significantly only in SW10, ST, and DKOSC cells. The effect of the PR inhibitor RU486 was cell type-specific, ranging from significant inhibition even below control levels (SW10 and PNF) to no significant effect (ST, D3SC, SKOSC, DKOSC; Fig. 4, P4; n = 5). Addition of E2 (Fig. 4, E2) or T (Fig. 4, T) significantly increased proliferation of malignant NF1 tumor cells (ST) and both DKOSC and D3SC cells. However, the NF1−/− cell lines ST and DKOSC cells were the only cell lines that showed a significant increase in proliferation with all three of the hormones tested. There was generally a slight trend, although not a significant decrease, seen when the respective inhibitors for the classic receptors (ICI182, 780 for ER, flutamide for AR) were used to block these receptors by preincubating cells with the inhibitors for 2 hr.

2ME2 Effects

To determine whether 2ME2, an estrogen metabolite that has been found to be up-regulated during normal pregnancies (Wang et al., 2000) and which has been found to affect the growth of various tumor cells (Fotsis et al., 1994; Maran et al., 2002; Djavaheri-Mergny et al., 2003; Mabjeesh et al., 2003), affected the growth of NF1−/− mES cells, we grew the SC-like mES cells, SW10, and the tumor cell lines for 3 days in 2ME2 concentrations between 0.1 μM and 100 μM. We determined that 10 μM was the threshold for significant changes in growth rates in all cells and cell lines tested (not shown). To determine whether the effect was cytotoxic (causing necrosis), apoptotic, or only decreased proliferation, we grew all cells for 2 days in 10 μM 2ME2. Malignant ST cells were the only cell type to show a significant *decrease* in cell number when compared with the initial cell number (Fig. 5A). All other cells had either static cell numbers (PNF, DKOSC, and D3SC, or merely decreased proliferation rates (SKOSC, SW10) compared with control cells grown without 2ME2 addition. We did not observe cell necrosis.

Effects of 2ME2 Exposure on MTs

The mechanism of 2ME2 action in cultured cells is reported to be through disruption of microtubules (Mabjeesh et al., 2003), and not through effects on the classic ER itself, for which it has very low affinity (Ireson et al., 2004). We, therefore, examined tumor cells grown with or without added 2ME2 for expression of αtubulin to visualize any changes in these cytoskeletal elements with increasing concentrations of 2ME2. We found that with the addition of 10 μM 2ME2 (Fig. 5B, middle column), the PNF cells rounded up but their nuclei (stained with 4′,6-diamidine-2-phenylidole-dihydrochloride [DAPI]) remained intact and cells retained some cytoskeletal structure. In the ST cells, however, cells appeared to have the classic apoptotic profile (Edinger and Thompson, 2004). The cells rounded up, nuclei were "broken up" and appeared as clusters of nucleic acid-containing material, and cell membranes were blebbed (Edinger and Thompson, 2004). The microtubules no longer were found in long extensions (Fig. 5B, left column), and tubulin protein was more diffuse in the cytoplasm. With 100 μM 2ME2 (Fig. 5B, right column), PNF cells also began to lose microtubule extensions, tubulin expression was diffuse, and 5–10% of the nuclei were becoming clustered and fragmented. ST cells became reduced in size (less than half the normal cell diameter) and apoptotic, with very little cytoplasm extending beyond the nucleus, thus visually exhibiting a much stronger effect from the 2ME2 on the cytoskeleton. To confirm that these malignant ST cells were becoming apoptotic in 2ME2, we assayed them for both caspase-3 expression and terminal deoxynucleotidyl transferase–mediated deoxyuridinetriphosphate nick end-labeling (TUNEL) staining. Although less than 1% of benign PNF tumor cells were TUNEL+ and Caspase-3+, approximately 20% of ST cells stained positive for these apoptotic markers after 24 hr (Fig. 5C).

DISCUSSION

Because NF1 tumors often grow in size and increase in number during pregnancy (Ansari and Nagamani, 1976; Dugoff and Sujansky, 1996), suggesting a hormonal influence, we conducted experiments to determine whether the mES-derived SC-like cell model of NF1 or human SC tumor cell lines with variable levels of neurofibromin responded differently to the steroid hormones that are up-regulated during pregnancy (P4, E2, and T; Fernandez-Valdivia et al., 2005; Okada et al., 2005; Rodriguez-Cuenca et al., 2006). We first determined that these cells expressed the appropriate receptors (PR, ER, AR) for the relevant classic steroid receptor pathways (Chen et al., 2005; Okada et al., 2005; Ozawa, 2005; Sonneveld et al., 2006). We found that the level of receptor expression varied depending on whether the cell type/line expressed neurofibromin and at what levels. NF1−/− (DKOSC, PNF, ST) cells had the most intense levels of PR expression, while ER and AR expression followed similar patterns to each other, with very low/no expression in the NF1+/+ (D3SC, SW10) cells, low levels of expression in NF1+/− (SKOSC) cells, and most intense expression in NF1−/− (DKOSC, PNF, ST) cells. The differences in expression levels were confirmed in the mouse SC-like cells by RTqPCR. These findings suggest that NF1 mutant cells can more

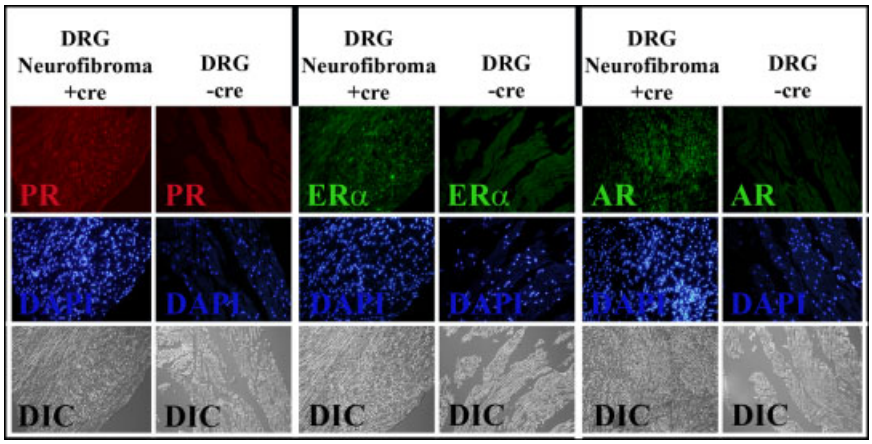

Fig. 3. Classic hormone receptor expression in mouse tissue. To assay for classic hormone receptor expression in vivo, we used mice in which cre recombinase expression targeted loss of floxed neurofibromatosis type 1 (NF1) expression to cells in the Schwann cell (SC) lineage (Zheng et al., in revision; Zhu et al., 2002). Mice transgenic for the cre transgene developed neurofibroma tumors in dorsal root ganglia (DRG), whereas mice without the cre transgene expressing normal NF1 levels did not. In vivo, mouse tissues with or without NF1 expression showed similar patterns of classic estrogen receptor (ER, green, middle columns) and androgen receptor (AR, green, right columns) steroid hormone receptor expression as SC-like mouse cells in vitro. The NF1-deficient tissues (cre+) had intense expression of ER and AR, whereas the NF1+ (cre−) did not. Progesterone receptor (PR) expression (red, left columns), however, was much more robust in NF1-deficient tissues (cre+) than that seen in cultured NF1−/− SC-like cells. This finding could be attributed to signaling from the surrounding cells in the heterogeneous, hypercellular tumor microenvironment, in contrast to the homogeneous NF1−/− SC-like cells in culture. 4′,6-Diamidine-2-phenylidole-dihydrochloride (DAPI) staining of cell nuclei is shown in blue, and differential interference contrast (DIC, aka Nomarski) images are seen in the bottom row. Photographs were taken at ×40 original magnification.

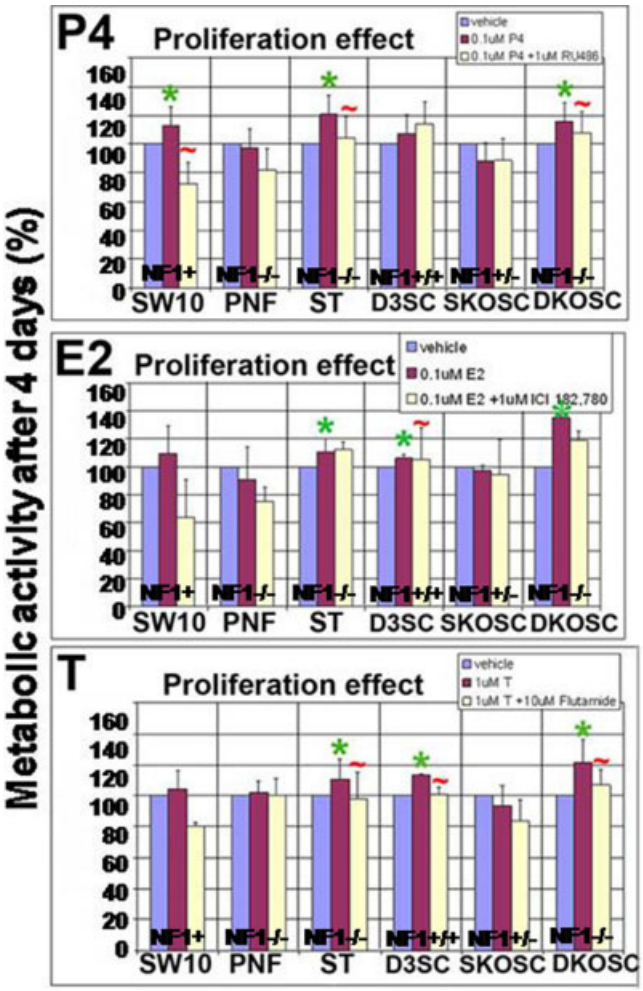

Fig. 4.

readily respond to hormones that rise during pregnancy. Because at least a part of this increase in cell numbers is inhibited by the classic receptor inhibitors, some of this increase must be mediated through these classic pathways. However, other possible nongenomic pathways include second messenger cascades involving G-protein coupling, cAMP and MAPK pathway activation that affects Ca^{++} channels, and PI3K and Akt pathways (Zhang et al., 2004), which are known to be involved in NF1. PR and AR localization was exclusively nuclear, and ER was seen in both the nucleus and the cytoplasm, in accordance with the findings of others (Ho and Liao, 2002; Zhang et al., 2004; Revankar et al., 2005). Breast cancer tumor cells

Fig. 4. Hormones that are increased during pregnancy affect the proliferation of Schwann cell (SC) -like cells and neurofibromatosis type 1 (NF1) tumor cells differently, depending on the level of neurofibromin expression. Progesterone (P4): Addition of P4 increased proliferation significantly only in SW10, ST, and DKOSC (asterisk), whereas the progesterone receptor (PR) inhibitor RU486 returned proliferation rates to control levels (plus sign). 17β-Estradiol (E2): E2 increased proliferation significantly in malignant NF1 tumor (ST), DKOSC, and D3SC cells (asterisk), whereas addition of estrogen receptor (ER) inhibitor ICI 182, 780 reduced proliferation rates to control levels only in D3SC cells, which had a small but significant difference (plus sign). Testosterone (T): Addition of T also significantly increased proliferation only in malignant NF1 tumor (ST), DKOSC, and D3SC SC-like differentiated mES cells (asterisk); addition of the AR inhibitor flutamide returned proliferation rates to control levels (plus sign).

that express both ER and PR have been found to have a better prognosis than those that do not express these receptors because they are more likely to respond to hormone treatment (Jacobsen et al., 2003), although tumors that express only ER or PR, but not both, have been reported to have a poorer outcome (Jacobsen et al., 2005).

A study done on both male and female neurofibroma tumors found that 75% expressed PR, while 5% expressed ER, regardless of the sex of the patient (McLaughlin and Jacks, 2003). This finding suggests an important role of P4 in tumor development; however, the tumor cell type was not identified and tumors were not tested for coexpression of ER and PR; neither AR expression nor number of receptors per cell was tested or reported in the study. Also, positive receptor expression of tumors was defined in their study as slides with 5 or more positive cells per 10 high power fields, and virtually none of the sections tested contained more than one hundred positive cells (McLaughlin and Jacks, 2003). We assayed for in vivo expression of classic hormone receptors (PR, ER, AR) in mouse tissues that had been engineered to target loss of NF1 in SC lineage cells carrying a cre transgene (Zheng et al., 2008; Zhu et al., 200), which subsequently developed neurofibroma tumors in the DRG. We found high levels of expression of all three classic receptors (PR, ER, AR) in NF1-deficient tissues (cre+) and low/no expression in tissues with normal levels of NF1 expression (cre−). This finding is in contrast to our in vitro findings, where ER and AR alone were up-regulated in NF1−/− cells, but PR was not. We attribute this difference to the importance of the tumor microenvironment in tumorigenesis, because surrounding cells and their resultant signals with and in addition to the NF1-deficient cells could also be affecting hormone receptor expression. Notably, DAPI staining and differential interference contrast visualization of the tissues demonstrated hypercellularity in the NF1-deficient cre+ tissues when compared with the cre− tissues with normal levels of NF1 expression, which could result in increased signaling in the tissues. Re-

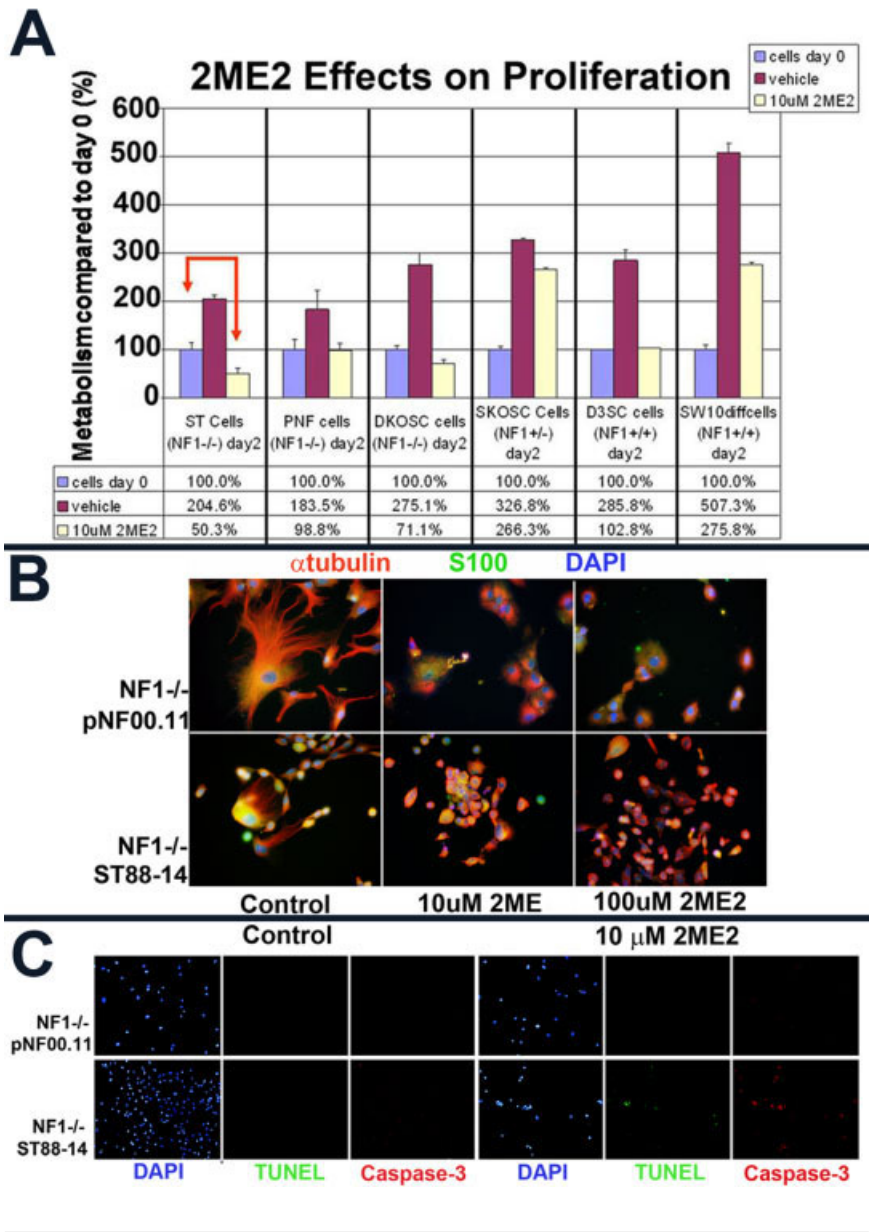

Fig. 5. 2-Methoxy estradiol (2ME2), a naturally occurring 17β-estradiol (E2) metabolite, is cytotoxic to a malignant neurofibromatosis type 1 (NF1) tumor cell line, but only slows or halts growth in other cell lines. Microtubules are disrupted in this process. **A:** When cells were grown for 2 days in 10 μM 2ME2, malignant NF1 tumor cells (ST) cells were the only cells that showed significant cell death compared with beginnnning cell numbers. All other lines (including the benign PNF tumor cells) either had static numbers (PNF, DKODC, D3SC), perhaps due to cell cycle arrest, or merely decreased proliferation (SKOSC, SW10). The *y*-axis indicates the percentage of cells actively metabolizing at day 2, compared with the number of cells actively metabolizing at day 0, which was set at 100%. **B:** Tumor cells were plated and attached overnight before the listed concentration (0 μM left, 10 μM middle, 100 μM right) was added to the medium. After an additional 24 hr incubation, cells were fixed and stained for α-tubulin (microtubules), S100 (SC origin of cells), and 4′,6-diamidine-2-phenylidole-dihydrochloride (DAPI) (nucleus), ×40 original magnification. Tumor cells grown without 2ME2 (left) had extensive tubulin networks. Addition of either 10 μM (middle) or 100 μM (right) 2ME2, however, caused the cells to round up and appear apoptotic, that is, nuclei were breaking up and appeared as clusters, and the cells showed blebbing. The microtubules no longer stained as strands, but tubulin showed a more diffuse expression. All of these effects were more pronounced in the malignant ST cells, which showed very little cytoplasm beyond the nucleus in the presence of 10 μM or 100 μM 2ME2. **C:** Tumor cells were grown as described and stained for terminal deoxynucleotidyl transferase–mediated deoxyuridinetriphosphate nick end-labeling (TUNEL) and cleaved caspase-3 expression. Whereas approximately 20% of the malignant ST cells (bottom row) were positive for apoptosis, only approximately 1% of the benign PNF cells were positive (top row).

cently, Fishbein et al. found differing heterogeneous levels of ER, PR, and AR in most NF1 tumor-derived SC samples and the normal SCs tested. Primary tissue samples they tested showed greater variation than cultured samples, suggesting that cells other than SC express hormone receptors (Fishbein et al., 2007). They also reported that tumor-derived SC cultures showed variable results for proliferation and apoptosis using steroid hormone ligands and receptors. Statistically significant changes were found in only a subset of tumor cells, regardless of gender (Fishbein et al., 2007). Our results indicate that E2 is likely also to be an important hormone, although its effects may be enhanced or influenced by P4. Because T is a precursor for E2, proliferative effects on cells could be mediated through aromatase activity (Gao et al., 2005), or through nonclassic indirect pathways by increasing intracellular Ca^{++} (Chen et al., 2005), rather than through the AR itself.

Expression of hormone receptors was found to be associated with the level of NF1 expression in the cells tested in the stem cell model of SC differentiation, with NF1−/− DKOSC cells expressing much higher levels (up to 400×) of the receptors than either the NF1+/+ D3SC or NF1+/− SKOSC cells. We, therefore, assayed the cells for hormonal effects on cell proliferation. Concentrations were chosen based on dose–response curves that determined the optimal proliferation response vs. differentiation (not shown). Although the increases in proliferation we found were modest, they were statistically significant. Addition of P4 (Fig. 4A) increased proliferation significantly only in SW10, ST, and DKOSC cells, possibly because P4 can also be involved in cell differentiation and modulation of E2 proliferative effects (Jacobsen et al., 2003). E2 and P4 can have complementary functions, with P4 inhibiting the ER (Jacobsen et al., 2003). P4 and E2 can be used in combination to stimulate tumor development by simulating pregnancy in mice with dormant mammary tumors (Gattelli et al., 2004), where the combination of E2 and P4 caused the tumor cells to break dormancy and begin proliferating. P4 may act synergistically with E2 to affect proliferation, although in these studies we determined each hormone's effect individually. Also, PR had the lowest expression of any of the receptors we tested in any of the SC-like mES cells with variable neurofibromin levels or in the tumor cell lines. Perhaps this is because in this assay we were testing cell lines, rather than the cellularly heterogeneous tumors assayed in the McLaughlin and Jacks paper (McLaughlin and Jacks, 2003) and their criteria for positive expression depended on only a small number of cells. We found that the effect of the PR inhibitor RU486 was variable, ranging from significant inhibition of cell proliferation even below control levels in some cell types (SW10 and PNF) to no significant effect (ST, D3SC, SKOSC, DKOSC). RU486 is also an inhibitor of AR and the glucocorticoid receptor, which could also influence the results (Ghoumari et al., 2003; Zhang et al., 2006). However, because these cells were grown in hormone-free medium with only P4 added, this influence should be minimal in these experiments. Addition of E2 or T significantly increased proliferation of the malignant NF1 tumor cells (ST) and both DKOSC and D3SC cells. However, the NF1−/− cell line ST, derived from the human malignant tumor and the mES-derived DKOSC were the only cell lines that showed a significant increase in proliferation with all three of the hormones tested. There was a slight trend or significant decrease in proliferation when their respective classic receptor inhibitors (ICI 182, 780 for ER, flutamide for AR) were used to preincubate cells for 2 hr. This may be because the hormone action is not mediated exclusively through classic pathways (McEwen and Alves, 1999; Ho and Liao, 2002; Zhang et al., 2004; Chen et al., 2005; Gao et al., 2005; Jacobsen et al., 2005; Revankar et al., 2005; Sonneveld et al., 2006). There have been reports of steroid hormones (P4, E2, T) influencing cells independent of their classic receptors (PR, ER, AR; McEwen and Alves, 1999; Ho and Liao, 2002; Zhang et al., 2004; Chen et al., 2005; Gao et al., 2005; Jacobsen et al., 2005; Revankar et al., 2005; Sonneveld et al., 2006). E2 has also been shown to modulate secondary messengers, such as Ca^{++} and NO, and activate the PI3K/Akt and MAPK pathways (McEwen and Alves, 1999; Ho and Liao, 2002; Revankar et al., 2005), which are known to be involved in NF1 (Klesse and Parada, 1998; Klesse et al., 1999). These effects are also not inhibited by ER inhibitors, suggesting they are not mediated through the classic receptors (Ho and Liao, 2002). Many of the E2-stimulated pathways are initiated at the plasma membrane, suggesting that they could be mediated by an unidentified G-protein coupled receptor (Ho and Liao, 2002). Nongenomic actions of androgen with plasma membrane-associated signaling pathways involve activation of kinase signaling cascades or modulation of intracellular Ca^{++} thought to be mediated through interaction of AR and cytosolic pathway proteins (Gao et al., 2005). Conversely, steroid receptors have been shown to exert their influence without hormone stimulation (Chen et al., 2005; Jacobsen et al., 2005; Sonneveld et al., 2006). Genes regulated by unliganded PR encode membrane associated, cell-cycle regulatory, DNA repair and apoptosis proteins (Jacobsen et al., 2005). ERα has been found to activate the PI3K/Akt pathway in an E2-independent manner by binding constitutively to the p85 subunit of PI3K and activating PI3K/Akt pathway (McEwen and Alves, 1999; Ho and Liao, 2002). ER expression has been seen outside the nucleus (McEwen and Alves, 1999; Ho and Liao, 2002; Zhang et al., 2004; Revankar et al., 2005), for example, ERβ localized to the cytoplasm and plasma membrane of neurons and astrocytes, and was also seen in the myelin of oligodendrocytes and glia (Zhang et al., 2004). PR also regulates a cluster of G-protein signaling pathways, ras, and multiple kinase pathways (Jacobsen et al., 2003). ERβ expression was not seen in any of the cell lines or tissues we tested (not shown), suggesting that ERβ is not a significant influence in the cells/tissues in this study.

We also hypothesize that the complex hormonal milieu during pregnancy or the response to these hormones may be different in women with NF1. For example, 2ME2, which is an estrogen metabolite, which appears to hold overproliferation of cells

in check, has been found to be upregulated during a normal pregnancy (Wang et al., 2000), but may either be present in lower levels systemically in women with NF1, resulting in tumor overgrowth, or cell receptors for 2ME2 may be lacking in NF1−/− cells. 2ME2 has been found to be cytotoxic to numerous tumor cells as well as some other rapidly growing cells (Mabjeesh et al., 2003), but not to normal or quiescent cells, by inducing apoptosis (Wang et al., 2000; Ireson et al., 2004). 2ME2 has no E2-like activity and has very low affinity for the ER, suggesting that its mechanism of action is not ER-dependent (Wang et al., 2000; Ireson et al., 2004). The mechanism of 2ME2 action is reported to be through disruption of microtubules by destabilization and disassembly, and impairing HIF-1 accumulation in the nucleus thus inhibiting VEGF expression (Mabjeesh et al., 2003). VEGF is required for angiogenesis, which in turn is needed for tumor growth beyond the size at which nutrients can diffuse. In vitro, 2ME2 competes with colchicine for tubulin binding sites and disrupts interphase microtubules, resulting in cell death (Mabjeesh et al., 2003). Neurofibromin has been found to associate and co-purify with microtubules, suggesting NF1 involvement in microtubule-mediated pathways (Gregory et al., 1993). We determined that 10 μM was the threshold at which 2ME2, a naturally occurring estrogen metabolite, disrupts microtubules and is cytotoxic to malignant NF1 tumor cells while its effect is to slow or halt the growth of the other cells lines tested, regardless of their NF1 status. This suggests that perhaps additional mutations, for example p53, which has been associated with MPNSTs (Menon et al., 1990), are involved in 2ME2 cytotoxic effects specific to malignant tumors, because nonmalignant NF1−/− tumor cells did not undergo apoptosis with 2ME2 treatment.

Another hypothesis we posit is that the effect of hormones on neurofibromas may be indirect through hormonal effects on angiogenesis. Increased blood vessel formation during pregnancy could allow existing tumors to be supplied with additional nutrients and gas exchange as they grow, as well as to induce previously microscopic tumors to grow to a size at which they are detectable. It is also worth noting that, although most of the cultures on which these studies were performed are of mouse cells, the tumor cell cultures are from human neurofibromas, which may explain some of the disparate results.

On the basis of these studies, we conclude that NF1−/− SC-like differentiated mES cells, as well as NF1-deficient mouse tissues and NF1−/− human tumor cells, express higher levels of classic steroid hormone receptors than cells and tissues with full expression of neurofibromin. Hormonal addition had a heterogeneous effect on cell proliferation, with a small but significant direct effect on the classic pathway in the NF1−/− SC-like and malignant NF1−/− human tumor cell lines tested. A naturally occurring estrogen metabolite, 2ME2 was able to induce apoptosis only in the malignant NF1−/− human tumor cells.

We have shown in a previous study that these SC-like differentiated mES cell lines (SKOSC, NF1+/− and DKOSC, NF1−/−) as well as two human NF1 tumor cell lines, are deficient in NF1 expression (Roth et al., 2007). We cannot, however, draw the general conclusion that increased steroid hormone receptor expression would be seen in all SC-like differentiated NF1-deficient mouse ES cell lines, because there are no other NF1+/− or NF1−/− mES cell lines available for comparison of which we are aware and the production of additional "knockout" ES cell lines is beyond the scope of this study. The effects of NF1 knockdown through RNA silencing and subsequent rescue by insertion of an NF1 construct into the knocked-down cells could also be used to verify the respective induction or suppression of steroid hormone receptors in NF1+/+ D3SC cells. However, interpretation of such experiments would be difficult, because silencing is seldom complete and the huge size of NF1 makes re-expression experiments extremely difficult. These steps are beyond the scope of this current analysis, which is intended to examine the effects of hormonal treatment on proliferation in a homogeneous NF1−/− cell population as a "proof of principle" that ES knockout cell lines can be used to test effects of neurofibromin loss, rather than a focus on the ES cell properties themselves.

Future studies will focus on the effects of these hormones separately and in combination on these stem cell-derived cell lines and other cells and tissues whose NF1 status is known, including other malignant NF1 tumor cell lines. Because of the complex hormonal milieu during pregnancy, it will be necessary to look for synergy among hormone effects. We will also investigate the mechanisms of these hormones' effects through other mechanisms than their classic receptors. Future analyses will also include in vivo assays that study the effect of steroid hormones on NF1-deficient tissues in the cre mouse models used in this study, which are also beyond the scope of the current study.

EXPERIMENTAL PROCEDURES

Cell Types

The cell lines used for these studies include the NF1+/+ (D3) mES cell line (Doetschman, 1985); NF1+/− (SKO) mES cells (Jacks et al., 1994); NF1−/− (DKO) mES cell line (Jacks et al., 1994); SW10 (NF1+/+) mouse Schwann Cell line with a temperature sensitive SV40 large T antigen, grown at 37°C (the nonpermissive temperature for transgene expression) for differentiation (ATCC; Hai et al., 2002); pNF00.11 (referred to as PNF cells in this report; NF1−/−) human plexiform neurofibroma (Muir et al., 2001); and ST88-14 (referred to as ST cells in this report; NF1−/−) human MPNST (gift of Dr. Larry Sherman, Oregon Health Sciences University; Su et al., 2004). Positive control cell lines for hormone receptors were ER+ and PR+ MCF-7 cells (gift of Dr. Dorraya El-Ashry, Univ. of MI) and AR+ LNCaP cells and mouse breast and prostate tissues (gift of Dr. Diane Robins, Univ. of MI).

Differentiation of mES Cells to SC-like Cells

We had previously found that mES cells that were wild type, heterozygous or homozygous for the NF1 gene could be differentiated into neuron-

like cells and SC-like cells, (Roth et al., 2007) the latter of which more closely approximate the initiating tumor cell type in NF1. SC-like differentiated mES cells will be referred to as D3SC (NF1+/+), SKOSC (NF1+/−) and DKOSC (NF1−/−), depending on the number of NF1 alleles expressed.

Media

Proliferating (ES) cells medium consisted of 81% DMEM without Phenol Red, 1% L-Glut, 1% Pen/Strep, 1% nonessential amino acids (Gibco, Carlsbad, CA), 15% fetal bovine serum (FBS; Atlanta Biological, Norcross, GA), 1% sodium pyruvate (2% stock), 7 μl/L βmercaptoethanol (Sigma, St. Louis, MO), and 1,000 U/ml ESGRO (Chemicon, Temecula, CA). Schwann cell differentiation (SC) medium contained 84% a-mod. MEM without Phenol Red, 1% Pen/Strep (Gibco), 10% FBS (Atlanta Biological), 5% 11-day chick embryo extract, 10 ng/ml neuregulin NRG-1 (R&D systems, Minneapolis, MN). Tumor cell medium for growth of PNF (Muir et al., 2001) and ST (Su et al., 2004) cell lines contained 84% DMEM without Phenol Red, 1% Pen/Strep (Gibco), 25 ng/ml NRG-1 (R&D systems), 15% FBS. SW10 SC cell line medium consisted of 88% DMEM without Phenol Red, 1% L-glutamine, 1% Pen/Strep, 10% FBS (Atlanta Biological). Note: Regular FBS was replaced by charcoal-stripped FBS (Valley Biomedical, Winchester, VA) in all medium used for hormone assays. Minimal medium contained 87% DMEM without Phenol Red, 10% FBS, 1% Pen/Strep, 1% L-glutamine, 1% sodium pyruvate (2% stock).

Antibodies

All antibodies were diluted in 10% donkey serum (Chemicon International, Temecula, CA) in 0.1% Tween20/phosphate-buffered saline (Sigma). ERα (rabbit polyclonal 1:50); AR (rabbit polyclonal 1:50) and NF1 (rabbit polyclonal 1:50; Santa Cruz, Santa Cruz, CA); Tuj1 (mouse monoclonal 1:500; Covance, Berkeley, CA); neurofilament (rabbit polyclonal 1:400; Chemicon International); S100 (rabbit polyclonal 1:200 Novocastra, Newcastle Upon Tyne, UK or mouse monoclonal 1:50 Abcam, Cambridge, MA); glial fibrillary acidic protein (mouse monoclonal 1:400; Chemicon); myelin (mouse monoclonal 1:10; Abcam); PR (mouse monoclonal 1:50; Abcam); αtubulin (mouse monoclonal 1:200); Caspase-3 (mouse monoclonal 1:1,000; BD Transduction, San Jose, CA); AlexaFluor 350, 488, 594, DAPI (Molecular Probes, Eugene, OR), goat α rabbit-horseradish peroxidase (Zymed, San Francisco, CA). Note: We also looked at ERβ expression, but did not see expression in any of the experimental cells or tissues tested. Therefore, ER = ERα in this study. Hormones and receptor inhibitors used included progesterone, RU486, 17β-estradiol, 2ME2 (Sigma) ICI 182,780 (Tocris), testosterone and flutamide (gift of Dr. Diane Robins, University of MI). All were diluted in 100% ethanol, which was also used for vehicle wells. Reagents used included CellTiter96 cell proliferation assay kit (Promega), Histomouse (Zymed), Prolong Gold anti-fade mounting medium (Molecular Probes), Porcine gel (Sigma), in situ cell death detection kit, fluorescein (TUNEL) (Roche, Indianapolis, IN), Citrisolv, ethanol, and sodium citrate dihydrate (Fisher Scientific, Fairlawn, NJ).

Immunocytochemistry

On day 0, 40,000 cells were plated onto 0.1% porcine gel-coated coverslips (Corning, Corning, NY) and grown overnight. For microtubule visualization in the 2ME2 assay, varying concentrations of 2ME2 were added to the medium; cells were grown an additional 24 hr. Cells were then fixed in 4% paraformaldehyde (Sigma), permeabilized in 0.2% Triton X-100 (Sigma), stained and mounted on Superfrost plus slides (Fisher, Pittsburgh, PA). Fluorescence micrographs were taken with an Olympus BX-51 microscope, and nonfluorescent micrographs with Nikon ACT-1 software on a Leitz Diavert inverted microscope.

Hormone Receptor Immunohistochemistry on Mouse Tissue

The control mice used in this study are a pool of phenotypically indistinguishable mice with four genotypes: NF1flox/+;P0A-cre+, NF1flox/flox; P0A-cre−, NF1flox/-;P0A-Cre−, and NF1+/−. The mutant mice used were of the genotype, NF1flox/−;P0A-cre (mutants). Twelve- to 20-month-old mice were monitored until signs of distress appeared, at which time they were subjected to necropsy. The P0A-cre transgenic strain was initially generated on the FVB background (Giovannini et al., 2000). After five generations of being backcrossed to the 129 Svj background, the P0A-cre transgenic mice were crossed to the NF1flox/− mice that were maintained on the 129 Svj background. Subsequent crosses generated control and mutant mice for analysis (Zheng et al., in revision; Zhu et al., 2002). The Rosa26-LacZ allele was maintained on the mixed 129 Svj and C57Bl6 backgrounds. The mutant mice with or without the Rosa26-LacZ allele exhibited similar phenotypes. All mice in this study were cared for according to the guidelines that were approved by the Animal Care and Use Committees of the University of Michigan at Ann Arbor. For histological analysis, control and mutant littermates at 12–22 months of age were perfused with 4% paraformaldehyde. Tissues were dissected, post-fixed overnight for 2 hr at room temperature, and transferred to 30% sucrose overnight. Tissues were embedded using OCT medium and sectioned longitudinally at 65 μm thicknesses using a cryostat. Mouse tissue slides were deparaffinized in Citrisolv and rehydrated in successive dilutions of ethanol. Antigen retrieval was performed be boiling slides for 10 min in 0.01 M sodium citrate buffer pH 6.0, followed by immunohistochemistry at room temperature in a humidified chamber. Nonspecific binding was blocked with 10% donkey serum, incubated with primary antibodies listed followed be secondary antibody incubation for 20 min and 5 min DAPI staining. Washes between steps were done in 0.1% PBST. After coverslips were applied using Prolong Gold antifade mounting medium and slides were dried overnight, photographs were taken at ×40 magnification using an Olympus BX-51 microscope.

Measures of Cell Proliferation

Hormones and receptor inhibitors.

Cells were grown overnight in hormone-free phenol red-free medium. The next day, cells were counted, plated, and allowed to attach for 2 hr in SC differentiation medium (containing hormone receptor inhibitor if specified) before hormone was added in the concentrations indicated. Inhibitors and hormones were replenished after 48 hr. At 4 days growth, proliferation was assayed using a Beckman Z1 Particle Coulter counter (Beckman Coulter, Inc., Fullerton, CA). Cell numbers were converted to percentages using proliferation of cells in ethanol-containing (vehicle) wells as 100%. Statistical analysis: data are expressed as mean ± SD, and the Student's *t*-test was used to gauge significance, which was $P < 0.05$.

2ME2.

Cells were counted, plated, and allowed to attach overnight in hormone-free medium and phenol-red free medium. Varying concentrations of 2ME2 were added to the media; cells were grown an additional 2 days, proliferation was assayed using the CellTiter96 (Promega) proliferation assay and absorbance was measured by microplate reader (Fisher). Absorbance was converted to percentages using absorbance of cells grown in vehicle (EtOH) as 100%. Equation used: treated well/vehicle well × 100.

RTqPCR

RTqPCR was performed using primer pairs designed using the Beacon designer program (Bio-Rad, Hercules, CA), target with Ta at 55°C, a length 18–22 bp, and amplicon size 100–200. Gene expression was normalized to glyceraldehyde-3-phosphate dehydrogenase (GAPDH). Total RNA from the samples was extracted using a Qiagen RNeasy Kit (Kit 74106, Qiagen, CA). RT-PCR was performed as follows: cDNA was synthesized from 2 μg of total RNA by reverse transcription using Super Script III transcriptase (Invitrogen, Carlsbad, CA) and oligo dT primer. A 2-μl aliquot of the cDNA of each sample was used for PCR with the hormone receptor primers. The PCR conditions included an initial denaturation at 94°C for 1 min, followed by 94°C for 1 min, 55°C for 30 sec, and 74°C for 30 sec and 34 cycles and final extension at 72°C for 5 min with a 4°C holding temperature. The PCR products were separated on 2.0% agarose gels and visualized using ethidium bromide under ultraviolet light.

PCR Primers

NF1: forward AGTTTCTCTCCTCGCTGGTCTTC reverse CGTTTCCTGCCACCCGTTTG; AR: forward GCGGTCCTTCACTAATGTCAACTC reverse TGCCTCATCCTCACACACTGG; PR: forward CTGGATGAGCCTGATGGTGTTTG reverse GGCACAGCGAGTAGAATGACAG; ER forward GAAAGGCGGCATACGGAAAGAC reverse TCAAGGACAAGGCAGGGCTATTC.

TUNEL Assay

Apoptosis was measured by TUNEL assay. PNF and ST cells were plated, grown, fixed, and permeabilized as in the 2ME2 immunocytochemical assay. The TUNEL assay was performed according to Roche kit specifications with the following modifications. Caspase-3 antibody was added at 1:1,000 to the TUNEL reaction mixture and incubated at 37°C for 60 min in the dark. After PBS rinses, DAPI was added at 1:1,000 for 3 min. Coverslips were mounted on slides with Molecular Probes' Antifade medium and dried 24 hr in the dark before fluorescence visualization.

ACKNOWLEDGMENTS

Thanks to Dr. Dorraya El-Ashry (Univ. of MI) for providing ER+ and PR+ MCF-7 cells, to Dr. Diane Robins (Univ. of MI) for very helpful discussions and critical comments on the manuscript as well as for AR+ LNCaP cells, testosterone, and flutamide. Thanks to Dr. Larry Sherman (Oregon Health Sciences University) for the ST88-14 MPNST cells. Thanks to Dr. Catherine Krull and Dr. Gary Hammer, both of the University of Michigan, for critical comments on the manuscript. Thanks to Naweah P. Attia, Luming Feng, Patricia Lenderman, Pierre Cornell, Dr. David Molea, and James Iannuzzi for excellent technical assistance and/or help with experiments. T.M.R. received a National Science Foundation Graduate Research Fellowship, K.F.B. was funded by the NIH and a Congressionally mandated AMRMC program, and M.R.W. and D.M. were funded by DAMD.

REFERENCES

Ansari AH, Nagamani M. 1976. Pregnancy and neurofibromatosis (von Recklinghausen's disease). Obstet Gynecol 47: 25S–29S.

Chen Y, Zajac JD, MacLean HE. 2005. Androgen regulation of satellite cell function. J Endocrinol 186:21–31.

Daschner K, Assum G, Eisenbarth I, Krone W, Hoffmeyer S, Wortmann S, Heymer B, Kehrer-Sawatzki H. 1997. Clonal origin of tumor cells in a plexiform neurofibroma with LOH in NF1 intron 38 and in dermal neurofibromas without LOH of the NF1 gene. Biochem Biophys Res Commun 234:346–350.

DeBella K, Szudek J, Friedman JM. 2000. Use of the national institutes of health criteria for diagnosis of neurofibromatosis 1 in children. Pediatrics 105(Pt 1): 608–614.

Dingli D, Timm M, Russell SJ, Witzig TE, Rajkumar SV. 2002. Promising preclinical activity of 2-methoxyestradiol in multiple myeloma. Clin Cancer Res 8:3948–3954.

Djavaheri-Mergny M, Wietzerbin J, Besancon F. 2003. 2-Methoxyestradiol induces apoptosis in Ewing sarcoma cells through mitochondrial hydrogen peroxide production. Oncogene 22:2558–2567.

Doetschman T. 1985. The in vitro development of blastocyst-derived embryonic stem cell lines: formation of visceral yolk sac, blood islands and myocardium. J Embryol Exp Morphol 87:27–45.

Dugoff L, Sujansky E. 1996. Neurofibromatosis Type 1 and pregnancy. Am J Med Genet 66:7–10.

Edinger AL, Thompson CB. 2004. Death by design: apoptosis, necrosis and autophagy. Curr Opin Cell Biol 16:663–669.

Fernandez-Valdivia R, Mukherjee A, Mulac-Jericevic B, Conneely OM, DeMayo FJ, Amato P, Lydon JP. 2005. Revealing progesterone's role in uterine and mammary gland biology: insights from the mouse. Semin Reprod Med 23:22–37.

Fishbein L, Zhang X, Fisher LB, Li H, Campbell-Thompson M, Yachnis A, Rubenstein A, Muir D, Wallace MR. 2007. In vitro studies of steroid hormones in neurofibromatosis 1 tumors and schwann cells. Mol Carcinog 46:512–523.

Fotsis T, Zhang Y, Pepper MS, Adlercreutz H, Montesano R, Nawroth PP, Schweigerer L. 1994. The endogenous oestrogen metabolite 2-methoxyoestradiol inhibits angiogenesis and suppresses tumour growth. Nature 368:237–239.

Gao W, Bohl CE, Dalton JT. 2005. Chemistry and structural biology of androgen receptor. Chem Rev 105:3352–3370.

Gattelli A, Cirio MC, Quaglino A, Schere-Levy C, Martinez N, Binaghi M, Meiss RP, Castilla LH, Kordon EC. 2004. Progression of pregnancy-dependent mouse mammary tumors after long dormancy periods. Involvement of Wnt pathway activation. Cancer Res 64:5193–5199.

Ghoumari AM, Dusart I, El-Etr M, Tronche F, Sotelo C, Schumacher M, Baulieu EE. 2003. Mifepristone (RU486) protects Purkinje cells from cell death in organotypic slice cultures of postnatal rat and mouse cerebellum. Proc Natl Acad Sci U S A 100:7953–7958.

Giovannini M, Robanus-Maandag E, van der Valk M, Niwa-kawakita M, Abramowski V, Goutebroze L, Woodruff JM, Berns A. Thomas G. 2000. Conditional biallelic NF2 mutation in the mouse promotes manifestations of human neurofibromatosis type 2. Genes Dev 14:1617–1630.

Gregory PE, Gutmann DH, Mitchell A, Park S, Boguski M, Jacks T, Wood DL, Jove R, Collins FS. 1993. Neurofibromatosis type 1 gene product (neurofibromin) associates with microtubules. Somat Cell Mol Genet 19:265–274.

Gutmann DH, Giovannini M. 2002. Mouse models of neurofibromatosis 1 and 2. Neoplasia 4:279–290.

Hai M, Muja N, DeVries GH, Quarles RH, Patel PI. 2002. Comparative analysis of Schwann cell lines as model systems for myelin gene transcription studies. J Neurosci Res 69:497–508.

Ho KJ, Liao JK. 2002. Nonnuclear actions of estrogen. Arterioscler Thromb Vasc Biol 22:1952–1961.

Ireson CR, Chander SK, Purohit A, Perera S, Newman SP, Parish D, Leese MP, Smith AC, Potter BV, Reed MJ. 2004. Pharmacokinetics and efficacy of 2-methoxyoestradiol and 2-methoxyoestradiol-bis-sulphamate in vivo in rodents. Br J Cancer 90:932–937.

Jacks T, Shih TS, Schmitt EM, Bronson RT, Bernards A, Weinberg RA. 1994. Tumour predisposition in mice heterozygous for a targeted mutation in Nf1. Nat Genet 7:353–361.

Jacobsen BM, Richer JK, Sartorius CA, Horwitz KB. 2003. Expression profiling of human breast cancers and gene regulation by progesterone receptors. J Mammary Gland Biol Neoplasia 8:257–268.

Jacobsen BM, Schittone SA, Richer JK, Horwitz KB. 2005. Progesterone-independent effects of human progesterone receptors (PRs) in estrogen receptor-positive breast cancer: PR isoform-specific gene regulation and tumor biology. Mol Endocrinol 19:574–587.

Klesse LJ, Parada LF. 1998. p21 ras and phosphatidylinositol-3 kinase are required for survival of wild-type and NF1 mutant sensory neurons. J Neurosci 18: 10420–10428.

Klesse LJ, Meyers KA, Marshall CJ, Parada LF. 1999. Nerve growth factor induces survival and differentiation through two distinct signaling cascades in PC12 cells. Oncogene 18:2055–2068.

Korf BR. 1999. Plexiform neurofibromas. Am J Med Genet 89:31–37.

Mabjeesh NJ, Escuin D, LaVallee TM, Pribluda VS, Swartz GM, Johnson MS, Willard MT, Zhong H, Simons JW, Giannakakou P. 2003. 2ME2 inhibits tumor growth and angiogenesis by disrupting microtubules and dysregulating HIF. Cancer Cell 3:363–375.

Maran A, Zhang M, Kennedy AM, Sibonga JD, Rickard DJ, Spelsberg TC, Turner RT. 2002. 2-methoxyestradiol induces interferon gene expression and apoptosis in osteosarcoma cells. Bone 30:393–398.

McEwen BS, Alves SE. 1999. Estrogen actions in the central nervous system. Endocr Rev 20:279–307.

McGaughran JM, Harris DI, Donnai D, Teare D, MacLeod R, Westerbeek R, Kingston H, Super M, Harris R, Evans DG. 1999. A clinical study of type 1 neurofibromatosis in north west England. J Med Genet 36:197–203.

McLaughlin ME, Jacks T. 2003. Progesterone receptor expression in neurofibromas. Cancer Res 63:752–755.

Menon AG, Anderson KM, Riccardi VM, Chung RY, Whaley JM, Yandell DW, Farmer GE, Freiman RN, Lee JK, Li FP, et al. 1990. Chromosome 17p deletions and p53 gene mutations associated with the formation of malignant neurofibrosarcomas in von Recklinghausen neurofibromatosis. Proc Natl Acad Sci U S A 87:5435–5439.

Muir D, Neubauer D, Lim IT, Yachnis AT, Wallace MR. 2001. Tumorigenic properties of neurofibromin-deficient neurofibroma Schwann cells. Am J Pathol 158: 501–513.

Okada A, Sato T, Ohta Y, Iguchi T. 2005. Sex steroid hormone receptors in the developing female reproductive tract of laboratory rodents. J Toxicol Sci 30:75–89.

Ozawa H. 2005. Steroid Hormones, their receptors and neuroendocrine system. J Nippon Med Sch 72:316–325.

Posma E, Aalbers R, Kurniawan YS, van Essen AJ, Peeters PM, van Loon AJ. 2003. Neurofibromatosis type I and pregnancy: a fatal attraction? Development of malignant schwannoma during pregnancy in a patient with neurofibromatosis type I. BJOG 110:530–532.

Rasmussen SA, Overman J, Thomson SA, Colman SD, Abernathy CR, Trimpert RE, Moose R, Virdi G, Roux K, Bauer M, Rojiani AM, Maria BL, Muir D, Wallace MR. 2000. Chromosome 17 loss-of-heterozygosity studies in benign and malignant tumors in neurofibromatosis type 1. Genes Chromosomes Cancer 28:425–431.

Revankar CM, Cimino DF, Sklar LA, Arterburn JB, Prossnitz ER. 2005. A transmembrane intracellular estrogen receptor mediates rapid cell signaling. Science 307:1625–1630.

Rodriguez-Cuenca S, Gianotti M, Roca P, Proenza AM. 2006. Sex steroid receptor expression in different adipose depots is modified during midpregnancy. Mol Cell Endocrinol 249:58–63.

Roth TM, Ramamurthy P, Ebisu F, Lisak RP, Bealmear BM, Barald KF. 2007. A mouse embryonic stem cell model of Schwann cell differentiation for studies of the role of neurofibromatosis type 1 in Schwann cell development and tumor formation. Glia 55:1123–1133.

Serra E, Rosenbaum T, Nadal M, Winner U, Ars E, Estivill X, Lazaro C. 2001. Mitotic recombination effects homozygosity for NF1 germline mutations in neurofibromas. Nat Genet 28:294–296.

Sonneveld E, Riteco JA, Jansen HJ, Pieterse B, Brouwer A, Schoonen WG, van der Burg B. 2006. Comparison of in vitro and in vivo screening models for androgenic and estrogenic activities. Toxicol Sci 89:173–187.

Su W, Gutmann DH, Perry A, Abounader R, Laterra J, Sherman LS. 2004. CD44-independent hepatocyte growth factor/c-Met autocrine loop promotes malignant peripheral nerve sheath tumor cell invasion in vitro. Glia 45:297–306.

Vandenbroucke I, Van Oostveldt P, Coene E, De Paepe A, Messiaen L. 2004. Neurofibromin is actively transported to the nucleus. FEBS Lett 560:98–102.

Virdis R. 2000. Neurofibromatosis type 1 and precocious puberty. J Pediatr Endocrinol Metab 13(Suppl 1):841–844.

Wang SH, Myc A, Koenig RJ, Bretz JD, Arscott PL, Baker JR. 2000. 2-Methoxyestradiol, an endogenous estrogen metabolite, induces thyroid cell apoptosis. Mol Cell Endocrinol 165:163–172.

Witorsch RJ. 2002. Low-dose in utero effects of xenoestrogens in mice and their relevance to humans: an analytical review of the literature. Food Chem Toxicol 40:905–912.

Woodruff JM. 1999. Pathology of tumors of the peripheral nerve sheath in type 1 neurofibromatosis. Am J Med Genet 89: 23–30.

Zhang Z, Cerghet M, Mullins C, Williamson M, Bessert D, Skoff R. 2004. Comparison of in vivo and in vitro subcellular localization of estrogen receptors alpha and beta in oligodendrocytes. J Neurochem 89:674–684.

Zhang J, Tsai FTF, Geller DS. 2006. Differential interaction of RU486 with the progesterone and glucocorticoid receptors. J Mol Endocrinol 37:163–173.

Zheng H, Chang L, Patel N, Yang J, Lowe L, Burns D, Zhu Y. 2008. Abnormal differentiation of stem/progenitor cells triggers tumor formation in peripheral nerves. Cancer Cell (in press).

Zhu Y, Ghosh P, Charnay P, Burns DK, Parada LF. 2002. Neurofibromas in NF1: Schwann cell origin and role of tumor environment. Science 296:920–922.

Development of mouse models of NF1-associated progressive peripheral nerve sheath tumor with therapeutic implications

Lou Chang[1], Huarui Zheng[1], Jessica Lee[1], Yinghua Li[1], Daniel T. Treisman[1], Seçkin Akgül[1], Neha Patel[1,2], Lori Lowe[3,4], David R. Lucas[4], Raf Sciot[5], Eric Legius[6], Luis F. Parada[7], Marco Giovannini[8] and Yuan Zhu[1]

[1]Division of Molecular Medicine and Genetics, Departments of Internal Medicine and Cell & Developmental Biology, [2]Department of Pediatrics and Communicable Diseases, Departments of [3]Dermatology and [4]Pathology, University of Michigan Medical School, Ann Arbor, MI 48109; [5]Morphology and Molecular Pathology Section, [6]Department of Human Genetics, Catholic University Leuven, 3000 Leuven, Belgium; [7]Center for Developmental Biology and Kent Waldrep Foundation Center for Basic Research on Nerve Growth and Regeneration, University of Texas Southwestern Medical Center, Dallas, TX 75390; [8]Center for Neural Tumor Research, House Ear Institute, Los Angeles, CA 90057

Running title: A progressive model for benign and malignant peripheral nerve sheath tumor

Author for correspondence:
Yuan Zhu, Ph.D.
Phone: (734) 647-3033
Fax: (734) 763-2162
E-mail: yuanzhu@umich.edu

ABSTRACT

Individuals with familial cancer syndromes frequently possess germline heterozygous mutations in a tumor suppressor gene. In the setting of neurofibromatosis type 1 (NF1), recent studies demonstrate that interaction with heterozygous cells ($NF1^{+/-}$) in tumor microenvironment is critical for *NF1*-deficient ($NF1^{-/-}$) cells to form plexiform neurofibromas, the only neurofibroma subtype with potential to progress to malignant peripheral nerve sheath tumors (MPNSTs). Importantly, preclinical studies suggest that *NF1* haploinsufficient tumor microenvironment may serve as an attractive therapeutic target for benign neurofibromas. However, the contribution of $NF1^{+/-}$ tumor microenvironment to MPNST development remains undetermined. Here, we use genetically engineered mice to demonstrate that $Nf1^{+/-}$ microenvironment is not required for neurofibroma initiation, which is characterized by developmental defects in axon/glial interaction. Instead, neurofibroma initiation is sensitive to mammalian target of rapamycin complex 1 (mTORC1) inhibition. Strikingly, $Nf1^{+/-}$ microenvironment greatly promotes the progression of $Nf1^{-/-}$ differentiated Schwann cells to plexiform neurofibromas. Upon acquiring somatic mutations in *p53* or *Ink4a*/*Arf*, $Nf1^{+/-}$ microenvironment becomes dispensable for formation of *Nf1*/*p53* and *Nf1*/*Ink4a*/*Arf*-deficient MPNSTs. These MPNST models feature step-wise tumor progression observed in human counterparts. Together, our study underscores the evolving relationship of tumor with stroma, and the need to develop therapeutic strategies appropriate to each stage of tumorigenesis.

INTRODUCTION

Familial cancer syndromes are frequently caused by a germline heterozygous mutation in a tumor suppressor gene (Weinberg 2007). In the case of haplosufficiency of tumor suppressors, germline mutation reduces second order kinetics to first order kinetic, accounting for tumor predisposition (Knudson 1971). The behavior of some familial cancer syndromes, such as Neurofibromatosis type I (NF1), do not follow the predicted kinetics of Knudson's two-hit hypothesis, attributed to tumor suppressor haploinsufficiency (Sherr 2004). Curiously, neoplastic cells isolated from NF1-associated tumors demonstrate that loss of heterozygosity (LOH) at NF1 locus, suggesting NF1 is a haplosufficient tumor suppressor (Rasmussen et al. 2000; Upadhyaya et al. 2008). This apparent contradiction may be explained by the consideration that familial cancer syndromes not only reduce the number of mutational events but also create a context in which tumor suppressor haploinsufficiency in stromal cells may produce an amenable microenvironment for tumorigenesis.

NF1 is a common inherited tumor syndrome afflicting 1 in 3000 to 4000 individuals (Friedman and Riccardi 1999). NF1 patients possess a heterozygous germline mutation in the tumor suppressor gene *NF1*, leading to 15 year decrease in expected life span due to their predisposition for developing malignant peripheral nerve sheath tumors (MPNSTs) (Rasmussen et al. 2001). Germline *NF1* heterozygousity ($NF1^{+/-}$) translates into an 8-13% life time risk of developing MPNSTs, an 10,000 fold increase, compared to the 0.001% risk for the general population (Ducatman et al. 1986; Evans et al. 2002). Another predictor of MPNSTs is the presence plexiform neurofibroma; patients with plexiform neurofibroma have a 20-fold increased likelihood of developing MPNSTs (Tucker et al. 2005). Plexiform neurofibromas are a congenital lesion that occurs in 30-50% of NF1 patients, but rarely in the general population (Lin

et al. 2004; Mautner et al. 2008). Thus, one of the important phenotypic consequences of NF1 germline heterozygousity is the conversion of an extremely tumor resistant organ, the peripheral nerve, into a highly cancer susceptible organ.

NF1 haploinsufficiency may produce an amenable microenvironment to tumorigenesis that is exclusively found in NF1 patients. Previous studies using mouse models of *NF1* have demonstrated that *Nf1*-deficient ($Nf1^{-/-}$) Schwann cells will develop plexiform neurofibromas in the context of a $Nf1^{+/-}$, but not wildtype ($Nf1^{+/+}$), tumor microenvironment (Zhu et al. 2002). Reciprocal bone marrow transplant and compound *Nf1*/c-kit receptor mutants have implicated $Nf1^{+/-}$ mast cell as a key mediator of plexiform neurofibroma tumorigenesis (Yang et al. 2008). Targeting the *NF1+/-* microenvironment has become a potential therapeutic management strategy, with clinical trials currently being conducted (Yang et al. 2008). However, it remains unknown whether NF1 haploinsufficiency in the tumor microenvironment contributes to malignancy.

MPNSTs are an aggressive soft tissue sarcoma with a 5 year survival of between 16% – 38% for NF1 patients and 42% – 57% for sporadic patients (Widemann 2009). Surgical resection of tumors with wide negative margins is the preferred treatment for MPNSTs (Grobmyer et al. 2008). Adjuvant therapy is based off protocols for soft tissue sarcomas, but the role of chemo- and radiotherapy in management of MPNSTs is disputed. This highlights the need for a relevant preclinical mouse model of MPNSTs. Plexiform neurofibromas can arise from a single (LOH) event for *NF1*, but MPNSTs accumulate addition somatic mutations, with *p53* and CDKN2A the most frequently altered loci (Brems et al. 2009). Based on this, mice carrying mutant *Nf1* and *p53* in cis (NPCis) were developed and now serve as the predominantly model for preclinical trials (Cichowski et al. 1999; Johannessen et al. 2008). Unfortunately, these mice do not

recapitulate the progression of tumorigenesis seen in humans; no neurofibromas have been documented in any NPCis mouse. A further concern is whether the Nf1-associated malignancies from NPCis mice recapitulate MPNSTs, as many of the tumors have a mesodermal, as opposed to neural crest, cell-of-origin such as rhabdomyosarcoma, leiomyosarcoma and malignant triton tumors (Vogel et al. 1999).

In this study, we use genetically engineered mouse (GEM) models of plexiform neurofibroma and MPNST to describe distinct stages of peripheral nerve tumorigenesis and the contribution of the $Nf1^{+/-}$ microenvironment to each stage. *Nf1* microenvironmental haploinsufficiency only contributes to the progression phase, but not to initiation or malignant transformation. In contrast, initiation can be prevented through mTORC1 inhibition. These GEM models recapitulate many of the features of NF1-associated MPNSTs, including stepwise progression and neural crest cell-of-origin. With this study, we present a case for the evolving relationship between neoplastic cells and their stroma and highlight the necessity to develop appropriate therapeutic interventions for each phase of tumorigenesis.

RESULTS

A framework for understanding peripheral nerve sheath tumorigenesis

We categorize PNST development into three distinct stages: (1) initiation, (2) progression and (3) malignant transformation. Initiation, as described in our previous publication, can be characterized by Schwann cell pocket defects at P22 and the appearance of abnormal non-myelinating Schwann cells, dissociating Schwann cells and unassociated Schwann cells at P90 (Zheng et al. 2008). Progression is typified by nerve hyperplasia, degeneration of myelinated axons, mast cell infiltration and the appearance of plexiform neurofibromas. Finally, malignant transformation is distinguished by the appearance of palpable masses that grow rapidly and invade into adjacent tissues.

Nf1 heterozygosity in the microenvironment is dispensable for neurofibroma initiation

To assess whether $Nf1^{+/-}$ in the microenvironment participates in initiation and progression, we crossed mice carrying the *P0*-Cre transgene to $Nf1^{flox/ko}$ mice. This cross resulted in littermate mice with the genotypes *P0*-Cre+;$Nf1^{flox/ko}$ and *P0*-Cre+;$Nf1^{flox/flox}$ termed $Nf1^{P0}$CKO1 and $Nf1^{P0}$CKO2, respectively. Notably, this is the same genetic comparisons used in the original *Nf1* microenvironment study (Zhu et al. 2002), where $Nf1^{P0}$CKO1 mice will generate $Nf1^{-/-}$ cells in an $Nf1^{+/-}$ environment and $Nf1^{P0}$CKO2 mice will generate $Nf1^{-/-}$ cells in an Nf1 wildtype ($Nf1^{+/+}$) environment (Supplemental Figure 1). For the sake of consistency in nomenclature, we use conditional knockout 1 (CKO1) to denote an $Nf1^{+/-}$ microenvironment and conditional knockout 2 (CKO2) to denote an $Nf1^{+/+}$ microenvironment. *P0*-Cre has a broader expression pattern compared to *Krox20*-Cre (Giovannini et al. 2000; Voiculescu et al. 2000; Zheng et al. 2008), conferring $Nf1^{P0}$CKO1 mice a robust plexiform and cutaneous neurofibroma

tumor burden (Supplemental Figure 2). *Nf1*^{P0}CKO2 mice permit assessment of whether extensive *Nf1* ablation during Schwann cell development throughout the peripheral nervous system is sufficient to generate plexiform neurofibromas in an *Nf1*$^{+/+}$ microenvironment.

The impact of an *Nf1*$^{+/-}$ microenvironment on neurofibroma initiation was analyzed by collecting sciatic nerves from littermate wildtype, *Nf1*^{P0}CKO1 and *Nf1*^{P0}CKO2 mice at P22. At this time point, we previously identified the earliest phenotype associated with plexiform neurofibroma formation: the generation of Schwann cell pocket defects, where bundles of axons fail to defasciculate into individually Schwann cell cytoplasm ensheathed domains in non-myelinating Schwann cells (Zheng et al. 2008). Sciatic nerves from *Nf1*^{P0}CKO1 and *Nf1*^{P0}CKO2 mice were subjected to light and electron microscopy. 8 wildtype, 3 *Nf1*^{P0}CKO1 and 3 *Nf1*^{P0}CKO2 P22 mice were collected for light microscopy and 3 wildtype, 4 *Nf1*^{P0}CKO1 and 3 *Nf1*^{P0}CKO2 P22 mice for electron microscopy. As expected, there were no detectable differences between control and either mutant sciatic nerve histology (Figure 1A-C). Semithin sections revealed no overt ultrastructural difference between controls and mutants (Figure 1D). No significant difference was found in the cellularity of the sciatic nerve, based on light microscopy (Figure 1E). Ultrastructurally, Schwann cell pocket defects occurred with greater frequency in both *Nf1*^{P0}CKO1 and *Nf1*^{P0}CKO2 sciatic nerves compared to control nerves (Figure 1A'-C'). We quantified the incidence of 1, 2-10 or >10 axons per Schwann cell pocket. Notably, more than 10 axons occupying a single Schwann cell pocket could be observed in both mutant nerves with regularity, but was extremely rare for control nerves. Using chi-squared goodness-of-fit test, we confirmed that while both *Nf1*^{P0}CKO1 and *Nf1*^{P0}CKO2 nerves had significantly greater incidence of Schwann cell pocket defects than in control nerves, they were not significantly different from each other (Figure 1F). From this, we conclude that there is no difference between *Nf1*^{P0}CKO1

and *Nf1*^{P0}CKO2 mice in terms of the incidence of abnormal Schwann cell differentiation, and *Nf1*-deficiency in NSCSs is sufficient to produce Schwann cell pocket defects, the first identifiable pre-neoplastic phenotype.

The next stage of plexiform neurofibroma initiation is characterized by the emergence of abnormal non-myelinating Schwann cells with impaired Schwann cell-axon interactions at approximately P90 (Zheng et al. 2008). The nmSC population undergoes striking morphological changes over the course of two months. Most of the abnormally differentiated Remak bundles with pocket defects observed in P22 mutant sciatic nerves are no longer detected. In their place, an entirely new spectrum of non-myelinating Schwann cell phenotypes appeared. Abnormal non-myelinating Schwann cells (anmSCs) are characterized by an association of morphologically abnormal axons (e.g., dilated or naked axons), focal dissociation and the appearance of deep crevasses disrupting the typically globular morphology of non-myelinating Schwann cells (compare Figure 2A and B). Dissociating Schwann cells (dSCs) were characterized by the presence of free Schwann cell processes (Figure 2C), which progressively dissociated from axons leading to the degeneration of unsheathed axons. Unassociated Schwann cells (uSCs) completely lost axonal contact in spite of the presence of a continuous basal lamina that occasionally ensheath collagen fibers (Figure 2C). The uSCs are morphologically identical to the tumor cells observed in both human and mouse neurofibromas (Lassmann et al. 1977; Cichowski et al. 1999; Zhu et al. 2002).

We thus assessed the propensity of *Nf1*$^{-/-}$ cells to generate pre-neoplastic non-myelinating Schwann cells in an *Nf1*$^{+/-}$ and *Nf1*$^{+/+}$ environment. Sciatic nerves from littermate wildtype, *Nf1*^{P0}CKO1 and *Nf1*^{P0}CKO2 mice at P90 were subjected to light and electron microscopy. 3 wildtype, 6 *Nf1*^{P0}CKO1 and 7 *Nf1*^{P0}CKO2 P90 mice were collected for light microscopy and 2

wildtype, 3 *Nf1*^{P0}CKO1 and 3 *Nf1*^{P0}CKO2 P90 mice for electron microscopy. Histological analysis of sciatic nerves revealed increased cellularity in both mutants compared to wildtype nerves (Supplemental Figure 3A-C, Figure 2D). X-gal staining (Supplemental Figure 3D-I) confirms recombined cell expansion, and p75^{NGFR} staining (Supplemental Figure 3J-L) implicates non-myelinating Schwann cell expansion. Ultrastructurally, from both *Nf1*^{P0}CKO1 and *Nf1*^{P0}CKO2 sciatic nerves, we identified a similar spectrum of abnormal non-myelinating Schwann cells (Figure 2B), dissociating Schwann cells (Figure 2C) and unassociated Schwann cells. The myelinating Schwann cell population was decreased by approximately 10% in both mutants, but due to large sample variation, this was not significant (Figure 2E). Concordantly, S100 staining (Supplemental Figure 3M-O) did not reveal any overt changes in the myelinating Schwann cell population. We quantified the number of abnormal, dissociating and normal non-myelinating Schwann cells in the wildtype, *Nf1*^{P0}CKO1 and *Nf1*^{P0}CKO2 sciatic nerve to determine if *Nf1* environmental heterozygosity impacted the efficacy of generating pre-neoplastic cell types. Both *Nf1*^{P0}CKO1 and *Nf1*^{P0}CKO2 mice had significantly greater cellularity than littermate controls, and a significant presence of abnormal or dissociating Schwann cells (Figure 2F). Although a trend was observed where *Nf1*^{P0}CKO1 had slightly more non-myelinating Schwann cells than *Nf1*^{P0}CKO2, this difference was not statistically significant. Finally, we noted that mast cells were not observed in P22 nerves, but were significantly increased in mutant nerves at P90 compared to control nerves (Figure 2G). Mast cells are unlikely contribute to the generation of Schwann cell pocket defects, as they are not present during this phase of peripheral nerve sheath tumor initiation. We cannot rule out the possibility that Nf1$^{+/+}$ or Nf1$^{+/-}$ mast cells may contribute to loss of axon/glial interaction at P90; previous reports suggest this may indeed be the case (Monk et al. 2007). Together, this data demonstrates

that *Nf1*$^{+/-}$ in the microenvironment has little, if any, effect on neurofibroma initiation. Consequently, targeting the *Nf1*$^{+/-}$ microenvironment likely will not successfully prevent peripheral nerve sheath tumorigenesis.

Rapamycin treatment can stabilize early Schwann cell/axon interaction in *Nf1*-deficient mice

The most promising therapeutic window that we have identified is neurofibroma initiation. We have previously demonstrated that there is a developmental window of susceptibility to *Nf1*$^{-/-}$ (Zheng et al. 2008), suggesting that intervention during this critical period may prevent future plexiform neurofibromas from arising. Unfortunately, targeting the *Nf1*$^{+/-}$ microenvironment does not appear to be a viable strategy to prevent neurofibroma initiation. To find potential alternative therapeutic approaches to treating pre-neoplastic nerves, we performed signal transduction analysis on *Nf1*^{P0}CKO1 and *Nf1*^{P0}CKO2 sciatic nerve at the P22 and P90 time points. No abnormal signal transduction activity was detected at P22 (Figure 3A). In contrast, the mutant P90 *Nf1*$^{-/-}$ nerves consistently had elevated phospho-Erk and phospho-S6 levels (Figure 3B). This suggests that the MAPK/ERK and mammalian target of rapamycin complex 1 (mTORC1) signal transduction pathways may be dysregulated during neurofibroma initiation. We elected to pursue the mTORC1 pathway for its therapeutic potential, as the FDA has approved its inhibitor, rapamycin, for use. Rapamycin is routinely used as an immunosuppressive medication for organ transplant patients and has also been documented to act as a temporary cytostatic agent in the treatment of MPNSTs (Johannessen et al. 2008; Johansson et al. 2008). If the mTORC1 pathway is necessary for neurofibroma initiation, it may be possible to revert the phenotype observed at P22 and stabilize the Schwann cell/axon interaction, preventing subsequent dissociation and tumor formation (Figure 3C).

To test the therapeutic efficacy of rapamycin in preventing early neurofibroma initiation phenotypes, two preliminary trials were conducted. Five *Nf1*^{P0}CKO1 mice were treated with rapamycin at a dose of 5 mg/kg every other day via intra-peritoneal injection every other day starting P30 until P90. A second batch comprised of 7 *Nf1*^{P0}CKO1 mice with the same regiment was treated starting at P21 until P90. Wildtype mice treated with rapamycin and *Nf1*^{P0}CKO1 mice treated with vehicle were also included as negative and positive controls for neurofibroma initiation, respectively. Western blot analysis of sciatic nerve (Figure 3D) and immunohistochemical analysis of splenic white pulp (Supplemental Figure 4A) demonstrates reduction of phospho-S6, confirming the efficacy of rapamycin-mediated inhibition of mTORC1. At P90, nerves were collected for light and electron microscopic analysis. Ultrastructural analysis revealed that rapamycin treatment was capable of stabilizing the Schwann cell/axon interaction in a subset of mice when administered during neurofibroma initiation. Despite the presence of abnormally differentiated Remak bundles with pocket defects at P22, when treated with rapamycin, 40% of mice with treatment starting at P30 and over 70% of mice with treatment starting at P21 had a dramatically less severe ultrastructural phenotype, with fewer aberrant non-myelinating Schwann Cells (Figure 3E). Rapamycin treated control mice had no abnormal Schwann cell phenotype (Figure 3Fa, e), while vehicle treated mutant mice displayed characteristic pre-neoplastic non-myelinating Schwann cell phenotypes: the presence of dissociating and unassociated Schwann cells (Figure 3Fb, f). We categorized rapamycin treated mutant mice as either “unrescued” (Figure 3Ed, h) or “rescued” (Figure 3Ec, g) based on the presence or absence of more than one unassociated Schwann cells per low magnification (1450X) field, respectively. At least one unassociated Schwann cell could be found in each “rescued” nerve, suggesting that these mice were indeed mutants and that there may be a

minority of *Nf1*-deficient cells that are unresponsive to rapamycin treatment. Corresponding levels of sciatic nerve cellularity was found using both ultrastructural and light microscopy quantification, suggesting that the ultrastructural cross-section is representative of the entire length of the nerve (Supplemental Figure 4B). Quantification of the cell types found in the vehicle treated mutants, rapamycin treated controls, rescued and unrescued mice and revealed a striking alteration in the number of dissociating cells in the rescued nerves (Figure 3G, H, top charts). The numbers of dissociating and unassociated Schwann cells have been reduced to rapamycin treated control levels, and are significantly different from the untreated and the unrescued mutants (Figure 3G, H, top charts). However, the total number of non-myelinating Schwann cells was not reduced to wildtype levels (Figure 3G, H, bottom charts). This suggests that rapamycin can stabilize Schwann cell/axon interaction but only after some Schwann cells have undergone proliferation. Nevertheless, this represents the first successful attempt at targeting the pre-neoplastic population of neurofibroma initiation and highlights the role of mTORC1 during the initiation phase of peripheral nerve sheath tumorigenesis.

***Nf1* heterozygosity in the microenvironment promotes neurofibroma progression**

The impact of the *Nf1* heterozygous microenvironment was assessed by analyzing 20 $Nf1^{P0}$CKO1 and 13 $Nf1^{P0}$CKO2 mice between 10 and 14 month of age. As previously documented, at this age, $Nf1^{P0}$CKO1 mice develop plexiform neurofibromas in the sciatic nerve (Zheng et al. 2008). Whenever possible, comparisons were made between littermates to decrease potential influences resulting from different genetic backgrounds. We performed a systematic analysis of seven distinct sites across the peripheral nervous system: sciatic nerves (SN), trigeminal nerves (TN), cutaneous nerves (CN), cervical dorsal root ganglia (C-DRG), thoracic dorsal root ganglia (T-DRG), lumbar dorsal root ganglia (L-DRG) and brachial plexus. These

nerves were histopathologically diagnosed based on their H&E staining patterns. This permit discernment of whether (1) mice with sufficient burden of *Nf1*$^{-/-}$ cells in the developing PNS could generate tumors and (2) the *Nf1*$^{+/-}$ microenvironment plays a significant role in peripheral nerve sheath tumorigenesis in a *Krox20*-Cre independent GEM.

One of the most salient observations we found upon dissecting the peripheral nerves was that while both *Nf1*^{P0}CKO1 and *Nf1*^{P0}CKO2 nerves were enlarged throughout the peripheral nervous system, *Nf1*^{P0}CKO1 nerves consistently had a more severe phenotype (Figure 4A-D). The degree to which nerves were enlarged varied between sites, where the sciatic and trigeminal nerves had a mild but appreciable enlargement, while cutaneous nerves and brachial plexi were often grossly enlarged (Figure 4A). Using previously established histological grading criteria (Zheng et al. 2008), each nerve was diagnosed into one of four categories based on H&E staining. Normal nerves have low cellularity (Figure 4Ba, e). Hyperplastic nerves exhibit higher cellularity, while maintaining tissue organization and often accompanied by increased blood vessels and mast cells (Figure 4Bb, f). Hyperplasia with focal neurofibroma (Hyperplasia/fNF) resemble hyperplastic nerves, and contain focal areas of increased cellularity, demyelination and loss of organization (Figure 4Bc, g). Finally, frank neurofibromas resemble human neurofibromas with high levels of collagen deposition, disruption of tissue organization and greatly increased cellularity (Figure 4Bd, h).

From these histological criteria, the neurofibroma penetrance (Figure 4C) was determined for the seven sites described above. For sciatic nerve, trigeminal nerves (Supplemental Figure 5), cutaneous/subcutaneous nerves (Supplemental Figure 6), and brachial plexus, one nerve was examined for each mouse. For DRGs, from 1-6 DRGs were examined for each site in each mouse, and used to generate an average penetrance of all DRGs per mouse (Supplemental Figure

7). Specifically, 46 C-DRG from 12 *Nf1*^{P0}CKO1 , 45 C-DRG from 10 *Nf1*^{P0} CKO2 ; 23 T-DRG from 12 *Nf1*^{P0}CKO1, 16 T-DRG from 9 *Nf1*^{P0}CKO2; 29 L-DRG from 12 *Nf1*^{P0}CKO1 and 20 L-DRG from *Nf1*^{P0}CKO2 mice were analyzed. A Z-test was used to determine whether a difference in neurofibroma penetrance exists based on the environmental genotype for sciatic nerves, cutaneous/subcutaneous nerves, trigeminal nerves and the brachial plexus. Linear mixed modeling was used to determine whether the penetrance in DRGs was different based on *Nf1*$^{+/-}$ in the environment. A more detailed breakdown consisting of the diagnosis made for each nerve is summarized in Figure 4D. In all cases analyzed, nerves from *Nf1*^{P0}CKO1 mice had a more severe phenotype than littermates from *Nf1*^{P0}CKO2 mice.

The cutaneous/subcutaneous nerve plexiform neurofibroma (Figure 4A, Supplemental Figure 6), while robust, remained intra-neural. This is in contrast to the dermal neurofibromas observed that were distinctly extra-neural (Supplementary Figure 2). We insist caution be used when ascribing a diagnosis of dermal neurofibroma to lesions near the surface of the skin to avoid confusion between subcutaneous intra-neural plexiform neurofibroma and extra-neural dermal neurofibromas.

It is evident from the summaries provided (Figure 4C, D) that there exists a significant difference in terms of tumor burden between *Nf1*^{P0}CKO1 and *Nf1*^{P0}CKO2 mice. This leads us to conclude that *Nf1*$^{+/-}$ in the microenvironment does indeed promote peripheral nerve sheath tumorigenesis. This is especially true for the sciatic and trigeminal nerves, where neurofibromas were never diagnosed in *Nf1*^{P0}CKO2 mice and were relatively common in *Nf1*^{P0}CKO1 mice (Figure 4D). Mast cell infiltration in the sciatic nerve was investigated as a potential mechanism to facilitate this difference. While the degree of mast cell infiltration was dependent on the degree of nerve damage, it was not dependent on Nf1$^{+/-}$ (Supplemental Figure 8). This leads us to

conclude that mast cell recruitment is not influenced by *Nf1* heterozygosity, but leaves open the possibility that heterozygous mast cells may have altered behavior once recruited. *Nf1*^{P0}CKO2 mice also developed plexiform neurofibroma with high penetrance at certain sites such as cutaneous nerves, DRGs and brachial plexi. This would suggest that an *Nf1*$^{+/-}$microenvironment is not necessary to permit plexiform neurofibroma formation provided sufficient quantities of *Nf1*$^{-/-}$ cells are introduced to the peripheral nerves. Regardless, this collection of results leads us to conclude that the *Nf1* heterozygous microenvironment promotes neurofibroma progression, and thus represents a potential therapeutic window for microenvironment targeted therapies.

***Nf1* heterozygosity and benign tumor burden does not impact malignant transformation**

To assess the role of an *Nf1*$^{+/-}$ microenvironment in the malignant transformation of PNSTs, we required mouse models that satisfy two criteria: (1) they must form MPSNTs and (2) they must allow for direct comparison of how *Nf1*$^{+/+}$ and *Nf1*$^{+/-}$ microenvironments contribute to MPNST formation. *Nf1*^{P0}CKO1 and *Nf1*^{P0}CKO2 mice rarely, if ever, developed malignant peripheral nerve sheath tumors. To address this question, we generated several novel MPNST mouse models.

The NPCis mice provided the groundwork for the development of our novel GEMs (Cichowski et al. 1999; Vogel et al. 1999). These mice demonstrate that cells double deficient for *Nf1* and *p53* can give rise to MPNSTs. Thus, we focused our attempt on generating *Nf1*/*p53* double deficient cells in either an *Nf1*$^{+/+}$ or *Nf1*$^{+/-}$ context. This was accomplished by producing mice that carry a chromosome with an *Nf1* flox allele and a *p53* knockout allele in cis. When these mice are crossed to *P0*-Cre positive mice carrying *Nf1* knockout, *Nf1* flox or *Nf1* wildtype alleles, three useful genetic configurations would be produced. Mice with the genotype of *P0*-Cre+; *Nf1*$^{flox/ko}$; *p53*$^{ko/+}$ termed NP^{P0}CKO1 possess a germline *Nf1* knockout allele, providing an

Nf1$^{+/-}$ microenvironment, and would be *Nf1*$^{-/-}$ after Cre-mediated recombination. These mice are predicted to develop a high burden of benign neurofibromas due to the presence of *Nf1*$^{-/-}$ cells in a heterozygous microenvironment. A LOH event at the *p53* locus after Cre-mediate recombination would produce *Nf1*/*p53* double deficient cells (Figure 5A). Mice with the genotype of *P0*-Cre+; *Nf1*$^{flox/flox}$; *p53*$^{ko/+}$ termed NP^{P0}CKO2 possessed two *Nf1* flox alleles and thus have an *Nf1*$^{+/+}$ microenvironment. Similar to NP^{P0}CKO1 mice, NP^{P0}CKO2 mice become *Nf1*$^{-/-}$ after Cre-mediated recombination and an LOH event at the *p53* locus after Cre-mediate recombination would produce *Nf1*/*p53* double deficient cells (Figure 5A). These mice are expected to develop a lower burden of benign neurofibromas due to the presence of *Nf1*$^{-/-}$ cells in a wildtype microenvironment. A comparison of the rate of malignant transformation and tumor burden between NP^{P0}CKO1 and NP^{P0}CKO2 mice would determine whether *Nf1*$^{+/-}$ affects malignant transformation. Finally as a control, we utilized mice with the genotype *P0*-Cre+; *Nf1*$^{flox/+}$; *p53*$^{ko/+}$ mice NP^{P0}Cis (Figure 5A). These mice will rarely have *Nf1*$^{-/-}$ cells alone as a co-LOH event that also inactivates *p53* is the most common mode of LOH in mice (Luongo et al. 1994). Thus NP^{P0}Cis nerves are not predicted to have the inflammatory response associated with the presence of *Nf1*$^{-/-}$ cells (Figure 2G, 4B). Thus these three *p53* based models, termed NP^{P0}CKO mice collectively, provide *Nf1*/*p53* double deficient cells with three distinct cellular microenvironments to develop in: nerves with high benign tumor burden in *Nf1*$^{+/-}$ microenvironment with NP^{P0}CKO1, nerves with lower benign tumor burden in *Nf1*$^{+/+}$ environment with NP^{P0}CKO2 and nerves with no tumor burden in *Nf1*$^{+/+}$ environment with NP^{P0}Cis (Figure 5A).

Benign tumor burden was assessed for 12 NP^{P0}CKO1, 16 NP^{P0}CKO2 and 6 NP^{P0}Cis mice through the systematic diagnosis of four sites from the peripheral nerves of these mice:

sciatic nerves (SN), cutaneous nerves (CN), trigeminal nerves (TN) and brachial plexi (BP). These nerves were diagnosed based on our previously described grading criteria (Figure 4B). The benign tumors in these mice are not as robust as previously documented, likely due to the different genetic background on which these mice were generated. Nevertheless, NP^{P0}CKO1 mice with a $Nf1^{+/-}$ microenvironment had a more robust benign tumor phenotype than NP^{P0}CKO2 mice with an $Nf1^{+/+}$ environment (Figure 5B). As expected, nerves from NP^{P0}Cis mice were histologically normal. Together, this data demonstrates that mice with germline *p53* heterozygosity carry benign tumor burdens in a similar pattern to their wildtype counterparts; $Nf1^{+/-}$ still contributes to plexiform neurofibroma formation.

Despite increased benign tumor and $Nf1^{+/-}$ environment in NP^{P0}CKO1 mice (n=20), they developed MPNSTs with the same rate and penetrance as NP^{P0}CKO2 (n=34) and NP^{P0}Cis mice (n=34, Figure 5C-E). This result suggests that neither $Nf1^{+/-}$ cells nor benign tumor burden impacts the propensity for cells to undergo malignant transformation, provided the cell is already *Nf1*/*p53* double deficient. We performed molecular characterization of the MPNST cells to verify that the genetics of malignant transformation is as predicted (Figure 5A). We found that recombination of the *Nf1* flox allele was detected in all tumors (Figure 5F). LOH of the *p53* allele could be detected in the majority of NP^{P0}CKO1, NP^{P0}CKO2 and NP^{P0}Cis tumors, as verified by genomic qPCR (Figure 5G). To confirm that P53 function was lost in tumors that do not display LOH, we extracted RNA and performed RT-PCR for *p53* transcripts. These tumors indeed only expressed the *p53* ko allele, suggesting loss of P53 function (Figure 5H). The levels of Neurofibromin and P53 were assayed for benign and malignant tumors, further confirming the loss of *Nf1* and *p53* gene products in MPNSTs (Figure 5I). Notably, benign plexiform neurofibromas consistently contained a contaminate population of unrecombined cells that retain

Neurofibromin while MPNSTs do not. Together, this molecular analysis confirms the genetic changes underlying malignant transformation occur as described in Figure 5A.

To verify that the *Nf1*$^{+/-}$ microenvironment does not play a role in malignant transformation, we generated a MPNST model that was independent of *p53*. *Ink4a*/*Arf* was used to model malignant transformation because the CDKN2a locus is frequently deleted in MPNSTs and *Nf1*/*Ink4a*/*Arf* compound mutant mice were demonstrated to generate MPNSTs with low frequency (Joseph et al. 2008; Brems et al. 2009). We acquired the *Ink4a/Arf* flox allele to generate compound conditional knockouts of *Nf1 and Ink4a/Arf (Krimpenfort et al. 2001)*. To examine the role of the *Nf1*$^{+/-}$ microenvironment in *Nf1/Ink4a/Arf* tumorigenesis, we used a similar strategy as previous described for *p53*. We generated *P0*-Cre+; *Nf1*$^{flox/ko}$; *Ink4a/Arf*$^{flox/flox}$ termed NI^{P0}CKO1 and *P0*-Cre+; *Nf1*$^{flox/flox}$; *Ink4a/Arf*$^{flox/flox}$ termed NI^{P0}CKO2 mice. Upon Cre-mediated recombination, NI^{P0}CKO1 would have *Nf1/Ink4a/Arf* deficient cells in an *Nf1*$^{+/-}$ microenvironment while NI^{P0}CKO2 mice will have those cells in a wildtype environment. NI^{P0}CKO1 (n=11) and NI^{P0}CKO2 (n=20) mice, termed NI^{P0}CKO mice collectively, developed MPNSTs rapidly, taking between four and five months, preventing a robust neurofibroma phenotype (Figure 6A). There were no distinguishing features when tumors from NI^{P0}CKO1 and NI^{P0}CKO2 mice were analyzed histologically. Furthermore, no histological differences were identified between tumors derived from NP^{P0}CKO or NI^{P0}CKO mice (Supplemental Figure 9). As seen with *p53*-based mouse models, neither the rate of tumor formation (Figure 6B, C) nor the tumor spectrum (Figure 6D) were influenced by the presence of *Nf1*$^{+/-}$ cells. These results again demonstrate that malignant transformation does not depend on the status of *Nf1* in the microenvironment.

A notable difference between MPNSTs derived from NP^{P0}CKO and NI^{P0}CKO mice is the status of the P53 pathway. Unlike MPNSTs derived from NP^{P0}CKO mice, NI^{P0}CKO tumors still express p53 mRNA (Figure 6E). A functional assay for P53 activity is exposure to ionizing radiation, where an intact P53 response will result in cell cycle arrest and apoptosis. The readout for P53-induced cell cycle arrest is transcription and accumulation of $P21^{WAF1}$ in the nucleus (Rowland and Peeper 2006). The readout for P53-induced apoptosis is cleavage of Caspase-3, an effector caspase that becomes activated via cleavage during the apoptosis caspase cascade (Lakhani et al. 2006). NP^{P0}CKO derived MPNSTs never displayed any P21 or cleaved Caspase-3 regardless of irradiation. NI^{P0}CKO derived MPNSTs rarely had elevated P21 in conjuction with stabilized P53 (1/11) and occasionally displayed cleaved Caspase-3 (3/11). In response to irradiation, increased P21 and cleaved Caspase-3 can be appreciated in the majority of NI^{P0}CKO MPNSTs (Figure 6F). Immunohistochemical analysis of p53, p21 and cleaved Caspase-3 confirms these pathways are active in INKCKO MPNSTs in response to irradiation (Figure 6G). These results suggest that in a subset of MPNSTs, the P53 pathway may still be intact, providing a potential avenue for therapeutic intervention.

By using five novel GEM models of MPNST, we have demonstrated that malignant transformation of peripheral nerve sheath tumors does not depend on $Nf1^{+/-}$ or an inflammatory nerve environment. Instead, the largest contributory factor to malignant transformation is the presence of additional oncogenic somatic mutations, such as *p53* and *Ink4/Arf*. Thus, therapies being developed for MPNSTs must target the cells carrying these mutations directly, as attempts to target the microenvironment will most likely be met with failure. Instead, therapeutic intervention must be directed at the cells carrying the somatic mutations that cause malignant transformation.

A neural crest-specific step-wise model of peripheral nerve sheath tumors

The mouse models that we have developed not only address the role of environmental *Nf1* haploinsufficiency in malignant transformation, but are also improvements over currently existing GEM models of MPNSTs. Frequently, in NP^{P0}CKO mice, MPNSTs develop juxtaposed to plexiform neurofibroma, a characteristic commonly found in NF1 patients (Figure 7A). Furthermore, benign tumors are distinguishable from malignant tumors through various histological markers such as Ki67 and phosphorylated-S6 (Figure 7A). Tumors collected from all five MPNST mouse models have a nearly identical spectrum of histopathology to their human counterparts, with the majority of tumors displaying a fasciculated pattern (Figure 7B, Supplmental Figure 9A). This similarity is also reflected at the ultrastructural level in terms of benign neurofibromas and MPNSTs (Figure 7C). Notably, neurofibroma cells retain differentiated characteristics with elongated spindle like cell bodies and basal lamina while MPNST cells resemble immature cells with high nuclei to cell body ratios and loss of basal lamina (Figure 7C, insets).

As all of these mouse models utilize Cre-mediated recombination to generate compound *Nf1*/*p53* or *Nf1*/*Ink4a*/*Arf* deficient cells, tumors are derived from the neural crest lineage. As a result, these mice produce relatively pure populations of MPNSTs (Figure 5E, 6D). Immunohistochemistry reveals that MPNSTs consistently display neural crest cell markers such as p75NGFR, BLBP and Sox10, while a subset of cells stain for immature Schwann cell markers such as S100 and GFAP (Figure 7D). In contrast, tumors never express muscle-differentiated markers (Figure 7E), nor have histology resembling muscle differentiated tumors. Immunocytochemistry demonstrates tumor spheres derived from MPSNTs have a propensity to undergo multilineage differentiation into glial (GFAP) lineage and rarely into neuronal

(peripherin) or myofibroblasts (αSMA) lineages, further supporting the notion MPNSTs are neural crest derived (Figure 7F). These characteristics underscore the neural crest nature of MPNSTs and advantages of using neural crest conditional mutations to model MPNSTs.

We have generated a mouse model that recapitulates the typical course of peripheral nerve sheath tumor development (Figure 8A). These mice develop both plexiform neurofibromas and MPNSTs that arise from a common neural crest lineage. To better understand the relationship between these tumors, we performed signal transduction analysis. From the sciatic nerves of *Nf1*^{P0}CKO1 and *Nf1*^{P0}CKO2 mice, we found phosphorylation of Akt and Erk were elevated compared to control nerves (Figure 8B). In contrast to three month old sciatic nerve, phosphorylation of S6 was not significantly increased compared to control (Figure 8B). Plexiform neurofibroma from the brachial plexus of NP^{P0}CKO mice revealed a similar pattern of activation (Figure 8C). In contrast, MPNSTs reveals a heterogenous pattern of activation in PI3K/Akt and Erk, but consistent activation of mTORC1 (Figure 8C). Similar results were observed in NI^{P0}CKO mice (Supplemental Figure 9C, D). These results highlight the dynamic changes in signaling between benign plexiform neurofibromas and MPNSTs. In summary, these mice provide insight to the underlying mechanisms behind MPNSTs and both direct and serve as platforms for future preclinical trials.

DISCUSSION

Tumor suppressors responsible for familial cancer syndromes are considered to be dominant on an organism level, but recessive at the cellular level. In accordance with Knudson's two-hit hypothesis, tumors involving these genes often display first or second order kinetics for familial and sporadic cancers, respectively (Knudson 1971). In the context of oncogenesis, tumor suppressors are considered haplosufficient with complete inactivation of the genes expected during the course of tumorigenesis. The concept of tumor suppressor haploinsufficiency has only recently been accepted, with a growing number of cases from both human and mouse that report dosage dependent phenotypes in response to loss of tumor suppressors (Berger and Pandolfi 2011). For example, *p53*, *p27* and *PTEN* haploinsufficiency in the neoplastic cell has been documented in GEM models of cancer (Fero et al. 1998; Venkatachalam et al. 1998; Trotman et al. 2003). Here, we further establish how NF1 haploinsufficiency of the tumor microenvironment can contribute to tumorigenesis. Thus, tumor suppressor haploinsufficiency needs to be considered in cases of familial cancer syndromes – as both neoplastic and microenvironmental cells may have additional phenotypes resulting from tumor suppressor haploinsufficiency that contribute to tumor burden.

The contribution of the *Nf1* heterozygous environment

There is some controversy regarding the role of $Nf1^{+/-}$ cells in tumor microenvironment. The initial report of this interaction implicated that $Nf1^{+/-}$ cells contributed to the tumor phenotype, but the experimental conditions left open the possibility that $Nf1^{flox/-}$ mice may generate more $Nf1^{-/-}$ cells than $Nf1^{flox/flox}$ mice as a consequence of Cre efficiency (Zhu et al. 2002). A follow-up study using reciprocal bone-marrow transplantation between $Nf1^{+/-}$ and $Nf1^{+/+}$ mice provide evidence that an $Nf1^{+/-}$ c-Kit expressing hematopoietic cell contributes

strongly to the plexiform neurofibroma phenotype, independent of Cre-mediated recombination (Yang et al. 2008). In contrast, recent studies have reported the generation of plexiform neurofibromas in a wildtype Nf1 environment (Wu et al. 2008) and that wildtype mast cells can contribute to tumor formation (Monk et al. 2007). With the data presented in this paper, we can now reconcile these seemingly disparate results, clarifying the role of the *Nf1*$^{+/-}$ microenvironment in peripheral nerve sheath tumorigenesis.

The observation that sciatic nerves derived from *Nf1*^{P0}CKO1 and *Nf1*^{P0}CKO2 mice have similar phenotypes during neurofibroma initiation (Figures 1 and 2) suggests that Cre-mediated recombination is not a contributory factor to the number of *Nf1*$^{-/-}$ cells generated. Indeed, a comparison between *Nf1*^{P0}CKO1 and *Nf1*^{P0}CKO2 nerves 9 months later reveals a dramatic difference in plexiform neurofibroma burden (Figure 4), despite having a similar number of *Nf1*$^{-/-}$ cells initially. Thus, plexiform neurofibroma initiation and progression can be separated into two distinct stages based off their dependency on the *Nf1*$^{+/-}$ microenvironment. In this light, prior studies implicating that *Nf1*$^{+/+}$ mast cell contribute to plexiform neurofibroma initiation is no longer contradictory with the role of *Nf1*$^{+/-}$ mast cells may play in progression (Monk et al. 2007; Yang et al. 2008).

Notably, we found plexiform neurofibromas develop in a wildtype environmental context, especially in the brachial plexus, DRGs and cutaneous nerves (Figure 4C, D). This is concordant with phenotype from *Dhh*-cre mediated recombination of *Nf1*$^{flox/flox}$ (*Nf1*^{Dhh}CKO2) mice (Wu et al. 2008), but a result that is at odds with *Nf1*^{Kx}CKO2 mice (Zhu et al. 2002). A potential rationale for this difference may be that only a limited number of cells undergo *Krox20*-Cre mediated recombination in the dorsal root ganglia and cranial nerves during the critical stages of Schwann cell development, making this GEM far more reliant on environmental *Nf1*

heterozygosity (Voiculescu et al. 2000; Maro et al. 2004). In contrast, both *P0*-Cre and *Dhh*-Cre target a substantially larger pool of neural crest cells, causing recombination of approximately 40% and 65% of Schwann cells, respectively (Joseph et al. 2004; Joseph et al. 2008). This high number of $Nf1^{-/-}$ cells may alleviate the necessity for an $Nf1^{+/-}$ environment, as mast cells are recruited in response to unassociated Schwann cells (Figure 2G) and nerve damage (Supplemental Figure 8). $Nf1^{Kx}$CKO mice may thus better represent what is occurring in NF1 patient populations by introducing only a limited pool of *Nf1*-deficient Schwann cell precursors. Nevertheless, this study firm establishes Nf1 haploinsufficiency as a contributory factor to plexiform neurofibroma tumorigenesis, reconciling seemingly disparate reports from previous studies.

Preclinical mouse models of MPNSTs

MPNSTs are rare tumors with a poor survival rate and ill-defined management techniques beside tumor resection (Grobmyer et al. 2008). A GEM model of NF1-associated MPNSTs that can recapitulate aspects of the human disease would provide a platform to investigate the mechanism underlying malignancy and provide a preclinical model to rapidly assess various therapeutic modalities. There are some concerns over the relevancy of the current GEM model of MPNSTs, the NPCis mouse. NPCis mice present a spectrum of tumors, primarily with soft tissue sarcomas, predominantly with Schwann cell differentiation such as MPNSTs and MTTs, but also with muscle differentiation such as rhabdomyosarcoma and leiomyosarcoma (Vogel et al. 1999). As LOH is a stochastic event during tumorigenesis in NPCis mice, it is possible that these tumors with muscle differentiation arise from a mesodermal cell-of-origin as opposed to a neural crest cell-of-origin. Indeed, the observation that no MTT, rhabdomyosarcoma or leiomyosarcoma arose in the neural crest specific NP^{P0}CKO and

NI^{P0}CKO mice suggests that only MPNSTs arise from a neural crest cell-of-origin (Figure 7D-F). Thus these neural crest specific GEMs provide confidence that tumors being studied are in fact MPNSTs.

MPNSTs from NF1 patients typically arise from pre-existing peripheral nerves after accumulation of somatic mutations in tumor suppressors such as *p53* and *Ink4a*/*Arf* (Brems et al. 2009). Similar to NF1 patients, cells that will give rise to MPNSTs from NP^{P0}CKO first become *Nf1* deficient and upon LOH of the *p53* allele, will become double deficient for *Nf1* and *p53* (Figure 5A). As a direct result of this stepwise inactivation of tumors suppressors, mice carry both benign plexiform neurofibroma and MPNST burden, allowing simultaneous assessment of both tumors' response to potential therapeutics (Figure 5B, E and Figure 7A, B). NI^{P0}CKO mice develop tumors extremely rapidly, permitting expeditious assessment of therapeutic outcomes. With NP^{P0}CKO and NI^{P0}CKO mice, we cover *p53* and *Ink4a*/*Arf*, the major somatic mutations responsible for malignant transformation of benign plexiform neurofibromas into MPNSTs. Together, the mouse models presented here provide relevant preclinical models that can serve as a platform for understanding the etiology and development of therapies for MPNSTs.

Therapeutic implications of mouse models of NF1-associated tumorigenesis

The reductionist view of a tumor being a cell-autonomous homogeneous population has all but become discarded in favor of a model in which neoplastic cells interact in a heterotypic fashion with their surrounding tumor microenvironment. Moreover, the relationship between neoplastic cells and their stroma change over the course of tumorigenesis; incipient neoplastic cells interact with their microenvironment differently from end-stage malignant cells (Hanahan and Weinberg 2011). Through GEM models of NF1 we provide a clear example of how the interactions of neoplastic cells with their microenvironment evolve over the course of

tumorigenesis, highlighting the need to develop appropriate therapeutic modalities tailored for each stage (Figure 8A, C).

Through our GEM models of NF1, we discovered two contributory factors that were differentially utilized during each stage of peripheral nerve tumorigenesis. First, the *Nf1*$^{+/-}$ tumor microenvironment does not contribute to initiation or malignant transformation but contributes significantly to the expansion of *Nf1*$^{-/-}$ Schwann cells. It is not surprising that therapeutic intervention targeting the *Nf1*$^{+/-}$ neurofibroma progression phase was met with success (Yang et al. 2008). Second, we found mTORC1 activity to be differentially regulated during tumorigenesis. Elevated phosphorylated-S6 was detected during late initiation (Figure 3A, B) and early inhibition of mTORC1 through rapamycin treatment rescued the axon/glial interaction defect characteristic of pre-neoplastic cells (Figure 3E-H). Similarly, elevated phosphorylated-S6 was detected in MPNSTs (Figure 8B), and rapamycin has been demonstrated to successfully act as a cytostatic agent for these tumors (Johannessen et al. 2008; Johansson et al. 2008). In contrast, the levels of phosphorylated-S6 was relatively low in plexiform neurofibroma (Figure 8B), and preclinical trials for rapamycin has resulted in a lack of response from established tumors (Wu et al. 2011). These findings provide encouragement that our GEM models of NF1 can be used to direct development of therapeutic avenues based on a basic scientific understanding of the different stages of tumorigenesis.

Finally, NP^{P0}CKO and NI^{P0}CKO mice provide evidence that the behavior of the MPNSTs in response to chemo- and radiotherapy may be dependent on the nature of the somatic mutations involved in malignant transformation. When MPNSTs have mutations in *p53*, the cell-cycle and apoptotic responses no longer become triggered by irradiation (Figure 6E-G). However, when *Ink4a*/*Arf* causes malignant transformation, irradiation can still activate cell

cycle arrest and apoptotic response in a subset of MPNSTs (Figure 6E-G). This observation suggests that consideration should be given to the mutations causing malignant transformation when developing a management strategy for MPNST patients.

In summary, by using GEM models of NF1, we have found peripheral nerve sheath tumorigenesis to be a highly dynamic process, with multiple dynamic cell-intrinsic and cell-extrinsic interactions that can influence tumor outcome. These GEM provide not only insight into the basic science of peripheral nerve sheath tumors, but also provide therapeutic implications relevant for NF1 patients.

Materials and methods

Control and Conditional Mutant Mice

For the benign tumor portion of this study mice carrying the genotype *P0*-Cre+; *Nf1*$^{flox/ko}$ was crossed to mice of the genotype *Nf1*$^{flox/flox}$; *Rosa26-stop-LacZ*/*Rosa26-stop-LacZ*. The progeny of this cross will carry the genotype *Nf1*$^{flox/ko}$; *Rosa26-stop-LacZ*/+ (control), *Nf1*$^{flox/flox}$; *Rosa26-stop-LacZ* /+ (control), *P0*-Cre+; *Nf1*$^{flox/ko}$; *Rosa26-stop-LacZ* /+ (*Nf1*^{P0}CKO1) and *P0*-Cre+; *Nf1*$^{flox/flox}$; *Rosa26-stop-LacZ* /+ (*Nf1*^{P0}CKO2). *Nf1*$^{flox/ko}$; *Rosa26-stop-LacZ*/+, *Nf1*$^{flox/flox}$; *Rosa26-stop-LacZ* /+. *Nf1*$^{flox/ko}$; *Rosa26-stop-LacZ*/+ and *Nf1*$^{flox/flox}$; *Rosa26-stop-LacZ* /+ are indistinguishable from wildtype mice and used as controls.

For *p53*-mediated malignant transformation analysis, we crossed mice carrying the genotypes *P0*-Cre+; *p53*$^{ko/+}$; *Nf1*$^{flox/+}$ (NP^{P0}Cis) to *Nf1*$^{flox/ko}$ mice. The progeny of this cross will carry the genotype *Nf1*$^{flox/+}$ (control), *Nf1*$^{ko/+}$ (control), *P0*-Cre+; *Nf1*$^{flox/+}$ (control), *P0*-Cre+; *Nf1*$^{ko/+}$ (control), *p53*$^{ko/+}$; *Nf1*$^{flox/ko}$, *p53*$^{ko/+}$; *Nf1*$^{flox/flox}$, *P0*-Cre+; *p53*$^{ko/+}$; *Nf1*$^{flox/ko}$ (NP^{P0}CKO1) and *P0*-

Cre+; *p53*$^{ko/+}$; *Nf1*$^{flox/flox}$ (NP^{P0}CKO2). *Nf1*$^{flox/+}$, *Nf1*$^{ko/+}$, *P0*-Cre+; *Nf1*$^{flox/+}$ and *P0*-Cre+; *Nf1*$^{ko/+}$ are indistinguishable from wildtype mice and used as controls.

For *Ink4a*/*Arf*-mediated malignant transformation analysis, we crossed mice carrying the genotypes *P0*-Cre+; *Ink4a/Arf* $^{flox/flox}$; *Nf1*$^{flox/ko}$ to *Ink4a/Arf* $^{flox/flox}$; *Nf1*$^{flox/flox}$ *Nf1*$^{flox/ko}$ mice. The progeny of this cross will carry the genotype *Ink4a/Arf* $^{flox/flox}$; *Nf1*$^{flox/ko}$ (control), *Ink4a/Arf*$^{flox/flox}$; *Nf1*$^{flox/flox}$ (control), *P0*-Cre+; *Ink4a/Arf* $^{flox/flox}$; *Nf1*$^{flox/ko}$ (NI^{P0}CKO1) and *P0*-Cre+; *Ink4a/Arf* $^{flox/flox}$; *Nf1*$^{flox/ko}$ (NI^{P0}CKO2). *Ink4a/Arf* $^{flox/flox}$; *Nf1*$^{flox/ko}$ and *Ink4a/Arf*$^{flox/flox}$; *Nf1*$^{flox/flox}$ mice are indistinguishable from wildtype mice and used as controls.

All mice in this study were cared for according to the guidelines that were approved by the Animal Care and Use Committees of the University of Michigan at Ann Arbor.

Tissue Processing

For histological analysis, we utilized paraffin sections. For neurofibroma initiation analysis, control and mutant littermates at P22 and P90 were collected. For end-stage analysis, mice were collected when they displayed signs of sickness including lethargy, ruffled hair, skin lesions, hindlimb paralysis, or tumors of >10 cm. Mice were perfused with 4% paraformaldehyde (PFA). Sciatic nerves, trigeminal nerves, brachial plexus, cutaneous nerves and MPNSTs, if present, were dissected for all mice, post-fixed in PFA overnight at 4°C and processed for paraffin embedding. Cervical, thoracic and lumbar dorsal root ganglia were collected from end-stage control, *Nf1*^{P0}CKO1 and *Nf1*^{P0}CKO2 mice and processed as other nerves. Nerves were sectioned longitudinally at 5 μm thickness.

Histology and Tumor Grading

Two to three paraffin sectioned slides were stained with hematoxylin/eosin (H&E). Diagnosis for each nerve or tumor was generated based upon histology from H&E stained sections under the light microscopy. The penetrance and frequency of neurofibromas or pre-neoplastic lesions in control and mutant mice was quantified based upon nerve diagnoses. Quantification of the number of cells per surface area (mm^2) in P22 and P90 control and mutant sciatic nerves was performed using ImageJ on digital images of H&E stained sections. For PCR analysis, tissues were dissected in ice-cold PBS and digested with proteinase K.

Western Blot analysis

Snap-frozen tissues from normal nerves and tumors were homogenized in 1X RIPA buffer [50 mM Tris-HCL (pH7.4), 150 mM NaCl, 1% Triton X-100, 1% sodium deoxycholate, 0.1% SDS, 1mM EDTA, complete protease inhibitor (Roche) and phosphatase inhibitor (Roche) and β-mercaptoethanol.] Samples were analyzed by SDS-PAGE and transferred onto PVDF membranes (Millipore). The blots were then blocked in 5% non-fat milk in TBST, followed by incubation of primary antibodies at 4°C overnight. After washing, the blots were incubated in horseradish peroxidase (HRP)-conjugated secondary antibodies at room temperature for 1 hour. Signals were detected using ECL or ECL plus (GE healthcare) followed by film development. The primary antibodies used are as follows: p-Akt (1:1000, rabbit, Cell Signaling), Akt (1:2000, rabbit, Cell Signaling), p-Erk (1:1000, rabbit, Cell Signaling), Erk (1:2000, rabbit, Cell Signaling), p-S6 (1:2000, rabbit, Cell Signaling), S6 (1:2000, rabbit, Cell Signaling), p53 (1:1000, rabbit, Novo Castra), Nf1 (1:1000, rabbit, Santa Cruz), cleaved caspase 3 (1:5000, rabbit, Cell Signaling), p21 (1:500, mouse, BD Pharmigen) and β-actin (1:10000, mouse, Sigma).

Immunohistochemistry

Immunohistochemistry was performed on paraffin sections. The visualization of primary antibodies was performed with the avidin-biotin horseradish peroxidase system (Vectastain ABC kit, Vector). The dilutions of primary antibodies used on sections in this study were: anti-p53 (1:500, rabbit, Novo Castra), anti-cleaved Caspase 3 (rabbit, 1:300, Cell signaling), anti-Ki67 (1:1000, rabbit, Abcam), anti-phosphorylated S6 (rabbit, 1:1000, Cell signaling), anti-$p75^{NGFR}$ (rabbit, 1:4,000, Chemicon), anti-BLBP (rabbit, 1:2,000, a gift from N. Heintz), anti-Sox10 (rabbit, 1:500, Chemicon), anti-S100 (rabbit, 1:200, Signet), anti-GFAP (rabbit, 1:2,000, DAKO) and anti-myoglobin (rabbit, 1:50, Signet). Sections were examined under a light microscope (Olympus).

Semithin and Ultrathin Preparation

Control and mutant littermates were perfused with 4% PFA and 2.5% gluteraldehyde. Sciatic nerves and MPNSTs were dissected and post-fixed in 4% PFA and 2.5% gluteraldehyde overnight at 4°C. Tissues were then post-fixed in OsO4 for 1 hour and embedded in epoxy resin. Semithin sections were cut with a glass knife at 0.5 μm and stained with toluidine blue for visualization. Ultrathin sections were cut with a diamond knife at 75 nm and visualized using transmission electron microscope (TEM). Each field was taken at the same low magnification, and total endoneurial area in each image calculated by the ImageJ software package. Higher magnification images for most areas in each field were taken. The number of mSCs, nmSCs, anmSCs, and dSCs were quantified for each field based on morphology in high magnification

images. Axons in each Schwann cell pocket was counted and categorized into single, 2-10 or 11-50. The cell density for each population was normalized by the surface area sampled.

Statistical Analysis for EM Data

Cell densities from the same low magnifications image cannot be considered independent since cells from the same nerve tend to be correlated as evident by an interclass correlation coefficient (ICC) of 0.2. Thus, we utilized linear mixed models from the SAS 9.2 statistical package in order to determine if there was a difference in population for nmSC, anmSC, dSC, mSC and axons per Remak bundle in control and mutant nerves. Genotype was set as the fixed factor while nerve was set as a random factor in order to generate accurate P-values and error bars. Chi-squared goodness-of-fit tests were used to compare control and mutant distributions for axon pocketing at P22. $P < 0.05$ was considered to be statistically significant.

LacZ Staining

Mice carrying the *Rosa26-stop-LacZ* and *P0*-Cre alleles allow for reporting of cells that have undergone Cre-mediated recombination. Sciatic nerves from control and mutant mice carrying the *Rosa-stop-LacZ* allele were dissected and 14 μm frozen sections were analyzed with X-gal and X-gal/anti-p75NGFR antibody staining.

Mast Cell Quantification

One to three H&E stained slides of sciatic nerves were taken from 22 day, 90 days old and end-stage mice for mast cells quantification. All of these H&E stained slides were scanned and the sections that had best histology were selected for analysis. Mast cells were counted for each

section individually using 40X magnification under a light microscope. The area of the nerve was calculated using the ImageJ software package and mast cell density was calculated as the number of cells per surface area (mm^2). Statistical analysis was carried out using two tail Student's *t*-test. $P < 0.05$ was considered to be statistically significant.

Neural crest sphere and differentiation assay

Enteric nerves and MPNSTs were dissected from control and mutant mice and collected in ice-cold PBS. Nerves were dissociated for 30 min at 37°C in 1 mg/ml type IV collagenase (Worthington) followed by 20 min at 37°C in Accumax (Innovated Cell Technologies). Cells were centrifuged, resuspended in DMEM, triturated, and filtered through nylon screen (45 mm, Sefar America) to remove aggregates. Cells were placed into ultralow attachment plates (Corning) in a media composed of 5:3 mixture of DMEMlow:Neurobasal medium (Invitrogen), 15% chick embryo extract (CEE; prepared as described, Stemple and Anderson, 1992), 20 ng/ml recombinant human bFGF (R&D Systems, Minneapolis, MN), 20 ng/ml IGF1 (R&D Systems), 1% N2 supplement (Gibco), 2% B27 supplement (Gibco), 50 mM 2-mercaptoethanol, 35 ng/ml retinoic acid (Sigma), 1% penicillin/streptomycin (Biowhittaker) and 1 nM NRG1 (NRG1-β1/HRG1-β1 EGF domain; R&D Systems, 396-HB). Spheres were induced to differentiate in fibronectin or laminin coated plates in media composed of 5:3 mixture of DMEMlow:Neurobasal medium (Invitrogen), 5% FBS (Invitrogen), 1% N2 supplement (Gibco), 2% B27 supplement (Gibco), 50 mM 2-mercaptoethanol and 1% penicillin/streptomycin (Biowhittaker). Cells were given 10-14 days to adhere before acid ethanol fixation.

Immunocytochemistry

Immunocytochemistry was performed on fixed differentiated cells. The visualization of primary antibodies was performed with the Alexa 488 and Alexa 555 secondary antibodies (Invitrogen). The dilutions of primary antibodies used on sections in this study were: anti-peripherin (rabbit, 1:1000, Millipore), anti-Tuj1 (mouse, 1:500, Covance), anti-αSMA (1:200, mouse, Signet), anti-GFAP (rabbit, 1:500, DAKO). Sections were examined under a fluorescent microscope (Olympus).

REFERENCES

Berger AH, Pandolfi PP. 2011. Haplo-insufficiency: a driving force in cancer. *J Pathol* **223**: 137-146.

Brems H, Beert E, de Ravel T, Legius E. 2009. Mechanisms in the pathogenesis of malignant tumours in neurofibromatosis type 1. *Lancet Oncol* **10**: 508-515.

Cichowski K, Shih TS, Schmitt E, Santiago S, Reilly K, McLaughlin ME, Bronson RT, Jacks T. 1999. Mouse models of tumor development in neurofibromatosis type 1. *Science* **286**: 2172-2176.

Ducatman BS, Scheithauer BW, Piepgras DG, Reiman HM, Ilstrup DM. 1986. Malignant peripheral nerve sheath tumors. A clinicopathologic study of 120 cases. *Cancer* **57**: 2006-2021.

Evans DG, Baser ME, McGaughran J, Sharif S, Howard E, Moran A. 2002. Malignant peripheral nerve sheath tumours in neurofibromatosis 1. *J Med Genet* **39**: 311-314.

Fero ML, Randel E, Gurley KE, Roberts JM, Kemp CJ. 1998. The murine gene p27Kip1 is haplo-insufficient for tumour suppression. *Nature* **396**: 177-180.

Friedman JM, Riccardi VM. 1999. *Neurofibromatosis : phenotype, natural history, and pathogenesis*. Johns Hopkins University Press, Baltimore.

Giovannini M, Robanus-Maandag E, van der Valk M, Niwa-Kawakita M, Abramowski V, Goutebroze L, Woodruff JM, Berns A, Thomas G. 2000. Conditional biallelic Nf2 mutation in the mouse promotes manifestations of human neurofibromatosis type 2. *Genes Dev* **14**: 1617-1630.

Grobmyer SR, Reith JD, Shahlaee A, Bush CH, Hochwald SN. 2008. Malignant Peripheral Nerve Sheath Tumor: molecular pathogenesis and current management considerations. *J Surg Oncol* **97**: 340-349.

Hanahan D, Weinberg RA. 2011. Hallmarks of cancer: the next generation. *Cell* **144**: 646-674.

Johannessen CM, Johnson BW, Williams SM, Chan AW, Reczek EE, Lynch RC, Rioth MJ, McClatchey A, Ryeom S, Cichowski K. 2008. TORC1 is essential for NF1-associated malignancies. *Curr Biol* **18**: 56-62.

Johansson G, Mahller YY, Collins MH, Kim MO, Nobukuni T, Perentesis J, Cripe TP, Lane HA, Kozma SC, Thomas G et al. 2008. Effective in vivo targeting of the mammalian target of rapamycin pathway in malignant peripheral nerve sheath tumors. *Mol Cancer Ther* **7**: 1237-1245.

Joseph NM, Mosher JT, Buchstaller J, Snider P, McKeever PE, Lim M, Conway SJ, Parada LF, Zhu Y, Morrison SJ. 2008. The loss of Nf1 transiently promotes self-renewal but not tumorigenesis by neural crest stem cells. *Cancer Cell* **13**: 129-140.

Joseph NM, Mukouyama YS, Mosher JT, Jaegle M, Crone SA, Dormand EL, Lee KF, Meijer D, Anderson DJ, Morrison SJ. 2004. Neural crest stem cells undergo multilineage differentiation in developing peripheral nerves to generate endoneurial fibroblasts in addition to Schwann cells. *Development* **131**: 5599-5612.

Knudson AG, Jr. 1971. Mutation and cancer: statistical study of retinoblastoma. *Proc Natl Acad Sci U S A* **68**: 820-823.

Krimpenfort P, Quon KC, Mooi WJ, Loonstra A, Berns A. 2001. Loss of p16Ink4a confers susceptibility to metastatic melanoma in mice. *Nature* **413**: 83-86.

Lakhani SA, Masud A, Kuida K, Porter GA, Jr., Booth CJ, Mehal WZ, Inayat I, Flavell RA. 2006. Caspases 3 and 7: key mediators of mitochondrial events of apoptosis. *Science* **311**: 847-851.

Lassmann H, Jurecka W, Lassmann G, Gebhart W, Matras H, Watzek G. 1977. Different types of benign nerve sheath tumors. Light microscopy, electron microscopy and autoradiography. *Virchows Arch A Pathol Anat Histol* **375**: 197-210.

Lin V, Daniel S, Forte V. 2004. Is a plexiform neurofibroma pathognomonic of neurofibromatosis type I? *Laryngoscope* **114**: 1410-1414.

Luongo C, Moser AR, Gledhill S, Dove WF. 1994. Loss of Apc+ in intestinal adenomas from Min mice. *Cancer Res* **54**: 5947-5952.

Maro GS, Vermeren M, Voiculescu O, Melton L, Cohen J, Charnay P, Topilko P. 2004. Neural crest boundary cap cells constitute a source of neuronal and glial cells of the PNS. *Nat Neurosci* **7**: 930-938.

Mautner VF, Asuagbor FA, Dombi E, Funsterer C, Kluwe L, Wenzel R, Widemann BC, Friedman JM. 2008. Assessment of benign tumor burden by whole-body MRI in patients with neurofibromatosis 1. *Neuro Oncol* **10**: 593-598.

Monk KR, Wu J, Williams JP, Finney BA, Fitzgerald ME, Filippi MD, Ratner N. 2007. Mast cells can contribute to axon-glial dissociation and fibrosis in peripheral nerve. *Neuron Glia Biol* **3**: 233-244.

Rasmussen SA, Overman J, Thomson SA, Colman SD, Abernathy CR, Trimpert RE, Moose R, Virdi G, Roux K, Bauer M et al. 2000. Chromosome 17 loss-of-heterozygosity studies in benign and malignant tumors in neurofibromatosis type 1. *Genes Chromosomes Cancer* **28**: 425-431.

Rasmussen SA, Yang Q, Friedman JM. 2001. Mortality in neurofibromatosis 1: an analysis using U.S. death certificates. *Am J Hum Genet* **68**: 1110-1118.

Rowland BD, Peeper DS. 2006. KLF4, p21 and context-dependent opposing forces in cancer. *Nat Rev Cancer* **6**: 11-23.

Sherr CJ. 2004. Principles of tumor suppression. *Cell* **116**: 235-246.

Trotman LC, Niki M, Dotan ZA, Koutcher JA, Di Cristofano A, Xiao A, Khoo AS, Roy-Burman P, Greenberg NM, Van Dyke T et al. 2003. Pten dose dictates cancer progression in the prostate. *PLoS Biol* **1**: E59.

Tucker T, Wolkenstein P, Revuz J, Zeller J, Friedman JM. 2005. Association between benign and malignant peripheral nerve sheath tumors in NF1. *Neurology* **65**: 205-211.

Upadhyaya M, Kluwe L, Spurlock G, Monem B, Majounie E, Mantripragada K, Ruggieri M, Chuzhanova N, Evans DG, Ferner R et al. 2008. Germline and somatic NF1 gene mutation spectrum in NF1-associated malignant peripheral nerve sheath tumors (MPNSTs). *Hum Mutat* **29**: 74-82.

Venkatachalam S, Shi YP, Jones SN, Vogel H, Bradley A, Pinkel D, Donehower LA. 1998. Retention of wild-type p53 in tumors from p53 heterozygous mice: reduction of p53 dosage can promote cancer formation. *EMBO J* **17**: 4657-4667.

Vogel KS, Klesse LJ, Velasco-Miguel S, Meyers K, Rushing EJ, Parada LF. 1999. Mouse tumor model for neurofibromatosis type 1. *Science* **286**: 2176-2179.

Voiculescu O, Charnay P, Schneider-Maunoury S. 2000. Expression pattern of a Krox-20/Cre knock-in allele in the developing hindbrain, bones, and peripheral nervous system. *Genesis* **26**: 123-126.

Weinberg RA. 2007. *The biology of cancer*. Garland Science, New York.

Widemann BC. 2009. Current status of sporadic and neurofibromatosis type 1-associated malignant peripheral nerve sheath tumors. *Curr Oncol Rep* **11**: 322-328.

Wu J, Dombi E, Jousma E, Scott Dunn R, Lindquist D, Schnell BM, Kim MO, Kim A, Widemann BC, Cripe TP et al. 2011. Preclincial testing of Sorafenib and RAD001 in the Nf(flox/flox) ;DhhCre mouse model of plexiform neurofibroma using magnetic resonance imaging. *Pediatr Blood Cancer*.

Wu J, Williams JP, Rizvi TA, Kordich JJ, Witte D, Meijer D, Stemmer-Rachamimov AO, Cancelas JA, Ratner N. 2008. Plexiform and dermal neurofibromas and pigmentation are caused by Nf1 loss in desert hedgehog-expressing cells. *Cancer Cell* **13**: 105-116.

Yang FC, Ingram DA, Chen S, Zhu Y, Yuan J, Li X, Yang X, Knowles S, Horn W, Li Y et al. 2008. Nf1-dependent tumors require a microenvironment containing Nf1+/-- and c-kit-dependent bone marrow. *Cell* **135**: 437-448.

Zheng H, Chang L, Patel N, Yang J, Lowe L, Burns DK, Zhu Y. 2008. Induction of abnormal proliferation by nonmyelinating schwann cells triggers neurofibroma formation. *Cancer Cell* **13**: 117-128.

Zhu Y, Ghosh P, Charnay P, Burns DK, Parada LF. 2002. Neurofibromas in NF1: Schwann cell origin and role of tumor environment. *Science* **296**: 920-922.

Figure Legends

Figure 1 – *Nf1* deficiency in non-myelinating Schwann sufficient to generate Schwann cell pocket defects.

The cellular density of postnatal day 22 (P22) (A) control, (B) *Nf1*^{P0}CKO1 and (C) *Nf1*^{P0}CKO2 sciatic nerves. Ultrastructural analysis of axon defasciculation in non-myelinating Schwann cells in P22 sciatic nerve of control (A'), *Nf1*^{P0}CKO1 (B') and *Nf1*^{P0}CKO2 (C') mice. (A'', B'' and C'') Schematized representations of A', B' and C'. color-coded by axons ensheathed per pocket: a single axon (green), between two and ten axons (yellow), or more than 10 axons (red). (D) Semi-thin analysis of P22 sciatic nerve reveals normal distribution and density of myelination Schwann cells in control and mutant mice. (E) Cellular density for the nerve is plotted as mean ± SEM. (F) Quantification and chi-squared analysis of Schwann cell axons ensheathed by Schwann cell pockets. Mutant nerves have elevated rates of non-myelinating Schwann cell pocket compared to control nerves, but have comparable rates to each other. Scale bars: (A-C, D) 50 μm. (A'-C'') 1 μm.

Figure 2 – Neurofibroma initiation and the spectrum of aberrant non-myelinating Schwann cells is not affected by *Nf1* environmental heterozygosity.

(A) Typical non-myelinating Schwann cells ensheath multiple axons without producing myelin; they are globular, with all processes ensheathing axon in an individual Schwann cell pocket. (B) A similar spectrum of abnormal Schwann cells (aSCs) could be identified in both *Nf1*^{P0}CKO1 and *Nf1*^{P0}CKO2 sciatic nerves. These aSCs are characterized by degenerating axons (a, a'), identified by the presence of bloated axons with sparse neurofilaments, focal dissociation (b, b', arrowhead), identified by Schwann cell processes that are not engaged in ensheathing axons,

crevassing (c, c', red dotted line) and axons with focal loss of ensheathment (c, c', inset). (C) A similar spectrum of dissociating Schwann cells (dSCs) could also be identified in both *Nf1*^{P0}CKO1 and *Nf1*^{P0}CKO2 sciatic nerves. Initial stages of dSCs are characterized by subcompartments of Schwann cells that are only attached to the main structure with only a thin Schwann cell process (a, a', red dotted line) in conjunction with a free Schwann cell process (a, a', arrowhead) while maintaining a globular form. Progressive stages of dSCs are characterized by progressive loss of globularity, with increased incidences of tenuous attachment (b, b', red dotted line) and free Schwann cell processes (b, b', arrow heads). Advanced stages of dSCs are characterized by complete loss of globular form, a decrease in total number of ensheathed axons, and a large proportion of Schwann cell processes that do not ensheath axons (c, c'). Finally, unassociated Schwann cells (uSCs) that ensheath no axons but still sent out Schwann cells structures can also be identified at similar levels in both *Nf1*^{P0}CKO1 and *Nf1*^{P0}CKO2 sciatic nerves (d, d'). These uSCs can be distinguished from fibroblasts and perineural cells from the presence of a continuous basal lamina. (D) P90 *Nf1*^{P0}CKO1 and *Nf1*^{P0}CKO2 sciatic nerves have significantly higher cellularity than controls but are similar to each other. (E) Ultrastructural analysis of P90 sciatic nerve myelinating Schwann cells reveals no significant difference in mutant nerves. (F) Ultrastructural analysis of non-myelinating Schwann cells in P90 sciatic nerves reveal the difference in cellularity between mutant and control nerves is caused by increased number of non-myelinating Schwann cells, retaining the pattern where both mutants are significantly higher in cellularity than the control, but are not significantly different from each other. (F) There is a similar distribution of normal non-myelinating Schwann cells, abnormal non-myelinating Schwann cells and dissociating Schwann cells between *Nf1*^{P0}CKO1 and *Nf1*^{P0}CKO2 nerves, but not to control nerves. 19 fields from 2 control nerves, 28 fields from

3 *Nf1*^{P0}CKO1 and 25 fields from 3 *Nf1*^{P0}CKO2 nerves were analyzed for the ultra structural study; linear mix modeling was used to calculate statistical significance. (G) Mast cell infiltration was not detected in P22 sciatic nerves and was significantly greater in mutant nerves at P90. Scale bars: 1 μm.

Figure 3 – Early Rapamycin intervention can stabilize axon-Schwann cell interactions in *Nf1* deficient mutants.

(A) Signal transduction analysis at P22 does not reveal any differences between control and mutant sciatic nerves. (B) Phosphorylated Erk and S6 are elevated in P90 mutant sciatic nerves. (C) Schematic diagram of the predicted effects of rapamycin mediated inhibition of mTORC1. (D) Sciatic nerves from rapamycin treated mice display reduced mTORC1 activity but no impact on Erk phosphorylation in both control and mutant mice. (E) A subset of mutant mice treated starting P21 or P30 display a stabilized or "rescued" phenotype reminiscent of control nerves using ultrastructural analysis at P90. (F) Ultrastructural analysis of vehicle and rapamycin treated control and mutant nerves. (a, a') Rapamycin treated control nmSCs have no phenotype. (Fb, b') Vehicle treated mutant nmSCs have a spectrum of aberrant non-myelinating Schwann cell phenotypes. (Fc, c') Rapamycin treated mutant nmSCs considered rescued have little or no phenotype. (Fd, d') Rapamycin treated mutant nmSCs considered unrescued have a phenotype resembling vehicle treated mutant nerves. (G and H) Successful rapamycin rescues have reduction of dSCs to control levels in both P21 and P30-initiated treatments. Successful treatment does necessarily decrease non-myelinating Schwann cell density. Scale bars: 1 μm.

Figure 4. *Nf1* heterozygosity in the environment promotes neurofibroma development. Representative whole-mount comparison of (A) sciatic nerves, (B) trigeminal nerves, (C) cutaneous/subcutaneous nerves, and (D) brachial plexus from control, *Nf1*^{P0}CKO1 and *Nf1*^{P0}CKO2 mice. *Nf1*^{P0}CKO1 nerves are markedly larger in size than those from age-matched *Nf1*^{P0}CKO2 littermates. The largest CKO1 trigeminal nerve (B, right panel) is also presented to demonstrate the range of trigeminal nerve sizes, while CKO2 trigeminal nerves have smaller variation. (E) Based upon previously established histological grading criteria, each nerve was diagnosed as normal (a, e), hyperplastic (b, f), hyperplastic nerves with focal neurofibroma (c, g; H – hyperplastia and fNF – focal neurofibroma) or frank neurofibromas (d, h; NF region). (F) Neurofibroma penetrance for *Nf1*^{P0}CKO1 and *Nf1*^{P0}CKO2 mice was determined for seven sites: sciatic nerves, cutaneous/subcuteneous nerves, trigeminal nerves, brachial plexus, cervical dorsal root ganglia (C-DRG), thoracic DRG (T-DRG) and lumbar DRG (L-DRG). A Z-test was used to determine whether a difference in neurofibroma penetrance exists based on the environmental genotype for sciatic nerves, cutaneous/subcuteneous nerves, trigeminal nerves and brachial plexus. Linear mixed modeling was used to determine whether the penetrance in DRGs was different based on Nf1 heterozygosity in the environment. (G) The summary of our diagnostics for all nerves examined, based on genotype, is presented. Frank neurofibromas (NF) are labeled by red, focal neurofibroma (H/fNF) by blue, hyperplasia (H) by green, and non-neurofibroma, degenerative lesions (DF) by yellow. Bars representing CKO1 nerves are on the left while CKO2 are on the right. A pattern emerges across the board, where the *Nf1* heterozygosity in the environment enhances the neurofibroma phenotypes caused by *Nf1* deficiency. Scale bars: (A-D) 1 mm. (E) 50 μm.

Figure 5. Step-wise mouse models of neurofibroma and MPNSTs demonstrate *Nf1* heterozygousity is dispensable for malignant transformation

(A) Schematic of the genetic configurations of NP^{P0}CKO1 , NP^{P0}CKO2 and NP^{P0}Cis mice. The green color is used to label functional alleles, including the wild-type allele (+) and the floxed allele (x1); the red color is used to label non-functional alleles, including the recombined floxed allele (Δ) and the knockout allele (−). Genotypes for each cell type are indicated in parentheses. While both NP^{P0}CKO configurations generate the same genotype after Cre-mediated recombination, unrecombined cells in NP^{P0}CKO1 are $Nf1^{+/-}$ while the unrecombined cells in NP^{P0}CKO2 are $Nf1^{+/+}$. NP^{P0}CKO mutant mice require an LOH event at the *p53* locus after recombination, while the NP^{P0}Cis mice require a co-LOH event after recombination, to generate a cell deficient for both *Nf1* and *p53*. (B) Nerves from NP^{P0}CKO1 and NP^{P0}CKO2 mice develop benign peripheral nerve sheath tumors; NP^{P0}CKO1 nerves have a more severe phenotype. No abnormalities were detected in NP^{P0}Cis nerves. (C) The survival curve and (D) MPNST-free curve for NP^{P0}CKO1, NP^{P0}CKO2 and NP^{P0}Cis mice were nearly identical ($P>0.5$). (E) The tumor spectrum of NP^{P0}CKO1, NP^{P0}CKO2 and NP^{P0}Cis mice are relatively similar, with MPNSTs the predominant tumors generated (60%, 78% and 68%, respectively). Malignant pheochromocytoma accounted for 20% of tumors in NP^{P0}CKO1 mice, and 6% in both NP^{P0}CKO2 and NP^{P0A}Cis mice. In some instances (10%, 11% or 18% for NP^{P0}CKO1, NP^{P0}CKO2 and NP^{P0A}Cis respectively), tumors arose from tissue that had not undergone Cre-mediated recombination. (F) PCR analysis of MPNST tissue confirms our schematic model of MPNST generation in these mice. All MPNSTs from these mice demonstrate recombination of the *Nf1* allele, and commonly demonstrate LOH of the *p53* allele. However, there is significant contamination with unrecombined tissue, resulting in a fainter band, as opposed to complete

absence of band. (G) Scatter plot of residual wildtype *p53* allele, as measured by qPCR of genomic DNA with primers against exons 6 and 7 of p53, confirms LOH of the wildtype p53 allele. (H) rt-PCR of tumors from NP^{P0}CKO mice demonstrate that regardless of LOH, only KO p53 cDNA is expressed. (I) Western blot analysis demonstrates an absence of Neurofibromin and P53 protein in MPNSTs.

Figure 6 –*Ink4a*/*Arf* mediated malignant transformation occurs independently of an *Nf1*$^{+/-}$ tumor microenvironment.

(A) NI^{P0}CKO1 mice have slightly higher neurofibroma tumor burden than NI^{P0}CKO2 mice. (B and C) Survival and MPNST-free curves demonstrate NI^{P0}CKO mice develop MPNSTs rapidly, accounting for relatively low benign tumor burden. (D) NI^{P0}CKO mice have high MPNST penetrance. (E) rt-PCR of tumors from NI^{P0}CKO mice demonstrate wildtype p53 cDNA is expressed. (F) Western blots demonstrates irradiation induces p53-mediated cell cycle arrest (p21) and apoptosis (cleaved Caspase 3) in spleen and some *Nf1*/*Ink4a*/*Arf* deficient MPSNTs but not in *Nf1*/*p53* deficient MPNSTs. (G) Immunohistochemistry confirms western blot findings. Upon irradiation (a, a') spleens stabilize both p53 and Cleaved Caspase3. Scale: 50 μm.

Figure 7. Mouse model recapitulates human peripheral nerve sheath features and MPNSTs display immature neural crest features.

(A) NP^{P0}CKO mice carry both benign and malignant peripheral nerve sheath tumor burden, recapitulating common feature of NF1 patients. (a) (B) MPSNTs from NP^{P0}CKO mice recapitulate common histopathological features of human MPNSTs. Commonly found features in mice are malignant spindle cells arranged in intertwining fascicles, with ill-defined cytoplasms

and a high mitotic rate (a, a'). Occasionally, geographic necrosis can be found, sometimes accompanied by peripheral palisading malignant spindle cells (b, b'). Another manifestation of MPNSTs seen are unoriented malignant cells dispersed in sheets (c, c'). In some tumors, nuclear pleomorphism can be found, with marked variation in size and shape of cells (d, d'). (B) MPNSTs collected from these mouse models often express $p75^{NGFR}$ (a, a') and BLBP (b, b') throughout the tumor tissues. Less frequently, MPNSTs express S100 (c, c'), GFAP (d, d'), and/or Sox10 (e, e') in approximately 50% of tumors analyzed, without correlations in expression patterns. While immunohistological markers varied highly between MPNSTs, staining patterns were indistinguishable between the NP^{P0A}CKO mice. (C) Ultrastructural analysis of murine benign (a, b) and malignant (c, d) peripheral nerve sheath tumors reveal a high degree of similarity with their human counterparts (a'-d'). Benign tumor cells retain differentiated phenotype: continuous basal lamina (inset, arrows), extended Schwann cell processes, sheet-like organization, low rates of proliferation. MPNST have immature and tumor phenotypes: loss of basal lamina (inset, arrows), prominent nuclei, ovoid shape, crowded and highly proliferative. Scale bars: (A, B) 50 μm, (C) 10 μm.

Figure 8 – Peripheral nerve sheath tumorigenesis and appropriate therapeutic windows.

(A) Based on observations from murine models of NF1, we have developed a model of peripheral nerve sheath tumorigenesis. $Nf1^{ko/+}$ neural crest stem cells will undergo normal development into well defasciculated non-myelinating or myelinating Schwann cells. If cells undergo LOH of *Nf1* during development, these $Nf1^{-/-}$ non-myelinating Schwann cells (red box) will have poorly defasciculated Remak bundles with Schwann cell pocket defects. These Schwann cells will dissociate from axons and proliferate to form unassociated Schwann cells.

Together, these events constitute Step I: Initiation. Interaction between unassociated Schwann cells and the *Nf1*$^{ko/+}$ microenvironment results in the progressive demyelination, proliferation of peripheral nerve cells and disruption of the peripheral nerve architecture. This results in neurofibromas composed of both *Nf1*-heterozygous and *Nf1*-deficient cells. Together, these events constitute Step II: Progression. Finally, as *Nf1*-deficient cells expand, they acquire additional genetic lesions such as *p53* or *Ink4a*/*Arf* mutations, resulting in Step 3: Malignant transformation. (B) Signal transduction analysis of end-stage nerves with neurofibroma reveals dynamic changes in activity with respect to mTORC1 activity. Whereas Initiation was dependent on mTORC1, nerves with neurofibromas have reduced activity (red box). (C) Comparison of benign and malignant tumors reveals further changes in signaling activity after malignant transformation. mTORC1 activity is once more elevated consistently (red box) while Ras/ERK and PI3K/Akt are no longer consistently activated. Notably, these results predict the ability of rapamycin to rescue the phenotypes of mutant mice. (D) Summary of dependencies on NF1 heterozygosity tumor microenvironments and NF1 based on Stage. Initiation has elevated mTORC1 activity and is susceptible to rapamycin mediated inhibition of mTORC1, but does not require a heterozygous NF1 microenvironment. In contrast, neurofibroma Progression is independent of mTORC1 activity, but is heavily dependent on interaction with NF1 heterozygous cells. Finally, upon Malignant Transformation, the dependency on a NF1 heterozygous microenvironment is lost and is once again dependent on mTORC1 activity for proliferation. Together, these results highlight the dynamic nature of peripheral nerve sheath tumors during their development and the need to determine the stage of tumors to develop appropriate therapeutic intervention.

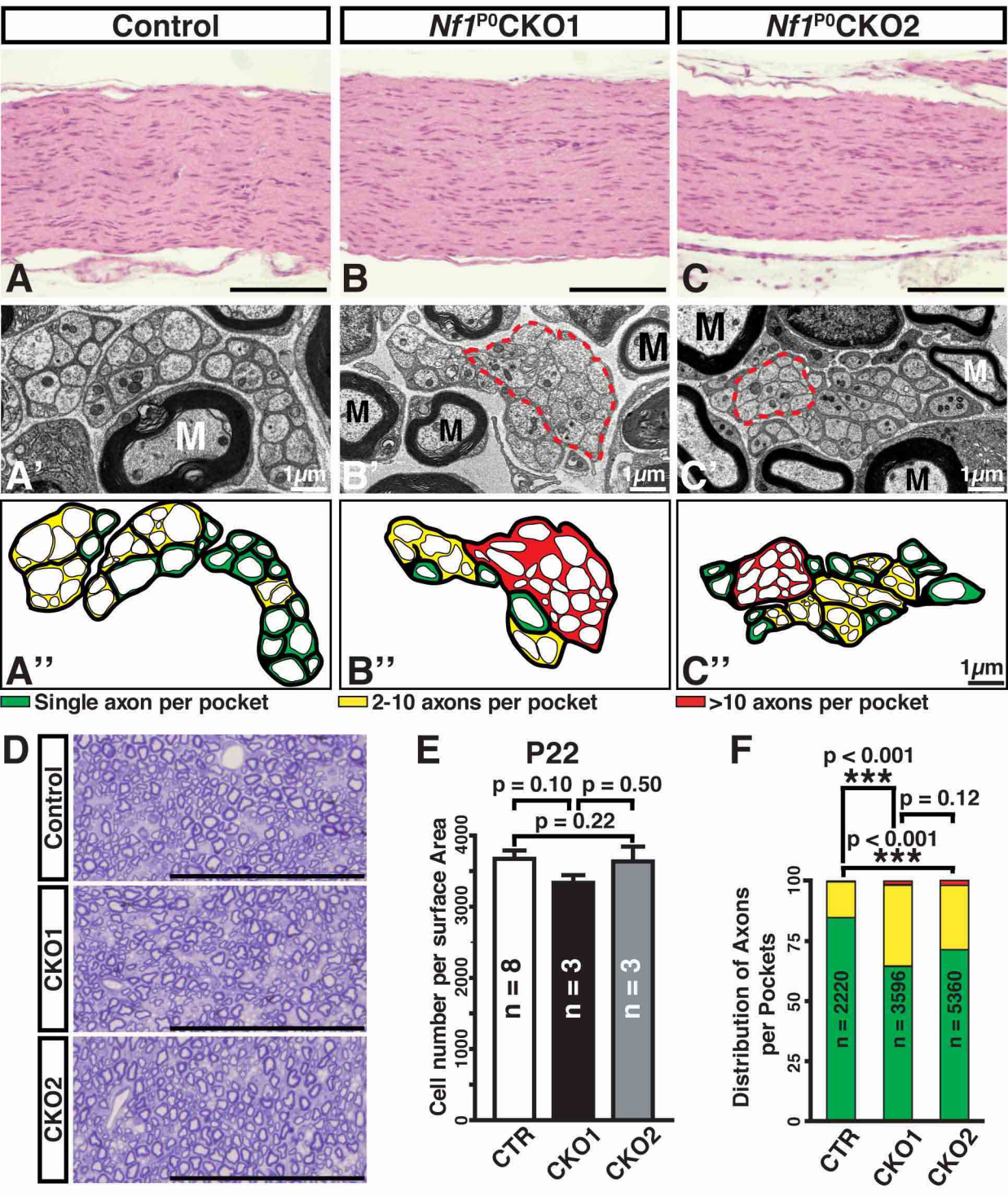
Control
Nf1P0CKO1
Nf1P0CKO2
A
B
C
A'
B'
C'
M
1μm
A''
B''
C''
Single axon per pocket
2-10 axons per pocket
>10 axons per pocket
D
Control
CKO1
CKO2
E
P22
p = 0.10
p = 0.50
p = 0.22
Cell number per surface Area
0
1000
2000
3000
4000
n = 8
n = 3
n = 3
CTR
CKO1
CKO2
F
p < 0.001
***
p = 0.12
p < 0.001
***
Distribution of Axons per Pockets
0
25
50
75
100
n = 2220
n = 3596
n = 5360
CTR
CKO1
CKO2

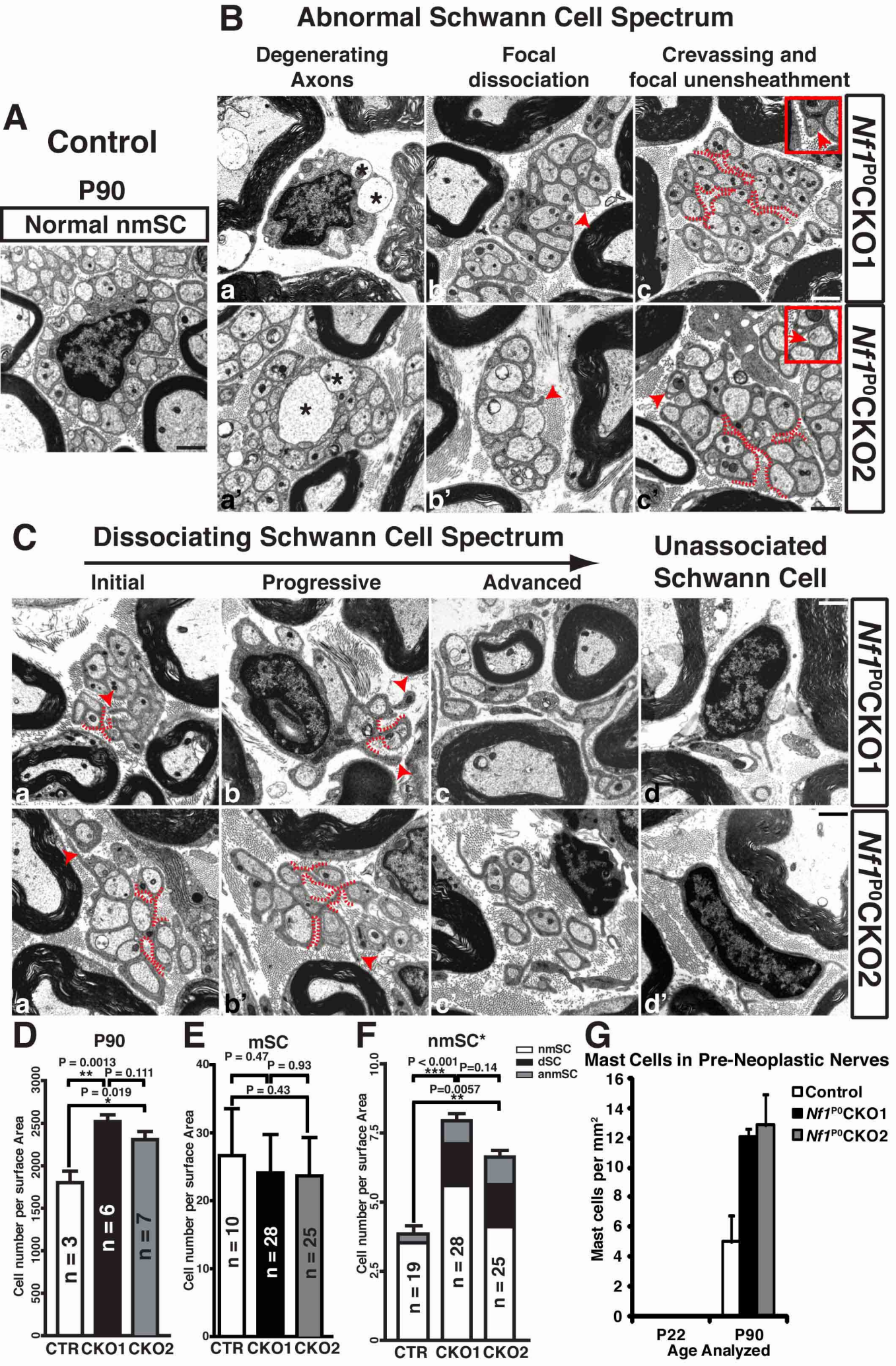
A
Control
P90
Normal nmSC
B
Abnormal Schwann Cell Spectrum
Degenerating Axons
Focal dissociation
Crevassing and focal unensheathment
Nf1P0CKO1
Nf1P0CKO2
a
b
c
a'
b'
c'
C
Dissociating Schwann Cell Spectrum
Initial
Progressive
Advanced
Unassociated Schwann Cell
Nf1P0CKO1
Nf1P0CKO2
a
b
c
d
a'
b'
c'
d'
D
P90
P = 0.0013
** P = 0.111
P = 0.019
*
Cell number per surface Area
n = 3
n = 6
n = 7
CTR CKO1 CKO2
E
mSC
P = 0.47
P = 0.93
P = 0.43
Cell number per surface Area
n = 10
n = 28
n = 25
CTR CKO1 CKO2
F
nmSC*
P < 0.001
*** P=0.14
P=0.0057
**
nmSC
dSC
anmSC
Cell number per surface Area
n = 19
n = 28
n = 25
CTR CKO1 CKO2
G
Mast Cells in Pre-Neoplastic Nerves
Control
Nf1P0CKO1
Nf1P0CKO2
Mast cells per mm2
P22
P90
Age Analyzed

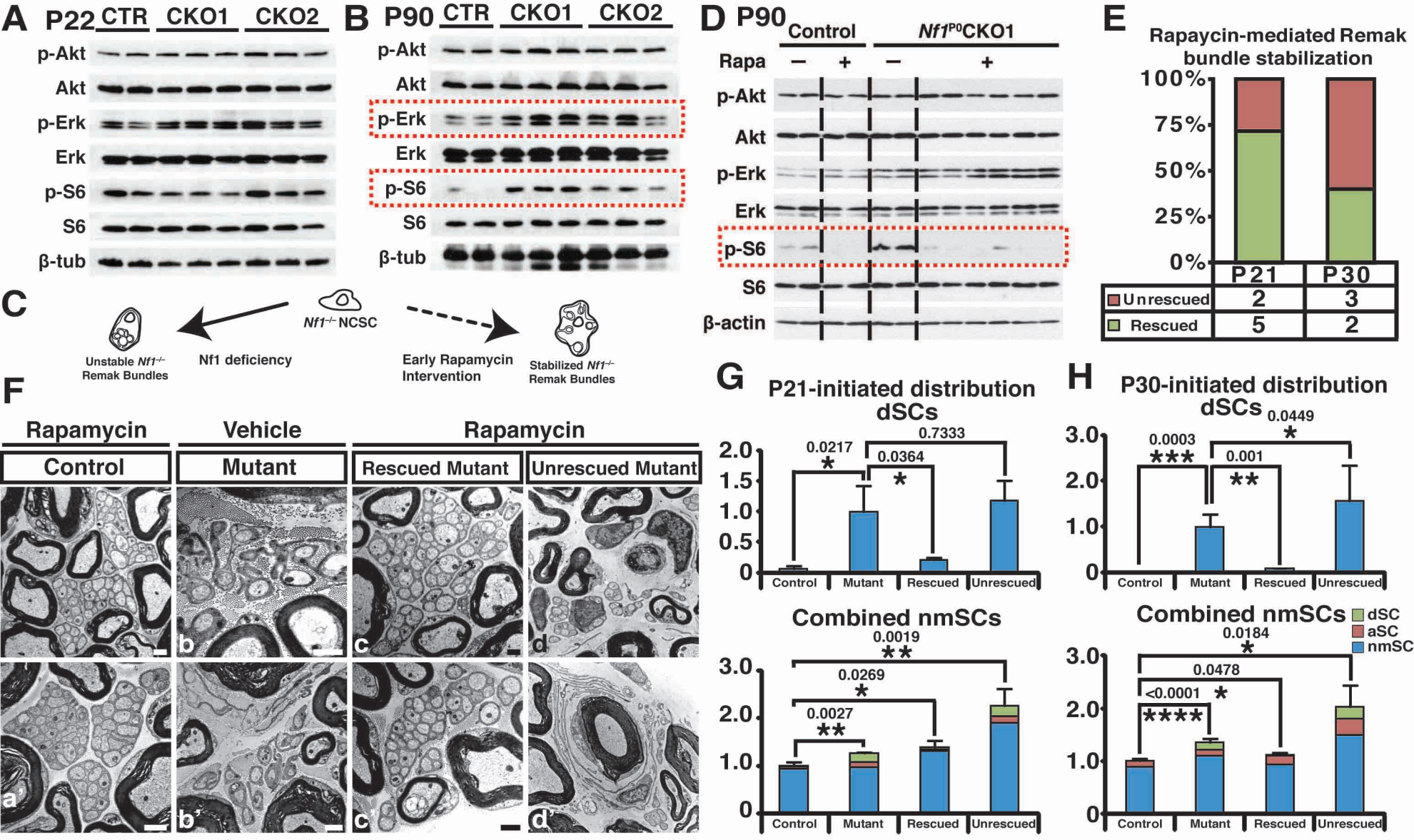
A
P22
CTR
CKO1
CKO2
p-Akt
Akt
p-Erk
Erk
p-S6
S6
β-tub
B
P90
CTR
CKO1
CKO2
p-Akt
Akt
p-Erk
Erk
p-S6
S6
β-tub
C
Unstable Nf1−/− Remak Bundles
Nf1 deficiency
Nf1−/− NCSC
Early Rapamycin Intervention
Stabilized Nf1−/− Remak Bundles
D
P90
Control
Nf1P0CKO1
Rapa
–
+
–
+
p-Akt
Akt
p-Erk
Erk
p-S6
S6
β-actin
E
Rapaycin-mediated Remak bundle stabilization
100%
75%
50%
25%
0%
P21
P30
Unrescued
2
3
Rescued
5
2
F
Rapamycin
Vehicle
Rapamycin
Control
Mutant
Rescued Mutant
Unrescued Mutant
a
b
c
d
a'
b'
c'
d'
G
P21-initiated distribution dSCs
0.0217
0.0364
0.7333
Control
Mutant
Rescued
Unrescued
Combined nmSCs
0.0019
0.0269
0.0027
Control
Mutant
Rescued
Unrescued
H
P30-initiated distribution dSCs
0.0003
0.001
0.0449
Control
Mutant
Rescued
Unrescued
Combined nmSCs
dSC
aSC
nmSC
0.0184
0.0478
<0.0001
Control
Mutant
Rescued
Unrescued

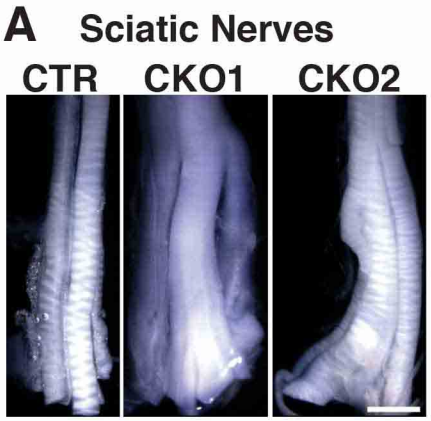

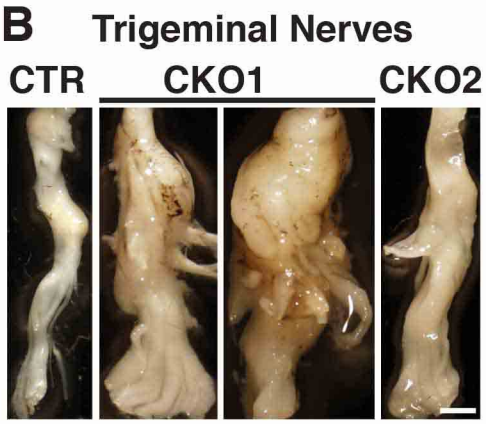

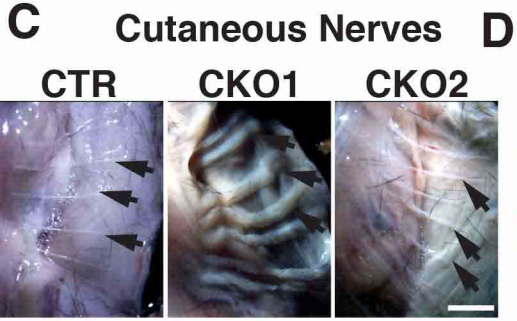

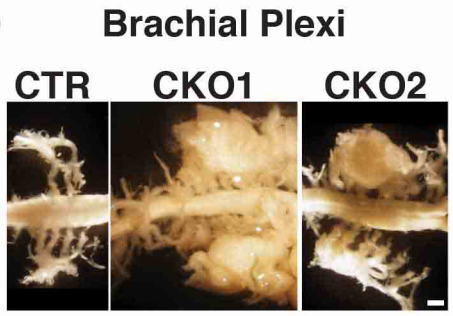

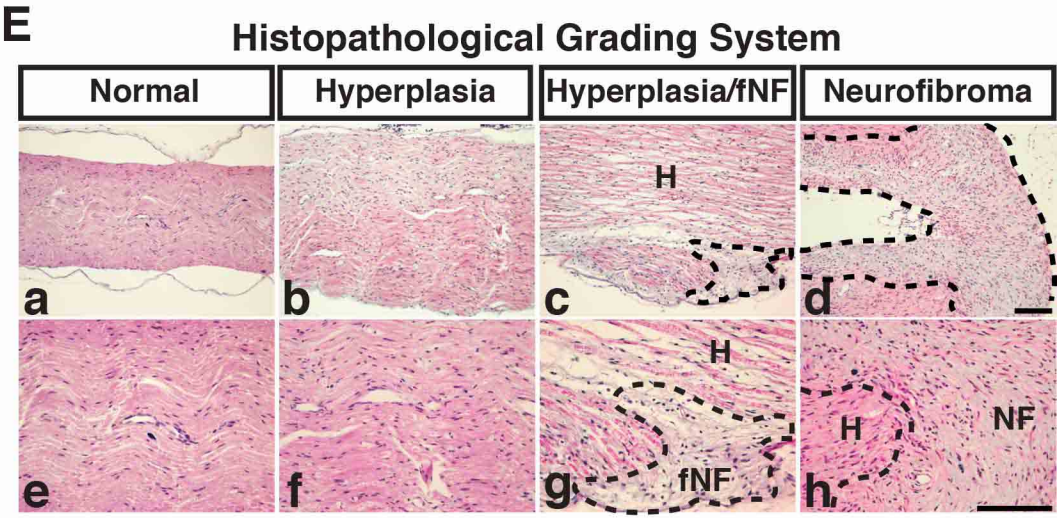

F Summary of Neurofibroma penetrance by site

Site	CKO1	CKO2	P-value
Sciatic	65% (n=20)	0% (n=13)	0.0002
Trigeminal	36% (n=14)	0% (n=12)	0.0425
Cutaneous	100% (n=20)	54% (n=13)	0.0015
CDRG*	73% (n=12)	35% (n=10)	0.027
TDRG*	58% (n=12)	31% (n=9)	0.086
LDRG*	36% (n=12)	23% (n=10)	0.472
Brachial Plexus	92% (n=13)	70% (n=10)	0.2806

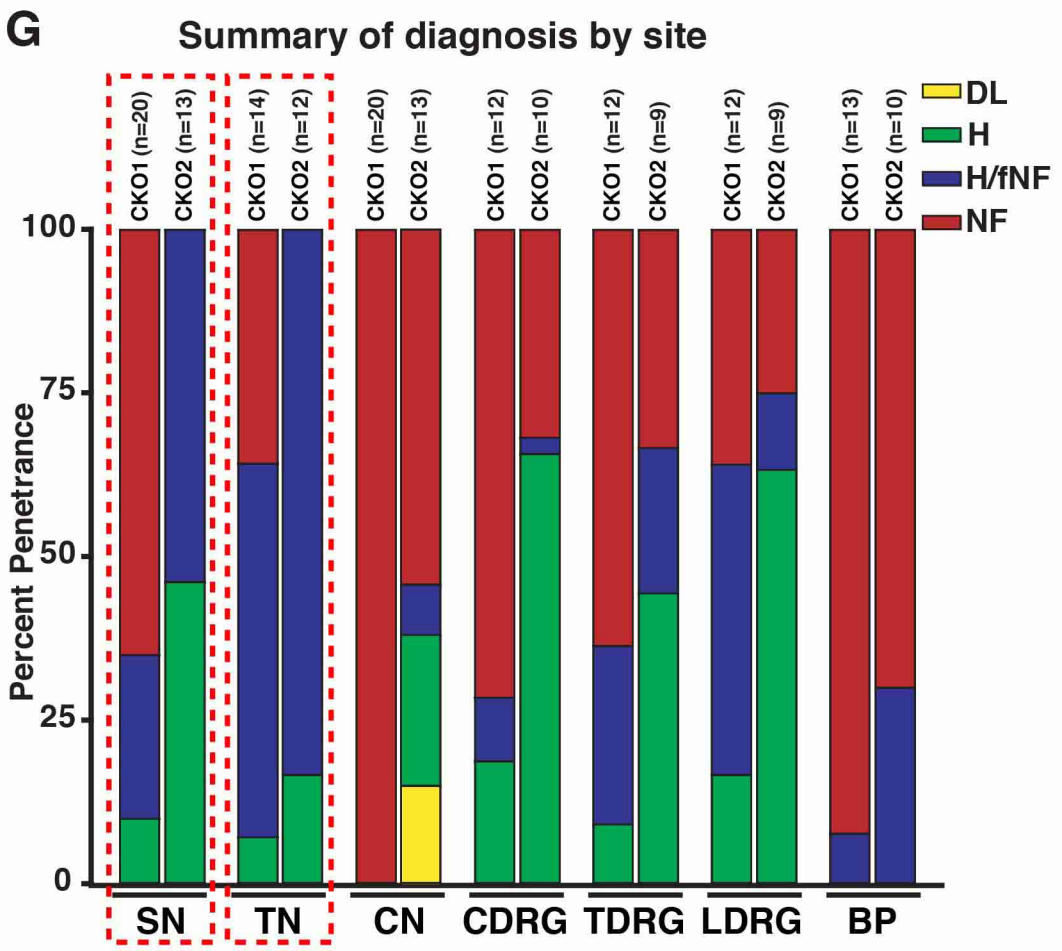

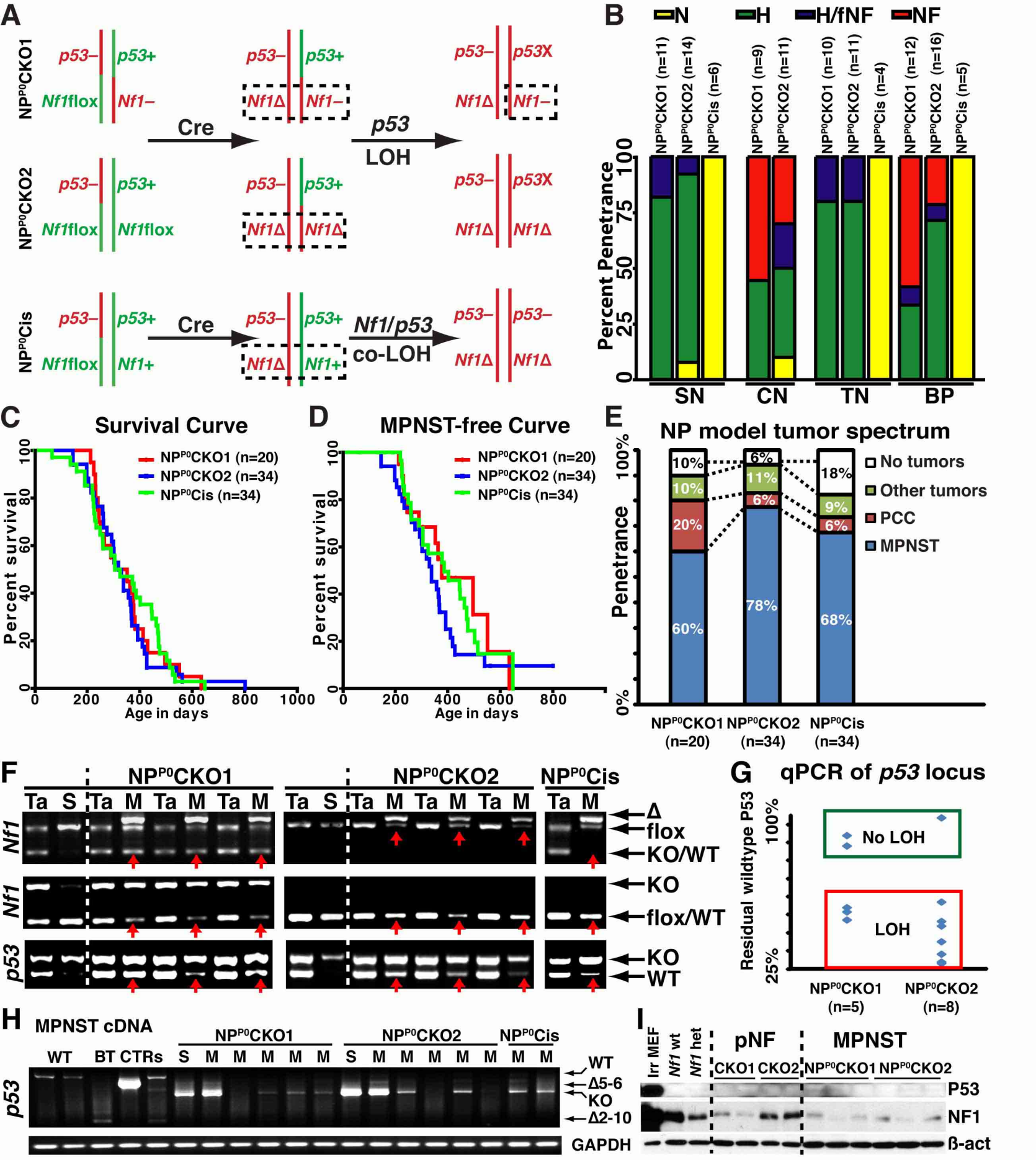
A
NP^P0CKO1
p53– p53+
Nf1flox Nf1–
Cre
Nf1Δ Nf1–
p53
LOH
p53– p53X
Nf1Δ Nf1–
NP^P0CKO2
p53– p53+
Nf1flox Nf1flox
Nf1Δ Nf1Δ
p53– p53X
Nf1Δ Nf1Δ
NP^P0Cis
p53– p53+
Nf1flox Nf1+
Cre
Nf1Δ Nf1+
Nf1/p53
co-LOH
p53– p53–
Nf1Δ Nf1Δ
B
N H H/fNF NF
NP^P0CKO1 (n=11)
NP^P0CKO2 (n=14)
NP^P0Cis (n=6)
NP^P0CKO1 (n=9)
NP^P0CKO2 (n=11)
NP^P0CKO1 (n=10)
NP^P0CKO2 (n=11)
NP^P0Cis (n=4)
NP^P0CKO1 (n=12)
NP^P0CKO2 (n=16)
NP^P0Cis (n=5)
Percent Penetrance
0 25 50 75 100
SN CN TN BP
C
Survival Curve
NP^P0CKO1 (n=20)
NP^P0CKO2 (n=34)
NP^P0Cis (n=34)
Percent survival
0 20 40 60 80 100
0 200 400 600 800 1000
Age in days
D
MPNST-free Curve
NP^P0CKO1 (n=20)
NP^P0CKO2 (n=34)
NP^P0Cis (n=34)
Percent survival
0 20 40 60 80 100
0 200 400 600 800
Age in days
E
NP model tumor spectrum
Penetrance
0% 100%
10% 10% 20% 60%
6% 11% 6% 78%
18% 9% 6% 68%
No tumors
Other tumors
PCC
MPNST
NP^P0CKO1 (n=20)
NP^P0CKO2 (n=34)
NP^P0Cis (n=34)
F
NP^P0CKO1
NP^P0CKO2
NP^P0Cis
Ta S Ta M Ta M Ta M
Ta S Ta M Ta M Ta M
Ta M
Nf1
Nf1
p53
Δ
flox
KO/WT
KO
flox/WT
KO
WT
G
qPCR of p53 locus
Residual wildtype P53
100%
25%
No LOH
LOH
NP^P0CKO1 (n=5)
NP^P0CKO2 (n=8)
H
MPNST cDNA
NP^P0CKO1
NP^P0CKO2
NP^P0Cis
WT BT CTRs S M M M M M S M M M M M M M
p53
WT
Δ5-6
KO
Δ2-10
GAPDH
I
Irr MEF
Nf1 wt
Nf1 het
pNF
MPNST
CKO1 CKO2
NP^P0CKO1 NP^P0CKO2
P53
NF1
ß-act

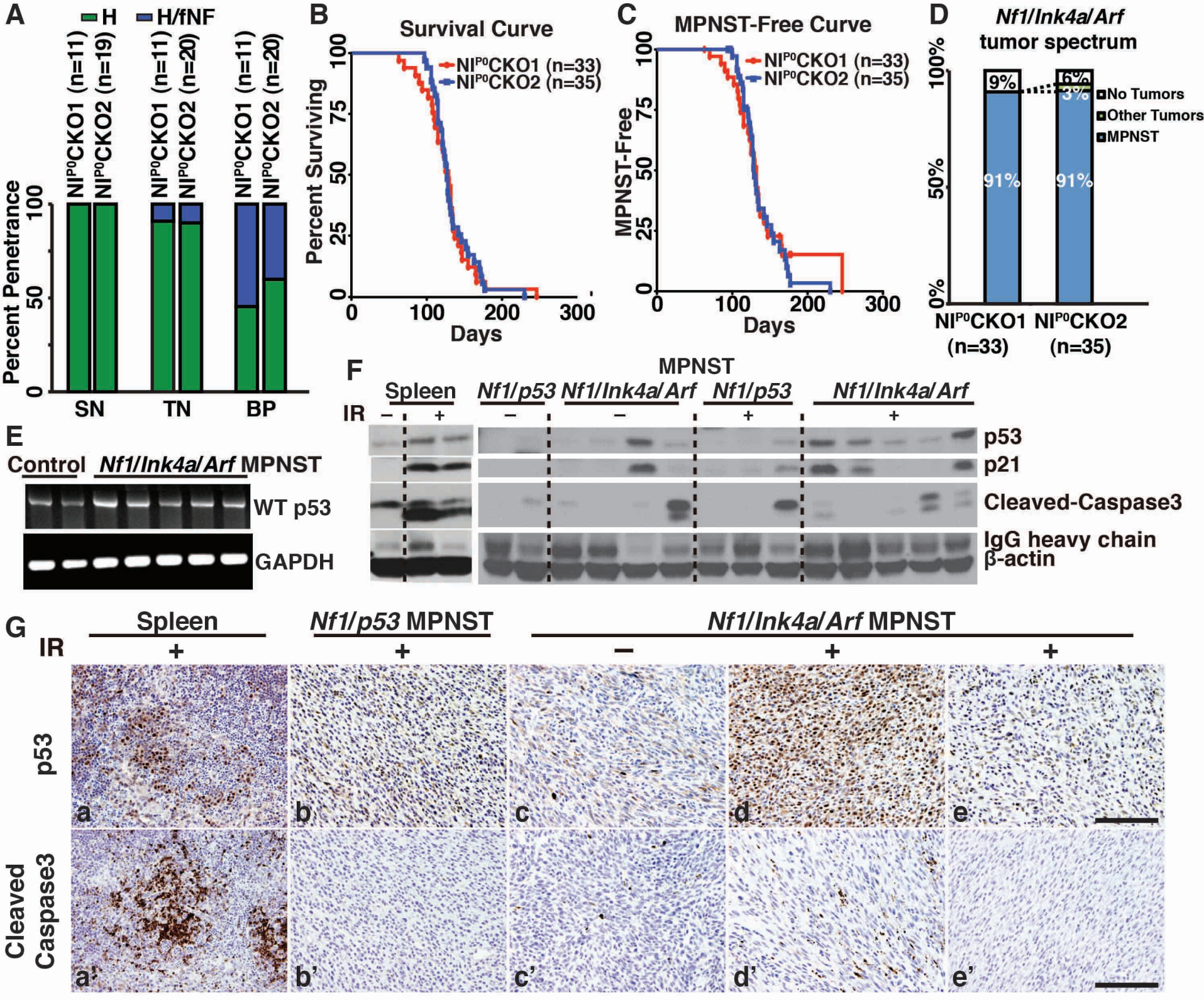
A
H
H/fNF
Percent Penetrance
NIP0CKO1 (n=11)
NIP0CKO2 (n=19)
NIP0CKO1 (n=11)
NIP0CKO2 (n=20)
NIP0CKO1 (n=11)
NIP0CKO2 (n=20)
SN
TN
BP
B
Survival Curve
Percent Surviving
NIP0CKO1 (n=33)
NIP0CKO2 (n=35)
Days
C
MPNST-Free Curve
MPNST-Free
NIP0CKO1 (n=33)
NIP0CKO2 (n=35)
Days
D
Nf1/Ink4a/Arf
tumor spectrum
9%
6%
3%
91%
91%
No Tumors
Other Tumors
MPNST
NIP0CKO1 (n=33)
NIP0CKO2 (n=35)
E
Control
Nf1/Ink4a/Arf MPNST
WT p53
GAPDH
F
MPNST
Spleen
Nf1/p53
Nf1/Ink4a/Arf
Nf1/p53
Nf1/Ink4a/Arf
IR
p53
p21
Cleaved-Caspase3
IgG heavy chain
β-actin
G
Spleen
Nf1/p53 MPNST
Nf1/Ink4a/Arf MPNST
IR
p53
Cleaved Caspase3
a
b
c
d
e
a'
b'
c'
d'
e'

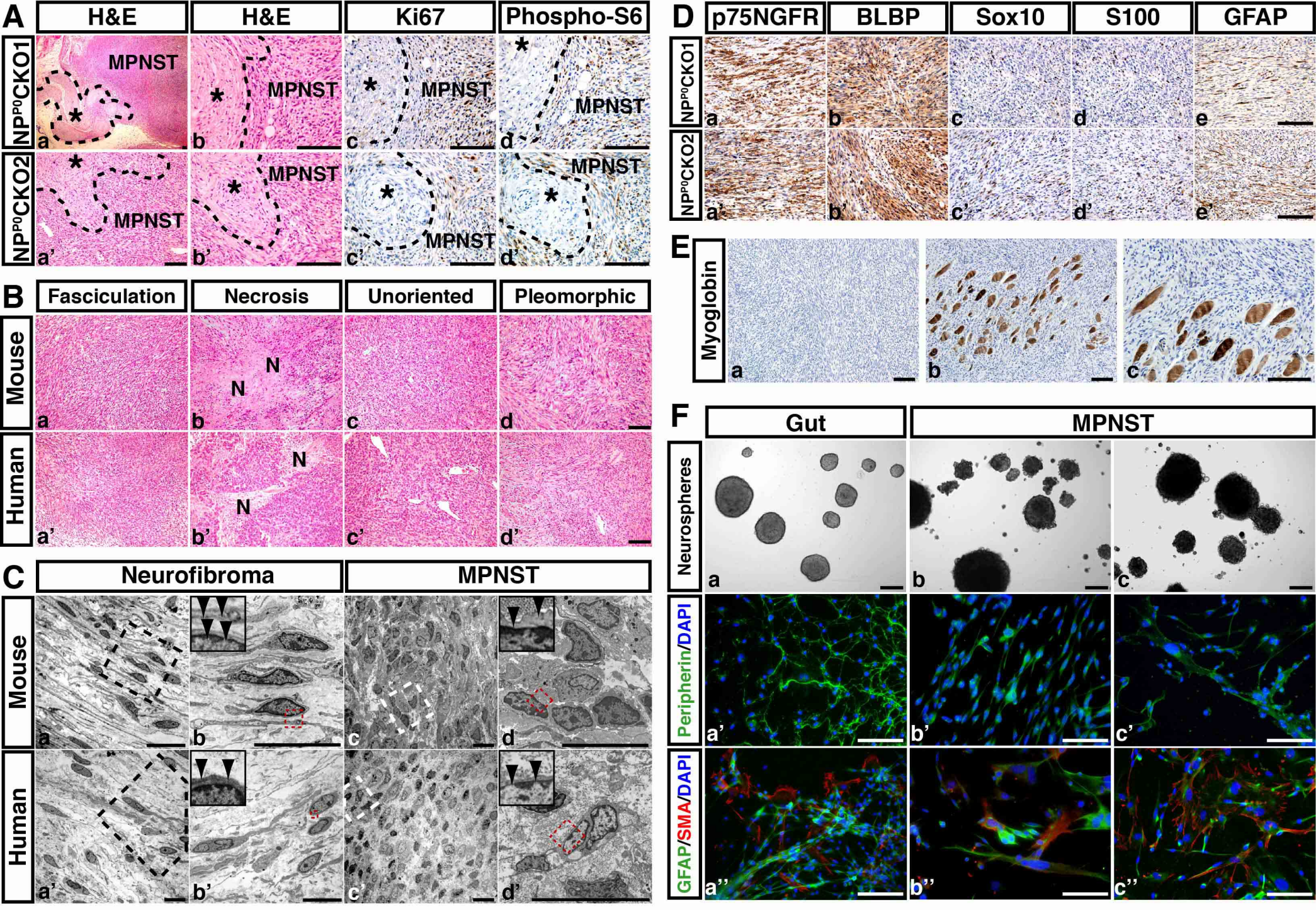
A
H&E
H&E
Ki67
Phospho-S6
NP^P0CKO1
NP^P0CKO2
MPNST
B
Fasciculation
Necrosis
Unoriented
Pleomorphic
Mouse
Human
N
C
Neurofibroma
MPNST
Mouse
Human
D
p75NGFR
BLBP
Sox10
S100
GFAP
NP^P0CKO1
NP^P0CKO2
E
Myoglobin
F
Gut
MPNST
Neurospheres
Peripherin/DAPI
GFAP/SMA/DAPI

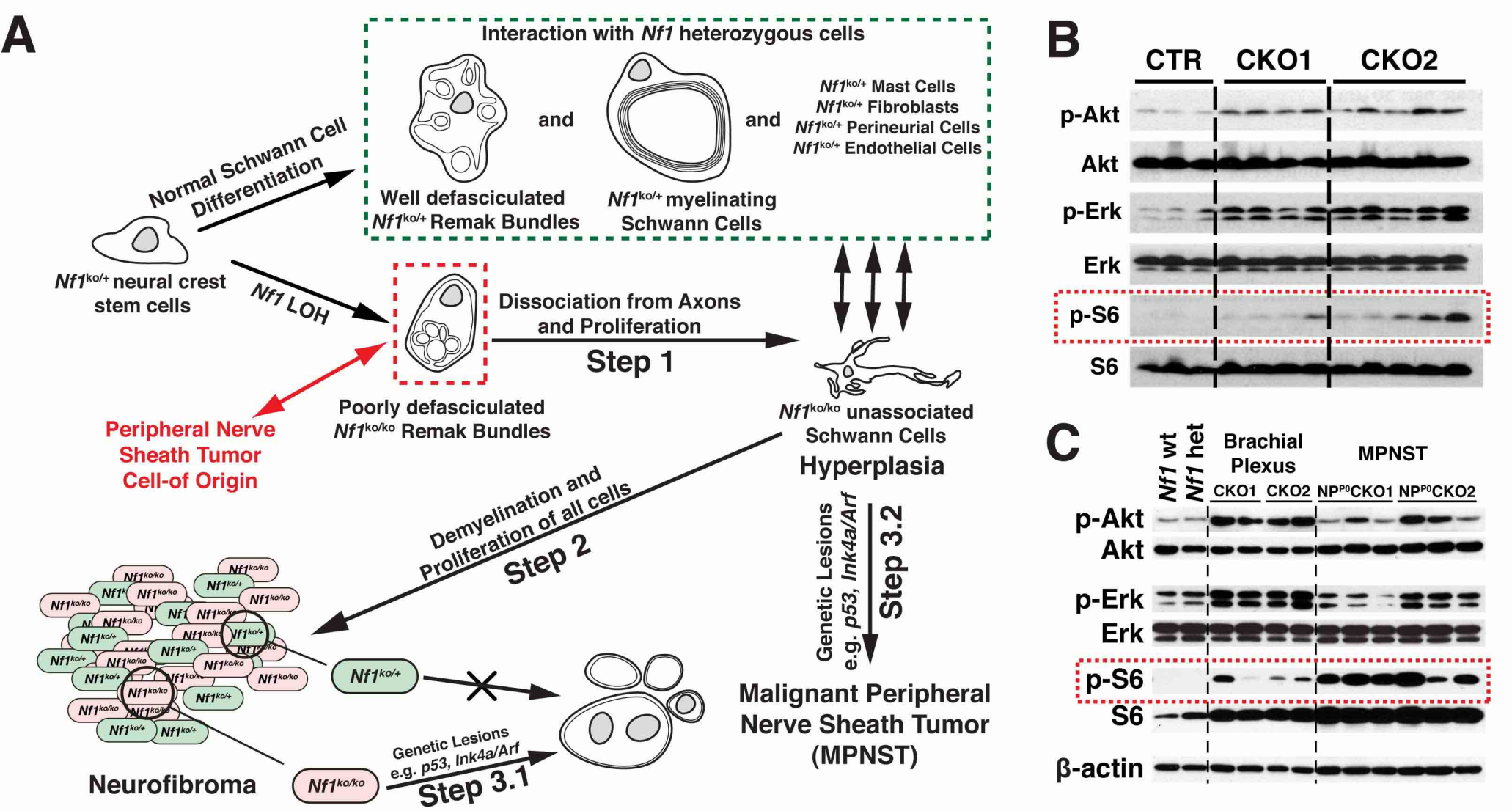

D

	NF1 heterozygous Microenvironment	mTORC1 Activity
Step 1: Initiation	Insensitive	Sensitive
Step 2: Progression	Sensitive	Insensitive
Step 3: Malignant Transformation	Insensitive	Sensitive

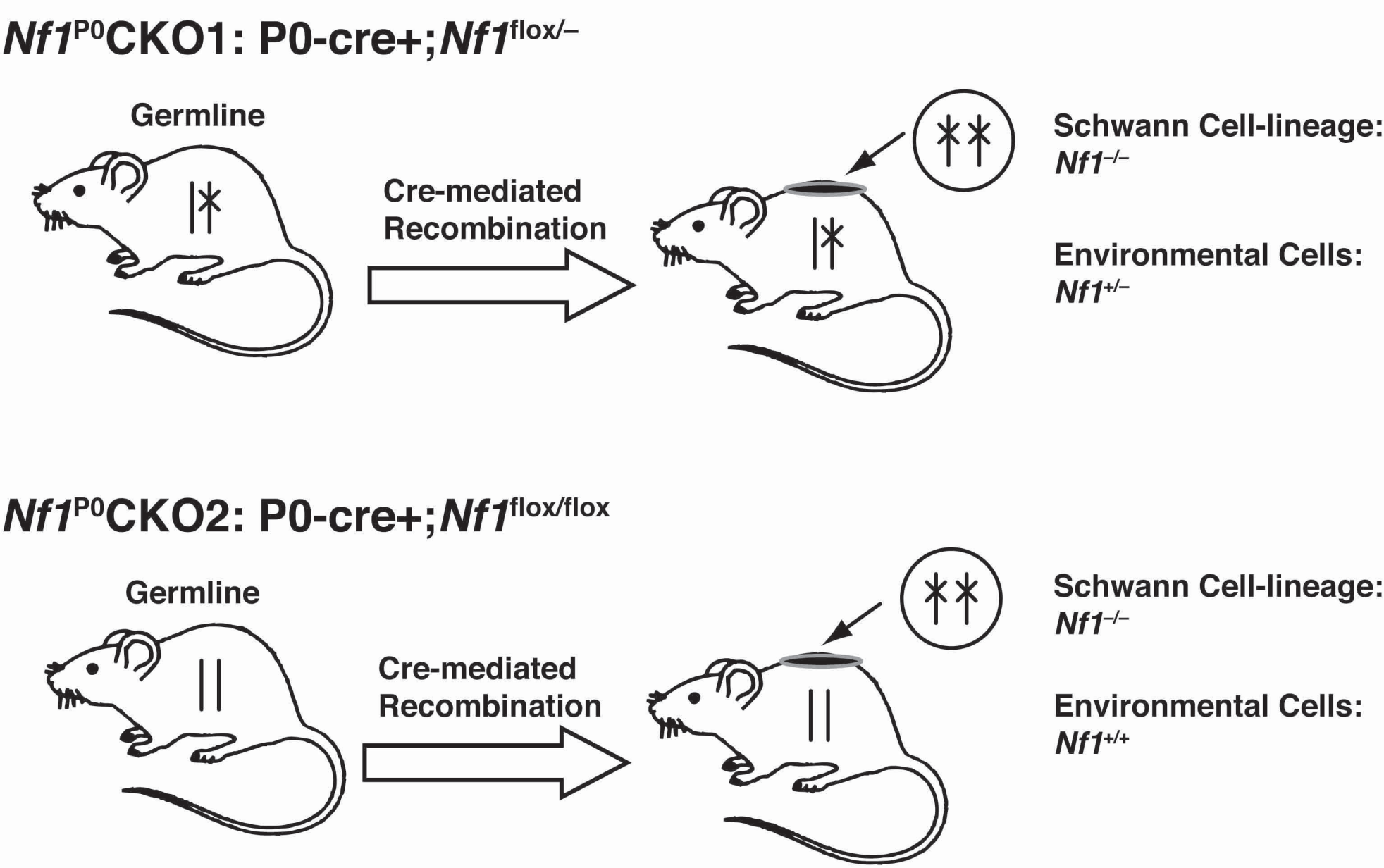
Nf1^{P0}CKO1: P0-cre+;*Nf1*$^{flox/-}$
Germline
Cre-mediated Recombination
Schwann Cell-lineage: *Nf1*$^{-/-}$
Environmental Cells: *Nf1*$^{+/-}$
Nf1^{P0}CKO2: P0-cre+;*Nf1*$^{flox/flox}$
Germline
Cre-mediated Recombination
Schwann Cell-lineage: *Nf1*$^{-/-}$
Environmental Cells: *Nf1*$^{+/+}$

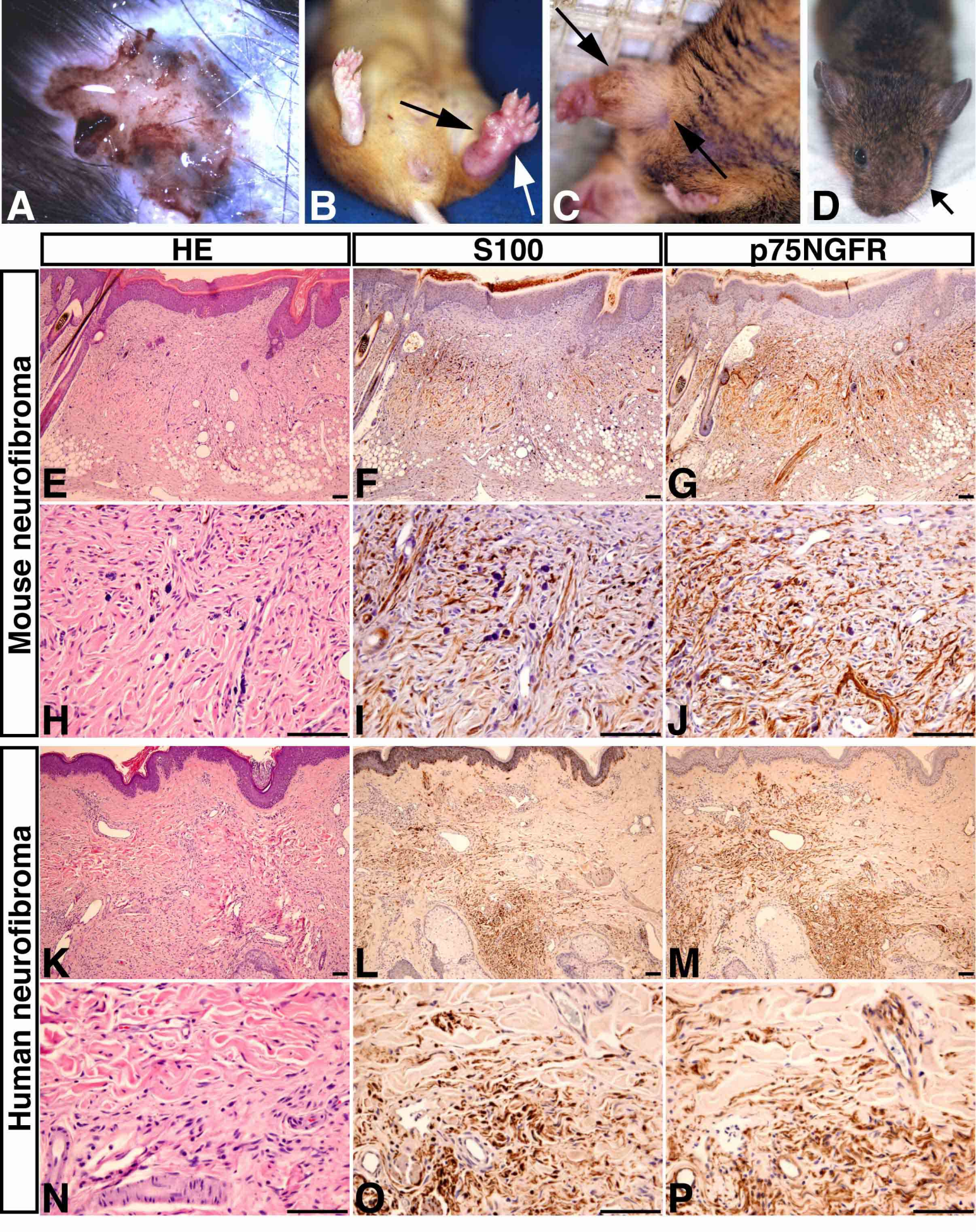
A
B
C
D
HE
S100
p75NGFR
Mouse neurofibroma
E
F
G
H
I
J
Human neurofibroma
K
L
M
N
O
P

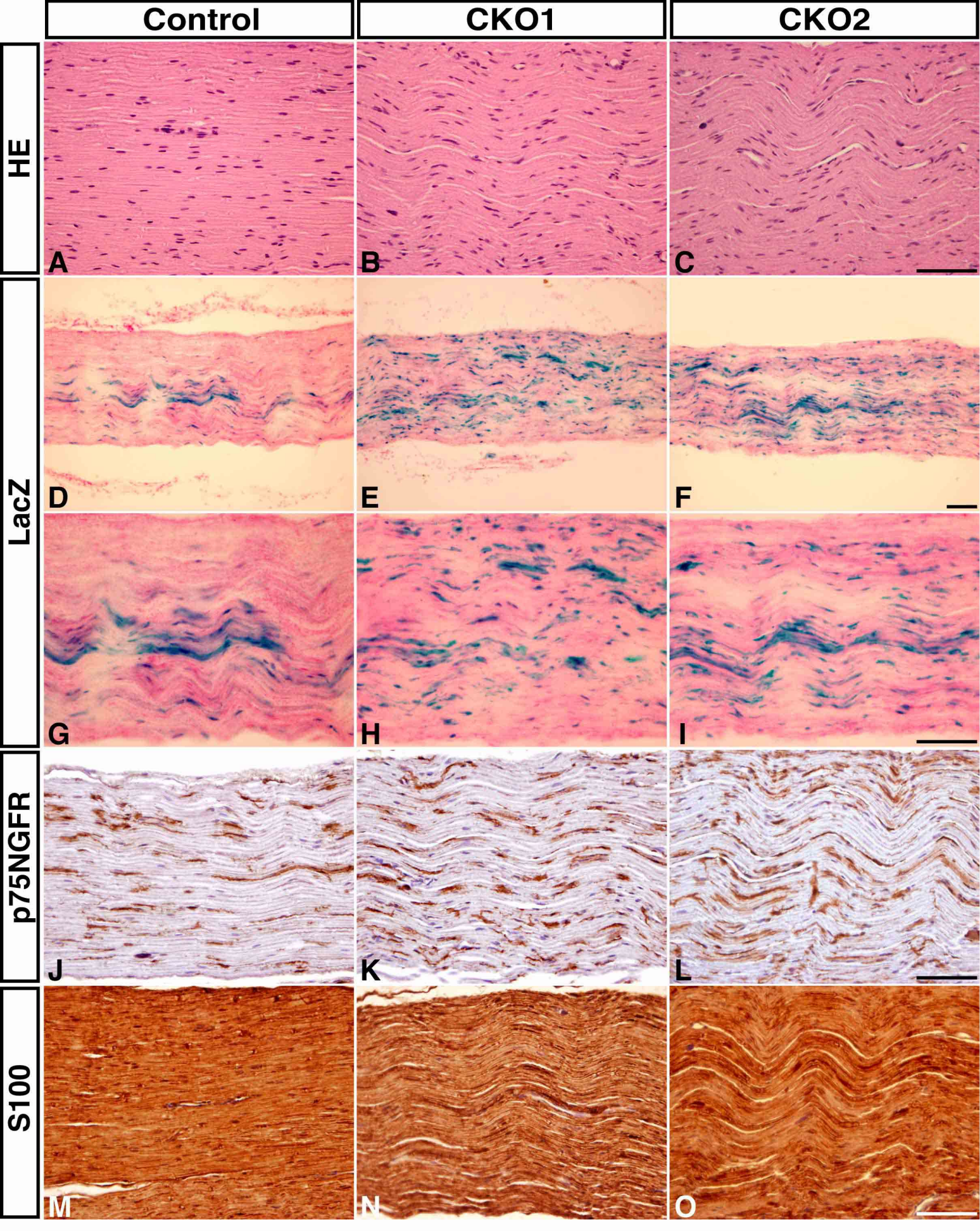
Control
CKO1
CKO2
HE
LacZ
p75NGFR
S100
A
B
C
D
E
F
G
H
I
J
K
L
M
N
O

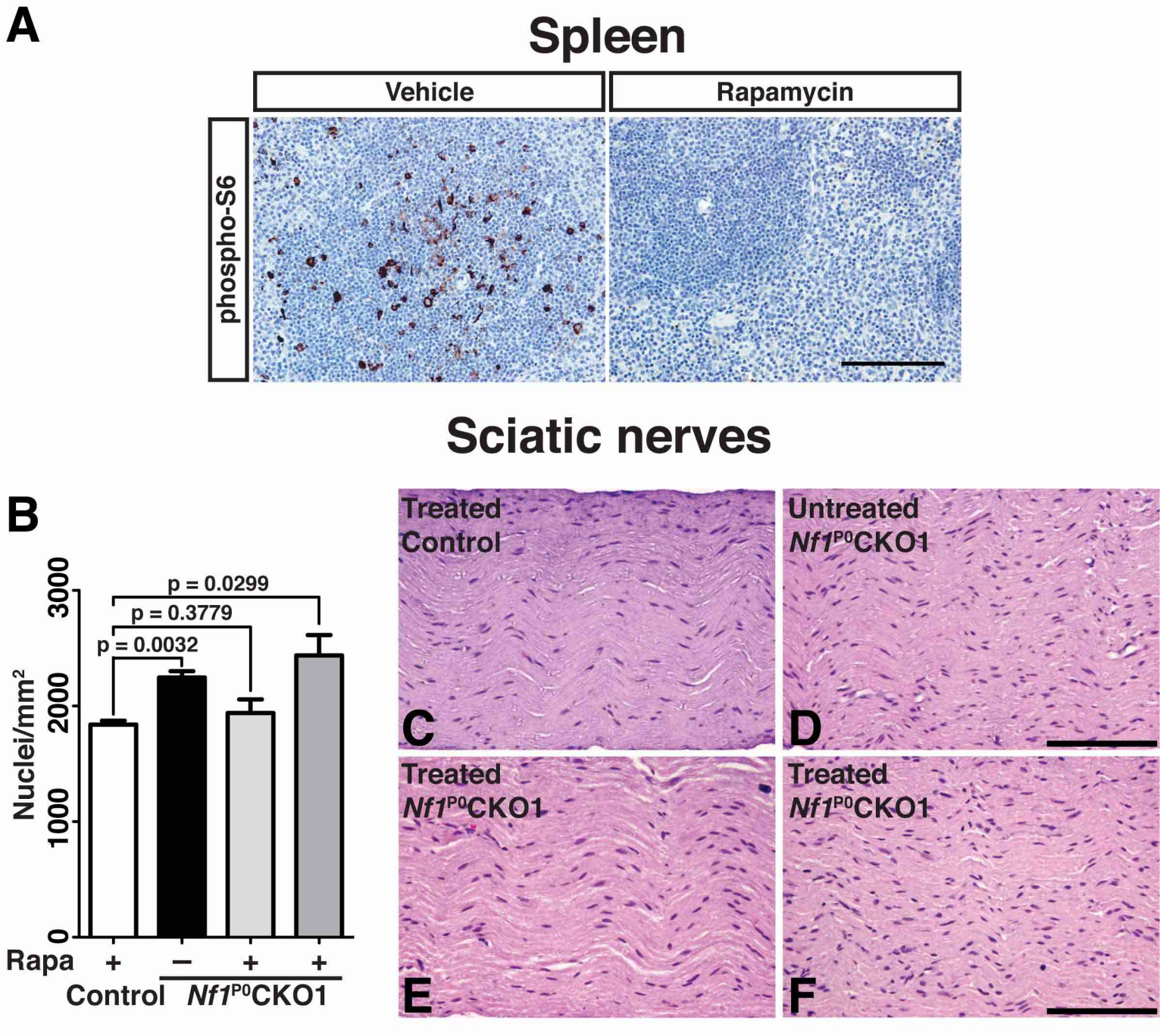
A
Spleen
Vehicle
Rapamycin
phospho-S6
Sciatic nerves
B
Nuclei/mm²
3000
2000
1000
0
p = 0.0299
p = 0.3779
p = 0.0032
Rapa + − + +
Control Nf1P0CKO1
Treated Control
C
Untreated Nf1P0CKO1
D
Treated Nf1P0CKO1
E
Treated Nf1P0CKO1
F

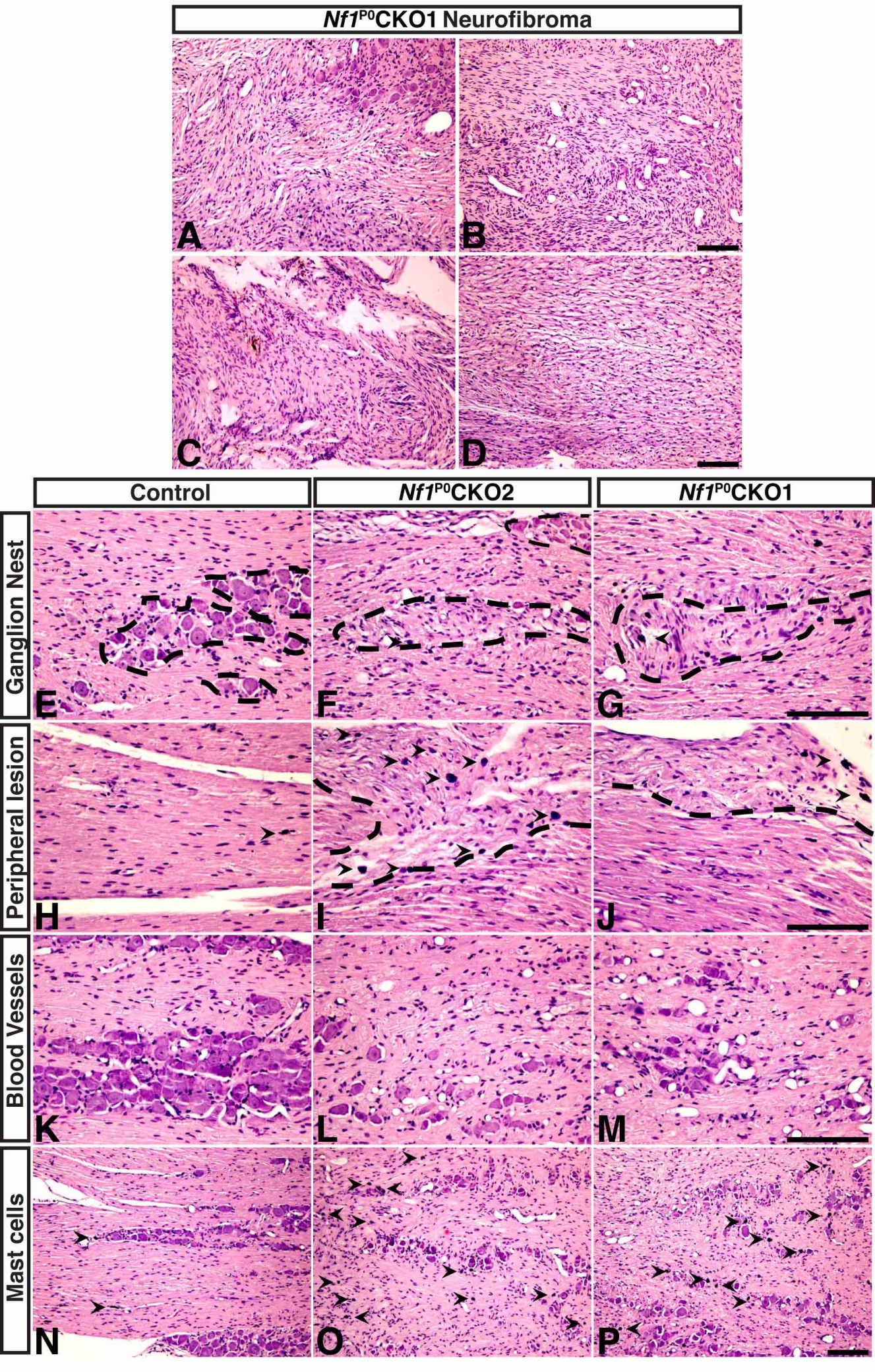
Nf1P0CKO1 Neurofibroma
A
B
C
D
Control
Nf1P0CKO2
Nf1P0CKO1
Ganglion Nest
Peripheral lesion
Blood Vessels
Mast cells
E
F
G
H
I
J
K
L
M
N
O
P

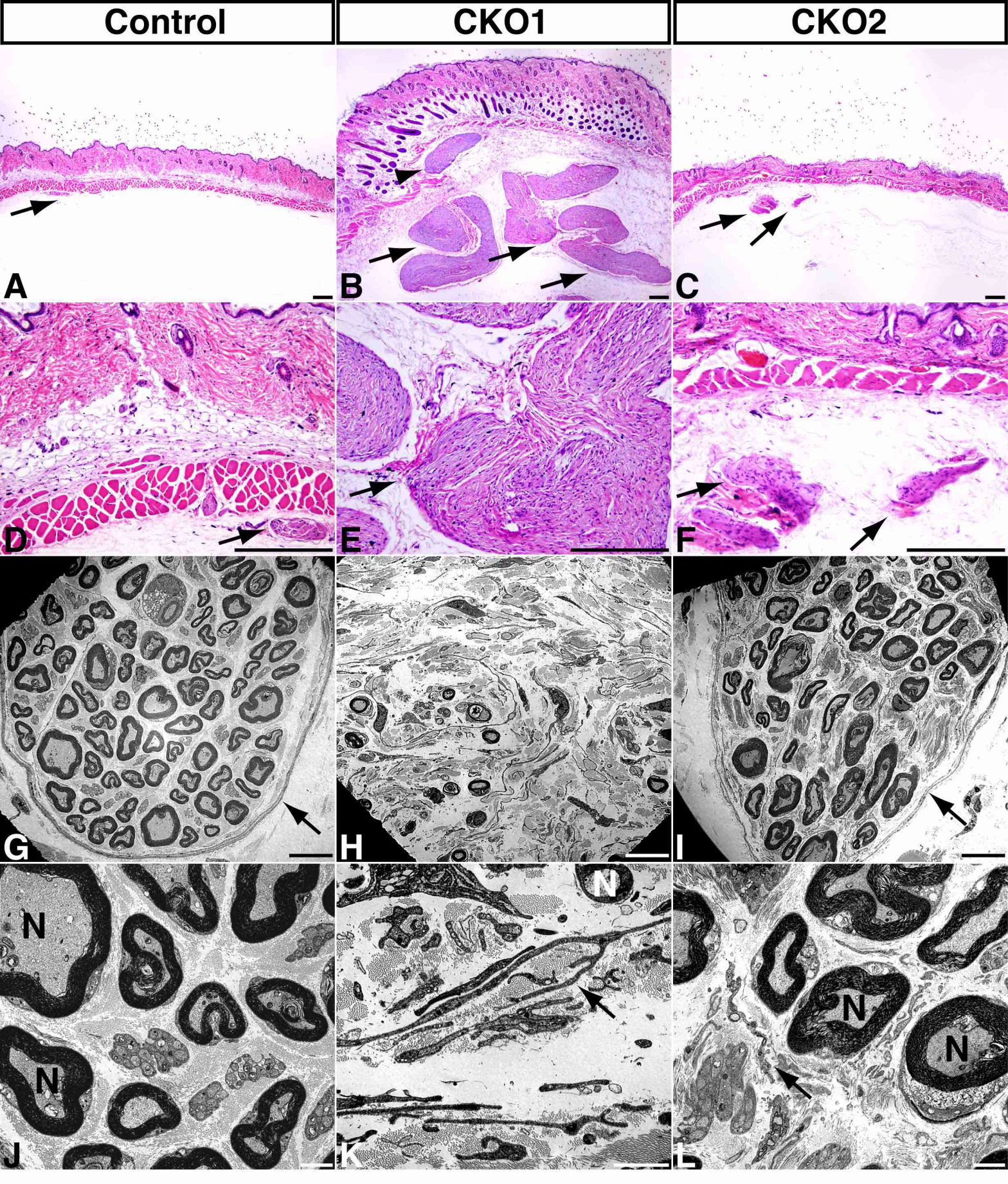
Control
CKO1
CKO2
A
B
C
D
E
F
G
H
I
J
K
L
N
N
N
N
N

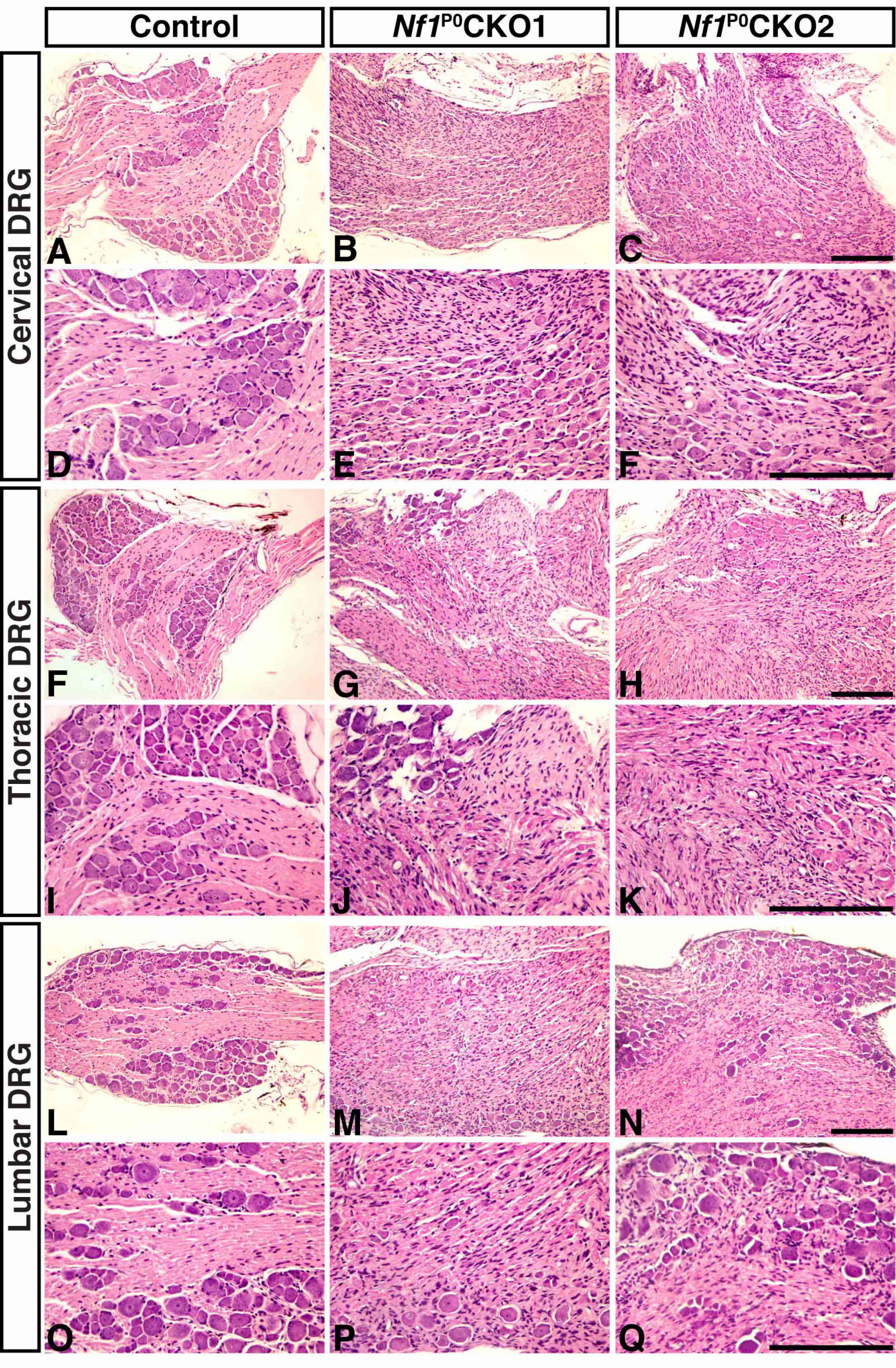
Control
Nf1P0CKO1
Nf1P0CKO2
Cervical DRG
Thoracic DRG
Lumbar DRG
A
B
C
D
E
F
F
G
H
I
J
K
L
M
N
O
P
Q

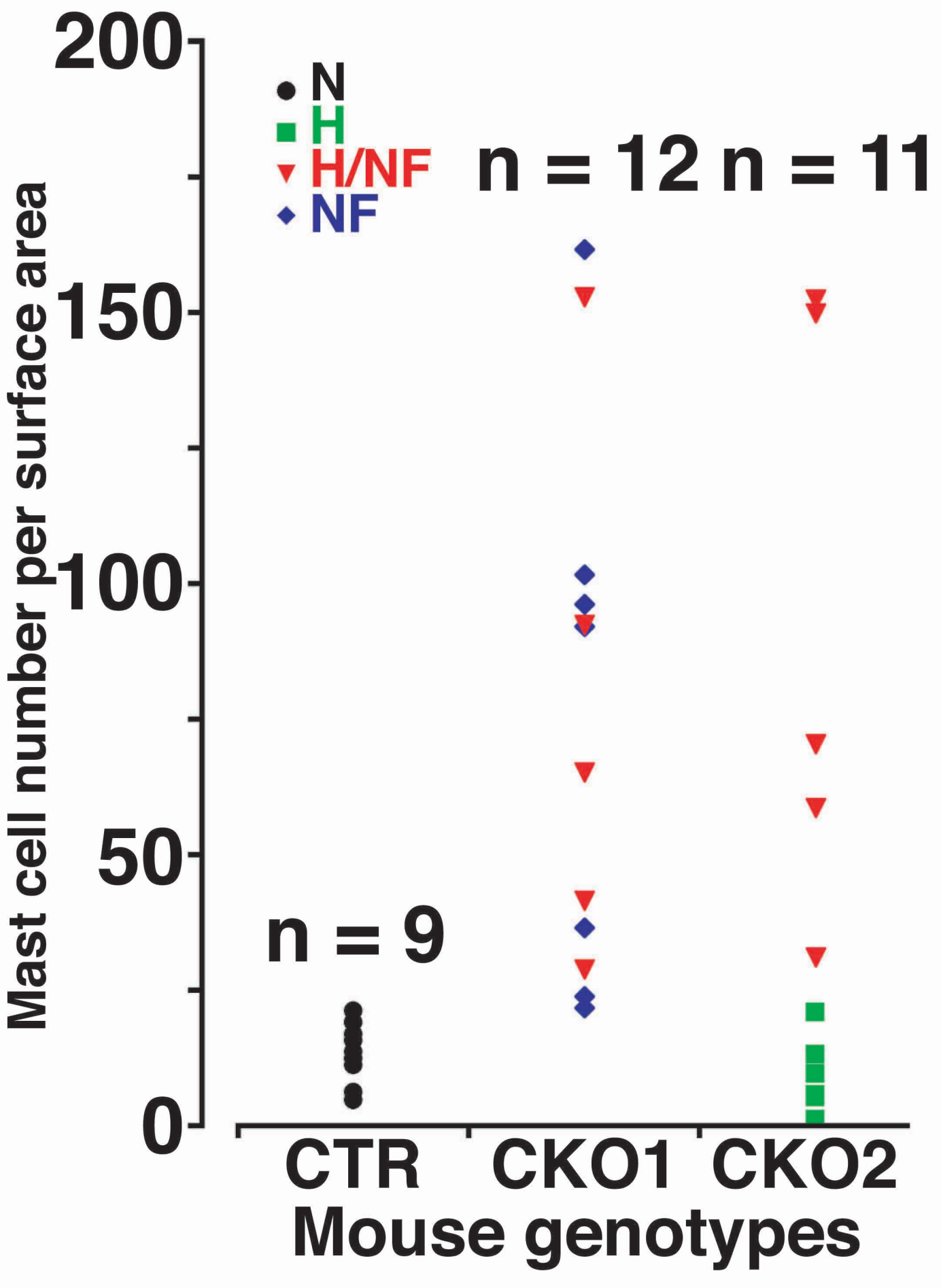
200
150
100
50
0
N
H
H/NF
NF
n = 12
n = 11
n = 9
Mast cell number per surface area
CTR
CKO1
CKO2
Mouse genotypes

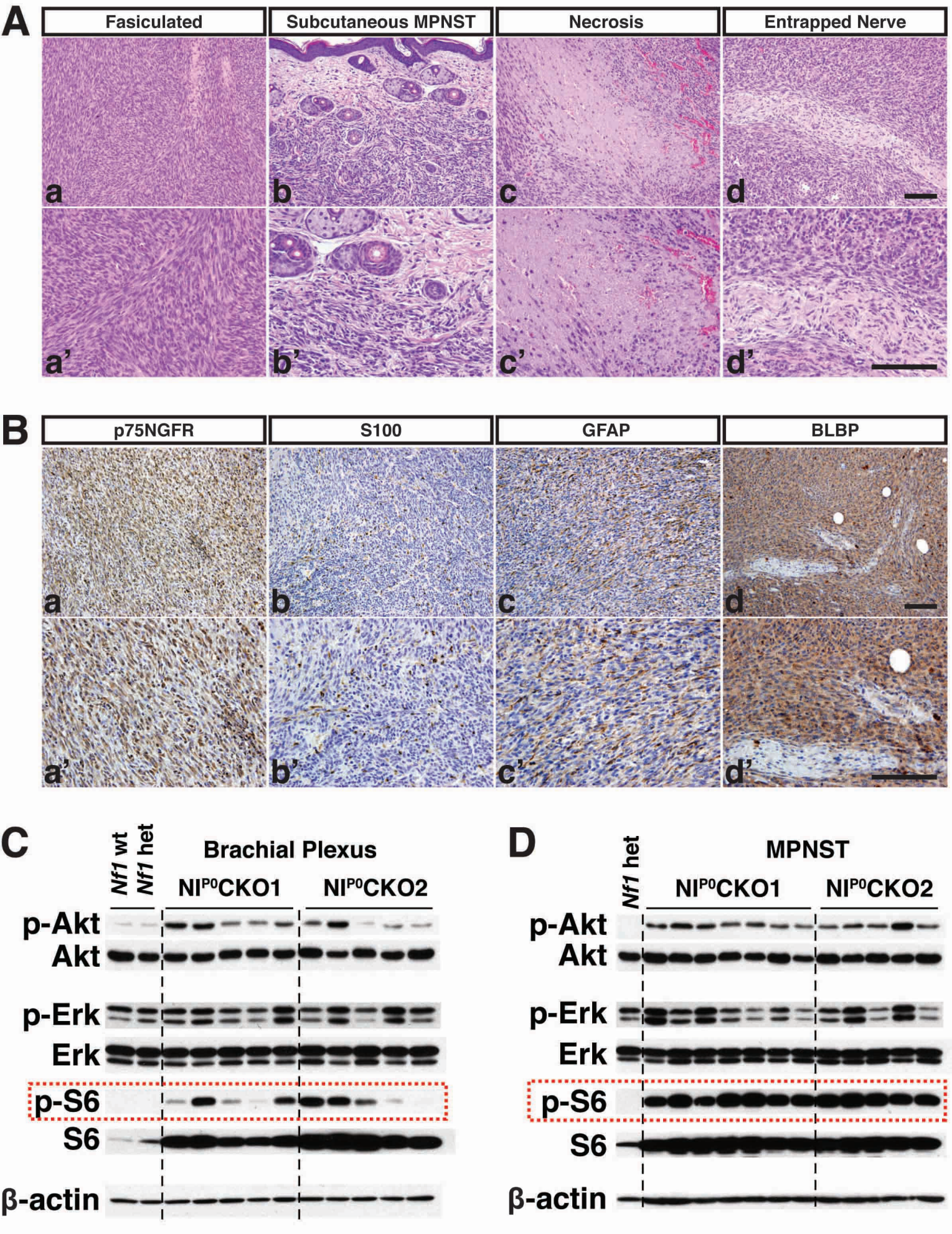
A
Fasiculated
Subcutaneous MPNST
Necrosis
Entrapped Nerve
a
b
c
d
a'
b'
c'
d'
B
p75NGFR
S100
GFAP
BLBP
a
b
c
d
a'
b'
c'
d'
C
Nf1 wt
Nf1 het
Brachial Plexus
NIP0CKO1
NIP0CKO2
p-Akt
Akt
p-Erk
Erk
p-S6
S6
β-actin
D
Nf1 het
MPNST
NIP0CKO1
NIP0CKO2
p-Akt
Akt
p-Erk
Erk
p-S6
S6
β-actin